The Thesis Committee for David Christopher Hull

Certifies that this is the approved version of the following thesis:

Stratigraphic Architecture, Depositional Systems, and Reservoir Characteristics of the Pearsall Shale-Gas System, Lower Cretaceous, South Texas

APPROVED BY

SUPERVISING COMMITTEE:

Co-Supervisor: _____
Robert G. Loucks

Co-Supervisor: _____
Kitty L. Milliken

_____
Charles Kerans

_____
Ronald Steel

Stratigraphic Architecture, Depositional Systems, and Reservoir Characteristics of the Pearsall Shale-Gas System, Lower Cretaceous, South Texas

by

David Christopher Hull, M.A.

Thesis

Presented to the Faculty of the Graduate School of

The University of Texas at Austin

in Partial Fulfillment

of the Requirements

for the Degree of

Master of Science in Geological Sciences

The University of Texas at Austin

August, 2011

Acknowledgements

Many people deserve recognition in this thesis for their support. Unfortunately these pages are not long enough to give each and every one their due.

First and foremost I would like to express my appreciation to Bob Loucks and Kitty Milliken, who co-advised me: Bob for his patience, advice, wanted and unwanted, and ability to recall geologic knowledge from decades past and Kitty for her inspiration at the microscope. Also I thank the rest of my committee, Charlie Kerans and Ron Steel, who enlightened me in regard to carbonates and clastics. In addition to the faculty at The University of Texas at Austin, I need to thank the geology department at Texas A&M University. Although they did not award me a degree, they facilitated my geologic education.

With respect to funding and research, I am also grateful to the STARR program, which has funded much of my work, and the MSRL consortium, which has provided both the venue to present it and much of the technical expertise. Thanks must also be extended to the QCL consortium and RCRL consortium, and Harry Rowe and his students from UT Arlington, as discussions with researchers from these groups have been particularly fruitful. Special thanks also must be extended to those have written on South Texas or mudrocks previously and concurrently. Many of the most worthwhile ideas and thoughts were generated in conversations with them. These people include Ryan Harbor, Ryan Phelps, and Dolores van der Kolk.

Data were also generously provided by Encana Oil and Gas (USA), Chesapeake Energy Corporation, Harry Rowe and his students at UT Arlington, Jason Jeremiah at Shell Oil Company, and Peter Rawson at the University of Hull at Scarborough.

Abstract

Stratigraphic Architecture, Depositional Systems, and Reservoir Characteristics of the Pearsall Shale-Gas System, Lower Cretaceous, South Texas

David Christopher Hull, MSGeoSci

The University of Texas at Austin, 2011

Co-Supervisors: Robert G. Loucks and Kitty L. Milliken

This study examines the regional stratigraphic architecture, depositional systems, and petrographic characteristics of the South Texas Pearsall shale-gas system currently developed in the Indio Tanks (Pearsall) and Pena Creek (Pearsall) fields. The Pearsall Formation was deposited as a mixed carbonate-siliciclastic system on a distally steepened ramp over a period of 11.75 million years. It was deposited between maximum floods of two second-order sequences and contains at least five third-order cycles. Up to three Oceanic Anoxic Events (OAE 1-A, Late Aptian Regional Event, and OAE 1-B) figure prominently in the deposition of the Pearsall sediments, and during these intervals, depending on the location within the Maverick Basin, sedimentation rates were between 0.5 and 2 cm/ky. Facies in the Pearsall section arise from interactions between pre-existing topography, oxygenation regime, eustatic sea-level fluctuation, and depositional processes.

In the Pearsall Formation, OAEs affected depositional environments and resulting facies patterns during several time periods. The OAEs occurred in association with transgressions but not necessarily in concert with them. Outer ramp OAE facies are siliciclastic-dominated, TOC-rich, and little-bioturbated. Conversely the outer ramp facies deposited under normally oxygenated paleoenvironmental conditions tend to be carbonate-rich, TOC-poor, and are more prominently bioturbated.

Table of Contents

List of Tables

List of Figures

Chapter 1: Introduction

INTRODUCTION

Since the 1970's the Pearsall Formation (Figure 1.1) has been recognized as a potential producer of oil and gas in the Maverick Basin of South Texas (Loucks, 1976; Loucks, 1978). Few conventional reservoirs have been discovered in the Pearsall Formation, despite great efforts by exploration companies and widespread acknowledgement of potential. Developments in technology and the advent of unconventional shale-gas production throughout the United States have made the outer ramp calcareous terrigenous mudstone facies of the Pearsall Formation an active gas exploration target. Although there is growing interest in the Pearsall calcareous terrigenous mudstones, our understanding of this shale-gas system is still limited. Until now, deposition of the calcareous terrigenous mudrocks in the distal portion of the ramp has not been systemically studied. Production characteristics of terrigenous mudrocks are poorly understood, inhibiting the development of predictive models in gas exploration. The primary purpose of this thesis is to document the stratigraphic architecture, depositional systems, and reservoir characteristics of the Pearsall Formation.

The Pearsall Formation was deposited primarily during Aptian time and is age-equivalent to a number of major oil and gas accumulations around the world (Loucks, 1976; Goldhammer and Johnson, 2001; Phelps, 2011). The Pearsall Formation at the time of deposition featured proximal areas dominated by shoreface and shoal-water carbonate complexes, and distal shelf areas which were the loci of calcareous terrigenous mudstone deposition. Lithostratigraphically the Formation is divided into three members, two clastic members with a carbonate member in between. The Bexar Shale Member, the

upper clastic member, is further subdivided into three units. The Cow Creek Member is also divided into two units.

This study characterizes the facies of the shale-gas interval in the outer ramp and places it in a sequence stratigraphic and temporal context. This study considers not only classical sequence stratigraphic events but also oceanic anoxic events (OAEs), which were important for organic carbon production and preservation. Figure 1.1 shows the approximate relationship between the OAE events, sequence stratigraphy, and lithostratigraphic terminology. The sequence stratigraphic events and the OAEs, whose relative timings are shown in Figure 1.1, interacted to produce the facies of the Pearsall shale-gas system.

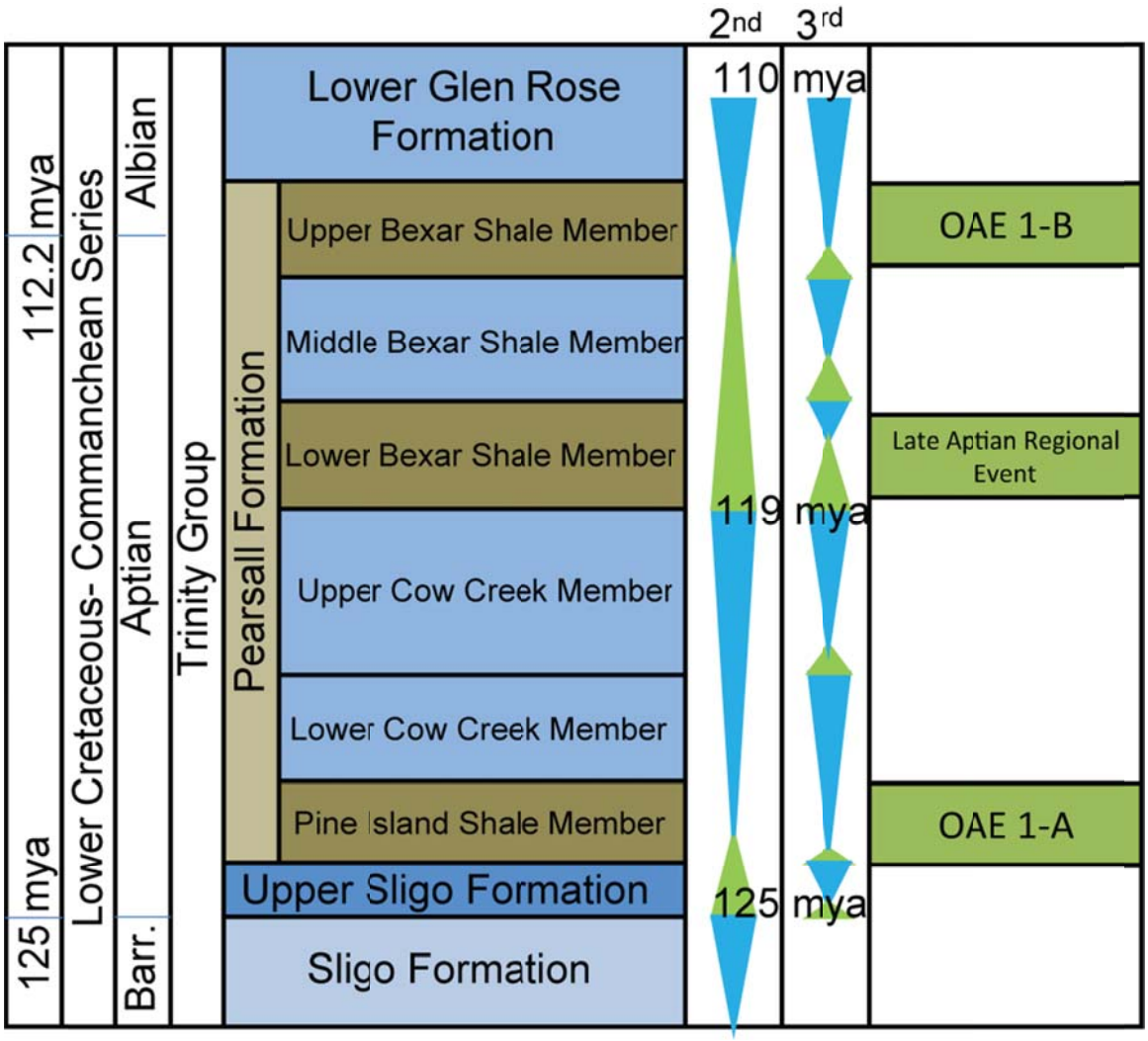

Figure 1.1: Stratigraphic chart of the Pearsall Formation. Second- and third-order sequence stratigraphic architecture and oceanic anoxic events are shown. 2nd order interpretation is based on Phelps (2011).

OBJECTIVES

The primary purpose of this study is to extend our understanding of the Pearsall shale-gas system by characterizing downdip Pearsall terrigenous mudrocks. This study further seeks to understand the drivers of and controls on the extent of this shale-gas system by describing:

1) Lithofacies in terms of lithology, mineralogy, sedimentology, and sequence stratigraphic position.

2) The oxygenation state of the various depositional environments and associated lithofacies at the time of formation.

3) Depositional systems affecting the development and extent of the shale-gas system given uncertainty and limited data.

4) Controls on total organic carbon (TOC), vitrinite reflectance (R_o), porosity, permeability, and other critical reservoir parameters in the South Texas area during Pearsall time.

STUDY AREA

The study area extends across South Texas from the Mexican border to the San Marcos Arch (Figure 1.2; Figure 1.3). To the north, the study area is bounded by the Balcones Fault Zone, which developed after the deposition of Pearsall Formation and roughly coincides with the deeper buried Paleozoic Ouachita Thrust Front (Ewing, 2003). To the south it is bounded by the paleo-Sligo Shelf Margin. The study area encompasses the bulk of the Maverick Basin, including the Pearsall Arch, and other paleogeographic features shown in Figure 1.3.

For this study the ramp is broken up into three areas, the inner ramp, the middle ramp and the outer ramp. The inner ramp is the foreshore area, within fair-weather wave base and the tidal range. The inner ramp includes the beach and supratidal environments The middle ramp is seaward of the inner ramp and largely within fair-weather wave base; it includes the offshore shoals and lagoonal environments below the foreshore. The outer ramp is below fair weather wavebase and mostly below storm weather wave base; it

includes all of the environments between the offshore shoals and the edge of the distally steepened ramp.

The study area spans the inner and the outer ramp sections. The middle ramp is where the carbonate shoal-water complexes developed, and the outer ramp is the lower energy area distal and seaward to the middle ramp. The carbonates actively aggraded on the middle ramp but not on the outer ramp. The extent of the middle ramp can thus be seen in Figure 1.3 as it matches the area where the shoal-water carbonates developed. Paleotopography controlled the location of the middle and the outer ramp. This study focuses on the outer ramp but draws critical information from the middle ramp area.

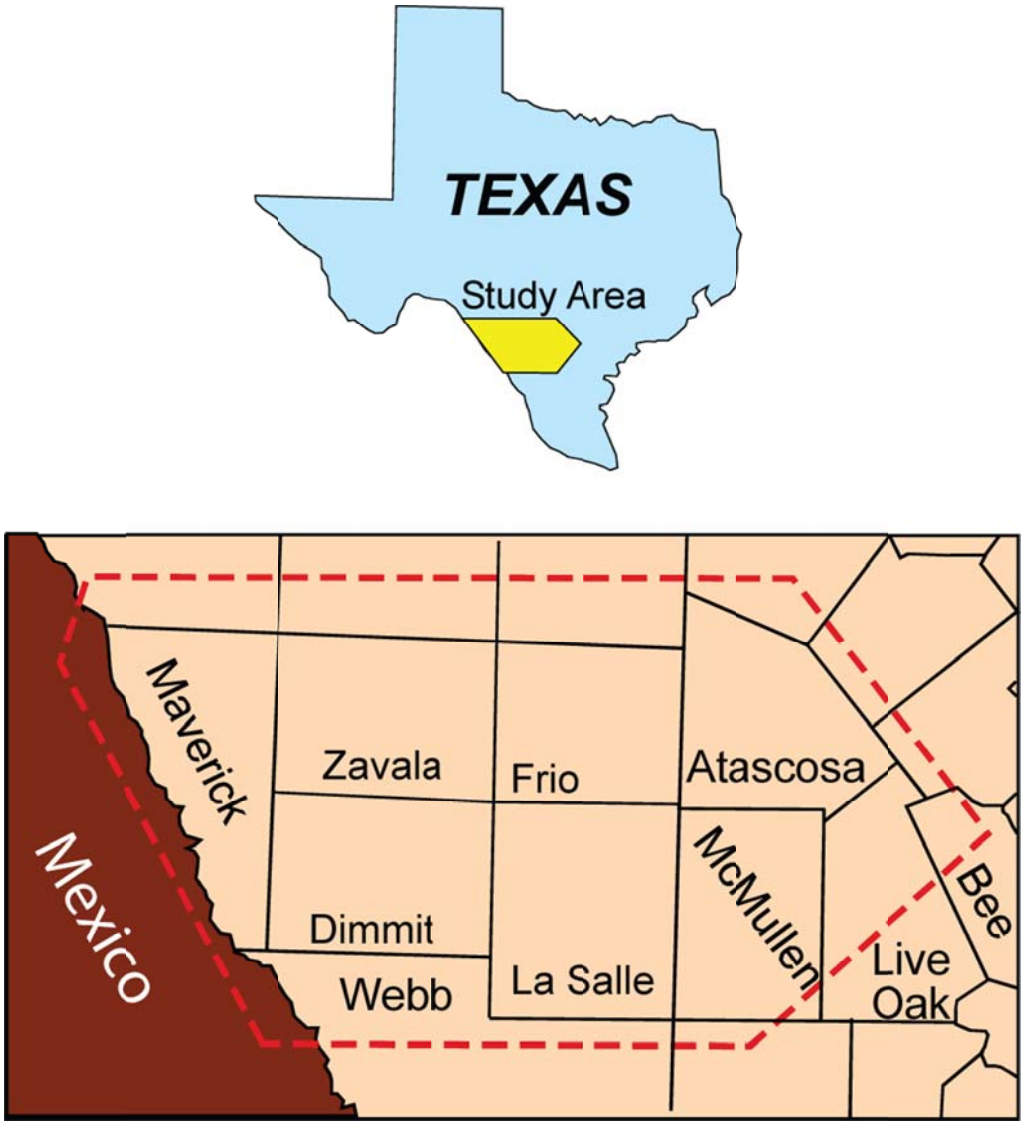

Figure 1.2: Map of study area.

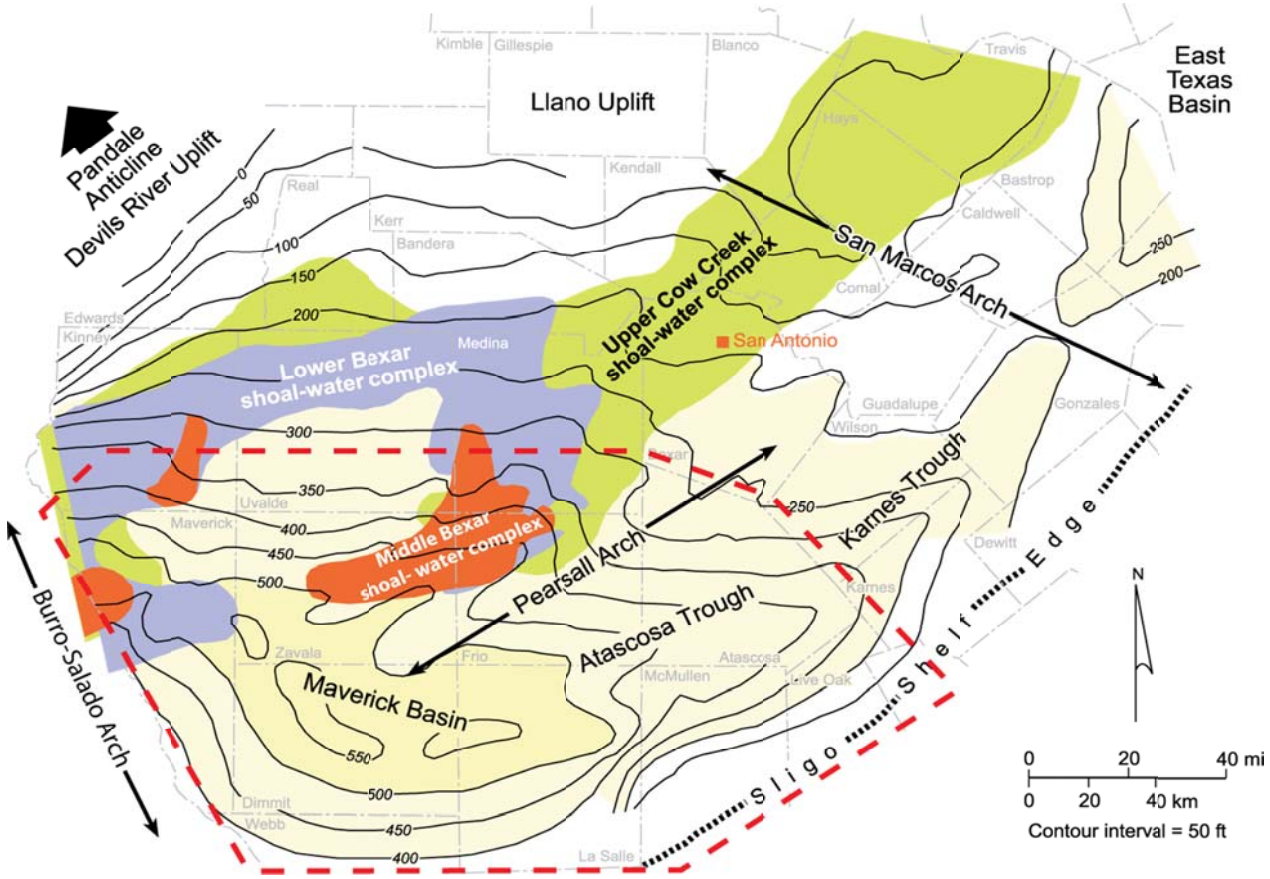

Figure 1.3: Paleogeography during Pearsall time. The study area is encircled by the red dashed line. The shoal-water complexes define the middle ramp and were surrounded by calcareous terrigenous mudstones and argillaceous wackestones (not pictured). These muddy facies largely comprised the outer ramp. Figure modified from Loucks (2002).

METHODS, DATA, AND SAMPLING TECHNIQUES

General Statement

Data for this study include wireline logs and conventional core. The main methods of analysis were by binocular microscope observations of core and thin sections, as well as other laboratory and SEM analyses. Various stratigraphic tools were applied, and available seismic information from the literature was utilized.

Stratigraphic Data

This study is based on approximately 185 wireline logs and 44 cores (Figure 1.4). The wireline-log suite was very similar to that used by Loucks (1976) as not many new wells have been drilled through the Pearsall Formation in recent times (Ewing, 2010). Thus, the majority of the wireline logs are SP-Resistivity logs; most wells lack gamma-ray and porosity wireline logs.

Cross-sections were created through the study area using the data set and maps from Loucks (1976). Cross-sections connect the cores and determine timelines and potential sequence stratigraphic surfaces. The characters of the wireline logs are affected by the amount of clay in the strata. In the Pearsall, the contrast of clay in the lime grainstones and packstones versus the argillaceous wackestones and terrigenous mudrocks produced characteristic responses of the different wireline-log curves, especially the SP and resistivity curves. This aided in correlating the wireline logs because of the ease of correlating alternating layers of terrigenous- and calcareous-dominated strata. Comparison of wireline logs and core descriptions reveals that facies in the middle ramp section can be delineated using core-calibrated log signatures (Loucks, 1976); however, this technique breaks down somewhat in the outer ramp as the

distinctive character of the logs is altered by the dominance of fine-grained terrigenous material in the mudrocks.

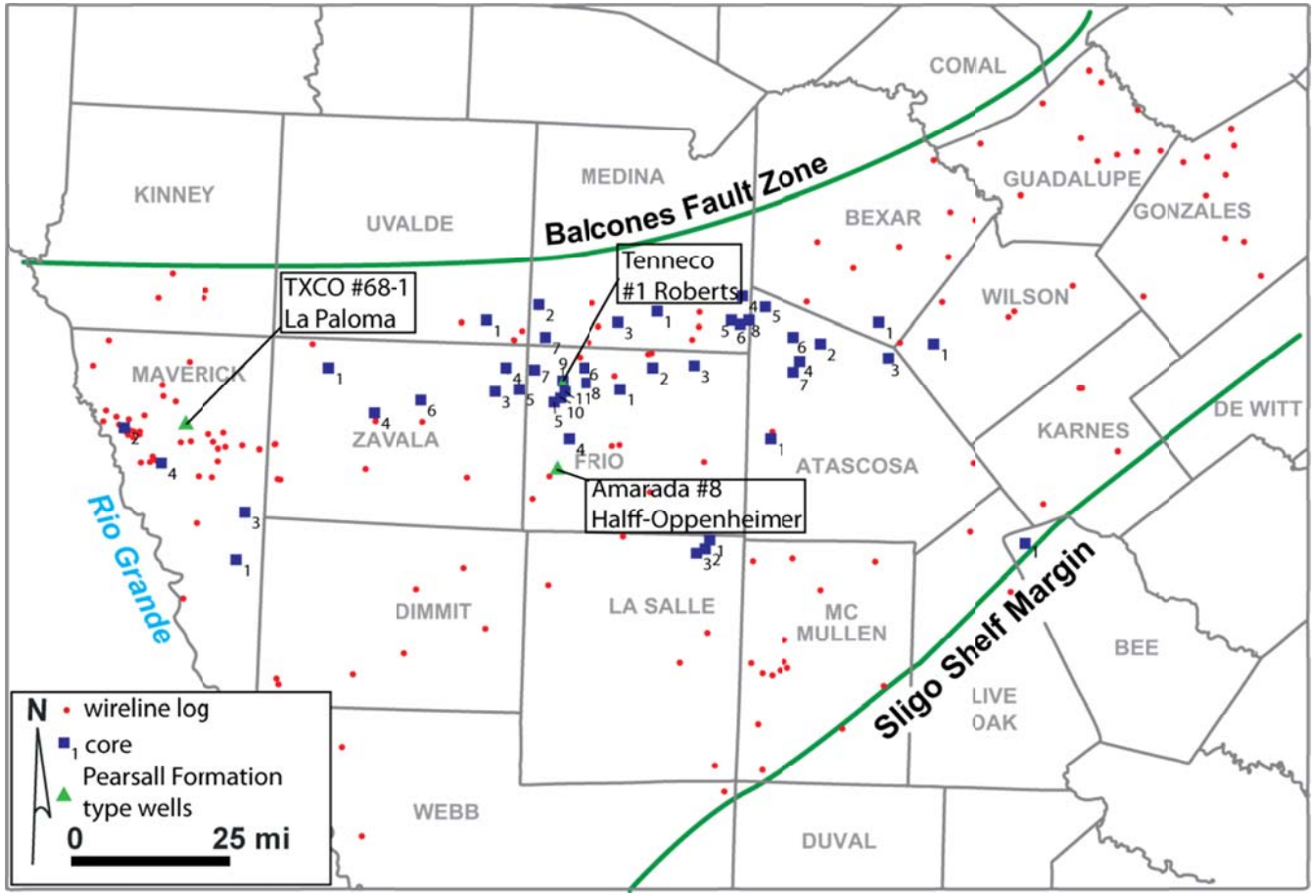

Figure 1.4: Map of wireline-logs and cores used in study. 3 type wells (2 informal) are marked with green triangles: Tenneco #1 Roberts in northern Frio County (with core), Amerada #8 Halff-Oppenheimer in southern Frio County, and TXCO #68-1 La Paloma in Maverick County. Numbers refer to cores listed in Table 1.1.

Core Description

Most of the 44 cores (Figure 1.4 and Table 1.1) are located in the middle ramp, and only 6 of those are positioned in the outer ramp. Descriptions of new cores from the downdip outer ramp are integrated with the previous core descriptions by Loucks (1976). In addition, several of the cores described by Loucks (1976) were redescribed.

The majority of the cores listed in Table 1.1 are housed in the permanent collection of the Core Research Center of the Bureau of Economic Geology in Austin Texas, but the TXCO #34-1 Commanche Ranch core was provided by EnCana Oil and Gas (USA), Inc.

Cores were described for information regarding: lithofacies, sedimentary structures, bulk mineralogy, and diagenetic features. The carbonate texture classification of Dunham (1962) is used to categorize the carbonated dominated facies, and the fine-grained terrigenous rock classification of Folk (1980) categorized the terrigenous mudrocks. Thin sections were selected to help collect detailed data on facies, mineralogy, diagenesis, and pore networks. Cores from the outer ramp were not etched with HCl as the associated middle ramp carbonates were, because it was found that etching is detrimental to observing the siliciclastic dominated lithologies. A binocular microscope and hand lens were used during core description.

Table 1.1: Pearsall cores and locations. Map numbers refer to cores plotted in Figure 1.4.

County	Map number	API number	Latitude	Longitude	Well name
Atascosa	1	42013023610000	28.865070	-98.742760	Humble 46 Pruitt
Atascosa	2	42013030480000	29.118630	-98.603130	Tenneco 1 Rogers
Atascosa	3	42013300060000	29.088390	-98.417170	Tenneco-Pennzoil 1 Suggs
Atascosa	4	42013300090000	29.069440	-98.667330	Tenneco-Pennzoil 1 Finch
Atascosa	5	42013030380000	29.204250	-98.766390	Tenneco 1 P. R. Smith
Atascosa	6	42013031000000	29.135960	-98.684160	Tenneco-Pennzoil 1 J.J Smith
Atascosa	7	42013310040000	29.051603	-98.673224	Tenneco 1 Climer
Bee	1	42025301480000	28.617450	-97.979050	Shell Oil 1-R Roessler
Bexar	1	42029026910000	29.215510	-98.454110	Tenneco 1 Herrera
Frio	1	42163016500000	28.991410	-99.156720	Tenneco 1 Stoker
Frio	2	42163016600000	29.043600	-99.069690	Tenneco 1 Sirianni
Frio	3	42163016660000	29.058580	-98.951300	Tenneco-Pennzoil 1 H. E. Edgar
Frio	4	42163016700000	28.859300	-99.288670	Tenneco-Pennzoil 1 H. A. Halff
Frio	5	42163200380000	28.957270	-99.334800	Tenneco-Pennzoil 1 Mack
Frio	6	42163300020000	29.040740	-99.262240	Tenneco-Pennzoil 1 Goad
Frio	7	42163300060000	29.033950	-99.395900	Tenneco-Pennzoil 1 Machen
Frio	8	42163300070000	29.006790	-99.250450	Tenneco-Pennzoil 2 Goad
Frio	9	42163300120000	28.999690	-99.316650	Tenneco-Pennzoil 1 Roberts
Frio	10	42163016620000	28.965662	-99.315880	W. A. Moncrief 1 Dan J. Rheiner
Frio	11	42163016640000	28.984362	-99.307850	W. A. Moncrief 2 Dan J. Rheiner
Frio	12	42163016690000	29.024893	-99.170037	Tenneco-Pennzoil 2 W. M. Wilbeck

Table 1.1 continued.

La Salle	1	42283006730000	28.360000	-98.900540	Skelly Oil Company 1-A La Salle
La Salle	2	42283000370000	28.610150	-98.911230	Auld-Shipman 1 Wilson
La Salle	3	42283000360000	28.604970	-98.916990	Tidewater Oil Company 2 Mabel Wilson
Maverick	1	42323011260000	28.539870	-100.182350	Union Producing Company 29-1 E. Halsell
Maverick	2	42323312580000	28.862770	-100.569344	Dilley Production Company 1 Ritchie
Maverick	3	42323329990000	28.591740	-100.323294	TXCO 34-1 Commanche Ranch
Maverick	4	42323305720000	28.769132	-100.429698	Cities Services 2A Kincaid
Medina	1	42325016540000	29.169220	-99.015340	Ralph A. Johnson 1A Howard
Medina	2	42325017210000	29.214100	-99.374000	Tenneco 1 W. J. Ney Jr. Trustee
Medina	3	42325017300000	29.150380	-99.164010	Tenneco 1 Roy Wilson
Medina	4	42325017320000	29.165310	-98.825960	Tenneco 1 Powell
Medina	5	42325017440000	29.174740	-98.861990	Hughes and Hughes 1 Plachy
Medina	6	42325017460000	29.166920	-98.810060	W. A. Moncrief 1 Joe. F. Collins
Medina	7	42325300030000	29.106070	-99.328360	Tenneco-Pennzoil 1 E. K. Hardie
Medina	8	42325300080000	29.224220	-98.828650	Tenneco-Pennzoil 1 John W. Carroll
Uvalde	1	42463300010000	29.143890	-99.532230	Tenneco Pennzoil 1 Kincaid
Wilson	1	42493019410000	29.121700	-98.298430	Tenneco 1 McKenzie
Zavala	1	42507002180000	28.945445	-99.704509	Tenneco 2 Kiefer
Zavala	2	42507004060000	28.900750	-99.826740	Continental Oil Company 1 Ike T. Pryor Jr.
Zavala	3	42507007360000	28.967810	-99.528060	Tenneco 1 Nixon

Table 1.1 continued.

Zavala	4	42507007680000	29.026680	-99.468760	Rowe 1 Kincaid
Zavala	5	42507007700000	28.979950	-99.433170	Zavala Property 1 Murphy
Zavala	6	42507300040000	29.015070	-99.961240	Tenneco-Pennzoil 1 K. B. & M.

Seismic Data

Several previously published seismic lines and published line drawings based on unpublished seismic lines were utilized (Fritz et al., 2000; Foster, 2003; Scott, 2003; Phelps, 2011) as no other seismic data were available for this study. In these seismic lines the Pearsall Formation appears as between one and six wavelets. These reflections are typically high-amplitude because of the impedance contrast between the siliciclastics of the Pearsall Formation and the surrounding and interbedded carbonates of the underlying Sligo Formation and overlying Glen Rose Formation. The Pearsall Formation reflectors do not commonly appear to be offset by faults, but seismic resolution is low and structural details are difficult to determine.

Thin-Section Analysis

One-hundred and forty four samples were collected for thin section analysis. These samples came principally from the outer ramp. The thin sections were prepared by Spectrum Petrographic Inc. with a low-viscosity surface impregnation with blue epoxy. Sections were ground to a thickness of 25 μm and polished to maximize their utility in both optical and SEM-based microscopy. Observations were made using a conventional transmitted polarized light microscope equipped with a UV epifluorescence, and bright-field polarized reflected light. Additional observations were made using a Technosyn cold cathode-luminescence microscope and a Philips 430 NovaNano field-emission SEM.

All instrumentation is housed at the Bureau of Economic Geology, in the Jackson School of Geosciences, The University of Texas at Austin.

Pore-Network Analysis

To analyze pore networks, ten samples from seven wells were prepared using an Ar-ion cross-section milling technique following a method established for the Barnett Shale (Loucks et al., 2009). The primary advantage of this method is that it eliminates differential hardness artifacts related to mechanical polishing. This method of sample preparation also minimizes artifacts related to heating and other beam damage (Rob Reed, The University of Texas at Austin, personal communication). Crushed-rock permeability and porosity data were also available for one core (well name is proprietary).

Total Organic Carbon and Rock-Eval Pyrolysis® Analysis

Total organic carbonate (TOC) analysis was done by GeoMark Geochemistry and by Dr. H. Rowe at The University of Texas at Arlington. Where the same intervals were analyzed by both laboratories, the results proved to be relatively consistent.

GeoMark used Rock Eval Pyrolysis® to analyze the samples for TOC. These samples were selected from strata in the lower Bexar Shale Member and from regularly spaced intervals in the Pine Island Shale Member. Bulk-rock samples weighing approximately 10 grams were sent to GeoMark for total organic carbon, kerogen typing, and rock maturity information calculated through rock pyrolysis. For TOC analysis the samples were crushed and acidized to remove inorganic carbon. The samples were then combusted in an LECO apparatus and the resultant gases were measured. The TOC, vitrinite reflectance (R_o), and kerogen type can be calculated from the measurements of

these gases with the knowledge of the temperatures at which the gas was produced (Espitalie, 1977; Peters, 1986). During the process GeoMark repeatedly tested the standards to ensure the continued accuracy of results (Jarvie and Tobey, 1999).

TOC profiles were produced by Krystin Robinson and Rolando Castillo at The University of Texas at Arlington. Samples were collected according to methods outlined in Hughes (2011). TOC was measured using a pyrolysis technique that does not test for R_o but does preserve the isotopic composition of the organic carbon isotopes, which can then be analyzed (Harry Rowe, University of Texas at Arlington, personal communication). Samples were pulverized, gently decarbonated, and analyzed using a Costech 4010 Elemental Analyzer interfaced with a Thermo Finnigan Conflo IV device and a Thermo Finnigan Delta V isotopic ratio mass spectrometer. For TOC the average standard deviation is 1.07% (Hughes, 2011).

Isotopic Analysis of Organic and Inorganic Carbon

Stable isotopes of both organic and inorganic carbon were analyzed. Oxygen isotopes were also determined for quality control purposes and more specifically, to evaluate diagenesis. Data were collected and compared to secular reference curves of the South Texas Cretaceous section constructed by Phelps (2011). The aim was to collect samples which reflected the original $\delta^{13}C$ composition of seawater at the time of deposition (Phelps, 2011). Terrigenous mudstones were targeted because they are least likely to incorporate bias from a single dominant allochem and late diagenetic cements (Gao and Land, 1991). Where no terrigenous mudstone was available for sampling, density of sampling was reduced as grain-rich carbonates are more likely to have undergone diagenesis, thus altering the original seawater $\delta^{13}C$ signature. Where evidence of diagenesis was noted in the core, such as discoloration and obvious grain replacement,

or where $\delta^{18}O$ values indicated substantial diagenesis, samples were not taken or were discarded, as they probably do not reflect the composition of Aptian seawater.

Isotopic curves for organic and inorganic carbon were provided by researchers at The University of Texas at Arlington. Samples were analyzed in conjunction with the TOC samples using the equipment and methods discussed in the previous section. These samples were also collected according to the methods outlined by Hughes (2011). Carbon isotope data are reported relative to the V-PDB standard, and the average standard deviation of $\delta^{13}C$ is 0.10 % (Hughes, 2011).

Samples were also sent to the Stable Isotope Laboratory at the University of Miami, where they were analyzed for $\delta^{13}C$ and $\delta^{18}O$ (Peter Swart, lab director). These samples were collected according to the methods outlined by Phelps (2011). Carbonate was separated using an acid bath of phosphoric acid at 90ºC, and isotopes were analyzed using a Finnigan-MAT 251 mass spectrometer. Results were reported relative to the V-PDB standard used by Harry Rowe at The University of Texas at Arlington. The Stable Isotope Laboratory at the University of Miami has a long-term replicate analysis of standards of 0.08%.

X-Ray Diffraction (XRD) and X-Ray Fluorescence (XRF) Analyses

Foot-by-foot XRF data were collected by workers from The University of Texas at Arlington. These data were collected using a Bruker Tracer III-V handheld energy-dispersive X-ray fluorescence instrument (ED-XRF). The methods for this process are detailed in Hughes (2011). Both major and minor elemental data were collected. These data are used to guide visual estimates of mineralogy in core descriptions.

XRD data were provided by Necip Guven of Clay Consultants. These data are calibrated with XRF data, but they are still semi-quantitative. The methods for this process are detailed in Harbor (2011).

Biostratigraphic Analysis

Ammonites and nannofossils were analyzed for biostratigraphic dating by Peter Rawson at the University of Hull at Scarborough and Jason Jeremiah (Shell Oil Company), respectively. Ammonites were found only in the downdip wells. Ammonites were typically crushed through compaction and were therefore difficult to identify. Thirteen ammonites were identified to some degree. The preservation of the nannofossils was also poor in many samples; however, samples were taken from 7 wells, and 95 species were identified.

PREVIOUS WORK

The Pearsall Formation was defined by Imlay (1945) in South Texas on the basis of the wireline-log signatures in the Amarada #8 Halff-Oppenheimer well in Frio County (Figure 1.4). The Pearsall Formation (Figure 1.1) is above the Sligo Formation and below the Glen Rose Formation. It has three units; the lowest is the Pine Island Shale Member, which is clastic-dominated. This is topped by the Cow Creek Member, which is a limestone and commonly broken into two separate subunits, the lower and upper Cow Creek Members (Loucks, 1976). The Bexar Shale Member is a clastic-dominated member which is commonly broken into three separate submembers, the upper, middle, and lower Bexar Shale Members (Loucks, 1976). Forgotson (1957) separated the Bexar Shale Member as a member in South Texas as distinct from the Hensel sand, which is partially time equivalent and found in the updip, shallow subsurface and outcrop.

Numerous workers from the Shell Research Laboratory and other groups contributed to an understanding of the Pearsall section, primarily in outcrop studies (Lozo and Stricklin, 1956; Stricklin et al., 1971; Amsbury, 1974). Loucks (1976,1977, 2002) focused mainly on the subsurface carbonate units. The Bexar Shale Member and the Cow Creek Member subdivisions primarily highlight the shoal-water carbonate complexes (Loucks, 1976, 1977), but also the tops of the members correspond to important sequence stratigraphic surfaces (the sequence stratigraphy is discussed in a later section).

Regional Perspective

The Pearsall Formation extends around the Gulf of Mexico, where it is known by a variety of names (Figure 1.5). To the southwest of the study area, in northeastern Mexico the Pearsall Formation is known as the La Pena Formation (Loucks, 1976; Tinker, 1985; Goldhammer and Johnson, 2001). It has similar characteristics to the Pearsall Formation in South Texas, but it was deposited on a divergent margin rather than a passive margin (Foster, 2003). Nonetheless, it is still described as a similar succession of carbonates and siliciclastics (Imlay, 1945; Bralower et al., 1999; Goldhammer and Johnson, 2001; Foster, 2003). To the northeast of the study area, the Pearsall Formation maintains similar succession lithologies, but the Cow Creek Member is known as the James Lime Member and the Pine Island Shale Member is often referred to as the Hammett Shale Member. The rock succession continues through the various salt basins of the eastern Gulf Coast extending to Mississippi and offshore Alabama (Bushaw, 1968; Achauer, 1974; Tinker, 1985; Loucks et al., 1996; Mancini and Scott, 2006).

The Pearsall succession can also be correlated globally with the aid of sequence stratigraphic and geochemical correlation techniques. It contains two major OAEs and one minor anoxic event. These can be tracked using secular carbon isotopes curves

combined with conventional stratigraphic methods (Bralower et al., 1999; Follmi et al., 2006; Phelps, 2011). This allows for the correlation of the Pearsall interval to major oil and gas reservoirs and source rocks in Arabia and elsewhere in the world (Phelps, 2011).

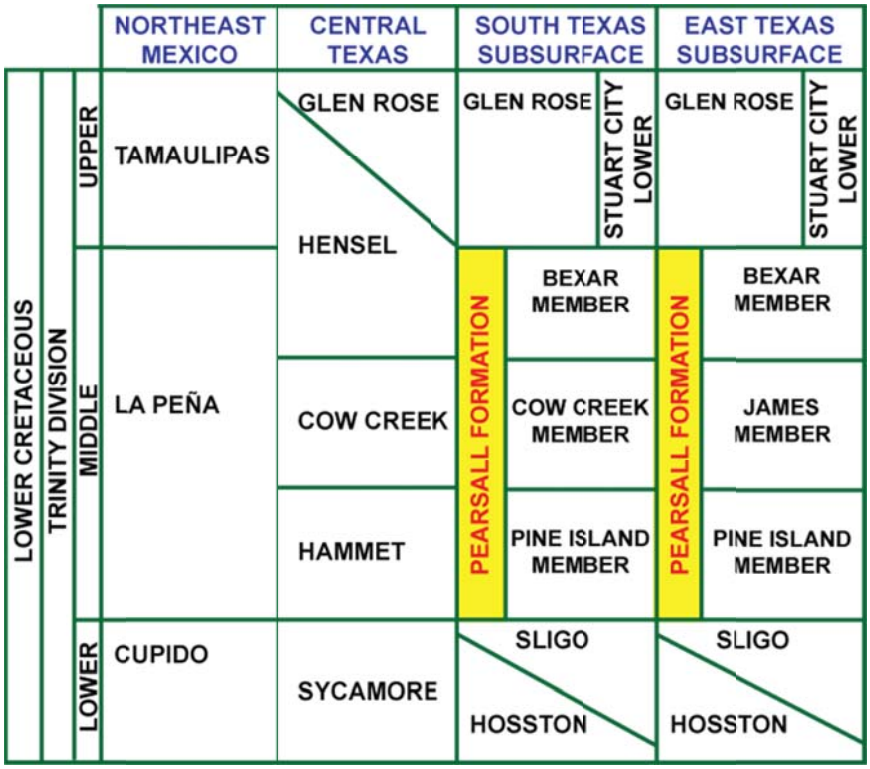

Figure 1.5: Regional stratigraphic chart showing the various equivalent units and their names around the Gulf of Mexico. Figure modified from Loucks (1976).

Informal Type Stratigraphic Sections

Two informal type sections (wireline logs) are used in the analysis of the Pearsall Formation (Figure 1.4; Figure 1.6) because the proximal succession of the middle ramp and distal mudrock and carbonate succession of the outer ramp comprise two different and contrasting sets of lithofacies. Loucks (1976) used the Tenneco #1 Roberts well as a type-log for the more proximal mixed carbonate/siliciclastic succession because it

highlights the carbonate shoal-water complexes found in the Pearsall interval. The Roberts well is located in Frio County and in the middle ramp depositional system (Figure 1.4). The Roberts well contains a succession of high-energy carbonate shoals with argillaceous wackestones and calcareous terrigenous mudstones above and below. The Pearsall carbonate complex succession lies above a transgressive ooid-shoal complex developed in the older Sligo Formation (Bebout and Schatzinger, 1978; Foster, 2003). Within the Pearsall interval the Pine Island Shale Member contains a second-order maximum flood and a regionally correlative oyster biostrome. This biostrome is clearly displayed in the Roberts well (Figure 1.6) by a spike in the resistivity in the middle of the Pine Island Shale Member (Loucks, 1976). Above the Pine Island Shale Member, the Cow Creek Member was deposited and developed into a shoal-water carbonate complex (shown in yellow in Figure 1.6) with a second-order sequence boundary at its top (Loucks, 1976, Phelps, 2011). Following the deposition of the Cow Creek Member, the Bexar Shale Member was deposited. The Bexar Shale Member features two transgressive shoal-water carbonate complexes (shown in yellow in Figure 1.6) before reaching a maximum flood in the upper Bexar unit (Loucks, 1976; Phelps, 2011). These carbonate complexes can be seen by the SP-log response in the Roberts type well (Figure 1.6).

The TXCO #1-68 La Paloma well (Figures 1.4 and 1.6) is used as the informal type well for the deeper water setting of the outer ramp where conditions were not suitable for shoal-water carbonate complexes to form (Hull and Loucks, 2010). In the La Paloma well the Pine Island Shale Member is similar to the Pine Island Shale Member in the Roberts well but lacks the oyster chondrodont biostrome (Figure 1.6). In the Cow Creek and Bexar Shale members the intervals of high-energy carbonates seen in the Roberts well are argillaceous wackestones in the area of the La Paloma well. These

wackestone units appear on the wireline log as positive resistivity spikes (Figure 1.6). Additionally, the lower Bexar Shale and upper Bexar Shale Members are dominantly terrigenous, whereas the Cow Creek and middle Bexar Shale Members are significantly more calcareous in the outer ramp.

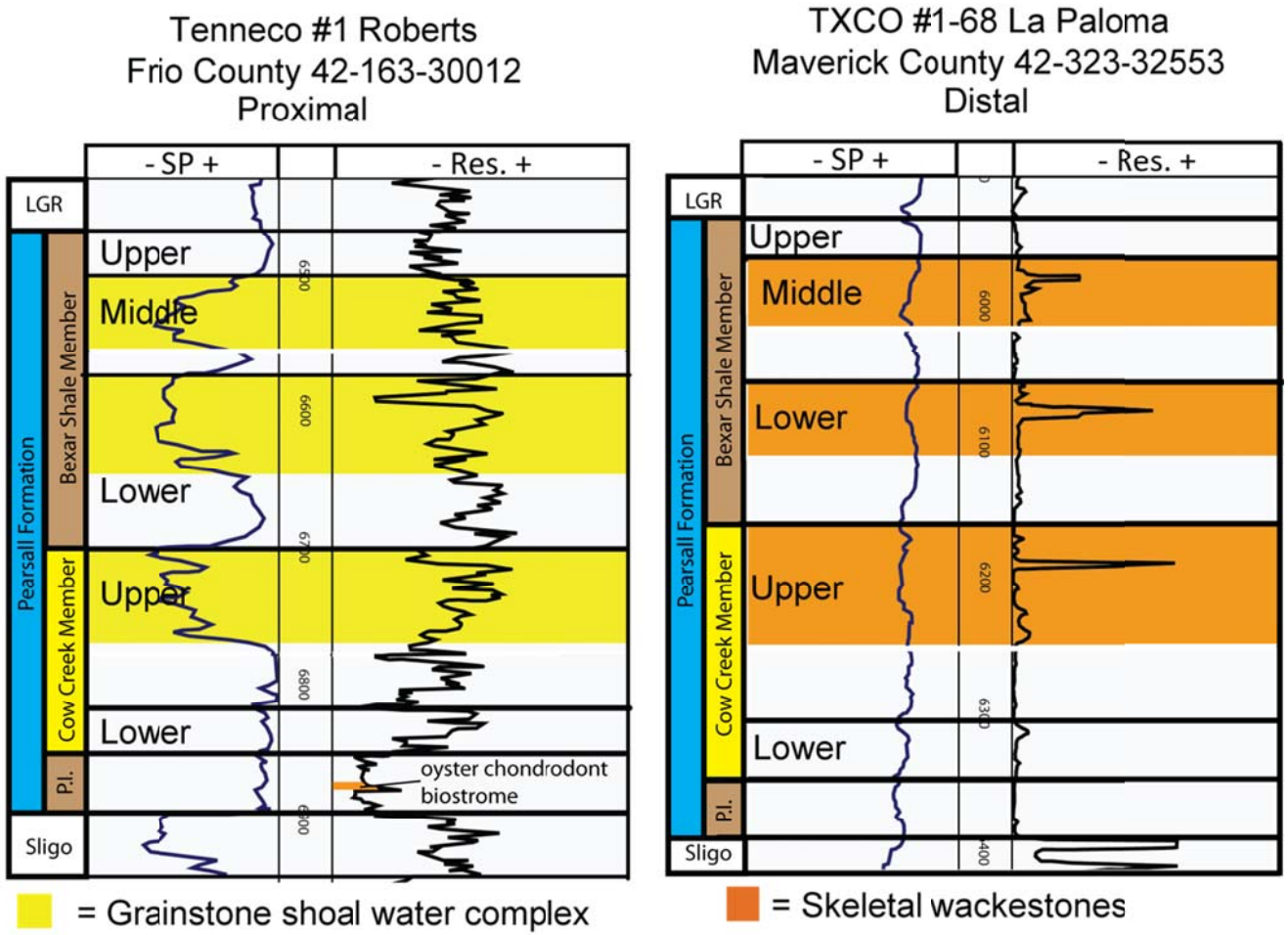

Figure 1.6: Informal type stratigraphic sections for the Pearsall inner and outer ramp (Loucks, 1976; Hull and Loucks, 2010). P.I. stands for Pine Island Shale Member.

Chapter 2: Regional Structure and Stratigraphy

GENERAL STATEMENT

Understanding the overall paleogeomorphology of the Pearsall Formation is critical in understanding the stratigraphic framework of the formation. This is because the paleotopography controlled the loci of carbonate versus terrigenous depositional regimes during several time intervals. The Pearsall Formation was deposited as the Maverick Basin subsided and compacted, producing changes in accommodation. This strongly impacted the lithofacies distributions. Sequence stratigraphic analysis of the middle ramp area was studied in detail to help delineate sequence packages that can be correlated to the outer ramp interval as the stratigraphic signals in the outer ramp were obscured by greater accommodation and environmental influences such as dysoxia, as suggested by Schlager (1991).

REGIONAL STRUCTURE AND PALEOGEOGRAPHY

General Statement

The depositional topography that existed for most of deposition of Pearsall deposition is interpreted to be that of a distally steepened ramp on a drowned shelf with a low-relief sill at the shelf margin, as seen in Figure 2.1C. This interpretation is supported by and based on seismic data from the literature (Fritz et. al, 2000; Foster, 2003; Scott, 2003). Prior to deposition of the Pearsall Formation, the Sligo Formation was a rimmed shelf system, and after the deposition of the Pearsall an active rimmed shelf slowly reemerged, forming the Stuart City Margin.

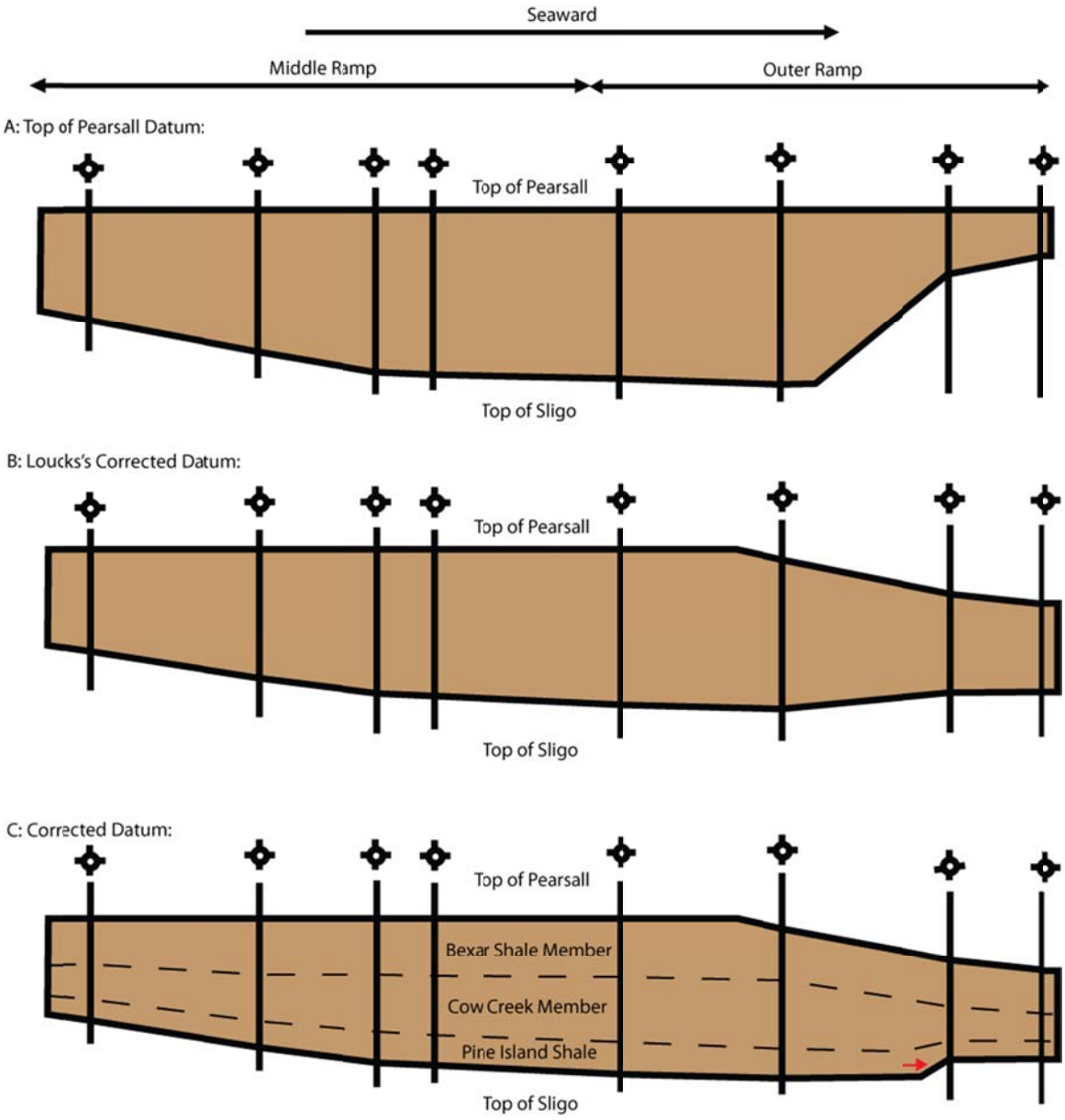

Figure 2.1: Depositional profile of the Pearsall Formation in the Maverick Basin. Section A shows the overall morphology of the section based on flattened cross-sections. Section B shows the correction to the profile done by Loucks (1976) , andsection C shows what seismic and other evidence indicates is the more likely depositional profile. Note the red arrow in section C, which illustrates the onlap of the Pine Island onto the previous margin. Figure modified from Loucks, 1976.

Structural Elements and Pre- and Post-Pearsall Paleotopography

Tectonic structural events/elements affecting Aptian deposition included

- the emplacement of stable cratonic terranes in the Coahuila Block and the Llano Uplift in Precambrian time (Ewing, 2003)
- The development of the Ouachita Orogen in Carboniferous time (Ewing, 2003)
- the opening of the Gulf of Mexico during the Jurassic
- the counterclockwise rotation of the Yucatan into its current position by the end of Cretaceous time (Pindell, 2001), and
- the connection of the paleo-Gulf of Mexico to Tethys and the wider ocean in Jurassic and early Cretaceous time (Scotese, 1997; Goldhammer and Johnson, 2001; Pindell, 2001; Ewing, 2003; Blakey, 2005).

These events produced high and low topographic areas, which affected Pearsall deposition and created areas of slower and faster subsidence. The regional paleogeography during Sligo deposition is shown in Figure 2.2.

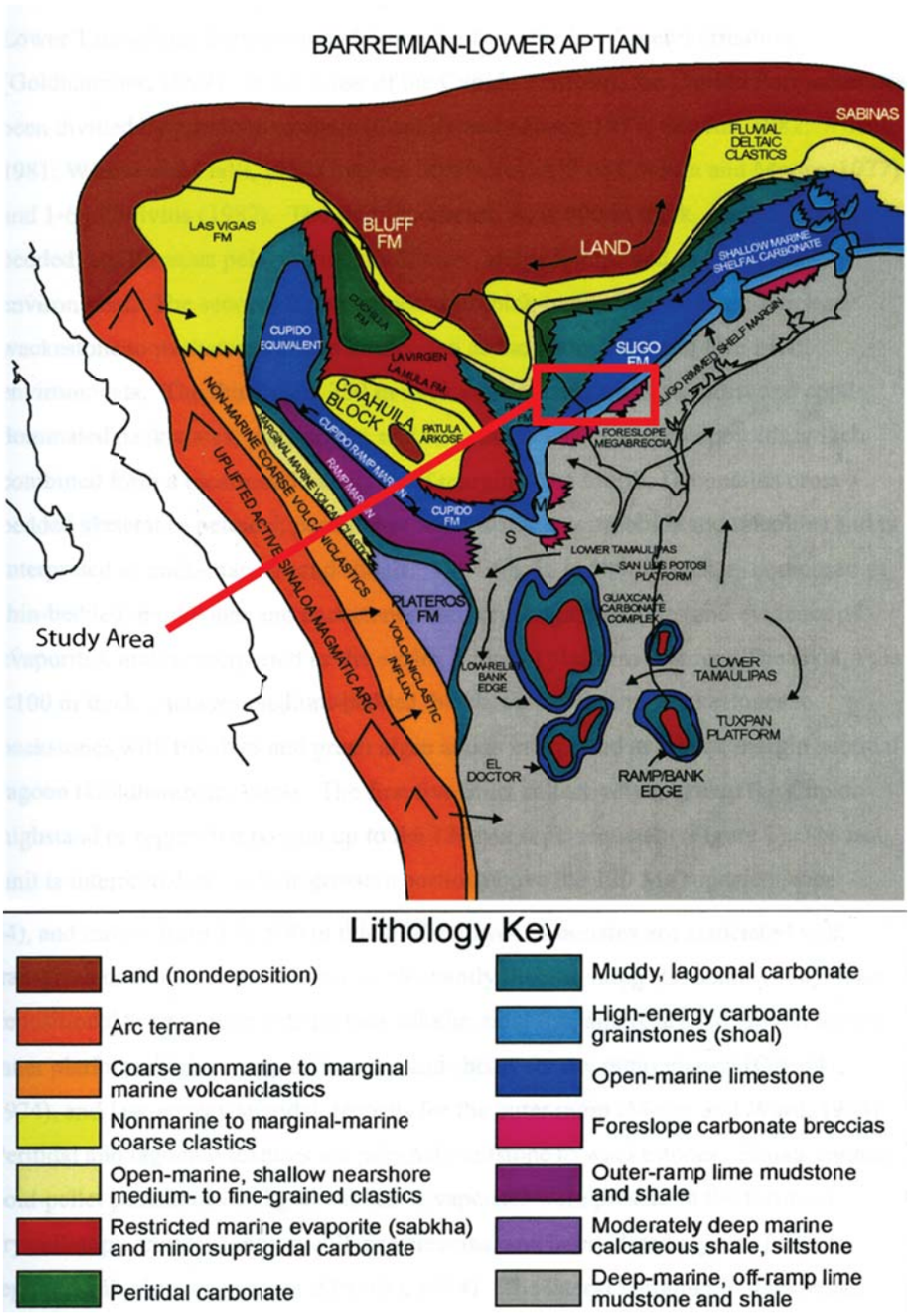

Figure 2.2: Regional paleogeography during Sligo time before deposition of the Pearsall Formation. The study area is highlighted by the red box. Figure modified from Goldhammer and Johnson, 2001 and Foster, 2003.

Some of the early paleogeographic features that formed prior to the deposition of the Pearsall Formation contributed to sedimentation during Pearsall time (Figure 2.3). The Llano and Coahuila highs sourced clastic sediment to the Maverick Basin; the Ouachita basement provided a stable terrain on which a coastline developed and carbonate shoals nucleated in South Texas (Loucks, 1976; Goldhammer and Johnson, 2001). Also, the Pearsall Arch was a depositional high with an active shoal-water carbonate factory (Loucks, 1976, 1977). The older Sligo Shelf Margin delineates the edge of the distally steepened ramp and separates the Pearsall shelf system geographically from the more basinal but concurrent Otates Formation (Tinker, 1985; Goldhammer and Johnson, 2001). No active shoaling areas were present at the shelf edge during Pearsall deposition. The older Sligo shoals on the Pearsall Arch and the Sligo Margin reef complex also resisted subsidence during Pearsall time as these areas were composed of mud-poor, well cemented lithofacies inherently more resistant to compaction. To the east the San Marcos Arch was underlain by stable continental crust and therefore remained a relatively higher area as it subsided at a slower rate than the rest of the Gulf of Mexico region (Loucks, 1976; Winkler and Buffler, 1988; Lopez, 1995; Waite, 2009).

Seaward of the inner-ramp shoal-water complexes other features contributed to increased levels of subsidence and the formation of the Maverick Basin. The underlying continental crust was either attenuated or transitional to new oceanic crust associated with the opening of the Gulf of Mexico (Winker and Buffler, 1988). This crust was weaker and thus more susceptible to subsidence (Figure 2.3). The opening of the Gulf of Mexico and the rotation of the Yucatan also caused formation of a half-graben in what is now Maverick County during Triassic time (Goldhammer and Johnson, 2001; Ewing, 2003; Scott, 2004). Although the graben filled prior to Pearsall deposition, the strata above it

were subjected to increased thermal subsidence until almost Cenozoic time (Winker and Buffler, 1988; Ewing, 2003). This thermally driven subsidence was increased by subsidence related to as much as 1,000 m of salt (Salvador, 1991) deposited in the Rio Grande Embayment, which later became the Maverick Basin. The salt was the underlying substrate for much of the outer ramp area. It is assumed that this salt began moving very early as it did in the eastern Gulf area (Hughes, 1968) soon after it was deposited, compounding the effect of thermal subsidence in the Maverick Basin (Foster, 2003; Ewing, 2010). The salt may have also contributed to the formation and increased subsidence associated with the Karnes and Atascosa Troughs (Figure 2.3) (Ewing, 2010).

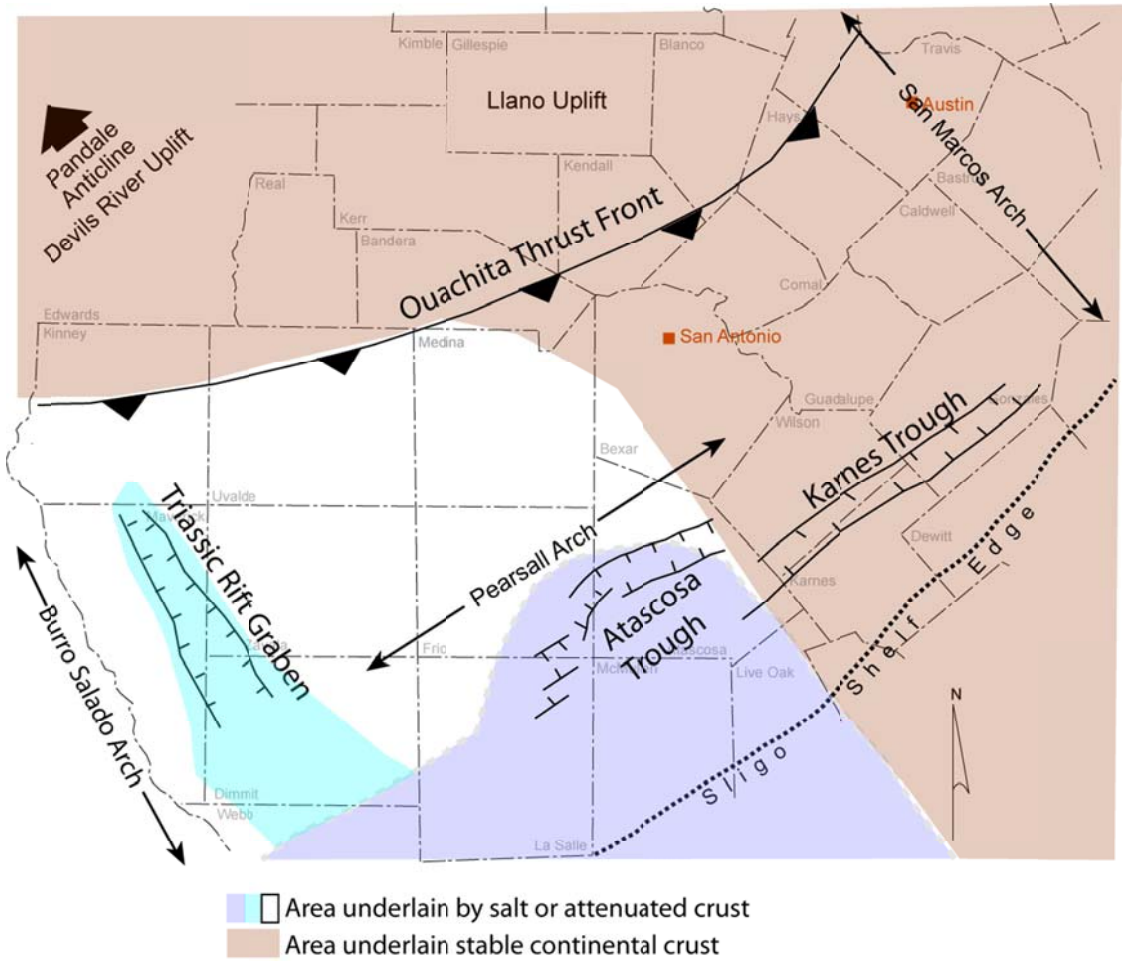

Figure 2.3: Paleostructure in the study area prior to deposition of the Pearsall Formation. Figure compiled from (Loucks, 1976; Winkler and Buffler, 1988; Lopez, 1995; Waite, 2009).

Following deposition of the Pearsall Formation, South Texas experienced structural change (Figure 2.4). The first change was the onset of Laramide compression at the end of Cretaceous time (Ewing, 2003). This compression inverted the Triassic graben and formed the Chittim Arch in the western area of the basin (Figure 2.4). The uplifted area extended into the middle of the study area and may have caused 1-2 km of erosion (Ewing, 2003). It is important to recognize that the Chittim Arch is a post-Pearsall high and that the area which underlies it was once a depositional low. This is clear when analyzing previously published seismic over the graben (Scott, 2004). Other key changes after the end of Pearsall deposition include the formation of the Balcones Fault Zone (Ewing, 2003). This feature parallels the Ouachita thrust front and marks the northern bound of the study area. To the south, Cenozoic Wilcox-age growth faults formed outboard of the Sligo Shelf Margin, causing the Pearsall section to be buried to even greater depths (Ewing, 2003).

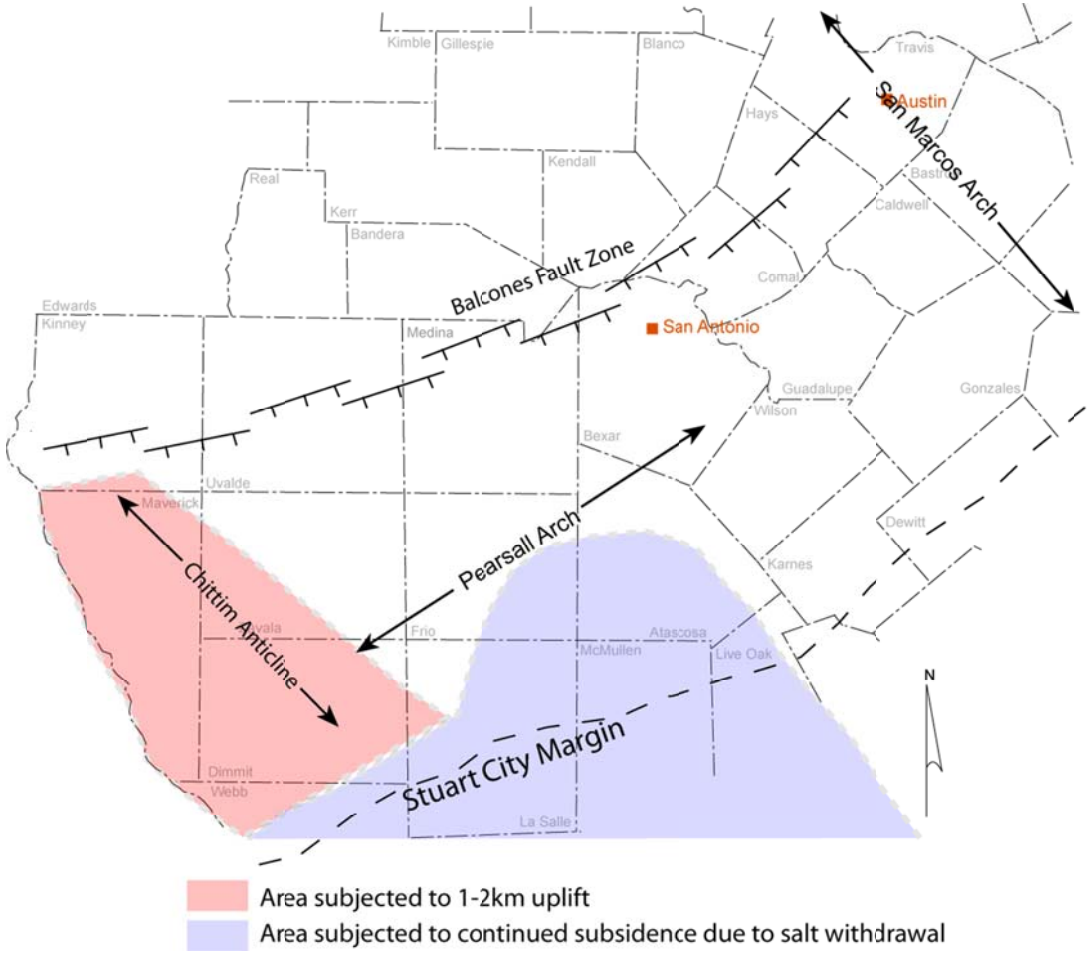

Figure 2.4: Paleostructure of the study area after the deposition of the Pearsall Formation. Figure compiled from Loucks, 1976, Ewing, 2003, and Waite, 2009.

Pearsall deposition marked a period of relatively consistent deposition around the Gulf of Mexico (Figure 2.5). Sea-level was at a relative high-stand during a major worldwide transgression (Goldhammer and Johnson, 2001), and the coastline in South Texas was located around the Llano Uplift area (Figure 2.6) (Lozo et al., 1962). The Coahuila Platform in Mexico was exposed, and the Burro-Salado Arch was submerged and covered with sediment, allowing sediment transport from the Coahuila Block into the study area (Goldhammer and Johnson, 2001). Localized shoal-water carbonate complexes and scattered pinnacle reefs developed in Mexico, South Texas, East Texas, and Mississippi (Achauer, 1974; Loucks, 1976; Loucks et al., 1996; Goldhammer and Johnson, 2001). Within the study area subsidence was an important factor in the Maverick Basin, for the reasons discussed in the pre-Pearsall structural elements section (Figure 2.3). The major center of the subsidence was the Maverick Basin. Subsidence was controlled by the salt withdrawal in the more distal parts of the basin and increased thermal subsidence where the basin was underlain by the Triassic rift. The present structure map reflects this subsidence and seaward dip, as seen in Figure 2.6. The Atascosa Trough and the Karnes Trough were also actively subsiding, as evidenced in the cross-sections and noted by Loucks (1976). Positive features included the Pearsall Arch and San Marcos Arch. The northern part of the study area is underlain by stable crust, and the bounding Burro-Salado Arch in Mexico (Figure 2.3). The older Sligo Shelf Margin appears not to have affected deposition but may have reduced the amount of accommodation generated at the shelf edge by limiting the subsidence rates in that part of the region. Several published seismic lines and line drawings show a slightly raised Sligo margin (Figure 2.8) (Fritz et al., 2000; Phelps, 2011). In some areas the Pine Island Shale reflectors on-lap against this raised margin, but other stratigraphically higher Pearsall

reflections drape over the top of the Sligo raised rim, indicating that relief was lost prior to deposition of much of the Pearsall .

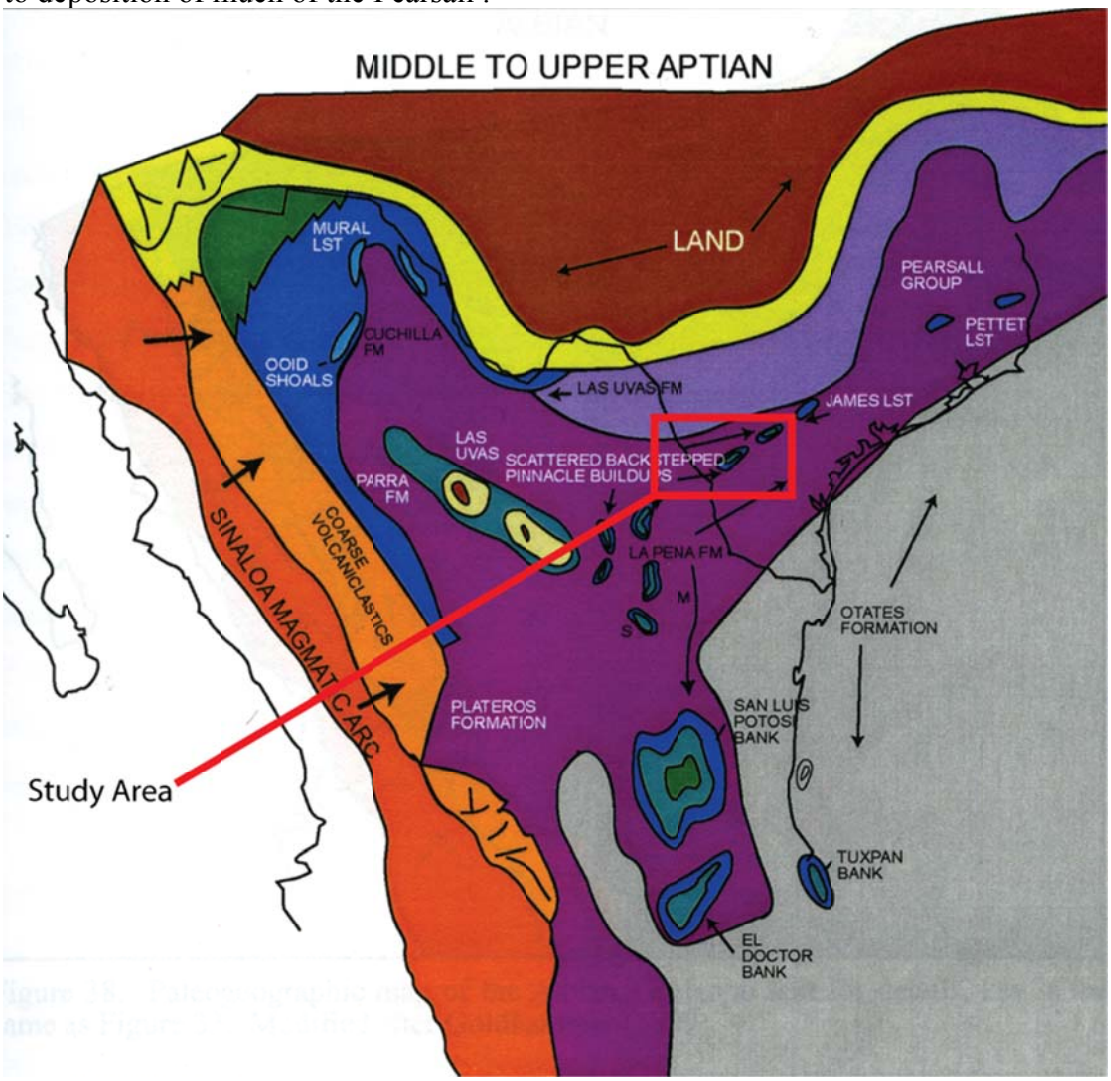

Figure 2.5: Regional paleogeography at the time of Pearsall deposition. Note that the Pearsall Formation (called the La Peña Formation in Mexico), extends all the way around the Gulf of Mexico. See Figure 2.2 for lithology key. Modified from Goldhammer and Johnson (2001) and Foster (2003).

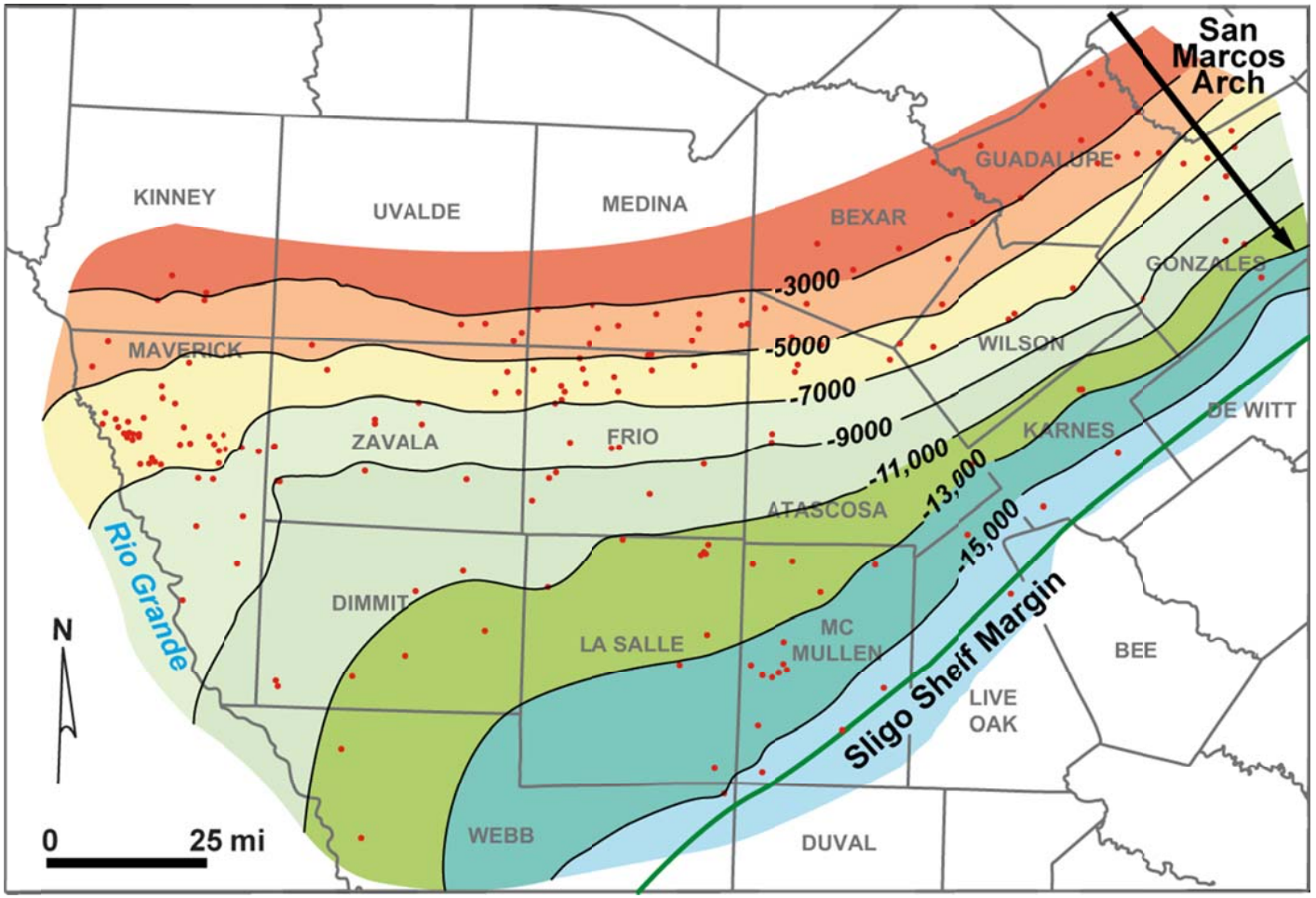

Figure 2.6: Structure map on top of the Sligo Formation.

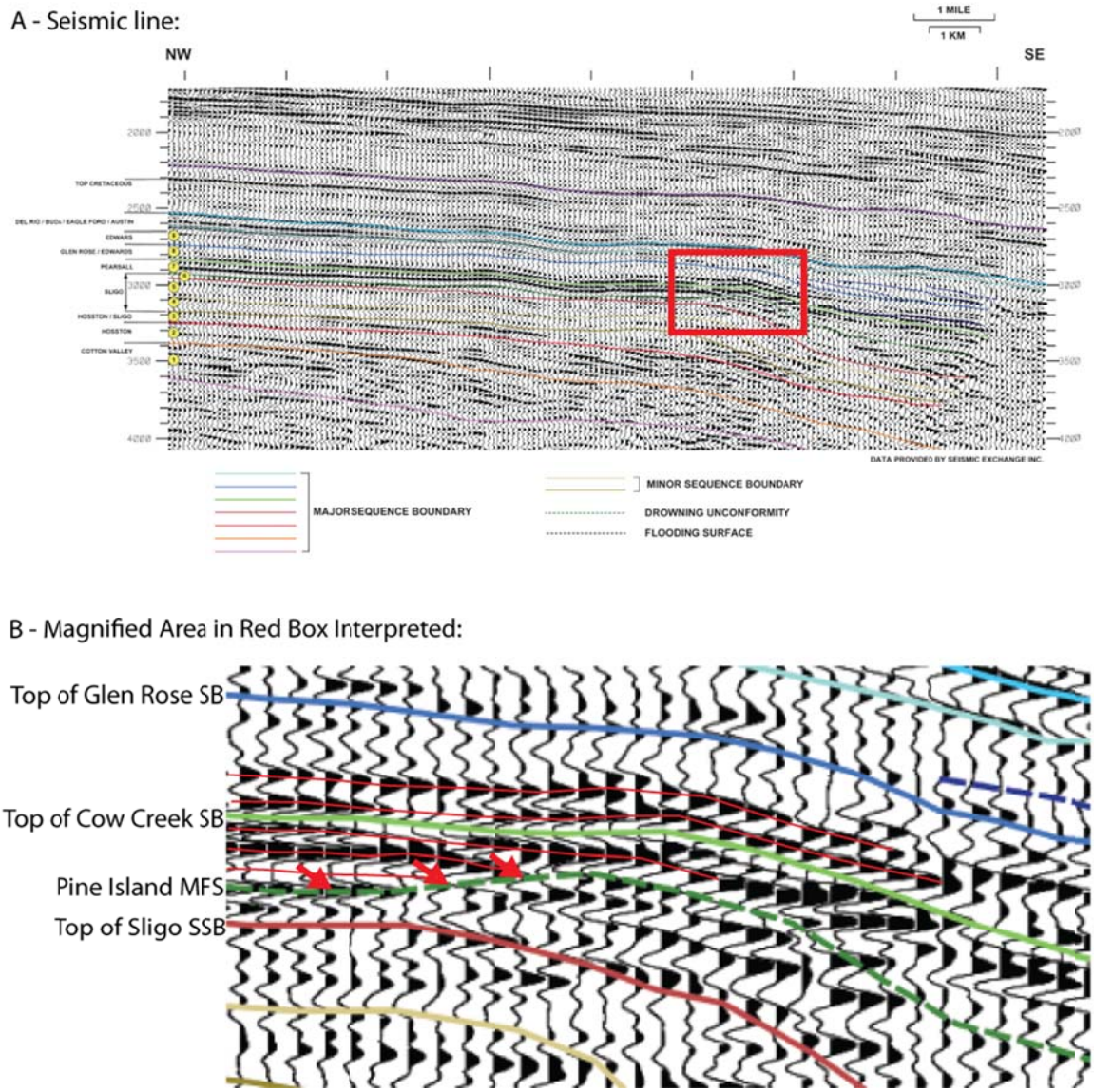

Figure 2.8: Seismic line showing ramp margin. A shows the whole line from Fritz et al.(2000). B shows the interpreted section in the red box featuring the ramp margin and showing the onlap of the Pine Island Shale Member, marked by the red arrows, onto the raised reef margin of the Sligo Shelf Edge. The seismic line is located in Lavaca County.

SEQUENCE STRATIGRAPHIC ARCHITECTURE

Lithostratigraphy versus Sequence Stratigraphy

The Pearsall lithostratigraphy and sequence stratigraphic interpretations do not differ significantly for a several reasons. First, the Pearsall Formation is a condensed section on the supersequence scale. Even, including the more rapidly deposited high-energy carbonates; average sedimentation rates for the whole section were slower than 20 μm a year (Li et al., 2008; Phelps, 2011; this study). The second reason is that the Pearsall stratigraphy is dominated by events that affected the whole ramp and altered the composition of sediments. This includes, but is not limited to, flooding events and OAEs. These events drive facies changes and affect whether siliciclastic or carbonate sediment was deposited. Therefore, the lithostratigraphy is connected to the sequence stratigraphy because of the relationship between the depositional processes and the depositional ramp profile. As such, a simple breakdown of facies dominated by carbonate-rich or siliciclastic-rich strata will generally identify timelines by default.

Lower Cretaceous Supersequences

The large-scale sequence stratigraphic approach used in this study is based on methods described by Phelps (2011), who analyzed the stratigraphic section on the San Marcos Arch. The interpretation by Phelps (2011) is reflected in the transgressive-regressive cycles shown in Figure 1.1. The study by Phelps (2011) focuses on a study area where subsidence and change in accommodation were minimal (Winkler and Buffler, 1988; Ewing, 2003; Phelps, 2011). As a result, high-frequency cycles and third-order sequences are more discernible in the Maverick Basin. Phelps (2011) recognized seven supersequences in the Lower Cretaceous interval. This includes two that contain a

portion of the Pearsall interval, which he terms the James and Bexar Supersequences (Figure 2.9). The Pearsall Formation was deposited between the maximum flooding events of these two supersequences (Phelps, 2011) during the transgressive part of the Zuni first order sequence defined by Sloss (1963). In the James Supersequence, Phelps (2011) identifies two third-order sequences and in the Bexar Supersequence three third-order sequences. The James Supersequence lasted 6 my and the Bexar Supersequence lasted 9 my (Phelps, 2011). The Pearsall interval accounts for 11.75 my of this time period. The interpretations by Phelps (2011) diverge from the interpretations of Goldhammer and Lehrmann (1999) relative to the equivalent interval in Mexico and the interpretations of Mancini and Puckett (2002) relative to the eastern Gulf of Mexico. These differences arise because neither Goldhammer and Lehrmann (1999) or Mancini and Puckett (2002) recognized the Bexar Supersequence as a separate unit at this stratigraphic rank. The sequence stratigraphic interpretation by Phelps (2011) is used in this study as it is based on a data set immediately adjacent to the study area.

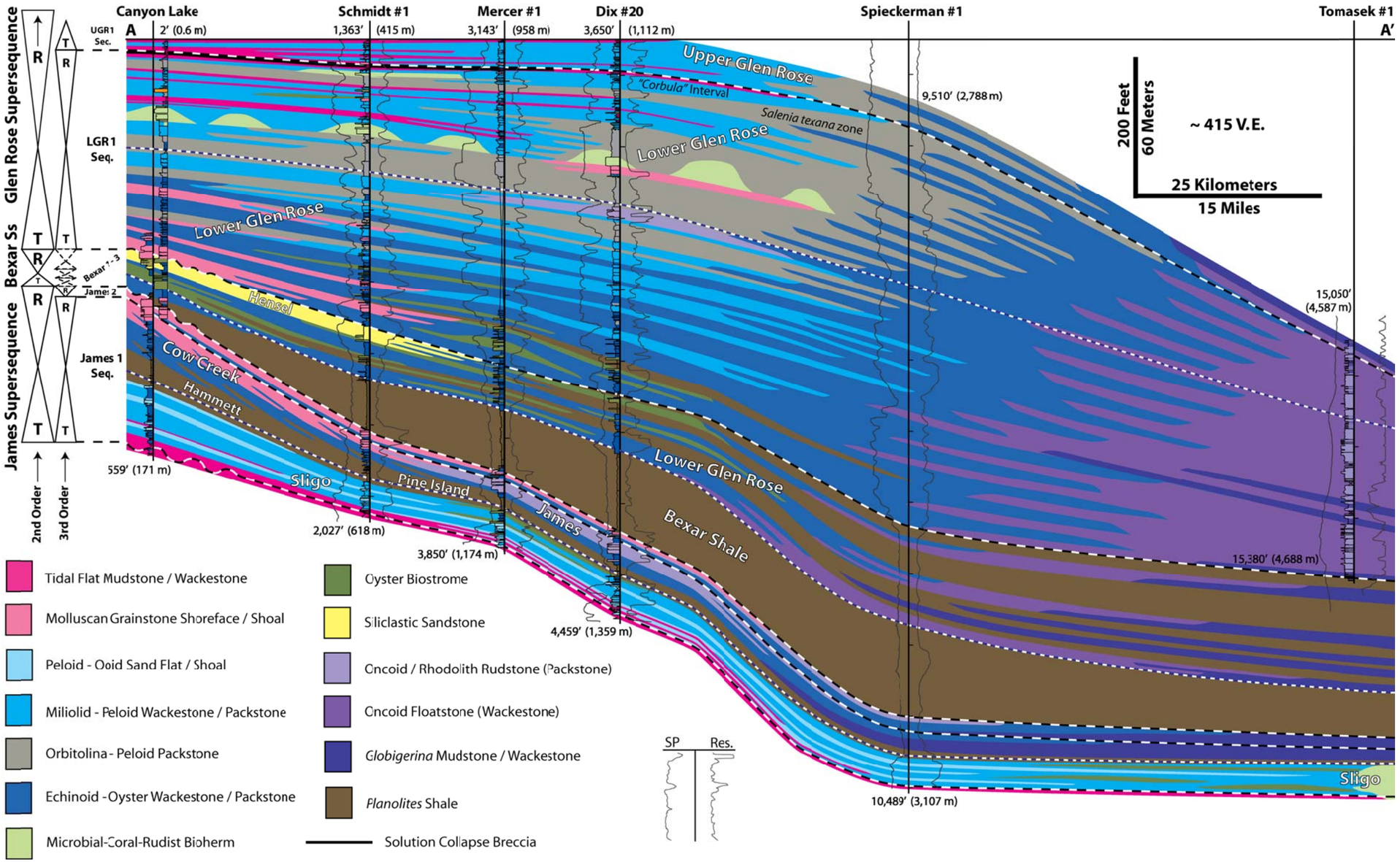

Figure 2.9: Sequence stratigraphic interpretation by Phelps (2011) on the San Marcos Arch. Figure taken from Phelps (2011). Figure reproduced with permission from R. Phelps

Supersequences

The James and Bexar Supersequences contain several third-order sequences, which lasted 1-3 million years each. Updip, in the middle ramp area, these sequences express themselves clearly whereas downdip in the outer ramp area the sequences are less well expressed but still present and identifiable. However, it is unclear how well the higher frequency cycles correlate in the downdip area.

James Supersequence

The James Supersequence of Phelps (2011) is composed of the upper Sligo Formation and the Pine Island Shale and Cow Creek Members of the Pearsall Formation. Phelps (2011) recognized two third-order sequences in the James Supersequence.

Phelps (2011) first third-order sequence is the James-1 third-order sequence (Figure 2.9). This sequence incorporates upper Sligo Formation the Pine Island Shale and lower Cow Creek Members. The transgressive portion of the supersequence initiated during upper Sligo time and could be interpreted as an additional third-order sequence, however further work is necessary to determine this conclusively. A tidal flats succession give way to subtidal facies and transgressive ooid shoals in the upper Sligo Formation to the deeper, fine-grained terrigenous Pine Island Shale Member of the Pearsall Formation (Bebout and Schatzinger, 1978; Foster 2003; Phelps 2011). The contact at the top of the Sligo Formation is erosional updip and transitional downdip (Bebout, 1977). In cores described in the present study, the top Sligo contact is a skeletal grainstone lag composed of abraded allochems. Above this skeletal lag there is an abrupt change to terrigenous claystones, mudstones, and siltstones, of the Pine Island Shale Member. The maximum flooding surface (MFS) for this third-order sequence coincides with the MFS of the

whole supersequence. The MFS is in the lower third of the Pine Island Shale Member where there is the greatest concentration of laminated terrigenous mudstone and finely laminated fissile shale. This also coincided with the highest gamma-ray and the lowest resistivity signature on the wireline-log curves. The Pine Island Shale Member has a transitional contact with the lower Cow Creek Member. This is because carbonates in the lower Cow Creek Member initiated deposition near land and then prograded over the distally deposited Pine Island Shale terrigenous sediments (Phelps, 2011). As such, downdip the lower Cow Creek is very terrigenous rich. This sequence also contains the OAE 1-A. The contact with the next third-order sequence is not well marked by a surface, but coincides with a deepening throughout the whole Maverick Basin and is characterized by a thin bed of calcareous mudstone deposition (Figure 2.9).

The final third-order sequence of the James Supersequence, called the James-2 by Phelps (2011) (Figure 2.9), consists of the upper Cow Creek Limestone. This includes the well-developed carbonate shoal-water complex and associated outer-ramp argillaceous lime wackestones. The shoals extend throughout the middle ramp section of the study area and over the San Marcos Arch (Loucks, 1977). The base of the sequence is a thin, transgressive shale overlain by a carbonate section (Figure 2.9). The carbonate section in the middle ramp includes packstone, grainstone, and boundstone. In the middle ramp area the sequence is capped by an erosional surface that contains oyster shell fragments and caliche in some wells (Loucks, 1976). Downdip the contact is transitional between the calcareous terrigenous mudstones and argillaceous lime wackestones of the upper Cow Creek Member and the terrigenous mudstones of the lower Bexar Shale Member (Figure 2.9). The fauna is limited to oysters, mollusks, and echinoids indicating a probable stressed environment.

Bexar Supersequence

In the Bexar Supersequence, Phelps (2011) identified three third-order sequences (Figure 2.9), all dominated by the transgressive portion of the sequences. The lower two sequences are within the Pearsall Formation, whereas the only the transgressive portion of the uppermost sequence is within the Pearsall Formation, the remaining part being within the overlying Glen Rose Formation.

The lowermost third-order sequence is the lower Bexar Shale Member (Figure 2.9). The lower section of the member is an argillaceous lime wackestone and siliciclastic mudstone. This interval is dominantly terrigenous and thins in the updip direction. The MFS of this third-order sequence occurs within this lower zone (Figure 2.9). The late Aptian regional OAE-1B also occurs within this zone. The OAE stressed the environment of deposition and limited the fauna. Above the terrigenous mudstone package a shoal-water complex developed in the western half of the study area (Figures 1.1, 1.3). This carbonate complex formed during a relatively minor regression and was progradational into areas of the Maverick Basin. The complex is also notably smaller than the Cow Creek shoal-water complex suggesting deeper water to the east. Again, similar to the upper Cow Creek Member, the updip area appears to have an erosional contact with the next sequence, the middle Bexar Shale Member, but downdip the contact is gradational.

The second third-order sequence in the Bexar Supersequence is within the middle Bexar Shale Member (Figure 2.9). This member also has a transgressive mudstone at its base and a regressive carbonate shoal-water complex above. A MFS separates the two units. The shoal-water complex is dominantly located in Zavala County and prograded into the Maverick Basin. The aerial extent of the shoal is more limited than the lower Bexar Shale Member shoal-water complex indicating continued overall transgression.

The middle Bexar sequence is also thought to be least-affected by paleoenvironmental OAEs as it contains a wider more calcareous lime wackestone apron around the shoals (Loucks, 1976; Figure 3.20). In the middle ramp, the contact with the upper Bexar Shale Member is erosional and shows cross-bedded grainstones. Downdip, in the outer ramp, the contact has not been sampled but it is thought to be gradational on the basis of wireline-log signatures.

The final third-order sequence of the Bexar Supersequence and the final third-order sequence in the Pearsall Formation is composed of the upper Bexar Shale Member and part of the lower Glen Rose Formation (Figure 2.9). The lower Glen Rose Formation was not investigated in this study. The upper Bexar Shale Member contains the MFS for the Bexar Supersequence and the upper Bexar Shale Member third-order sequence. The terrigenous matrix of the upper Bexar Shale Member distinguishes it from the lower Glen Rose Formation which is dominantly carbonate mudstones and wackestones (Bay, 1977). The contact between the lower Glen Rose and the upper Bexar Shale Members is similar to the contact between the Pine Island Shale and the lower Cow Creek Members in that it is a gradational contact from a terrigenous mudstone to a carbonate. Additionally, the siliciclastic deposition and biota of the upper Bexar Shale Member are altered by the OAE 1-B (Phelps, 2011).

Middle Ramp High-Frequency Stratigraphy

It was necessary to develop the sequence stratigraphic architecture of the Pearsall Formation in the middle ramp before attempting the sequence stratigraphic analysis of the outer ramp because the sequences are easier to identify in the middle ramp interval. In the middle ramp the changes in energy of the depositional environment and accommodation

had a more distinct effect on the sequences. The anoxic and dysoxic depositional environments of the outer ramp may have altered sequence stratigraphic signatures and masked interpretations (Schlager, 1991). Because the middle ramp was well oxygenated throughout deposition of the Pearsall Formation and consequently interpretations are predominately based on energy and accommodation changes. Downdip changes in facies can relate to changes in oxygenation regime as well as changes in energy of depositional processes and accommodation. The sequence stratigraphic architecture developed for the middle ramp was therefore was carried into the outer ramp.

To understand the higher order sequences using rock-based observations, the Tenneco #1 Ney core, which recovered the complete Pearsall interval, was described in detail (Figures 2.10, Figure 1.4). A number of higher frequency cycles (HFC) were deciphered in the core and then assigned to third-order and second-order packages. This hierarchy of cycles is shown with the core description in Figure 2.10. There are five third-order sequences identified in the Pearsall interval of the Ney core. This coincides with the interpretation of Kerans and Loucks (2002). The cycles are generally capped by coarse-grained carbonate units. Some units are capped by higher energy features, such as cross bedding and scour surfaces with skeletal and clast lags. The correlativity of the HFC was not determined.

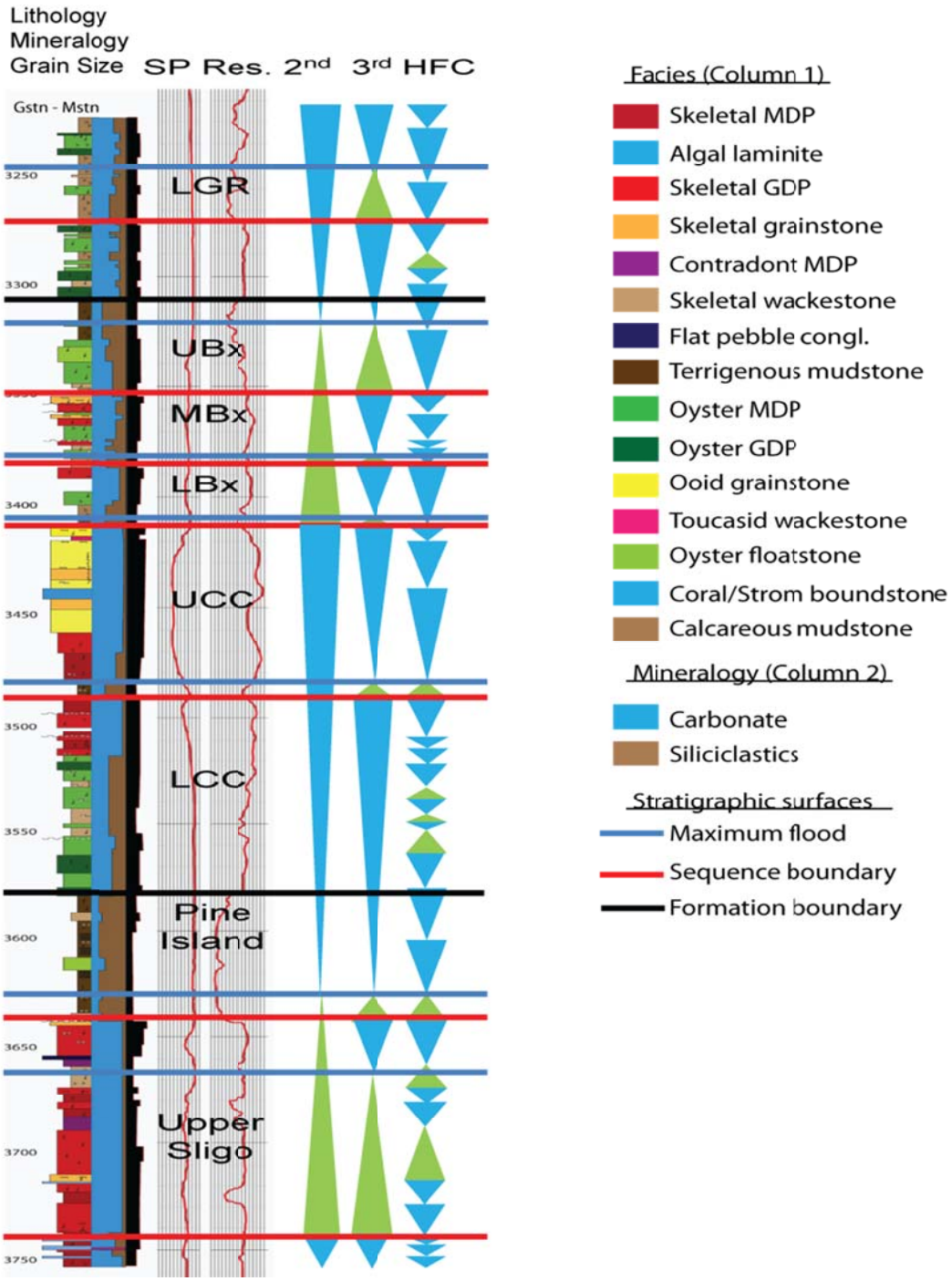

Figure 2.10: Tenneco #1 Ney well description with lithological description, mineralogy, grain size, wireline logs and second-order, third-order, and high-frequency cycles.

SEQUENCE STRATIGRAPHIC FRAMEWORK

General Statement

Four cross-sections, two dip and two strike, were constructed for this study (Figure 2.11). The dip lines were arranged to be perpendicular to the Sligo Reef Margin and the strike lines roughly parallel to it. The cross-sections were chosen to incorporate as many cored wells as possible. The lines were flattened on top of the middle Bexar Shale Member as this is thought to be a temporally consistent pick, which is widespread and easily identified. Picks within the upper Bexar Shale Member and Glen Rose Formation were determined to be questionable because of their lack of lateral consistency (Figure 2.12). The cross-sections reveal the effects of the preexisting topography and the variations in carbonate and clastic sedimentation. The wireline-log responses to facies transitions are fairly subtle given the SP and resistivity logs which penetrate the Pearsall Formation.

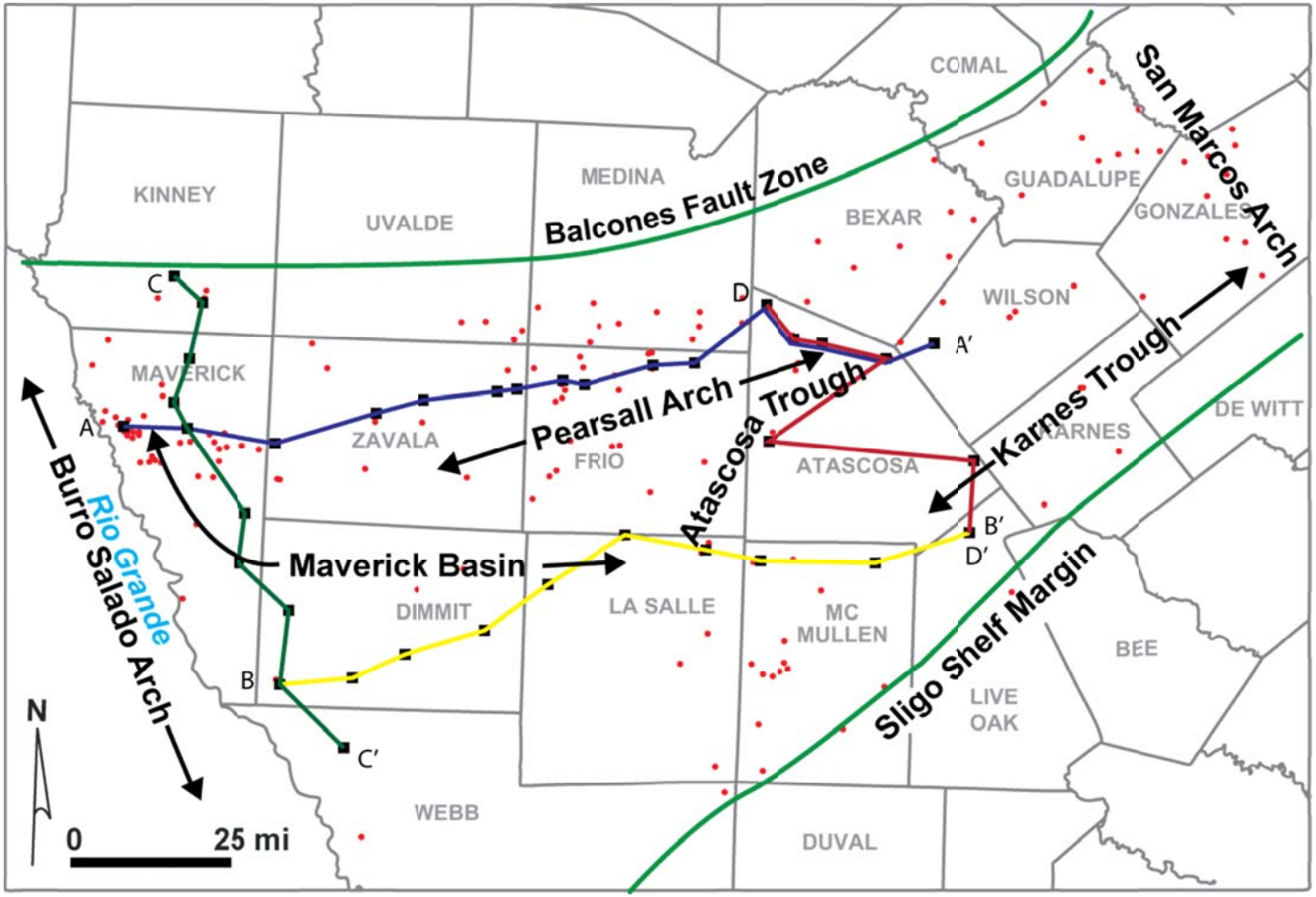

Figure 2.11: Map of the study area showing the locations of cross-sections.

Cross-section A-A'

Cross-section A-A' through the middle ramp (Figure 2.12) extends from the west in Maverick County near the Mexican Border to Wilson County on the San Marcos Arch to the east. Thinning occurs at the edge of the Burro Salado Arch in the westernmost well. This is evidenced by the presence of higher energy facies in the Dilly #1 Ritchie core as well as thinning of the clastic dominated members of the Pearsall Formation. In the case of the Dilly #1 Ritchie core, an abundant amount logged in this well. There is substantial thickening in the next wells, moving east from the Dilly #1 Ritchie, of the Pearsall section in the northern arm of the Maverick Basin underlain by the Triassic rift. This is the result of increased subsidence rates creating additional accommodation resulting in a depocenter. Still further east there is thickening of the carbonate-rich upper Cow Creek and middle Bexar Shale Members over the Pearsall Arch, which was a topographic high during this time. This thickening of the carbonate units along with high-energy carbonate facies is well documented in Loucks (1976). The thickness of the high-energy carbonates in this area was ultimately probably controlled by eustasy and accommodation. All the members of the Pearsall Formation show thinning at the eastern end of the cross-section over the San Marcos Arch. The area of the San Marcos Arch is also thought to be influenced by prodelta terrigenous sedimentation, which suppressed carbonate sedimentation in this area (Loucks, 1976).

The most prominent feature of the cross-section is the notable difference between the San Marcos Arch area and much thicker area to the west of the arch. This difference reflects 11.75 my of differential subsidence in the Maverick Basin. This subsidence occurred as a result the underlying features discussed in connection with Figure 2.3. The Burro Salado Arch, Pearsall Arch, and the San Marcos Arch all subsided slowly while the

area in the Maverick Basin, underlain by the Triassic rift, subsided at a significantly higher rate. In addition carbonates developed on the highs and clastics were deposited in the lows, further altering the thicknesses.

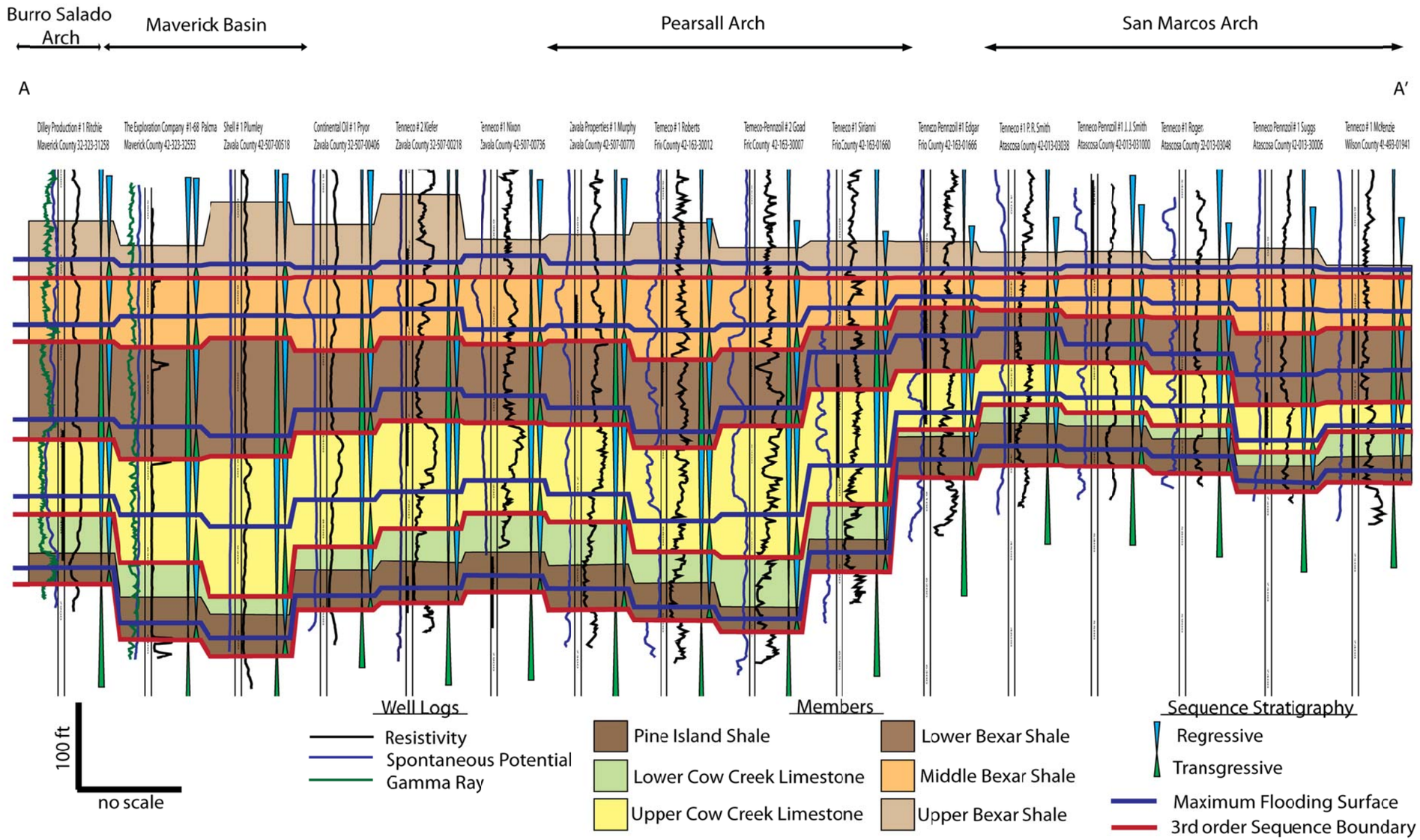

Figure 2.12: Cross-section A-A'. See Figure 2.11 for location.

Cross-section B-B'

Cross-section B-B' (Figure 2.13) is a strike line, which is oriented east-west across the Maverick Basin in the southern part of the outer ramp. It is somewhat oblique to the Sligo Shelf Margin, moving closer to the edge of the Sligo Shelf Margin on the eastern end. The cross-section also contains wells drilled in the last few years to target the Pearsall shale-gas system. Some of the wells are have modern wireline-log suites with gamma-ray logs.

The effect of the paleogeography was notably different in cross section B-B,' particularly with respect to the area affected by subsidence (Figure 2.12). There is thinning on the western end of the cross-section associated with the western edge of the Maverick Basin and the Burro Salado Arch. This thinning can be seen in the Catarina West well and the wells west of it. In the middle of the cross-section there is a large depocenter in the Maverick Basin created by the withdrawal of salt originally deposited in the Rio Grande Embayment and the distal edge of the subsidence caused by the Triassic rift. It is unclear to what extent each feature is responsible for subsidence in the area. This area is notably wider than the area of high subsidence in cross-section A-A,' which was underlain solely by the Triassic rift. Moving eastward, there is an increase in thickness as seen in the Tidewater #2 Mabel Wilson well. This well is centered in the Atascosa Trough shown in Figure 2.3. The thickening of strata in the Atascosa Trough is, however, a local phenomenon as the Pearsall interval thins onto the San Marcos Arch. This increased area of thickness hosts greater accumulations of potentially TOC-rich shale-gas reservoir facies.

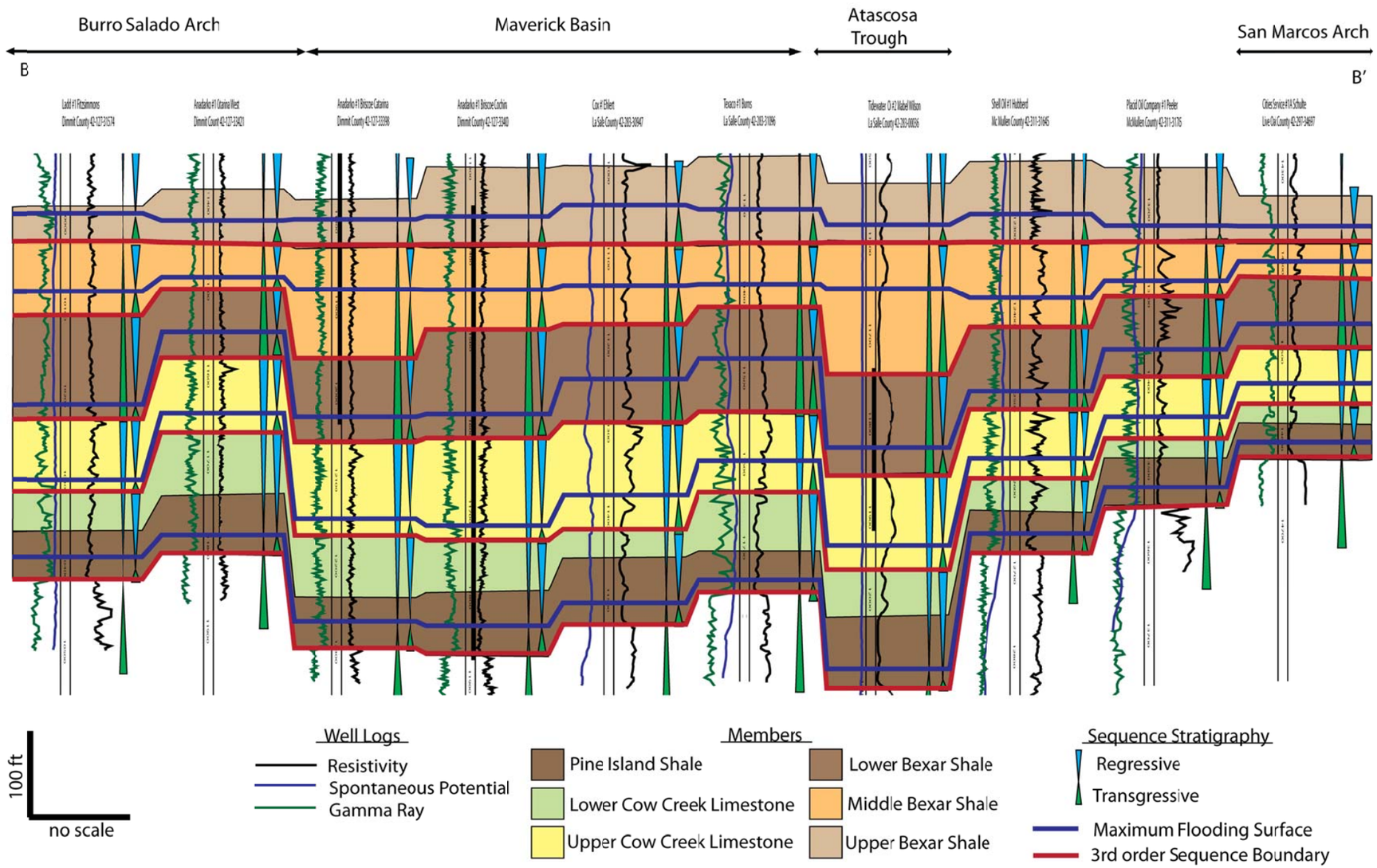

Figure 2.13: Cross-section B-B'. See Figure 2.11 for location.

Cross-Section C-C’

Cross-section C-C’ (Figure 2.14) runs north to south along the western part of the study area but does not reach the shelf edge, as no wireline logs were available. The southern end of the cross-section includes many wells that provide nearby well control for development of the Pearsall shale-gas play.

The cross-section runs roughly down the axis of the buried Triassic rift. It includes wells showing a rapid transition from inner ramp facies in Kinney County to outer ramp facies in northern Maverick County. The wells in the middle of the cross-section are affected dominantly by the northern arm of the Maverick Basin, which is underlain by the Triassic rift and had an anomalously higher rate of subsidence (Figure 2.3). The last two downdip wells on the cross-section are not underlain by the graben but were affected by the Burro Salado Arch. This arch trends southeast, as shown in Figure 2.11, and a deeper thicker section would be expected to the east of these wells. South of cross-section C-C', the Pearsall interval would probably thicken before thinning over the shelf edge. It would then drop off into the deep basin.

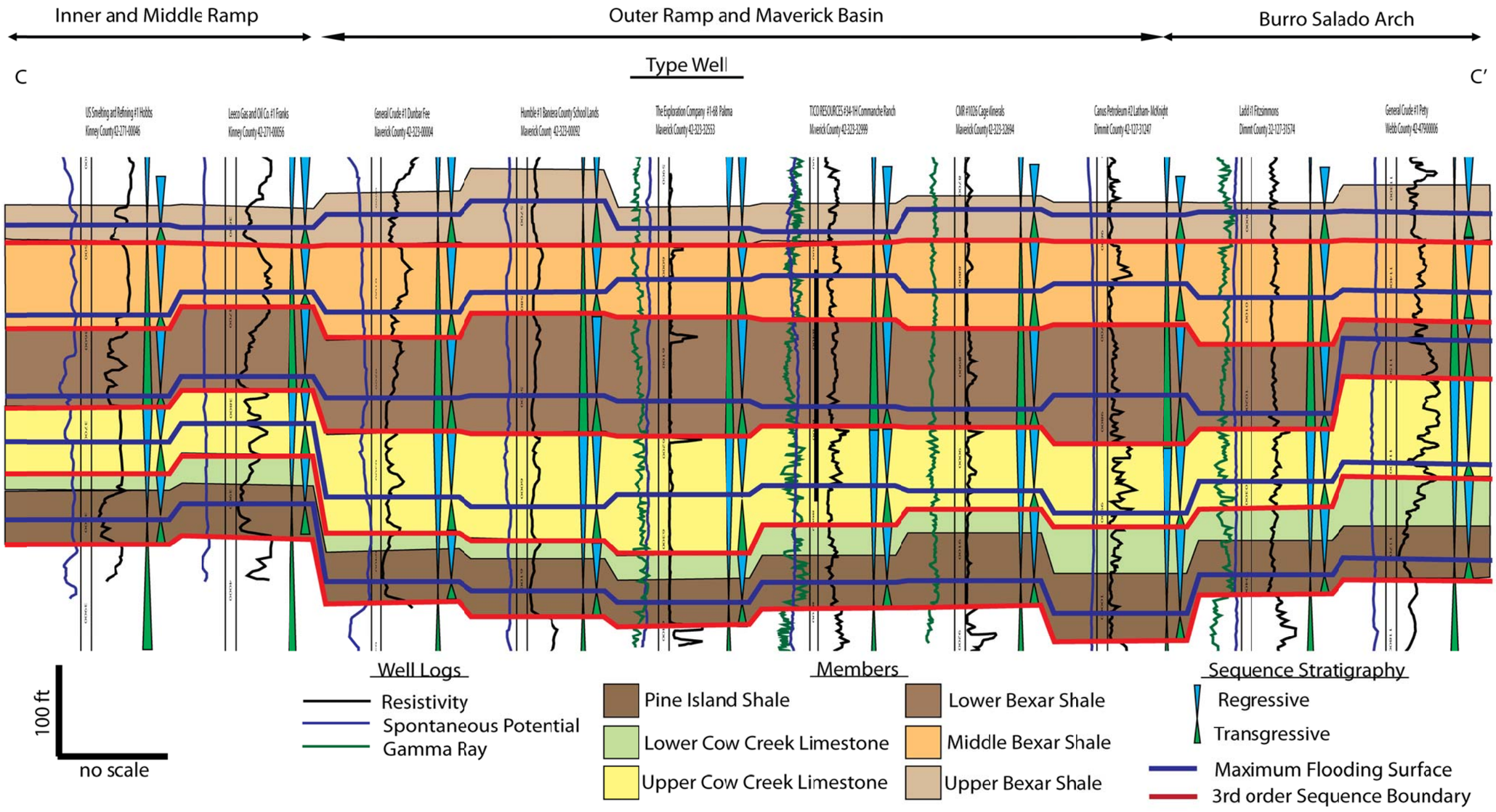

Figure 2.14. Cross-section C-C'. See Figure 2.11 for location.

Cross-Section D-D'

Cross-section D-D' (Figure 2.15) runs roughly north to south along the San Marcos Arch (Figure 2.11). The cross-section reaches all the way to the edge of the distally steepened ramp and passes from the middle ramp to the outer ramp. The section expands gradually downdip towards the shelf margin. An exception to this thickness trend is seen in the Shell #1 Urbancyzk well that penetrated the eastern edge of the Karnes Trough. This trough displays higher accommodation and thus a thicker Pearsall section accumulated in it. After passing through the Trough, the section thins again as it comes under the influence of the shelf edge and the underlying Sligo Reef Margin. This is evidence that the older Sligo reef complex produce a rim shelf with a deeper basin landward.

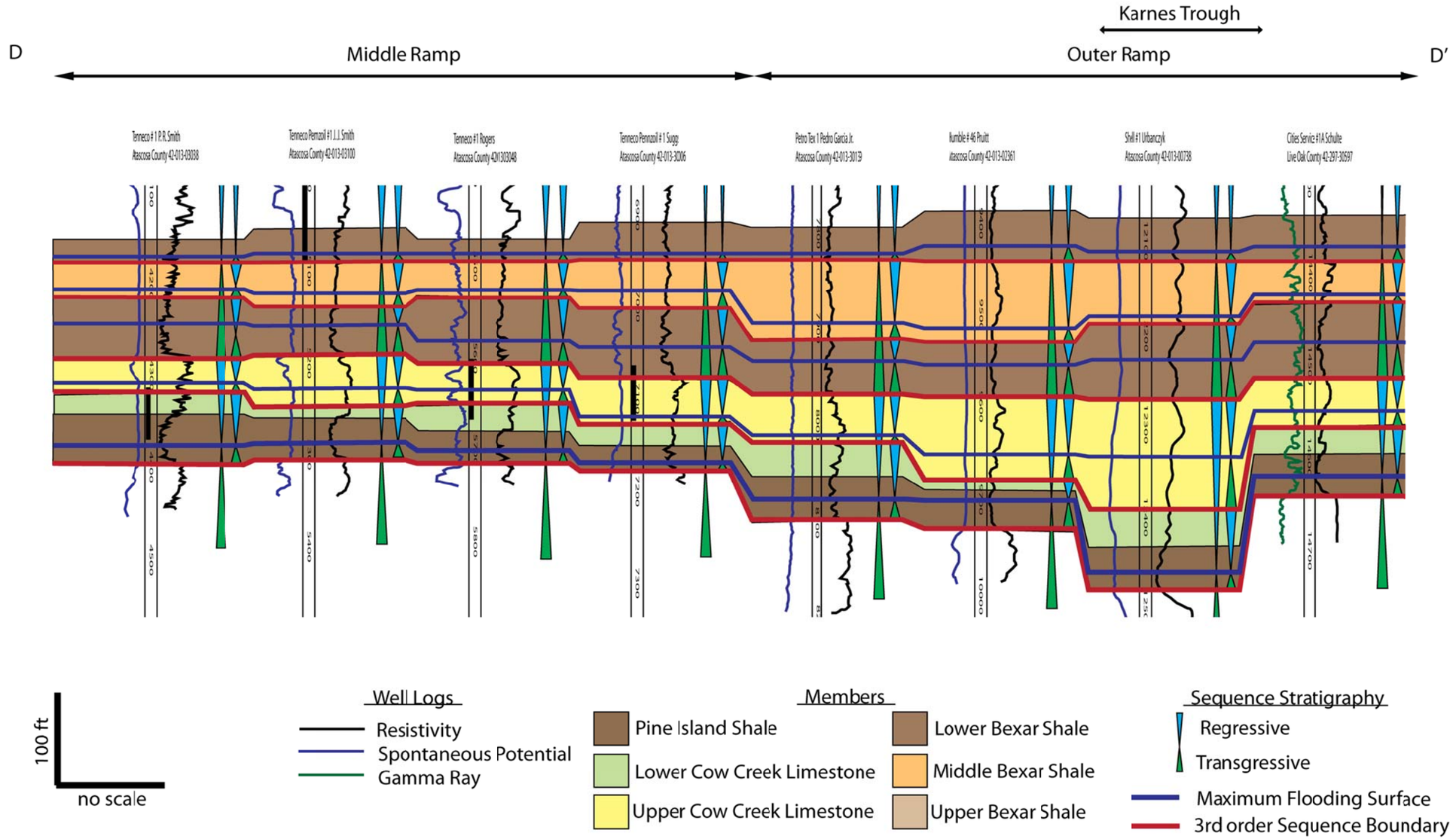

Figure 2.15. Cross-section D-D'. See Figure 2.11 for location.

DEPOSITIONAL TOPOGRAPHY AND CHANGES IN ACCOMMODATION

Depositional topography is important because it reflected the subsidence that controlled depositional lows. In these lows restricted conditions prevailed, which affected oxygenation and thus the preservation of TOC. These lows are related to antecedent topography and changes in accommodation related to the paleostructure.

The original distally steepened ramp morphologies were affected by the presence of the Pearsall Arch (Figure 1.3), and the Burro Salado Arch, which promoted development of shallow-water, high-energy carbonate deposition in the middle ramp. This produced thickening, which can be best seen over the Pearsall Arch in the cross sections, of the carbonate members of the Pearsall Formation in the middle ramp as carbonate sediment aggraded and prograded during third-order regression.

In the outer deeper ramp, drowned-shelf conditions prevailed on the distally steepened ramp. These conditions persisted because of low sedimentation rates (discussed later), which allowed subsidence to become a dominant control. The amount of subsidence was controlled by buried, older structures which profoundly affected deposition and salt withdrawal (Figure 2.3). The critical structures in the study area were the Triassic rift and the Atascosa and Karnes Troughs (Figure 2.10). The combination of these factors manifested itself in thickening in the outer ramp sections dominated by fine grained siliciclastic sediment, deposited primarily during transgressions. This deeper water section was below fair-weather wave base and was largely unaffected by shallow-marine processes. This led to low-oxygen conditions in the basin.

Water depth, circulation patterns, and cycles have an effect on TOC preservation (Arthur and Sageman, 1994), and thus it is important to understand these parameters in investigating shale-gas reservoir facies and associated reservoir properties.

Chapter 3: Lithofacies Analysis

General Statement

Depositional environments of the Pearsall Formation can be separated into facies belts with certain lithofacies dominating each depositional environment. The inner ramp is dominated by a carbonate foreshore, the middle ramp is dominated by shoal-water carbonate complexes, and the outer ramp is dominated by deeper water, siliciclastic sedimentation and an oncolite producing area. The outer ramp sediments grade from terrigenous dominated sediment landward to pelagic and hemipelagic clastics and carbonates seaward across the drowned shelf. Beyond the outer ramp is a distal basinal environment thought to be starved of most terrigenous sedimentation. Loucks (1976) summarized the middle ramp facies and his interpretation has been modified and extended into the outer ramp (Figure 3.1). Detailed facies descriptions used in this model can be found in Loucks (1976, 1978). Facies descriptions by Loucks (1976, 1978) do not highlight some aspects of the environments on the outer ramp. Therefore, the mudstone-dominated outer ramp facies are described in more detail in this chapter. These outer ramp facies are mapped and their stacking patterns in the Pine Island Shale and Bexar Shale Members are discussed, as these two members are the potential shale-gas reservoirs.

Review of Ramp Facies Belts

Inner Ramp Lithofacies

The inner ramp facies in the updip outcrops are dominated beach complexes (Figure 2.4) (Stricklin and Smith, 1959; Inden and Moore, 1983; Kerans and Loucks, 2002). The stratigraphy of the inner ramp is slightly different from the middle and outer ramp. At the base of the Pearsall section the Pine Island Shale Member is dominantly

terrigenous and contains abundant oysters. Above the Pine Island Shale Member are the foreshore and beach complexes of the Cow Creek Member. These beach complexes can be divided into shoreface, foreshore, beach-berm, and back-beach facies (Inden and Moore, 1983; Kerans and Loucks, 2002). Oyster banks offshore provided much of the skeletal material incorporated into the beach complex (Stricklin and Smith, 1959; Kerans and Loucks, 2002). Additionally terrigenous material was sourced from the exposed Llano Uplift. The Cow Creek beaches are capped by an erosional sequence boundary featuring caliches (Amsbury, 1996; Kerans and Loucks, 2002). Above the sequence boundary lies the Hensel Sand Member. This sandstone is equivalent to the siliciclastic shoreline of the Bexar Shale Member (Loucks, 1976; Amsbury, 1996; Phelps, 2011).

Middle Ramp Lithofacies

In the middle ramp there are well-developed shoal-water complexes, as documented by Loucks (1976; 1978). The shoals developed within fair-weather wavebase (Loucks, 1976). Laterally the extent of the shoals in the Bexar Shale Member is controlled by the input of terrigenous sediment in the area of the San Marcos Arch (Loucks, 1976). To the west of the San Marcos Arch, terrigenous mudstone facies developed at the base of the shoal-water complexes during high-frequency flooding events allowing for easy discrimination between the subdivisions within the Bexar Shale Member and Cow Creek Member (Figure 3.1). These mudstones also mark the transgressions during the five third-order sequences that comprise Pearsall time.

The facies of the middle ramp reflect third-order sequence cyclicity. The transgressive portion of the cycles is generally composed of muddy, terrigenous, echinoid mollusk argillaceous lime wackestones and argillaceous lime mudstones. These grade into ammonite terrigenous mudstones downdip (Figure 3.1). The regressive portions of

the sequences are primarily echinoid mollusk lime grainstones and lime packstones, which grade into oncolitic lime packstones and argillaceous lime wackestones downdip. An exception to this is the predominantly oolitic shoal-water complex of the middle Bexar Shale Member.

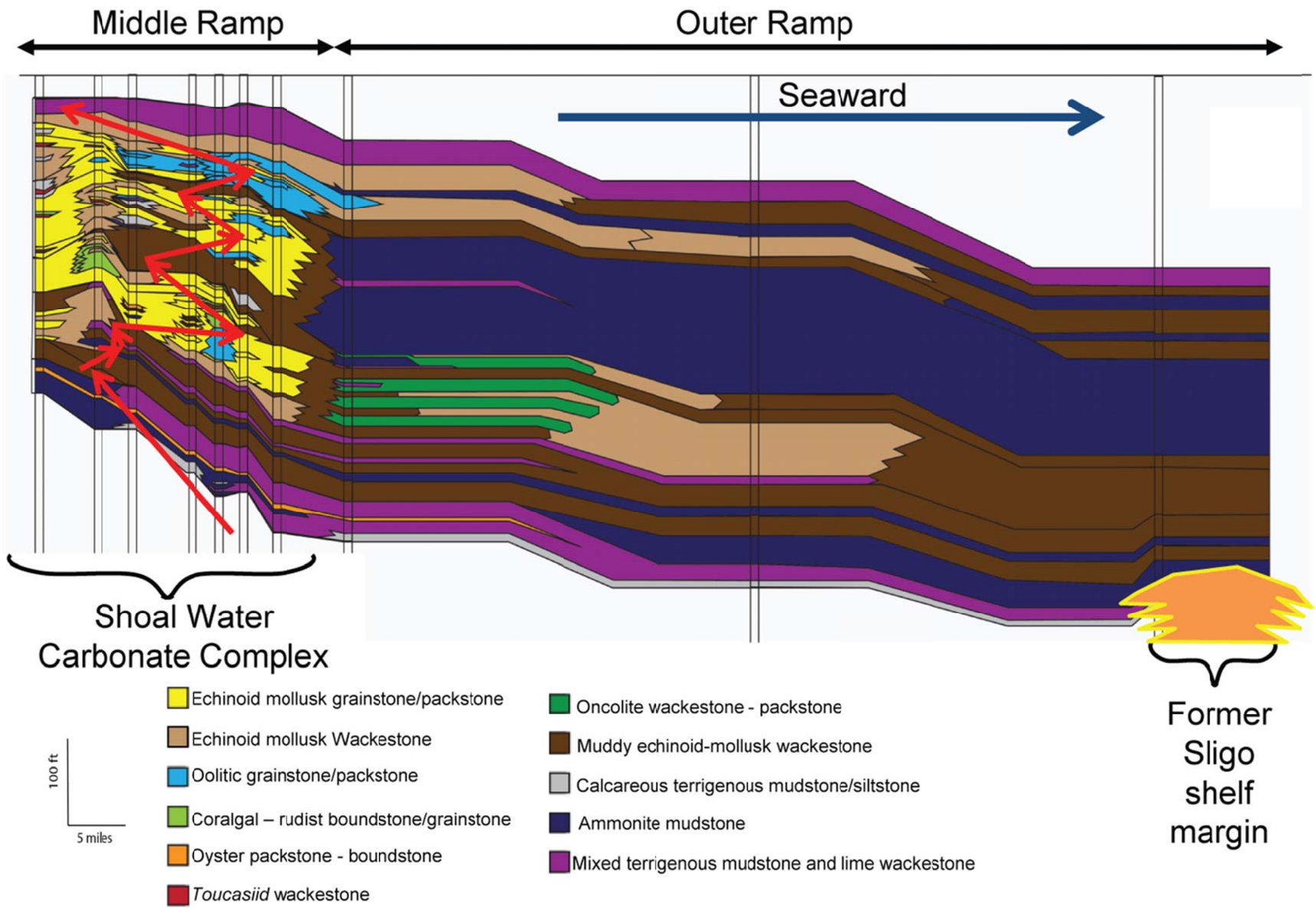

Figure 3.1: Middle and outer ramp facies diagram. The red arrows show the trajectory of the shoreline with transgression and regression.

Outer Ramp Lithofacies

The outer ramp is the area seaward of the shoal-water complexes where sediment was not subject to constant wave agitation (being below fair-weather wavebase, but occasionally affected by storms (above storm wavebase). Downdip of the middle ramp shoal-water carbonate complexes aprons of argillaceous lime wackestone and oncolitic lime wackestone and lime packstone extended onto the outer ramp (Figure 3.1). The lithologies of the outer ramp are primarily argillaceous lime wackestones and terrigenous mudstones. Gravity flows, including turbidity currents and debris flow transported carbonate sediment composed of lime mud and skeletal debris from the middle ramp. The argillaceous lime wackestone facies with some areas of packstones correlate in time with the shoal-water complexes. The skeletal material in these wackestones is mainly echinoids and mollusks. Pectinids or inoceremids, mollusks that can survive in poorly oxygenated water (Thiede and van Andel, 1977), are common but not abundant in the outer ramp, whereas oysters are rare. The terrigenous mudstones generally correlate to deeper water facies updip of the middle ramp. During the Cow Creek and middle Bexar Shale intervals, larger aprons of argillaceous lime wackestones surrounded the shoal-water complexes. Within the Pine Island Shale and upper Bexar Shale Members terrigenous mudstone and argillaceous wackestones are more common throughout the Pearsall interval. This is also true to a lesser extent in the lower Bexar Shale Member.

PINE ISLAND SHALE AND LOWER BEXAR SHALE LITHOFACIES

General Statement

Within the terrigenous mudstone-dominated outer ramp units of the Pearsall Formation, 13 lithofacies are identified. These are summarized in Table 3.1. The facies were described from cores in the Pine Island Shale, lower Cow Creek Member, and

Bexar Shale Members. Six facies occur are that are primarily associated with the Pine Island Shale Member, and seven others are primarily associated with the Bexar Shale Members. The facies are described according to 11 parameters: location on ramp, thickness, dominant matrix, texture, lithology, dominant grain types, lamination type, sedimentary structures, degree of bioturbation, total organic carbon, and early diagenetic products. From these 11 factors the oxygenation level at the time of deposition and the depositional mechanism are interpreted.

The 11 factors are observational groupings chosen to interpret depositional processes and depositional environment. The location on the ramp refers to inner, middle, or outer ramp position. Thickness refers to the thickness range of individual lithofacies packages. The dominant matrix refers to the primary mineral composition. Petrographic evidence indicates that much of the silica and clay was derived from land so terrigenous is used to refer to the siliceous component of the rocks. The classification of fine-grained rocks by Folk (1980) is used for terrigenous mudrock texture. The carbonate rock texture classification is from Dunham (1964). Lamination type refers to fine-scale layering within the rock. Numerous sedimentary structures are noted in the different facies and are described in the discussion of facies. The degree of bioturbation is based on the semi-quantitative classification of Drosser and Bottjer (1986). The six categories that they used to describe bioturbation, from none to total, are grouped into three categories, as it is commonly difficult to conclusively identify bioturbation in fine-grained rocks. A rock with rare bioturbation has most of its primary sedimentary structures preserved, whereas a rock with abundant bioturbation may be completely homogenized. TOC was determined by methods described previously. Early diagenesis, such as compaction, pyrite precipitation, dolomitization, carbonate cementation, and others are described

where important. Early diagenesis is noted when thin section and core observations indicate that the depositional fabric has been substantially modified.

Interpreted of oxygenation level (Figure 3.2) is based predominantly on the degree of bioturbation and the dominant biota (Arthur and Sageman 1994). The general approach used here follows Arthur and Sageman (1994) with additional insights from Rhodes and Morse (1971), Thompson et al. (1985), Arntz et al. (1991), Wignall and Hallam (1991), Kaminski et al. (1993), and Pemberton et al. (2008).

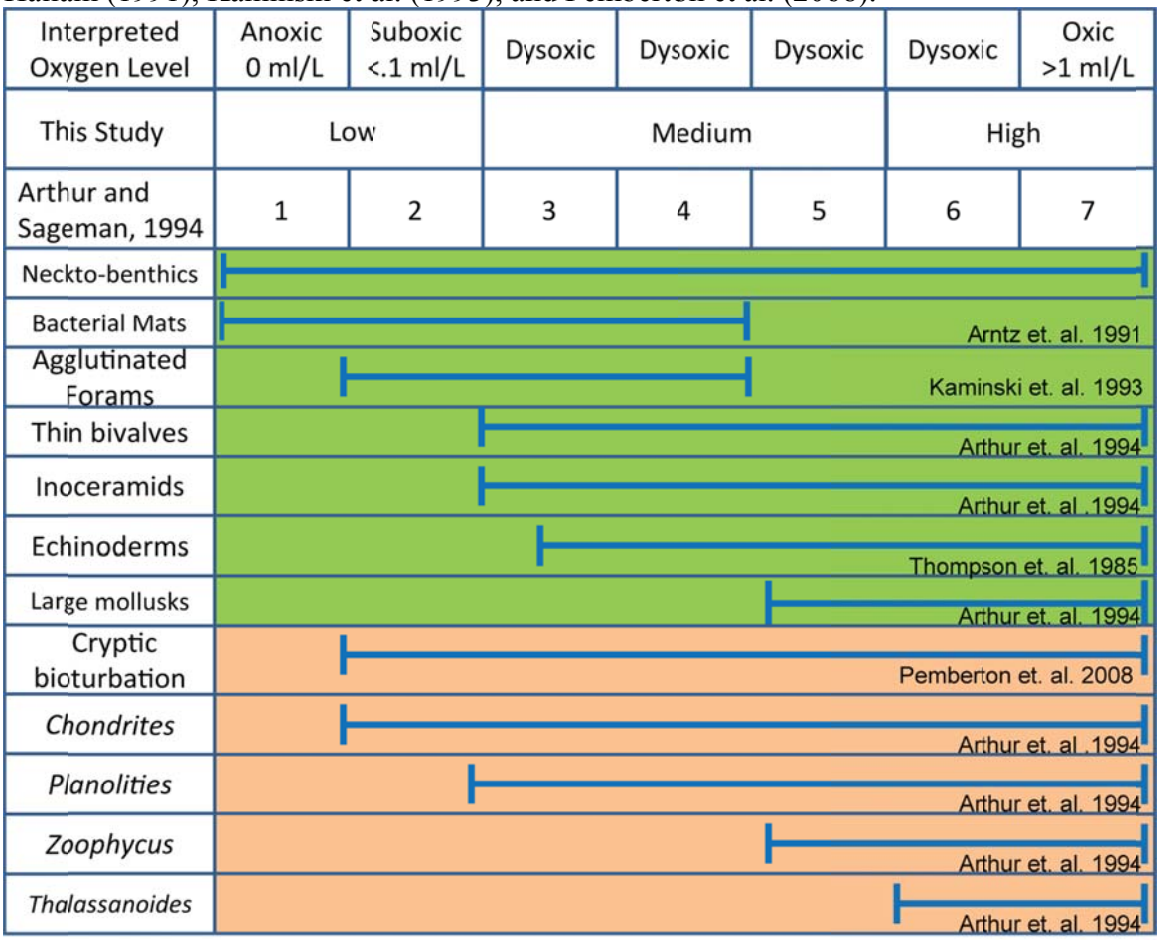

Figure 3.2: Degree of oxygenation from fauna (green) and bioturbation (orange).

In the interpretation of the oxygenation level, the skewing effects of time and transport are taken into account qualitatively. Under oxic water conditions at least 10 cm of sediment are subject to bioturbation, and under dysoxic conditions it takes less than 5 years for bioturbators to destroy all sedimentary structures (Wetzel, 1984; Soutar et al., 1981). The Pearsall Formation was deposited at an average rate of less than 2 cm/ky (Li et al., 2008; Phelps, 2011; this study). As such, 10 cm of sediment would only have to be subject to oxic or slightly dysoxic conditions for less than 0.5% of the Pearsall time to be totally bioturbated. This could easily have occurred on the basis that deposition was in relatively shallow water, less than 100 m, and poikiloaerobic conditions, periodically oxygenated, were highly probable given the water depth. “Doomed pioneers” may have also been present in the dysoxic portion of the basin (Follmi and Grimm, 1990). These organisms were transported into the dysoxic zone, and were able to continue living but not able to reproduce. Therefore they leave isolated trace fossils but few body fossils.

Lithofacies Descriptions

Interpretation of depositional processes is based mainly on textures, lithology, sedimentary structures, fauna, and lamination types. Other petrographic information was also incorporated, and factors that may introduce uncertainty, such as diagenesis and bioturbation, were taken into account.

Table 3.1: Descriptions and interpretation of lithofacies.

Facies	Ramp location	Thickness	Dominant matrix	Lithology / texture	Allochems/ dominant grains	Lamination/ sedimentary structures	Degree of bioturbation	TOC	Early diagenesis	*Oxygenation level*	*Depositional processes*
	Inner, middle, and outer	Range in thickness	Bulk mineralogy	(Dunham, 1964)/ (Folk, 1980)			(Modified from Drosser and Bottjer; 1986)	(Law, 1999)		Interpreted from biota, bioturbation, and TOC (Arthur and Sageman, 1994)	Interpreted from lamination types and sedimentary structures
Oyster chondrodont packstone/ boundstone	Middle	3-5 m	Carbonate	Packstone/ boundstone (rudstone) with siltstone matrix. Silt size: very fine to medium	Oysters, chondrodonts, and other fauna with rare clay floccules and quartz and feldspar silt	Mostly nonlaminated except for internal sediment. Irregular terrigenous silt laminate, fining upward laminate, mud drapes, and cross bedding	High. Individual burrow traces indistinguishable.	Low (>1%)	Sparse dolomite	High	Biota developed in place and reworked by storms and shallow-marine processes (Loucks, 1976; Ross, 1992)
Echinoid mollusk argillaceous wackestone	Middle	1-4 m	Carbonate	Wackestone/ mud-dominated packstone with terrigenous mud and silt in matrix. Silt size: medium to very coarse. Concentrated in burrows and ripples.	Oysters, large mollusks, echinoids, miliolids, serpulids, pellets, peloids, and quartz and feldspar silt	Nonlaminated. Irregular thin terrigenous beds and fining upward beds	High. *Planolites*, and others.	Low (>1%)	Sparse dolomite and blocky pyrite	High	Biota developed in place and reworked by storms (Loucks, 1976; Boggs, 2006)
Peloidal terrigenous siltstone	Middle	1-10 m	Terrigenous	Terrigenous mudstone with siltstone matrix and rare terrigenous mudstones and claystones. Silt size: fine to coarse silt relatively evenly distributed.	Peloids, coprolites, large mollusks, echinoids, serpulids, fish bones, and quartz and feldspar silt.	Nonlaminated, except for fissile shale layers, coarsening and fining upward beds, soft-sediment deformation, and storm-lag beds.	High. *Planolites*, *Chondrites*, *Thalassanoides*	Low (>1%)	Blocky pyrite	Medium	Hemipelagic sedimentation with density flows and storm-lag deposits (Stow and Piper, 1984; Mulder and Alexander, 2001; Boggs, 2006)

Table 3.1 continued.

Peloidal terrigenous mudstone (hemipelagic)	Outer	1-4 m	Terrigenous	Terrigenous mudstone. Silt size: carbonate- fine silt to medium sand (forams) and siliciclastic- fine silt to medium silt.	Peloids, pelagic forams (globigerinids), radiolarian, ammonites, wood material, fish bones, pellets, rare thin walled mollusk fragments (pyritized), and very fine albite and quartz silt.	Lamination <0.2 mm, starved ripples, and cryptic bioturbation.	Low. Rare cryptic bioturbation.	Medium (1-2%)	Blocky pyrite	Low	Hemipelagic and pelagic sedimentation, reworked by bottom currents (Stow and Piper, 1984)
Peloidal calcareous terrigenous mudstone (pelagic)	Outer	1-5 m	Terrigenous	Calcareous terrigenous mudstone. Silt size: forams forming fine sand to v. fine sand and other fine to medium carbonate silt) (commonly aggregated into larger particles),some siliciclastic- medium to v. fine.	Peloids, pelagic forams (globigerinids), radiolarians, coccoliths pellets, demosponge spicules, wood material, fish bones, ammonites, and very fine feldspar and quartz silt	Lamination <0.2 mm. alternating with layers of discontinuous laminae composed of carbonate aggregates or kerogen-rich peloidal clay	Low. None identified.	High (1.5-4%)	Early seafloor cementation of carbonate aggregates	Low	Pelagic sedimentation that may have been reworked by bottom currents (Stow and Piper, 1984; Wignall, 1994)
Fe-rich dolomitic mudstone	Outer	>1 m	Terrigenous	Dolomitic mudstone with siltstone matrix. Silt size: very fine to coarse silt with silt-sized dolomite crystals	Pelagic forams (globigerinids), coccolith aggregates, and peloids	Nonlaminated pseudocrystalline texture.	Low. None identified. Sediment heavily influenced by dolomite produced by bacteria.	Medium (1-2%)	Organogenic dolomitization related to methanogenesis)	Low	Pelagic sedimentation with early diagenesis (Wignall 1994; Mazzullo, 2000)

Table 3.1 continued.

Skeletal oncolitic wackestone/ mud-dominated packstone	Middle/outer	1-2 m	Carbonate	Wackestone and mud-dominated packstone. Carbonate mud matrix. Oncolites are 2-6 mm in length.	Oncolites, oysters, mollusks, echinoids, forams, carbonate peloids, reworked intraclasts, and rare rudist fragments.	Nonlaminated. Soft-sediment deformation.	High. Bioturbated to homogenous with individual *Planolites* and *Thalassanoides*.	Low (>1%)	Cemented nodules	High	In place biota. Sediments reworked by storms. (Loucks, 1976)
Lime mudstone	Middle/outer	1-3 m	Carbonate	Lime mudstone. Contains very coarse- coarse siliciclastic silt.	Echinoid and thin-walled mollusks fragments, oyster fragments, carbonate peloids, *Favorina* pellets, reworked intraclasts, and quartz and albite silt.	Nonlaminated. Soft sediment deformation.	High. Bioturbated to homogenous with individual *Planolites* and *Thalassanoides*.	Low (>1%)	Early carbonate cement expressed as nodules.	High	Hemipelagic and pelagic carbonate mud (Stow and Piper, 1984).
Skeletal siltstone/ terrigenous mudstone	Outer	1-4 m	Terrigenous	Terrigenous mudstone, siltstone, and some mud-dominated packstone. Matrix: Terrigenous siltstone and mudstones. Siliciclastic silt size: very fine sand to coarse silt and carbonate-medium sand to medium silt.	Peloids, thin-walled mollusks, echinoids, fish bones, abraded large mollusk fragments, rare oncolites, rare oysters, pelagic forams, and quartz and feldspar silt.	Diffuse laminations, weakly laminated to massive. Apparent laminations generally greater than 5 mm thick. Shell beds. Fining and coarsening upwards beds.	Low or high. *Chondrites* and *Planolites* burrows. Sediment may be homogenous as a result of bioturbation.	Medium (1-3%)	Aragonitic shells partially or completely replaced by calcite, apatite, and/or pyrite	Low to high	Sediment was deposited by hyperpycnal flows, hemipelagic plumbs and bottom-current reworking. Biota developed in place, but some was transported into the area. High-frequency cycles dominate, as well as oxygenation events

Table 3.1 continued.

Weakly laminated to massive calcite silt-bearing terrigenous mudstone	Outer	1-7 m	Terrigenous	Terrigenous mudstone. Silt size: medium to fine.	Peloids, inoceramid shells, rare thin-walled mollusks, rare echinoids, pelagic forams, ammonites, wood fragments, rare radiolarians, and quartz and albite silt	Diffusely laminated to weakly laminated to massive. Laminations are commonly greater than 5 mm. Rare starved ripples, graded beds, distinct burrows.	Low to high. Very rare *Chondrites* and *Planolites*. Sediment predominantly homogenous.	Medium (1-2%)		Low with some oxygenation events	Sediment was deposited by hyperpycnal flows and hemipelagic setting in an anoxic environment. Some bottom current reworking. (Stow and Piper, 1984; Bhattacharya and MacEachern, 2009)
Burrowed calcite silt-Bearing terrigenous mudstone	Outer	1-2 m	Terrigenous	Terrigenous mudstone Silt size: medium to fine.	Peloids, inoceramid mollusk, rare thin-walled mollusks, rare echinoids, pelagic forams, ammonites, wood fragments, rare radiolarians, pellets, *Favorina* pellets, reworked intraclasts, and quartz and albite silt.	Diffusely laminated to weakly laminated to massive. Laminations are commonly greater than 5 mm. Soft-sediment deformation. ,.	Low to high. *Chondrites* and *Planolites* Commonly with early calcite cement.	Medium (1-2%)	Early carbonate cementation of burrows	Low with some oxygenation events	Sediment was deposited by hyperpycnal flows and hemipelagic setting in an anoxic environment. Some bottom current reworking. (Stow and Piper, 1984; Bhattacharya and MacEachern, 2009)
Winnowed nonbioturbated calcite silt-bearing terrigenous mudstone	Outer	1-5 m	Terrigenous	Terrigenous mudstone with some siltstone. Silt size: medium to fine.	Inoceramid shells, very rare mollusks, pelagic forams, rare radiolarians, sponge spicules, hemipelagic aggregates, and quartz and feldspar silt, ,	Diffusely laminated to weakly laminated to massive. Laminations are commonly greater than 5 mm. Starved ripples, fining and coarsening upward laminae, ungraded silt laminae, and scour surfaces. Graded deposits may be bioturbated.	Low. Rare *Planolites* or *Chondrites*. Rare burrows are attributed to doomed pioneers.	High (1-4%)	Pyrite	Low with some oxygenation events	Sediment was deposited by hyperpycnal flows and hemipelagic setting in an anoxic environment. Some bottom current reworking. (Stow and Piper, 1984; Scheiber, 1996; Bhattacharya and MacEachern, 2009)

Table 3.1 continued.

Lithoclast-rich skeletal lime rudstone	Outer	>1 m	Terrigenous	Rudstone. Matrix: siltstone or terrigenous mudstone. Rare lime mudstone. Grain size: v. fine sand-medium silt. Clast are up to 5 cm in diameter.	Rare mollusks, rare oysters, large angular carbonate clasts with sponge and algal borings.	Nonlaminated. Show some coarsening upward, chaotic bedding	Low. Clasts were probably bored pretransport.	Low (>1%)		n/a	Debris flows into the outer ramp (Mulder and Alexander, 2001)

The following sections are brief summaries of the salient features of the facies listed in Table 2. Associated photographs and photomicrographs are presented.

Oyster Chondrodont Packstone/Boundstone

The oyster chondrodont packstone/ boundstone (Figure 3.3) is found in the middle ramp Pine Island Shale and upper Bexar Shale intervals, where it forms widespread correlative biostromes (Loucks, 1976). The biostromes are characterized by the large oysters and chondrodonts primarily preserved as disarticulated shells and large fragments, many of which are greater than 5 cm long (Figure 3.3). The chondrodonts are found either upright in clusters or flat-lying; both occurrences can be interpreted as living positions according to Ross (1992). Much of the matrix between the fossils is laminated internal carbonate sediment. This facies was deposited on a shallow, open-marine shelf within fair-weather wavebase as currents are necessary to transport food into the area and excrement out. These currents would have also ensured that the water was well-oxygenated (Arthur and Sageman, 1994). Siliciclastic layers and mud-drapes reflect the impact of storms. The fauna is low in diversity despite the well-oxygenated waters and high-energy conditions. This is thought to be connected to the OAE 1-A and OAE 1-B events, which coincide with the development of this facies in the middle ramp. This facies was also recognized by Phelps (2011) in the OAE 1-A interval to the east on the San Marcos Arch. OAEs created a stressed environment, limiting the fauna and creating the conditions for this facies to develop.

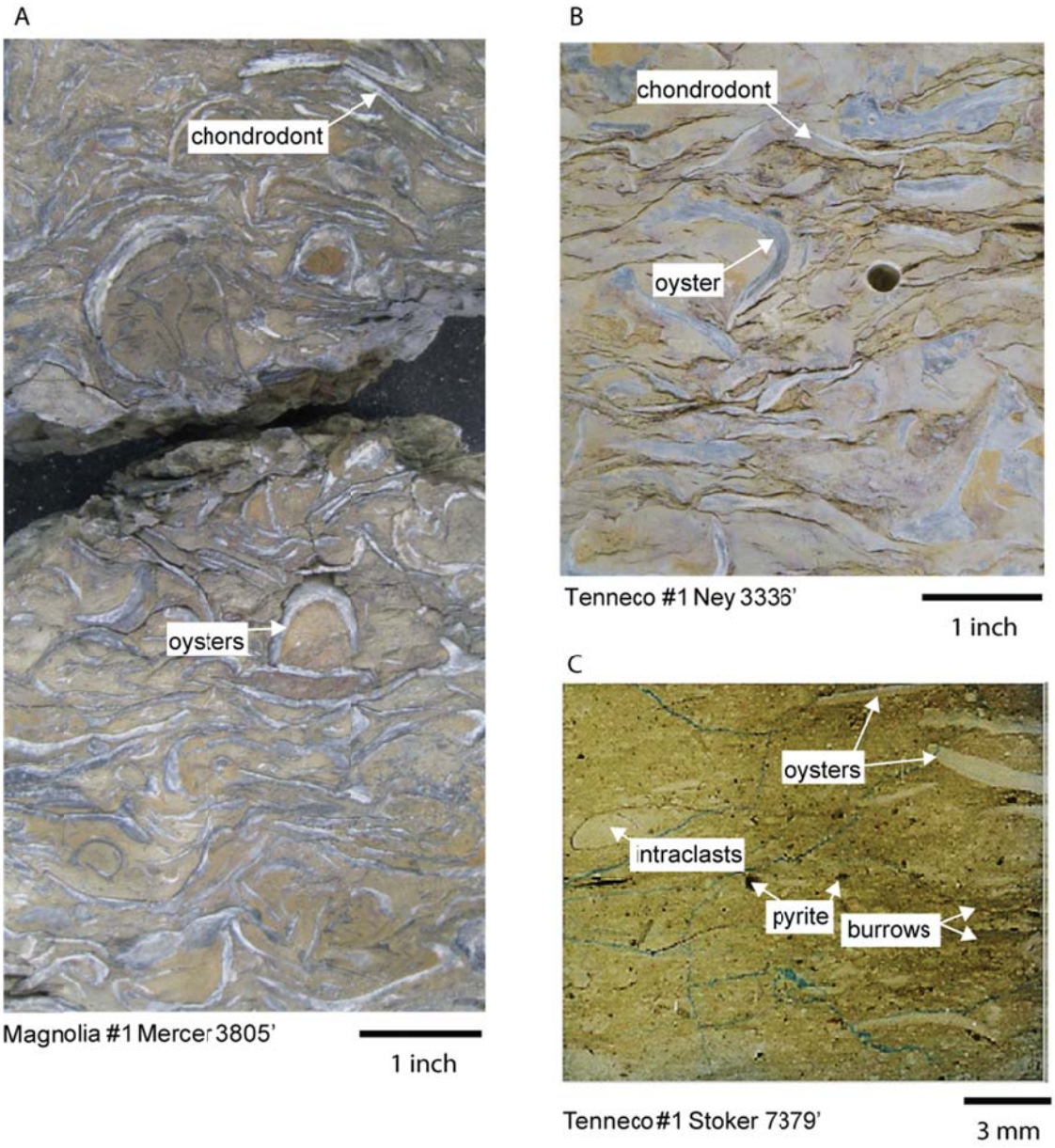

Figure 3.3: Oyster chondrodont packstone/boundstone. (A) and (B) Core slabs showing whole oysters and chondrodonts. (C) Plane-polarized light photomicrograph showing oyster fragments as well carbonate intraclasts and quartz silt. The black particles are diagenetic pyrite framboids in matrix and blocky pyrite replacing shell fragments.

Echinoid Mollusk Argillaceous Wackestone

The echinoid mollusk argillaceous wackestone (Figure 4.4) has a mixture of terrigenous and calcareous matrix and is present in the Pine Island Shale Member, lower Cow Creek Member, and Bexar Members of the middle ramp. The facies locally includes siltstone containing carbonate, quartz, and feldspar silt. In some areas this facies appears as a mud-dominated packstone where mud accumulation was lower and storm events produced better sorted sediment (Loucks, 1976). In the terrigenous mudstone-dominated parts of the Pine Island Shale Member, this facies is anomalous because of its high diversity of fauna and distinct bioturbation. It also appears to be only locally developed and not correlative between wells. In the Tenneco #1 Stoker well and other middle ramp wells, very fine crystalline dolomite is present. It is not a significant feature in the wider area and may also be attributed to other mechanisms such as seawater pumping and microbial activity (Tucker and Wright, 1999).

This facies displays a high degree of bioturbation and a high-diversity of fauna. It is interpreted to have been deposited in an open-marine environment above storm-weather wavebase in well-oxygenated water. This facies was not subjected to constant reworking. Although silt and storm features are present, they are not well-preserved because of the high degree of bioturbation. In the Pine Island Shale Member this facies was subjected to fewer-frequent high-energy events than in the lower Cow Creek Member where many of these bedded skeletal packstones developed.

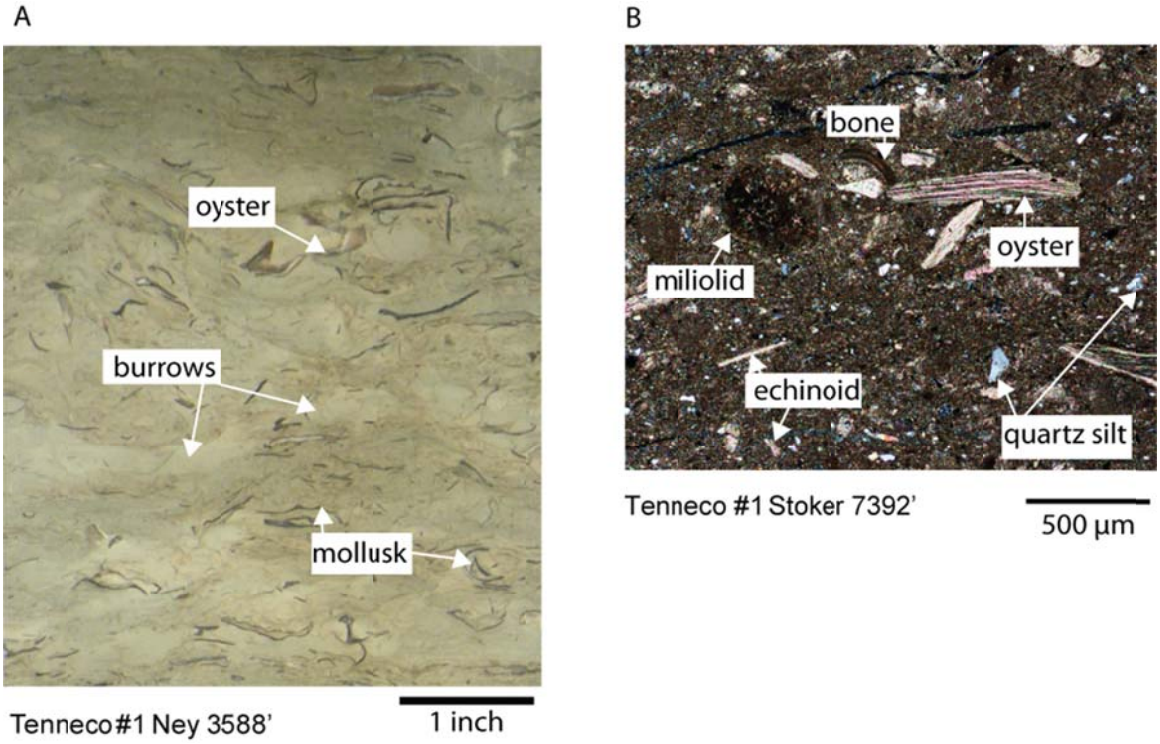

Figure 3.4: Echinoid mollusk argillaceous wackestone: (A) Core slab showing intense burrowing and abundant skeletal material. (B) Cross polar photomicrograph showing a peloidal texture. Oyster, mollusk, and echinoid fragments, miliolids, intraclasts, and quartz silt are present.

Peloidal Terrigenous Siltstone

This facies dominates the middle ramp mudrock system in the Pine Island Shale and Bexar Shale Members. It is a peloidal terrigenous siltstone (Figure 3.5) with some argillaceous wackestones and claystones intermixed. It contains both siliciclastic and carbonate silt. The siliciclastic silt is predominately detrital quartz and albite and the carbonate silt appears to be broken and abraded shell fragments as well as miliolids. There is sparse shell material scattered in the matrix. Much of this skeletal material was derived from organisms that require well-oxygenated water. They appear to have been transported into place, as they are broken and never articulated. Other organisms that are

more tolerant to adverse environmental conditions (Figure 3.2), such as thin-walled mollusks and whole echinoids, are present and probably grew in place.

The rock is largely bioturbated and displays abundant distinct burrows. There are preserved storm event-beds that are partly bioturbated. These are generally coarsening upward sequences and are commonly finely laminated. Many of the laminations are parallel, but some are truncated, suggesting scour (Figure 3.5). These laminations may be evidence of hummocky cross-bedding created by storms, as described by Lamb (2008); however, it is very difficult to make such a conclusion based on limited observations from core. The mixed terrigenous and carbonate composition results from the lateral transport of terrigenous mud on the open-marine shelf. Such processes have been described for the Modern by several authors and are commonly related to storms and bottom currents (Kelling and Mullins, 1974; Mount, 1984; Rine and Ginsburg, 1985). Even though there is bioturbation, it is clear that the environment of deposition was suitable neither for many sessile organisms nor TOC preservation.

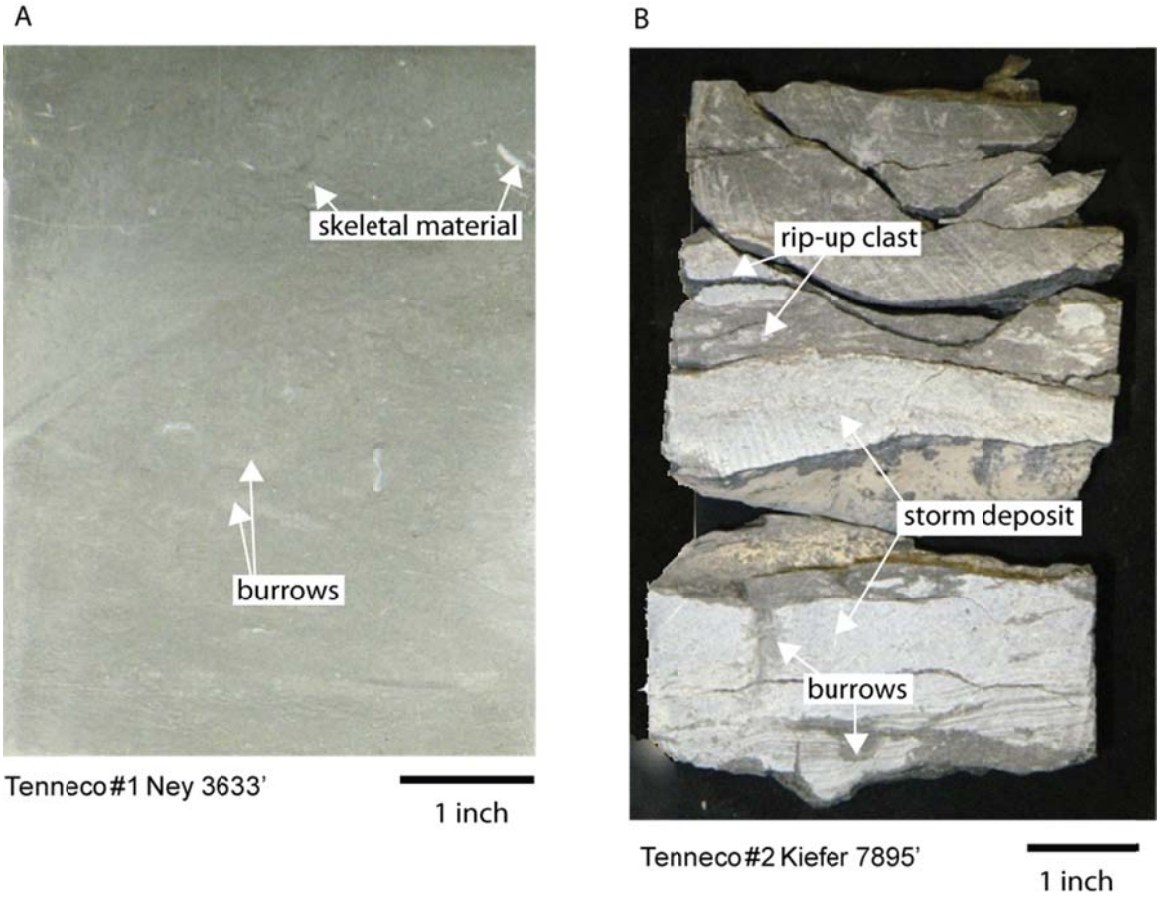

Figure 3.5: Peloidal terrigenous siltstone. (A) Core slab showing homogenous peloidal terrigenous mudstone with scattered broken fossils and burrowing. (B) Core slab showing burrowed carbonate storm deposits in peloidal terrigenous mudstone.

Peloidal Terrigenous Mudstone

The peloidal terrigenous mudstone (Figure 3.6) occurs in the most distal part of the outer ramp near the top of the Pine Island Shale interval. This facies probably extends into the downdip outer ramp area of the Bexar Shale Member as well. The facies is predominately fine-grained terrigenous mud. The facies is finely laminated with a peloidal texture and displays no evidence of bioturbation. The skeletal material is almost entirely composed of pelagic forams, radiolarians, fish bones, and ammonites. Rare,

larger skeletal fragments show evidence of transported and are commonly pyritized (blocky crystals). Pyrite in the matrix is disseminated as large framboids, which did not form in euxinic conditions (Wignall and Newton, 1998). This form of pyrite formed in poorly oxygenated sediment. The framboidal pyrite suggests that the redox line was not above the sediment-water interface and that the water column was not euxinic (Raiswell and Berner, 1985; Loucks and Ruppel, 2007).

This facies is interpreted as being deposited in a distal open-marine setting. It formed in very low-oxygenation conditions as evidenced by the lack of sedimentary structures, bioturbation, and benthic fauna. There are some textures observed in the thin sections which could be cryptic bioturbation or dewatering features; thin-section artifacts cannot be ruled out. There are very subtle laminations of less than 0.2 mm as visible in core and thin sections. The laminations are generally parallel and are composed of peloids and silt. The majority of the sediment was probably deposited by hemipelagic suspension settling (O'Brien, 1996; Stow and Piper, 1984). There is also some medium to fine-grained quartz and feldspar silt. This may have been transported as windblown dust or it may have been transported by dilute turbidity currents (Schieber et al., 2010). Some ripples composed of silt are present (Figure 3.6) and may have formed by erosion and transport of the particles along the seafloor by bottom currents, or they may be primary depositional features associated with dilute turbidity currents. In general, this facies is considered to be composed of hemipelagic sediment with some pelagic sediment input.

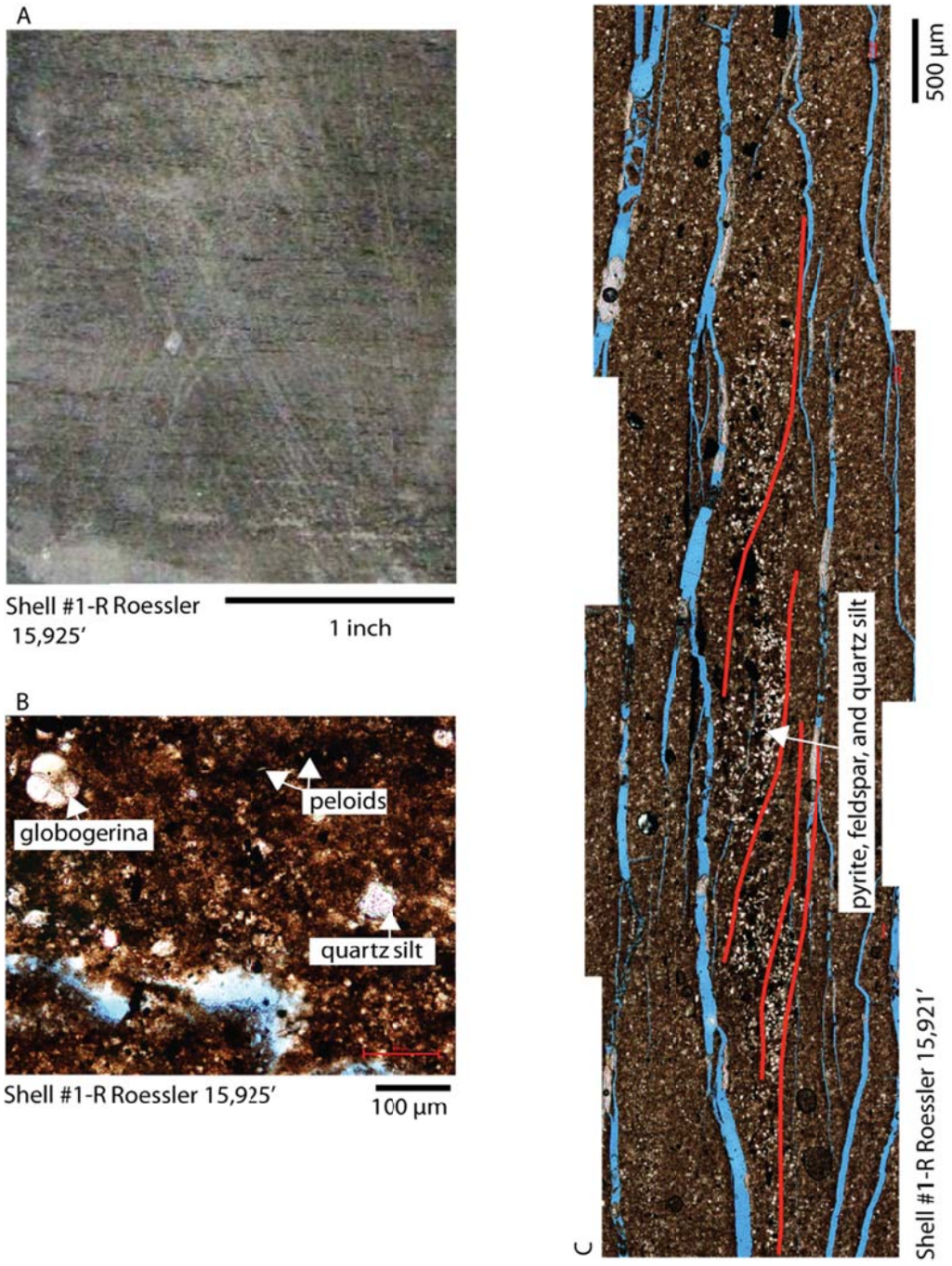

Figure 3.6: Peloidal terrigenous mudstone. (A) Core slab showing the poorly formed, sub-millimeter-scale laminations. (B) Photograph of peloidal texture, Globigerina foraminifera and quartz silt are visible. (C) Thin-section photograph of a ripple structure in a mudstone.

Peloidal Calcareous Terrigenous Mudstone

The peloidal calcareous terrigenous mudstone (Figure 3.7) occurs in the most distal part of the outer ramp near the paleo-Sligo Reef Margin. It is composed of alternating carbonate aggregates that are predominantly composed of coccoliths and other small pelagic organisms and kerogen-rich clay-dominated laminae. The smallest laminae are less than 0.2 mm thick, but range up to 2 mm through the aggradation of individual thin carbonate lamina. The carbonate aggregates appear to have been cemented early and reworked based on the discontinuous, ungraded character of the laminae. While the carbonate aggregates appear to be somewhat recrystallized the coccolith plates and other small pelagic fauna are still visible within them. There are also abundant pelagic foraminifers as well as radiolarians, fish bones, and ammonites. The facies also has a high TOC.

These rocks were deposited by pelagic sedimentation in dysoxic to anoxic environment. The oxygenation state is evidenced by the high TOC, the lack of benthic fauna, and the lack of substantial trace fossils. The laminations are also ungraded, indicating that the sediment was deposited primarily by dilute turbidites (Molder and Alexander, 2001). The alternating laminae are attributed to different hydrodynamic properties of the particles, as suggested by Arthur et al. (1984). The clay-rich peloids were probably deposited in suspension as marine snow, bound together as organomineralic aggregates (Wignall, 1994; MacQuaker, 2010). It is possible that the carbonate aggregates are in fact fecal pellets, as these would have been able to sink out of suspension rapidly (Arthur et al., 1984).

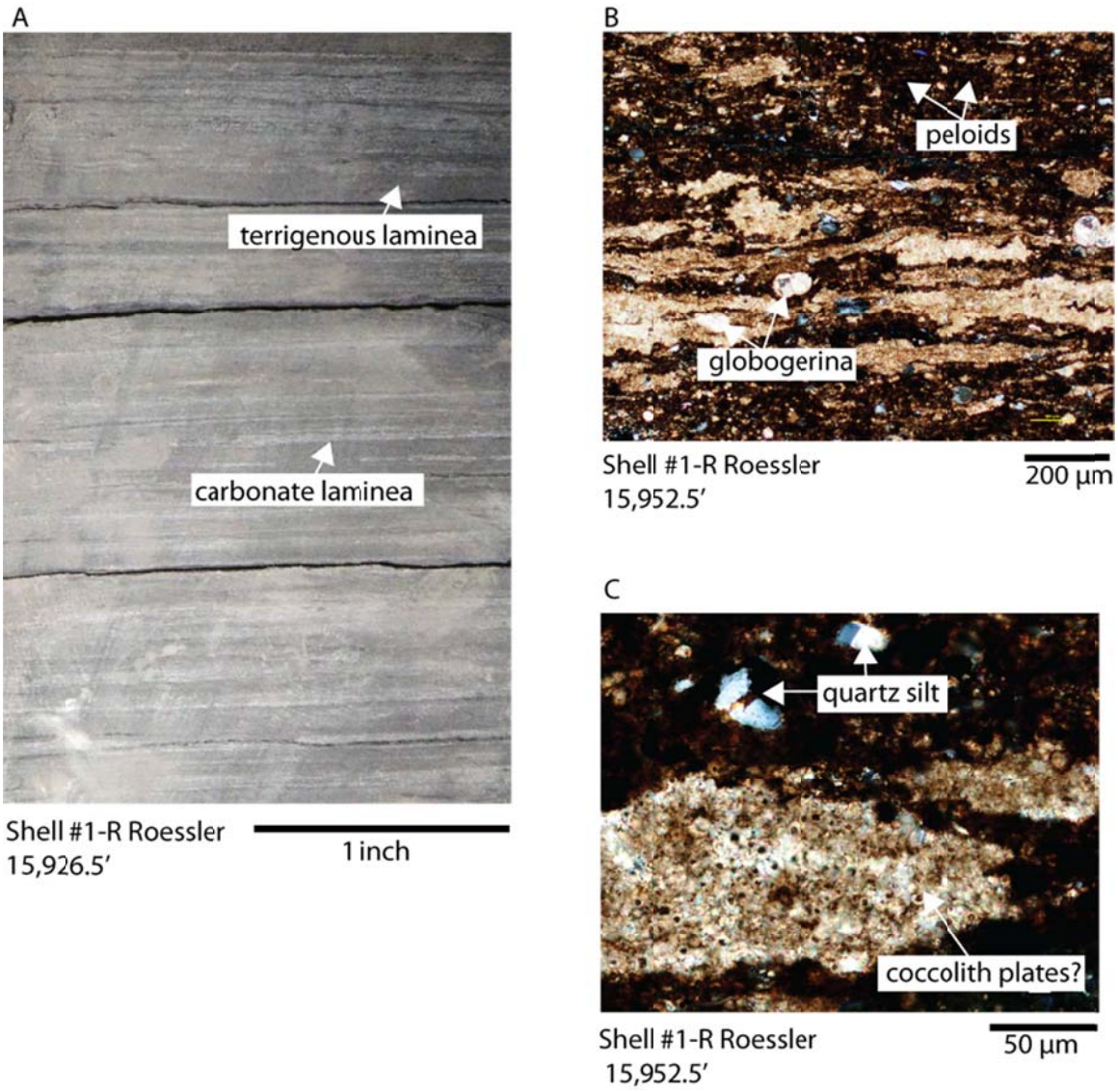

Figure 3.7: Peloidal calcareous terrigenous mudstone. (A) Core slab showing discontinuous laminations of alternating layers of carbonate aggregates and clay. (B) Laminations of intermixed silt and pelagic foraminifera. (C) Close-up of a carbonate aggregate showing evidence that it is composed of early cemented pelagic material, possibly coccoliths.

Fe-Rich Dolomitic Mudstone

The Fe-rich dolomitic mudstone (Figure 3.8) facies is one of the few facies defined in the basis of the presence early diagenetic products. The fabric and mineralogy

is almost entirely composed of silt-sized dolomite crystals. These are intermixed with clay and pelagic forams. The facies is almost unidentifiable in core except by its lack of layering and its relatively extreme hardness produced by a pseudocrystalline matrix.

XRD analysis, as well as microprobe analysis, reveals that the matrix is composed of mostly ankerite. Pelagic forams are also present in the matrix and the remains of carbonate peloids similar to those observed in the peloidal carbonate pellet-rich mudstone facies are observed. Therefore, it is thought that this facies was probably deposited under similar conditions to those of the peloidal carbonate pellet-rich mudstone. The dolomite is interpreted as a by-product of anaerobic respiration produced during bacterial respiration and methanogenesis (Mazzullo, 2000).

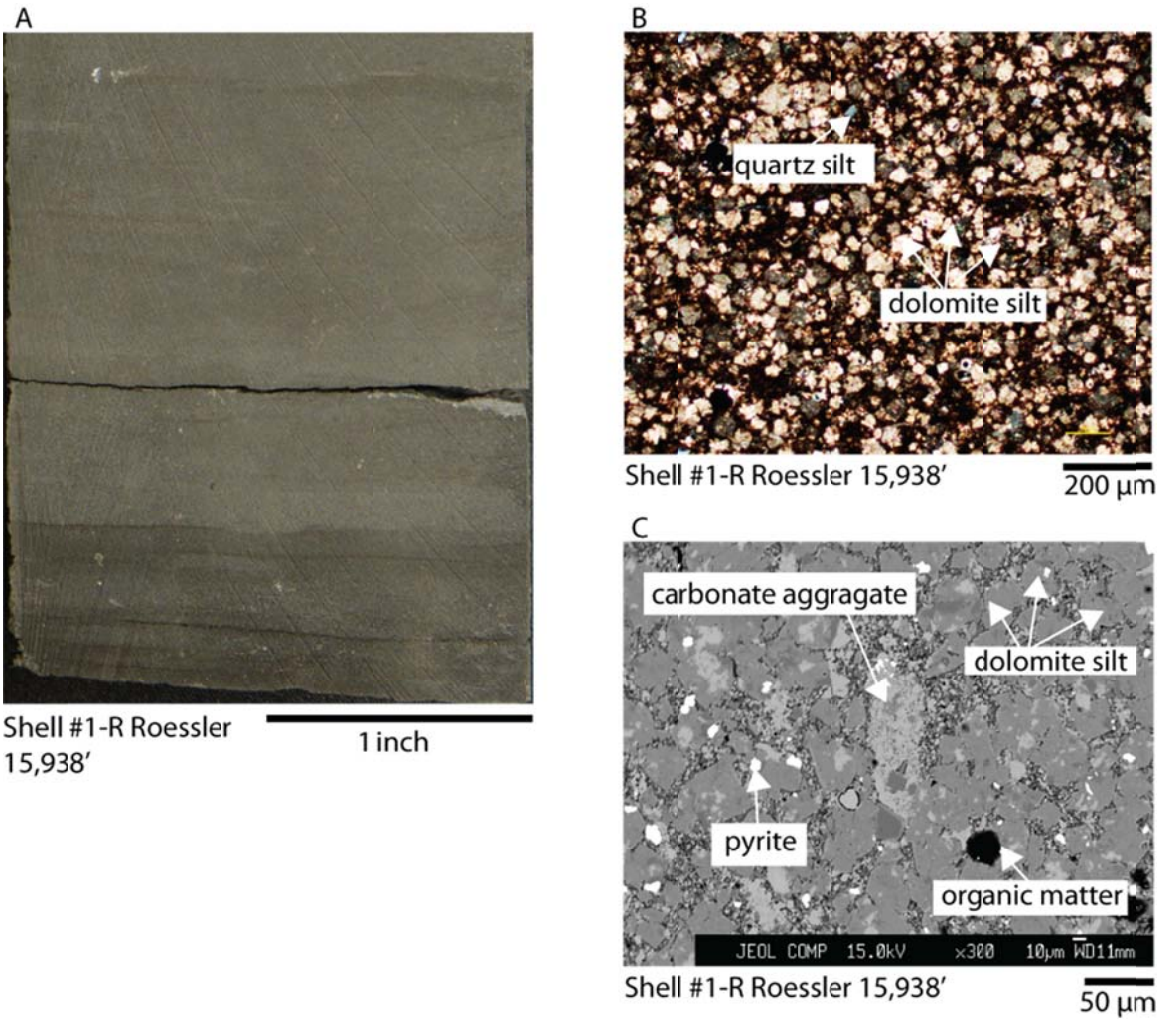

Figure 3.8: Fe-rich dolomitic mudstone. (A) Core slab. (B) Photomicrograph showing Fe-rich dolomite crystals. (C) SEM backscatter electron image displaying the dolomite crystals, carbonate aggregates. In (C)Up is to the left.

Skeletal oncolitic wackestone/ mud-dominated packstone

The skeletal oncolite wackestone and mud-dominated packstone (MDP) (Figure 3.9) developed in an apron around the Cow Creek Member shoal-water complex (Loucks, 1976). It is predominantly wackestone. The matrix is carbonate mud and highly bioturbated.

The facies has a high diversity of fauna and was deposited in clear water above storm-weather wavebase, as evidenced by the growth and development of green algal oncolids (Tucker and Wright, 1999). Oyster fragments and large mollusks are abundant, indicating that the facies was deposited in normal marine conditions. Some of the oysters and mollusks show signs of reworking, as evidenced by abrasion and rounding of the shells, as well as unique shell fills that do not match the surrounding matrix.

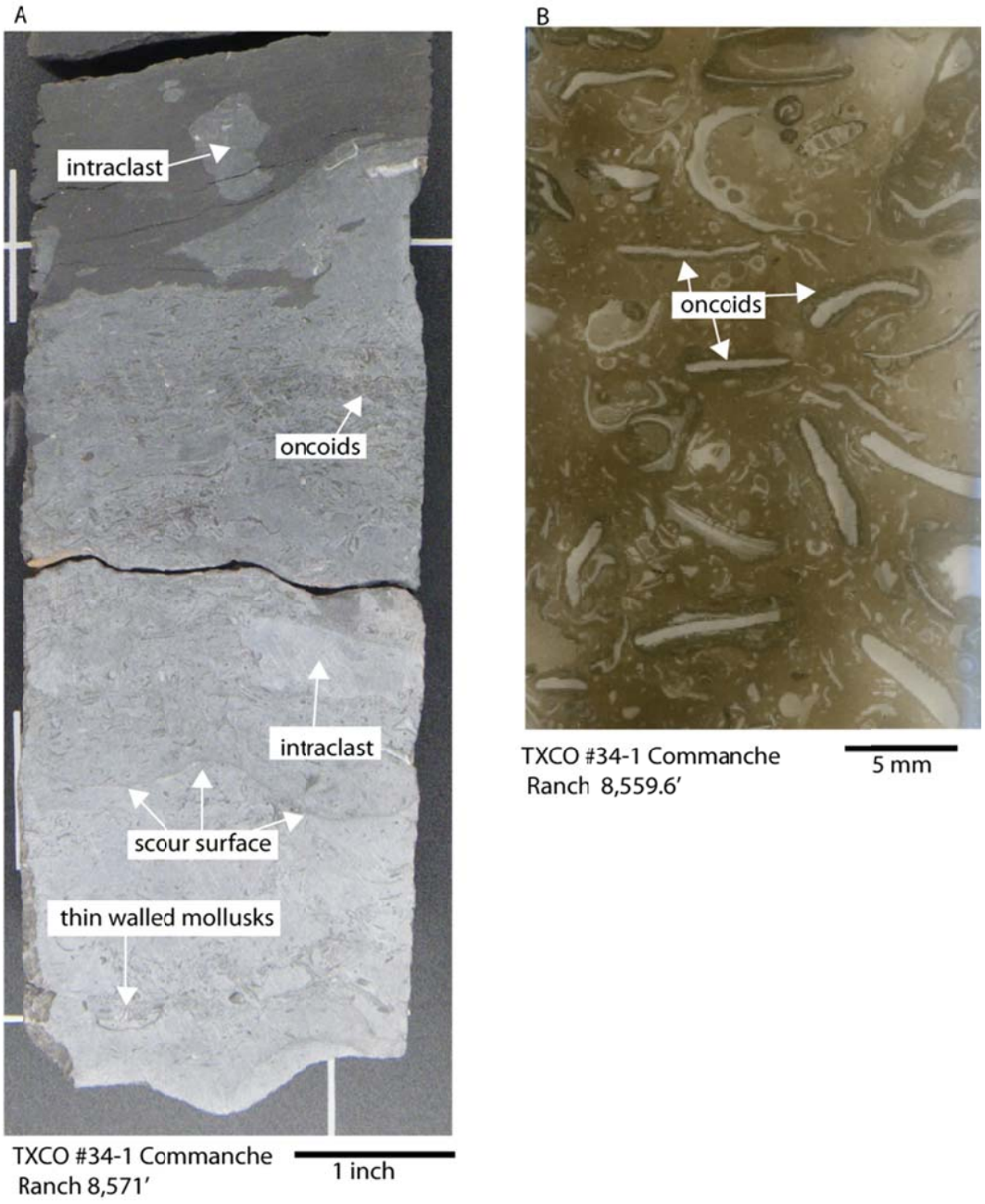

Figure 3.9: Skeletal oncolitic wackestone/ mud dominated packstone. (A) Core slab showing layers of skeletal material and intraclasts. (B) Thin-section scan showing some oncoids in a lime mud matrix.

Lime Mudstone

Lime mudstone (Figure 3.10) is composed mainly of lime mud with minor terrigenous material, and it is highly bioturbated. The lime mud shows a peloidal texture. The most common faunal components are foraminifers and fragments of echinoids and mollusks. Quartz and feldspar silt are present. The carbonate-rich mud is also distributed in nodules and beds (Figure 3.10B). The same textures found in the surrounding mud are not preserved inside the cemented lime mudstone, indicating that the facies never contained terrigenous mud. Some of the carbonate masses are interpreted as burrows filled with lime mud. Where there is a contact between carbonate mud and terrigenous mud there is evidence of differential compaction (Figure 3.10C). The terrigenous mud commonly exhibits some layering, whereas the carbonate mud exhibits none. Well-preserved *Favorina* pellets have been identified in the carbonate matrix. The facies was deposited on a low-energy, open-marine shelf and was periodically exposed to high-energy events, as evidenced by intraclasts and scour surfaces. Indicators of high-energy events and bioturbation suggest oxygenated conditions.

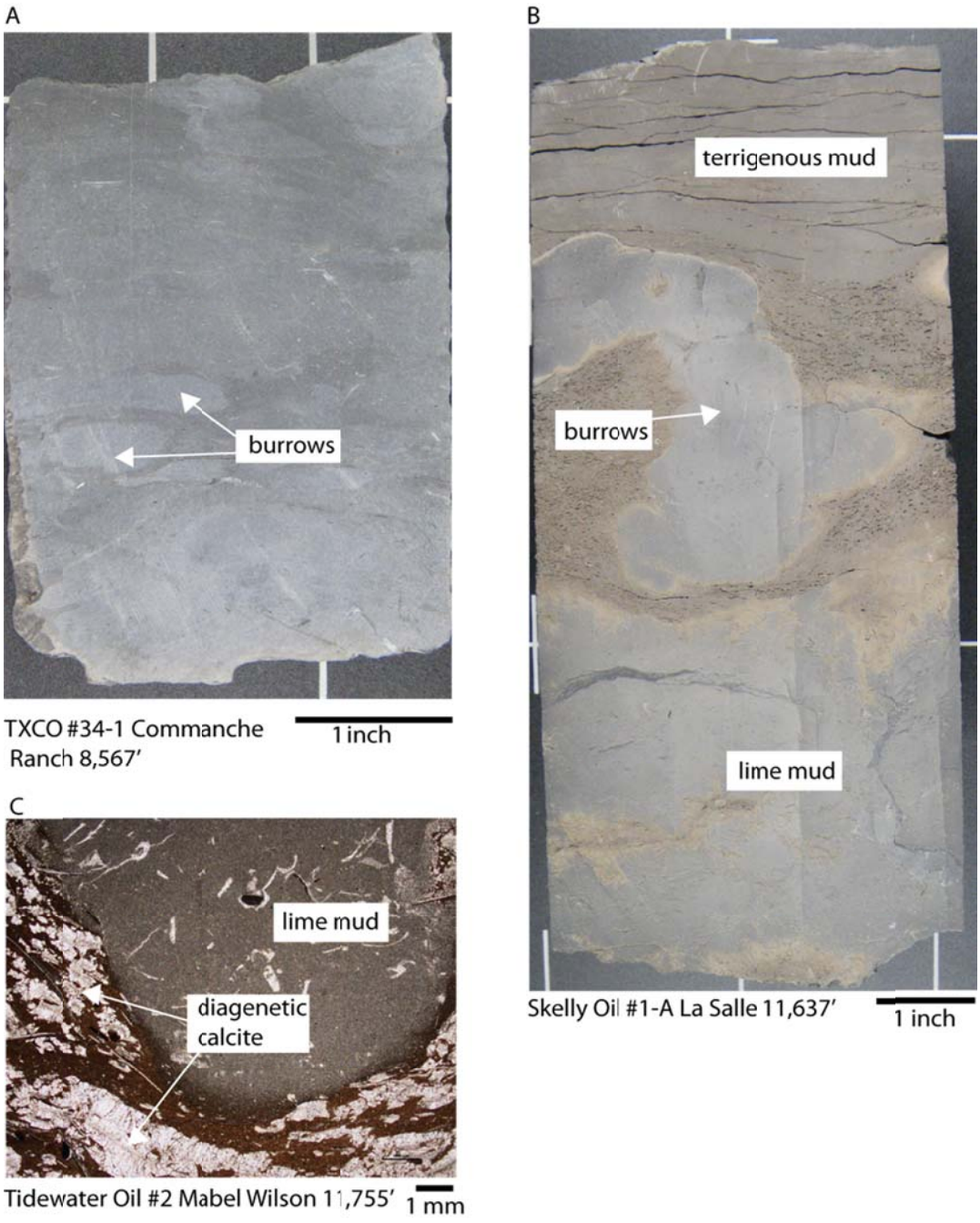

Figure 3.10: Lime mudstone. (A) Core slab showing the burrowed lime mudstone facies intermixed with terrigenous mud. The contact is dominated by burrowing structures, which were cemented early. (B) Core slab shell bed containing a large-mud-filled burrow with lime mudstone below. (C) Photomicrograph of the contact between lime mudstone and terrigenous mudstone. The mollusk shells in the terrigenous mudstone have diagenetic calcite overgrowths.

Skeletal Siltstone/ Terrigenous Mudstone

The skeletal siltstone/ terrigenous mudstone facies (Figure 3.11) was deposited on the outer ramp facies and has primarily terrigenous matrix. It is broadly equivalent in time to the shoal-water complexes that developed in the lower Bexar Shale and middle Bexar Shale Members. The facies is dominated by echinoids, thin-walled bivalves, and inoceramids. In some areas it contains layers of grain-dominated packstones several centimeters thick. These layers have large mollusks and oyster fragments, which are not noted elsewhere within the facies. TOC in this facies is highly variable, but the variability does not coincide with rock texture.

This facies contains fauna that was both living in place and transported into the area. Fragments of the larger mollusks and oysters are abraded and disorganized, therefore, they were probably reworked or transported. Transportation of fauna and shell material also probably occurred on a smaller scale in the form of cohesive mudflows (Mulder and Alexander; 2001). Some organisms, mainly echinoids and thin-walled mollusks are unbroken, which may indicate that they lived in place. These organisms, unlike the larger more robust mollusks, also required less oxygenated conditions than large mollusks and oysters (Arthur and Sageman, 1994). *Chondrites* and *Planolites* burrows are found in this facies, confirming that not all of the organisms were transported and that some organisms were living in the environment of deposition.

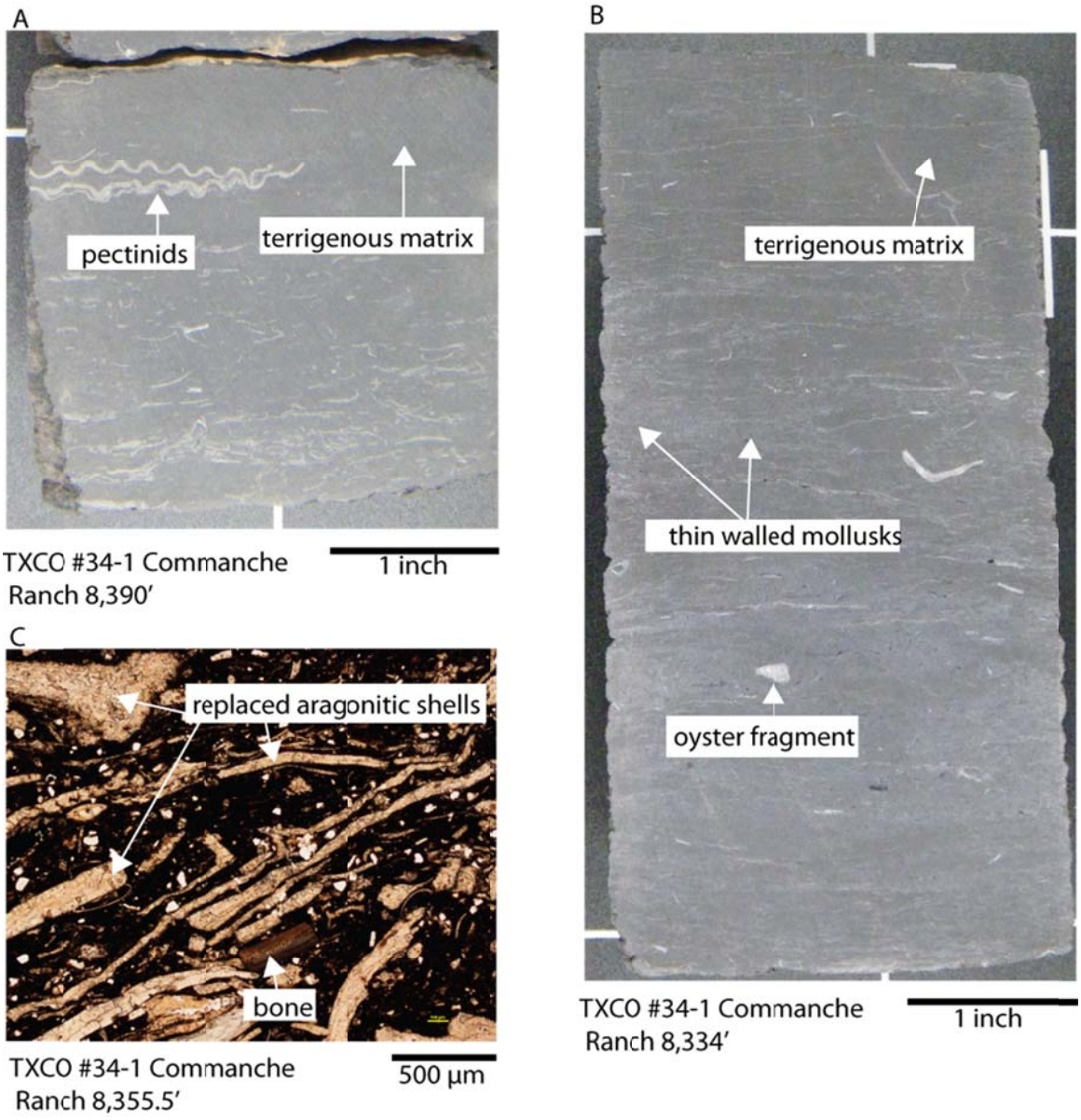

Figure 3.11: Skeletal siltstone/terrigenous mudstone. (A) Photograph of core showing larger pectinids. (B) Photograph displaying some fragmented oyster shells in a terrigenous mud matrix. (C) Photomicrograph showing the fragmented mollusks in a debris flow within the skeletal mudstone.

Weakly Laminated to Massive Calcite Silt-Bearing Terrigenous Mudstone

The weakly laminated to massive calcite-silt bearing terrigenous mudstone facies (Figure 3.12) contains few sedimentary structures and minor fauna. The laminations are

parallel and horizontal where they are distinct and are wide where they are diffuse. Some of the rocks in this facies are nonlaminated. The matrix contains approximately 40% silt and sand particles. The silt is siliciclastic and carbonate in composition. Much of the carbonate silt is inoceramid columns, pelagic foraminifera, and calcispheres. The fragmentation of the inoceramid columns indicates that the skeletal debris was reworked. There are also rare sponge spicules and radiolarians replaced with calcite. The siliciclastic silt is feldspar and detrital quartz. Ammonites, fish bones, echinoid fragments, and thin-walled mollusk fragments are also present. Most of the remaining matrix is peloidal clay with minor carbonate content.

The sediment was deposited in an open-marine setting on the outer ramp. There are several explanations for the weakly laminated to massive character of this facies. It is possible that it was deposited by hypopycnal plumes, by dilute hyperpycnal flows, or by slowly accumulating suspension deposits of anoxic laminites under restricted conditions (Bhattacharya and MacEachern, 2009). Alternatively the sediment could have been bioturbated by meiofauna, which would subtly mix the sediment while still preserving some lamination (Levin, 1994; Pike, 2001; Pemberton et al., 2008). This biological activity, if it occurred, had little effect on TOC preservation. Given the slow rates of deposition calculated (Li et al., 2008; Phelps, 2011; this study), this facies was most likely deposited as an anoxic laminite rather than by a process which requires faster rates of sedimentation (Bhattacharya and MacEachern, 2009). Based on the peloidal texture it was probably transported by bottom currents and dilute turbidites (O'Brien, 1996; Mulder and Alexander, 2001; Loucks and Ruppel, 2007; Schieber et al., 2007). Hyperpycnal flows may have transported some of the sediment and deposited finely laminated layer, but evidence of these laminations was destroyed by compaction.

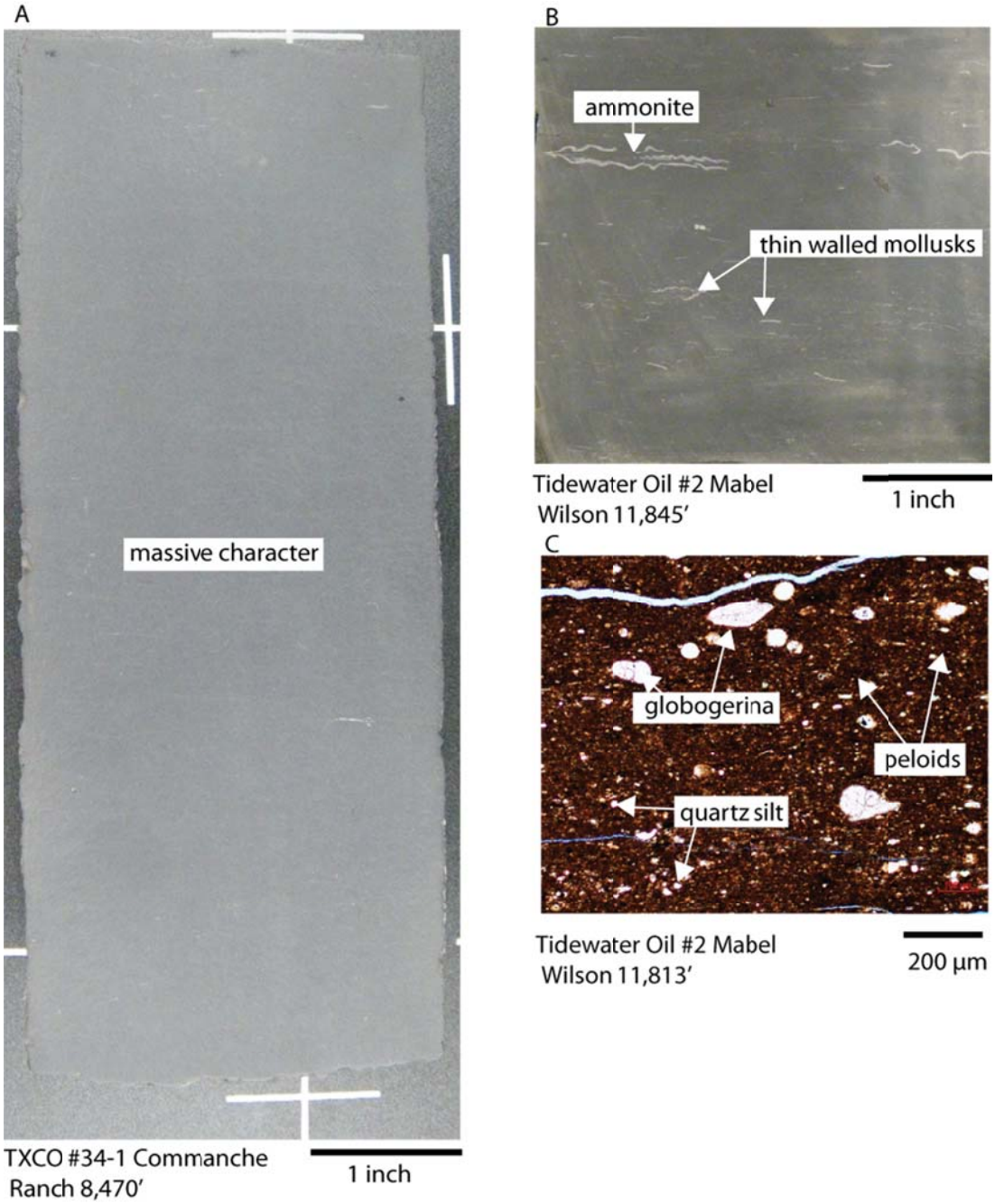

Figure 3.12: Weakly laminated to massive calcite silt-bearing terrigenous mudstone. (A) Core slab showing massive mudstone. (B) Core slab with ammonite cross-section visible in the upper left corner and evidence of lamination can be seen because of the slight increase in skeletal material. (C) Abundant pelagic forams and calcispheres are visible in a peloidal matrix.

Burrowed Calcite Silt-Bearing Terrigenous Mudstone

The burrowed carbonate silt-bearing siliciclastic mudstone (Figure 3.13) has a matrix very similar to that of the weakly laminated to massive calcite silt-bearing terrigenous mudstone. They both have similar silt content, sedimentary structures, fossils, and laminations. However, the critical difference is that this facies commonly features large *Planolites* and *Chondrites* burrows, whereas the massive to weakly laminated mudstone facies do not. These burrows indicate that environmental conditions were different with respect to oxygenation level. The burrows are carbonate cemented, adding to the carbonate content of this facies. The size and shape of some of the burrows match those made by echinoids (Kanazawa, 1992).

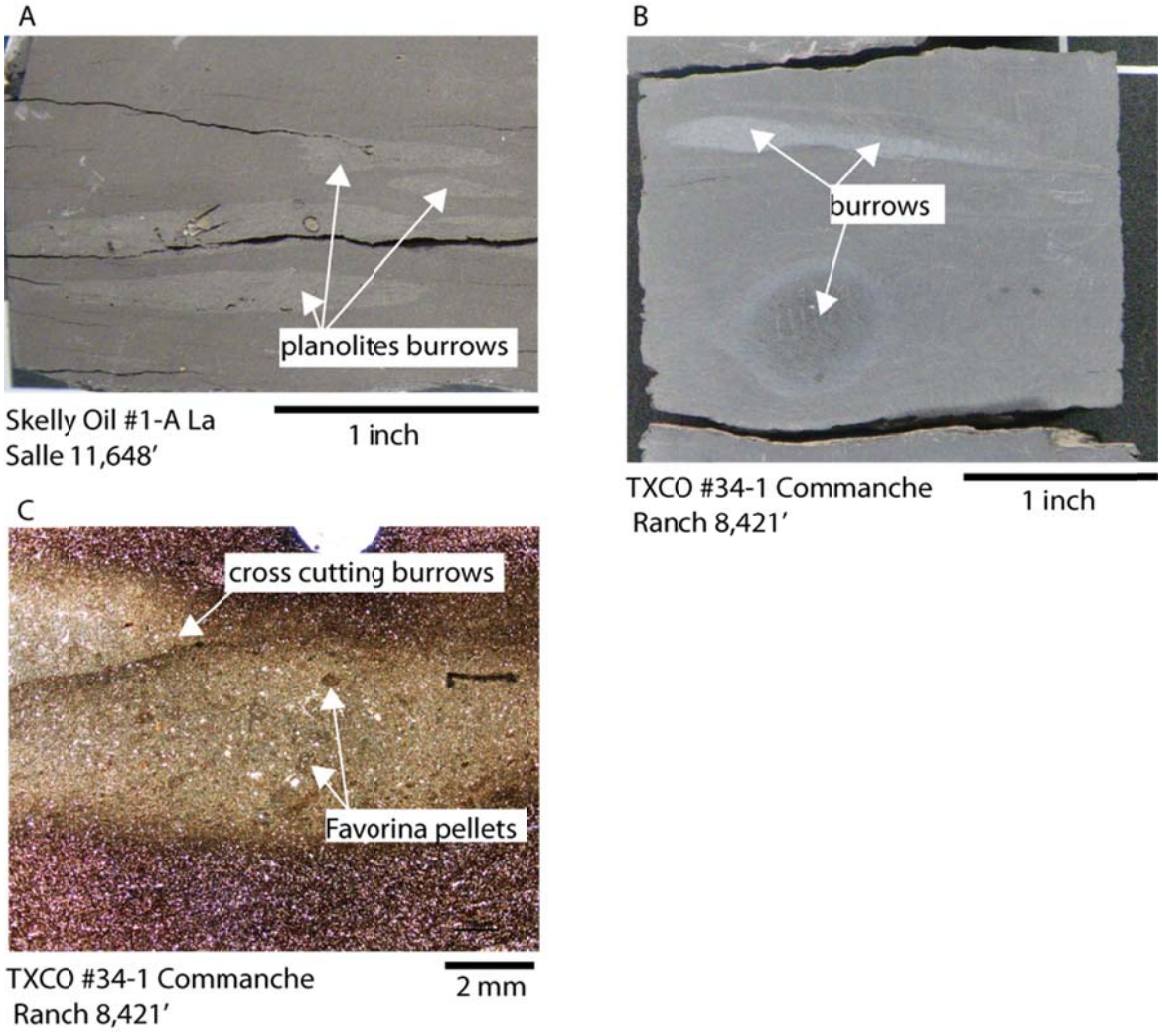

Figure 3.13: Burrowed calcite silt-bearing terrigenous mudstone. (A) Photograph displaying *Planolites* burrows in a massive matrix. (B) Photograph showing different burrow morphologies. The burrows are interpreted as being cemented early because of compaction of sediment around them. (C) Early calcite cemented burrows. Burrows contain well-developed *Favorina* pellets, as can be seen in this thin section.

Winnowed Nonbioturbated Calcite Silt-Bearing Terrigenous Mudstone

Similar to the burrowed calcite silt-bearing terrigenous mudstone facies, the winnowed nonbioturbated calcite silt-bearing terrigenous mudstone bears a strong resemblance to the weakly laminated to massive calcite silt-bearing terrigenous

mudstone. This facies is distinguished by abundant silt-rich laminae and lack of fossils or bioturbation. Many of these laminae are graded and truncated by scour surfaces. The deposits are ungraded or fining-upward. Many of the fining-upward deposits cap a scour surface and are interpreted to be dilute turbidites. Some of the silt layers are interpreted to be starved ripples similar to those seen in the Barnett Shale (Loucks and Ruppel, 2007) There are also ungraded deposits of reworked and concentrated pyrite and sponge spicules material on scoured mud contacts. These deposits along with the starved ripples are interpreted to be winnowed lag deposited by deep bottom currents. These lags form when bottom currents remove the mud from the sediment and concentrate the silt-size particles (Schieber, 1996). Truncation surfaces tend to be very low angle and normally contain rare grains, which are concentrated by the winnowing processes. The lack of burrowing and silt deposits coincides with the presence of higher TOC values. This facies consistently shows some of the highest TOC values (between 1 and 6%) in the Pearsall Formation. This facies is interpreted to having been deposited in one of the most oxygen-starved facies of the Pearsall Formation. Additionally, there are aggregates probably related to hemipelagic sedimentation.

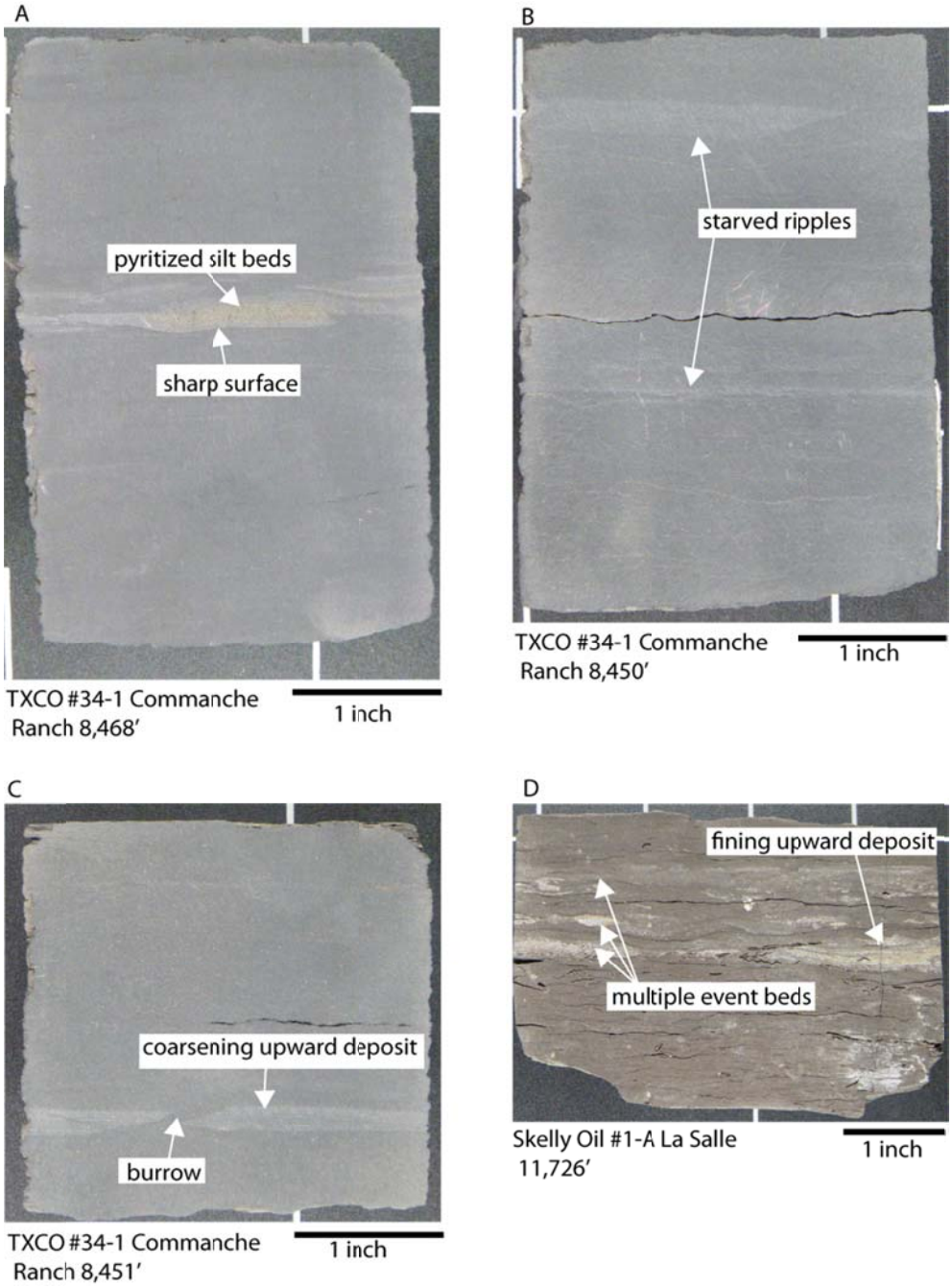

Figure 3.14: Winnowed nonbioturbated calcite silt-bearing terrigenous mudstone. (A) Core slab showing pyritized winnowed deposit. (B) Core slab with multiple starved ripples (C) Core slab with winnowed deposit and a solitary cross cutting burrow, likely by a "doomed pioneer." (D) Multiple stacked fining upward deposits; many of the grains have been pyritized.

Lithoclast-Rich Skeletal Lime Rudstone

In several of the cores, debris flow deposits were consisting of lithoclast-rich skeletal lime rudstone were noted (Figure 3.15). These deposits contain large angular clasts, some of which measure at least 5 cm across (Figure 3.15). The clasts are predominantly limestone and show borings related to sponges and algae. Pyrite replacement of the clasts is common, especially in proximity to the borings. The clasts are suspended in a relatively structureless mud matrix. Bedding thicknesses of this facies are rarely more than 0.3 m thick and may be as thin as 1 cm. The largest clasts are commonly found at the top of the beds, which is characteristic of debris flow (Mulder and Alexander (2001). Large skeletal fragments are also found in these flows.

These density flows are interpreted as debris flows, following the classification of Mulder and Alexander (2001). This is based on the sorting of the larger clasts to the top of the flow and the angular shape of the clasts. These flows are dominantly cohesive in that the particles do not typically move within the flow as they are transported. Therefore particles can be transported unbraided. The flows are supported by the matrix strength, pore pressure, and grain to grain contacts rather than suspension from the turbid currents created by the flow itself (Mulder and Alexander, 2001). These debris flows were most prominently identified in the cores found in the area of the northeast corner of La Salle County. There the cores are positioned in a reentrant associated with the Atascosa Trough. The skeletal-rich debris flows are may be associated with highstand shedding similar to what Schlager et al. (1994) observed. This is based on the position of the deposits near major third-order sequence boundaries, notably in the lower Bexar Shale Member, and the prevailing interpretation of the paleogeography.

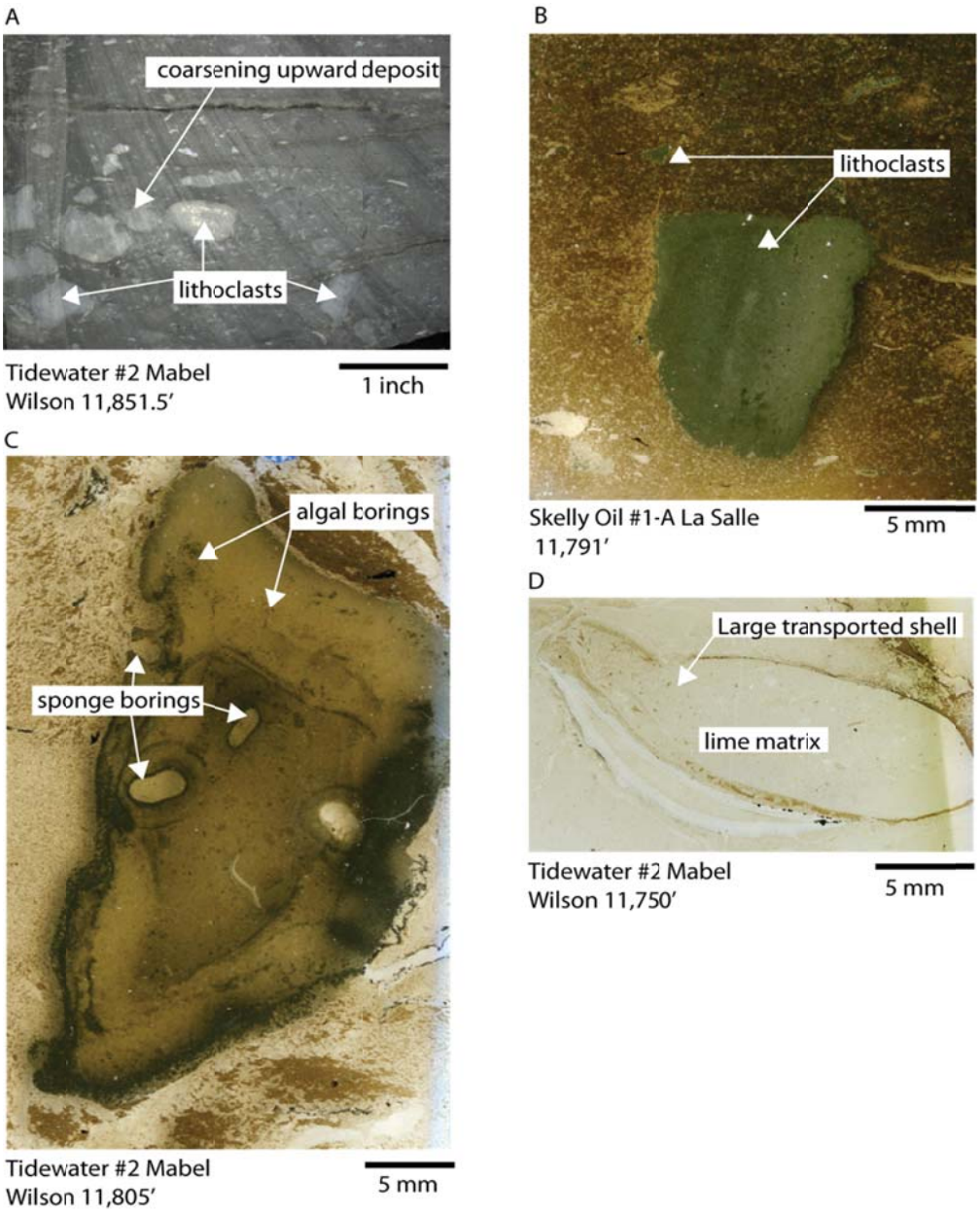

Figure 3.15: Lithoclast-rich skeletal lime rudstone. Core (A) Debris flow with larger lithoclasts sorted to the top. (B) Large unbored lithoclasts. (C) Large bored lithoclast with both sponge and algal borings and diagenetic alteration. (D) Example of larger skeletal material incorporated into the flows and lime matrix. These deposits are associated with highstand shedding.

PEARSALL LITHOFACIES MAPS

General Statement

Lithofacies maps were developed for all the members of the Pearsall Formation by combining core descriptions with wireline-log data. Paleogeographic information is incorporated into the facies interpretations. The goal of facies mapping is to document the distribution of the mudrock-rich units and to predict facies in the outer ramp area that is potential for shale-gas reservoirs. Similar to what was done in the middle ramp mapping by Loucks (1976, 1977) the wireline logs are calibrated with core data. In many cases this is very difficult given the age of the logs and the homogeneity of wireline-logs in mudrocks, adding an element of uncertainty to the maps produced.

Pine Island Shale Member Lithofacies Distribution

The interval of the Pine Island Shale Member that was mapped in Figure 3.16 is near the middle of the unit, which includes the oyster chondrodont biostrome in the area of the Pearsall Arch. Surrounding this biostrome is a peloidal terrigenous siltstone that grades updip into a clastic shoreface complex around the Llano Uplift, which is not preserved (Stricklin et al., 1971) The peloidal terrigenous siltstone is bioturbated. This facies contains storm deposits. Seaward return of flow during storms may have transported terrigenous mud into the outer ramp as suggested by Kelling and Mullins, (1974). Downdip the facies rapidly grades into less bioturbated terrigenous mudstones that are also probably related to storms. More distally the formation grades into nonbioturbated pelagic and hemipelagic facies deposited in the oxygen minimum zone (dysoxic to anoxic environment). The majority of carbonate material in this distal sediment is derived from pelagic and nektonic organisms. The Atascosa Trough and the Maverick Basin depocenter (Figure 2.3) had a pronounced effect on facies distribution,

causing outer ramp facies to extend north. The San Marcos Arch is significant as it causes the Maverick Basin to narrow and constricts the facies belts.

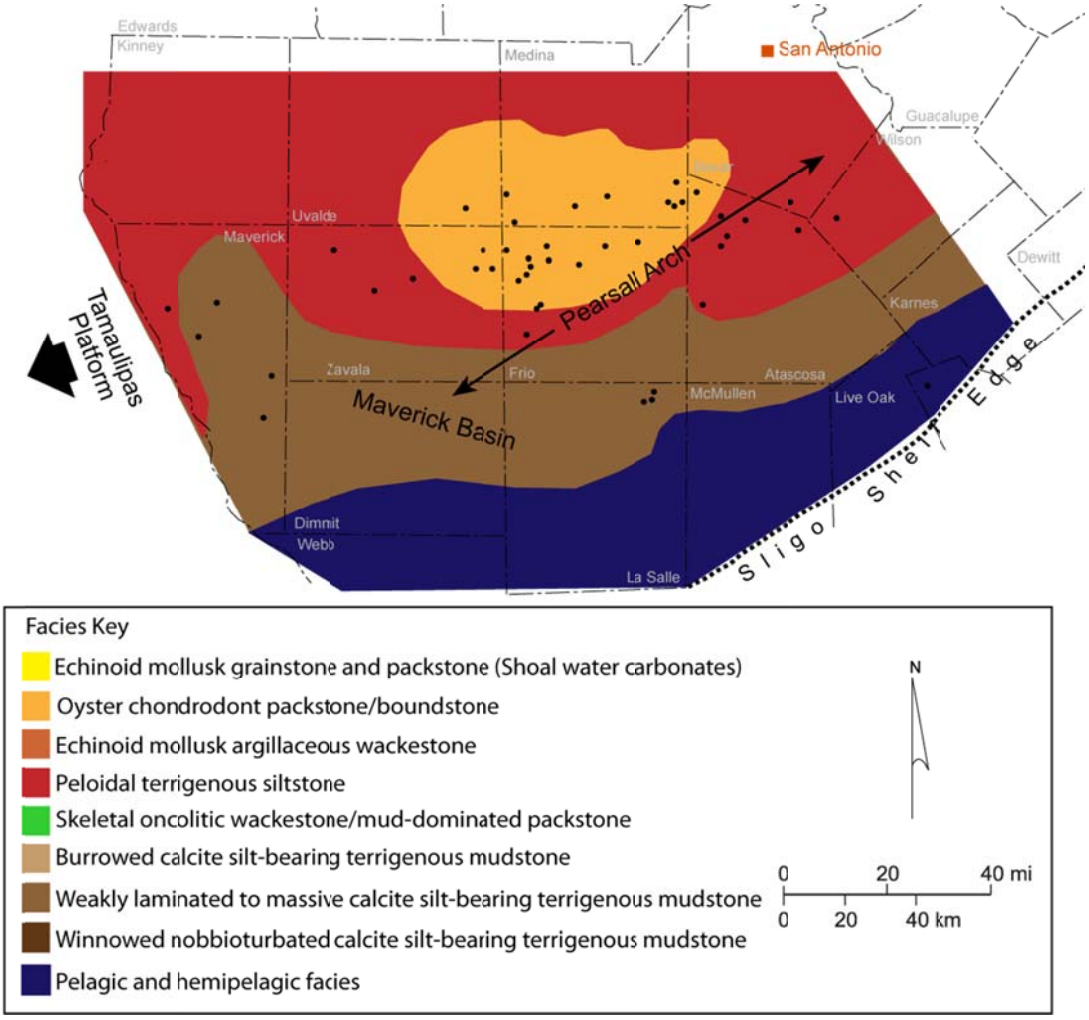

Figure 3.16: Pine Island Shale Member lithofacies map (Modified from Loucks, 1976).

Lower Cow Creek Member Lithofacies Distribution

The lower Cow Creek Member lithofacies map (Figure 3.17) shows the limited recovery of the carbonate system following deposition of the Pine Island Shale Member. Although much of the lower Cow Creek Member is still composed of terrigenous sediment, larger areas of carbonate sediment appear in this interval. The carbonate

organisms are mostly echinoderms and mollusks, both of which are tolerant of low-oxygen conditions (Arthur and Sageman, 1994). These and other organisms were abundant enough to produce argillaceous wackestones in the outer ramp. Robust carbonate sedimentation began on top of the Pearsall Arch (Loucks, 1976). In addition, carbonate shoals started to form and prograde adjacent to the Burro Salado Arch in the west. These shoal-water complexes are seen in the Dilly #1 Ritchie core. Seaward of the Pearsall Arch the ramp remained starved of carbonate sediment during the lower Cow Creek deposition. In this area the sediment was dominated by laminated muds that were preserved as weakly laminated to massive calcite silt bearing terrigenous mudstones.

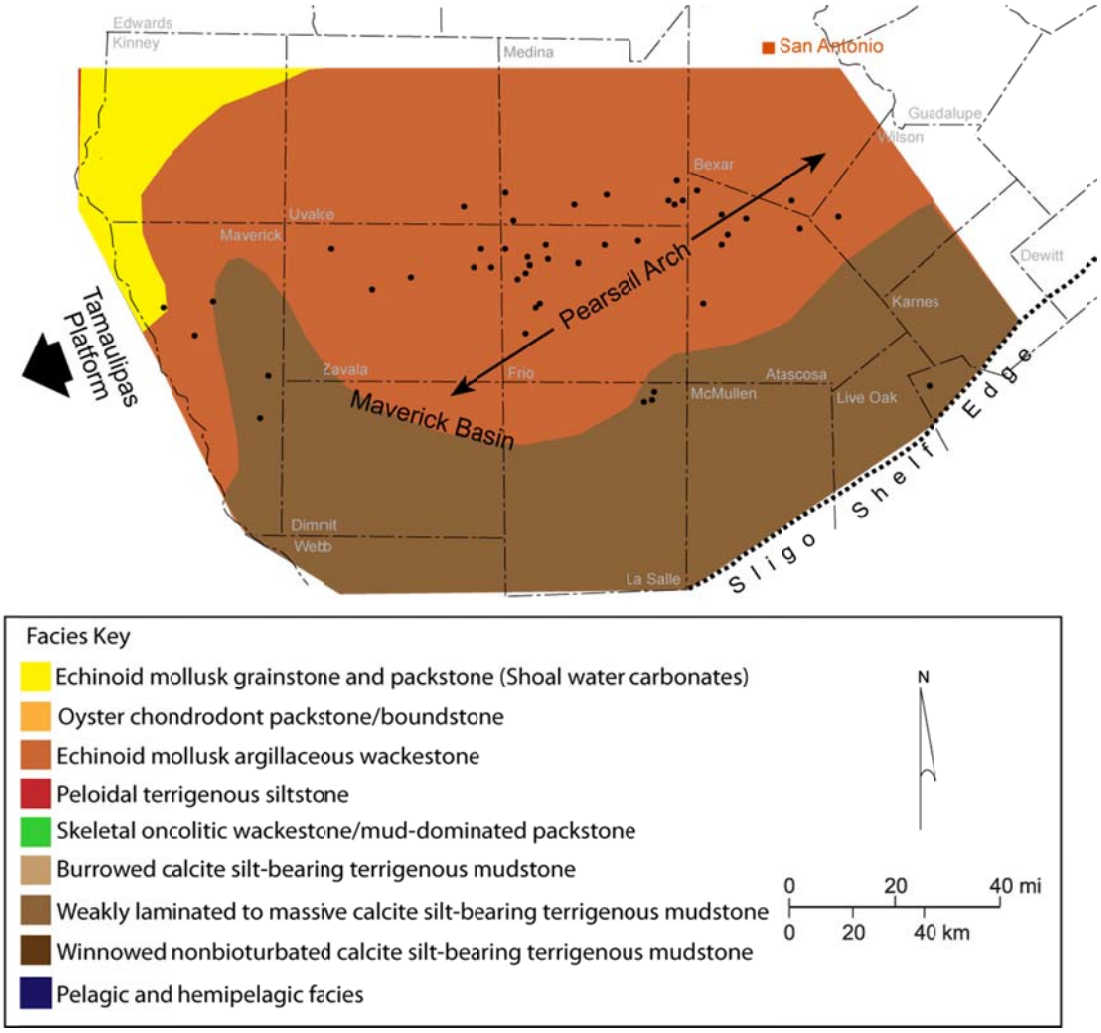

Figure 3.17: Lower Cow Creek Member lithofacies map (Modified from Loucks, 1976).

Upper Cow Creek Member Lithofacies Distribution

The upper Cow Creek Member (Figure 3.18) features the largest carbonate complex developed during Pearsall time (Loucks, 1976). This complex extends from north of the San Marcos Arch all the way across the study area. Seaward of the complex is an apron of skeletal oncolitic wackestone/ mud-dominated packstone that was deposited in moderate energy and water depths. Also in front of the shoals echinoid mollusk wackestone was deposited. Further seaward is the burrowed calcite silt bearing

terrigenous mudstone. Weakly laminated to massive calcite silt bearing terrigenous mudstone and pelagic and hemipelagic mudstones are expected on the outer most area of the ramp near the shelf edge.

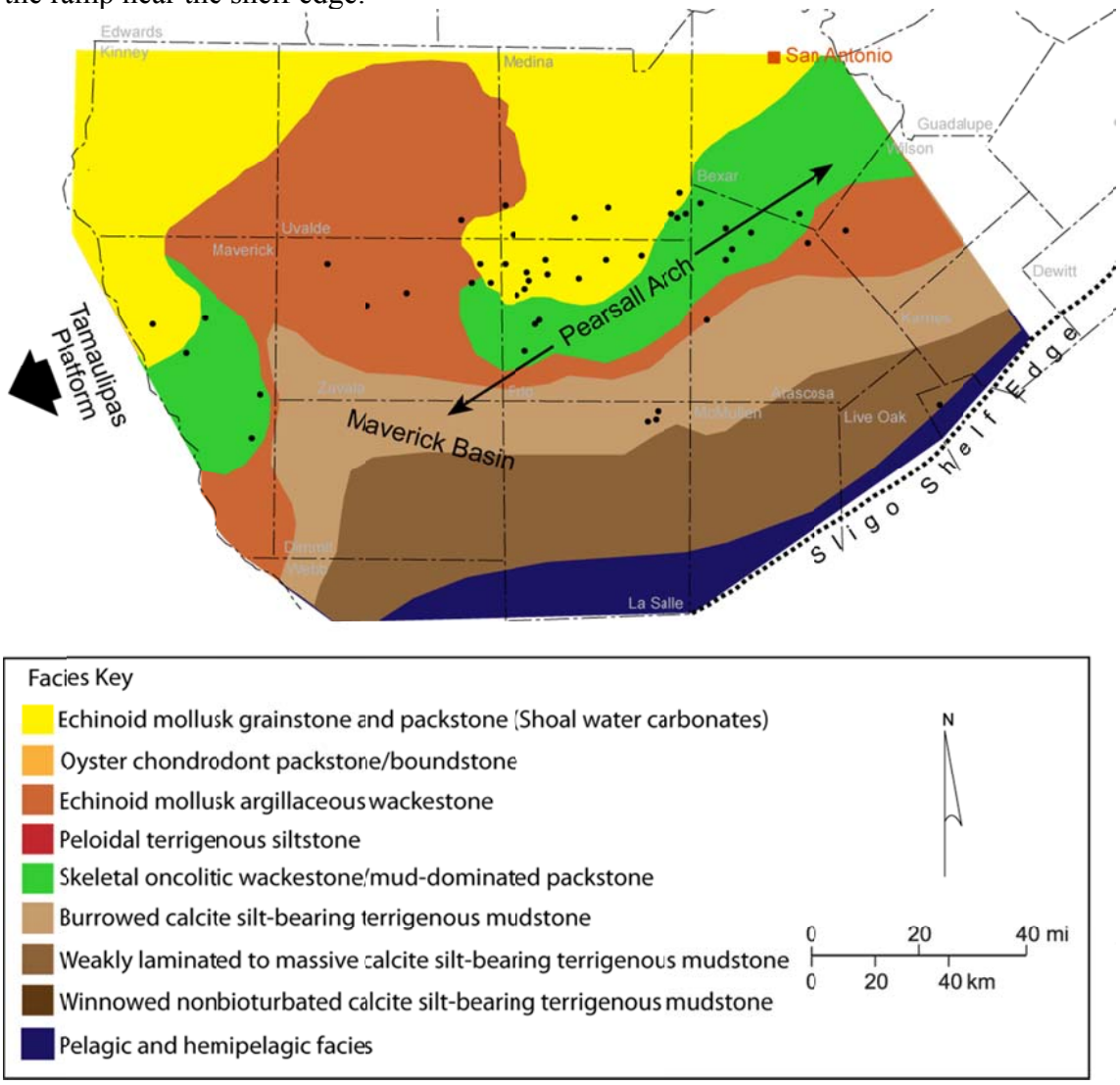

Figure 3.18: Upper Cow Creek Member lithofacies map (Modified from Loucks, 1976).

Lower Bexar Shale Member Lithofacies Distribution

Most of the lower Bexar Shale Member lithofacies (Figure 3.19) in the outer ramp are dominated by terrigenous material. In the middle ramp during lower Bexar Shale

sedimentation echinoid mollusk argillaceous wackestones and peloidal terrigenous siltstones formed. These deposits show storm influence similar to that seen in the Pine Island Shale Member, but the middle ramp terrigenous siltstones tend to be very thin because of non-deposition or erosion. In the later part of the lower Bexar Shale time, a shoal-water complex developed on the middle ramp. Moving down-dip, in this time interval, the succession becomes muddier. Further seaward, there is less silt and skeletal material and more preserved organic matter. Lithofacies grade from peloidal terrigenous siltstones into burrowed calcite silt-bearing terrigenous mudstones, into massive to weakly laminated calcite silt-bearing terrigenous mudstone, and finally into the winnowed calcite silt-bearing terrigenous mudstone facies. This winnowed terrigenous mudstone facies grades into a mixed hemipelagic and pelagic facies near the paleo-Sligo Reef Margin. The paleostructure affected the lower Bexar facies deposition in a similar manner as it did the Pine Island Shale deposition.

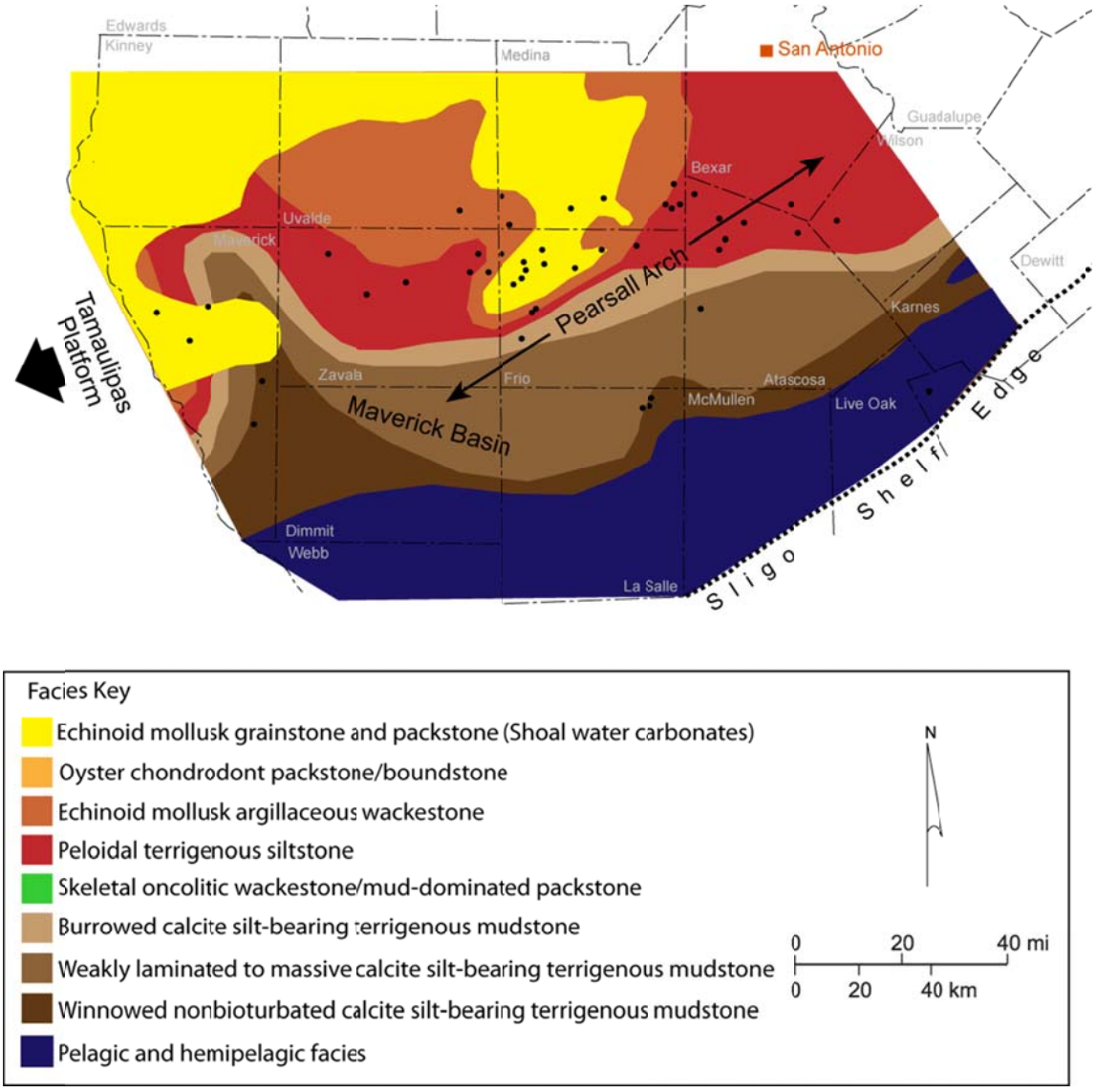

Figure 3.19: Lower Bexar Shale Member lithofacies map (Modified from Loucks, 1976).

Middle Bexar Shale Member Lithofacies Distribution

The middle Bexar Shale Member (Figure 3.20), unlike the Pine Island Shale and lower Bexar Shale Members, was deposited in a period of worldwide paleo-ocean oxygenation. Figure 3.20 shows the lower middle Bexar Shale Member with scattered shoal water carbonate complexes in the western half of the study area. Wackestones

developed around the shoal-water carbonate complexes in the middle ramp. These argillaceous wackestones developed with abundant carbonate fauna and large silt in a primarily terrigenous matrix. Storms, bottom currents, and bioturbation mixed and transported this sediment. The limited and scattered distribution of carbonate shoal complexes relative to the shoal complexes of the lower Bexar Shale Member reflects continued transgression through Bexar Shale time.

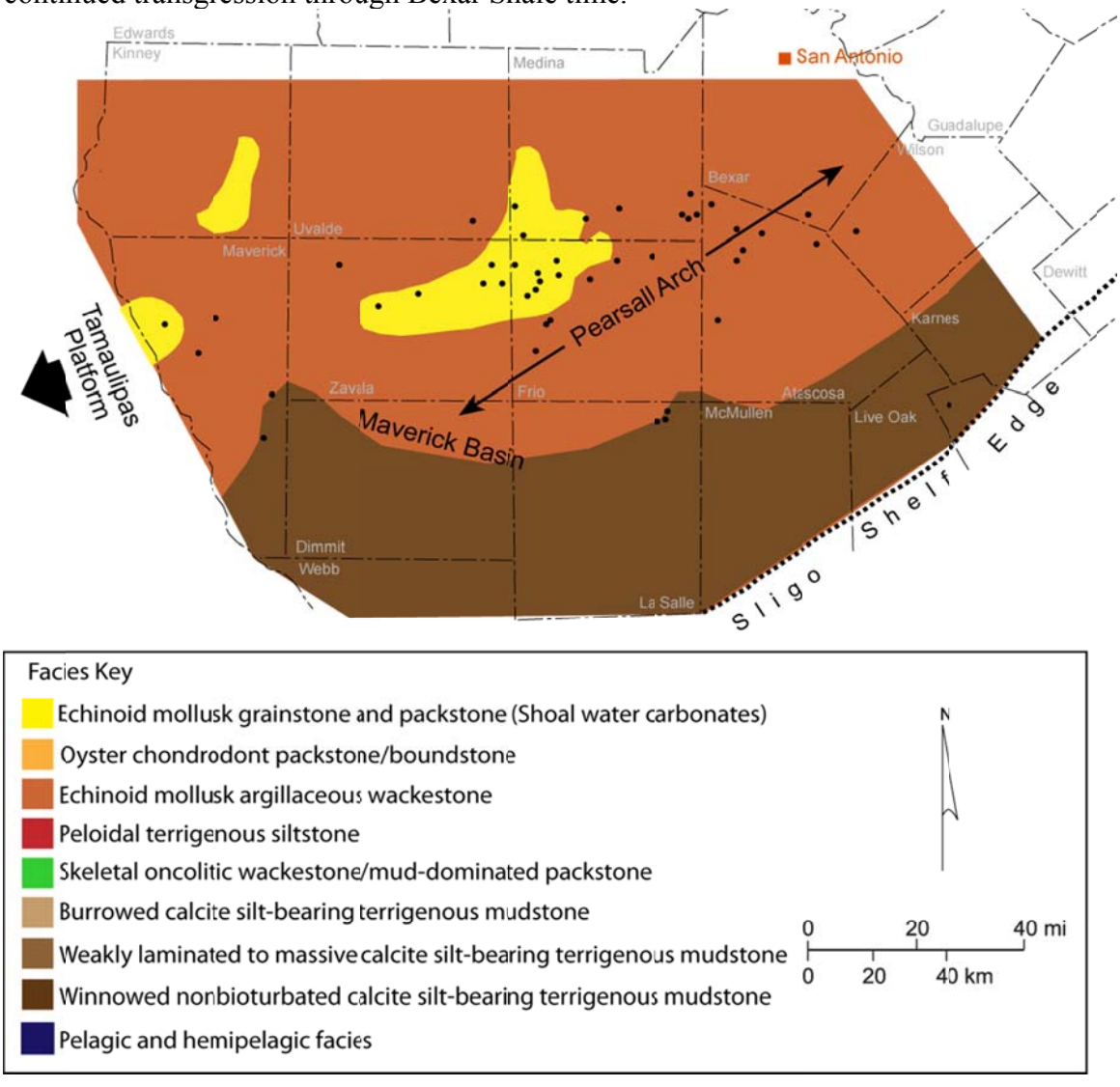

Figure 3.20: Middle Bexar Shale Member lithofacies map (Modified from Loucks, 1976).

Upper Bexar Shale Member Lithofacies Distribution

The upper Bexar Shale Member (Figure 3.21) had the least amount of core to analyze in the study area. It also has associated problems in correlation because the poorly defined boundary with the Glen Rose Formation and the boundary may be highly diachronous. The upper Bexar Shale Member was deposited during the OAE 1-B in South Texas, and it has similar lithofacies as the Pine Island Shale Member, which was deposited during the OAE 1-A event. Neither subsidence over the paleo-Triassic rift, nor the Atascosa and Karnes Troughs appear to have had an effect on the lithofacies distributions. The San Marcos Arch still prominently affected the facies distributions. Above the Pearsall Arch an oyster chondrodont biostrome developed as it did in the Pine Island Shale Member surrounded by peloidal terrigenous siltstone.

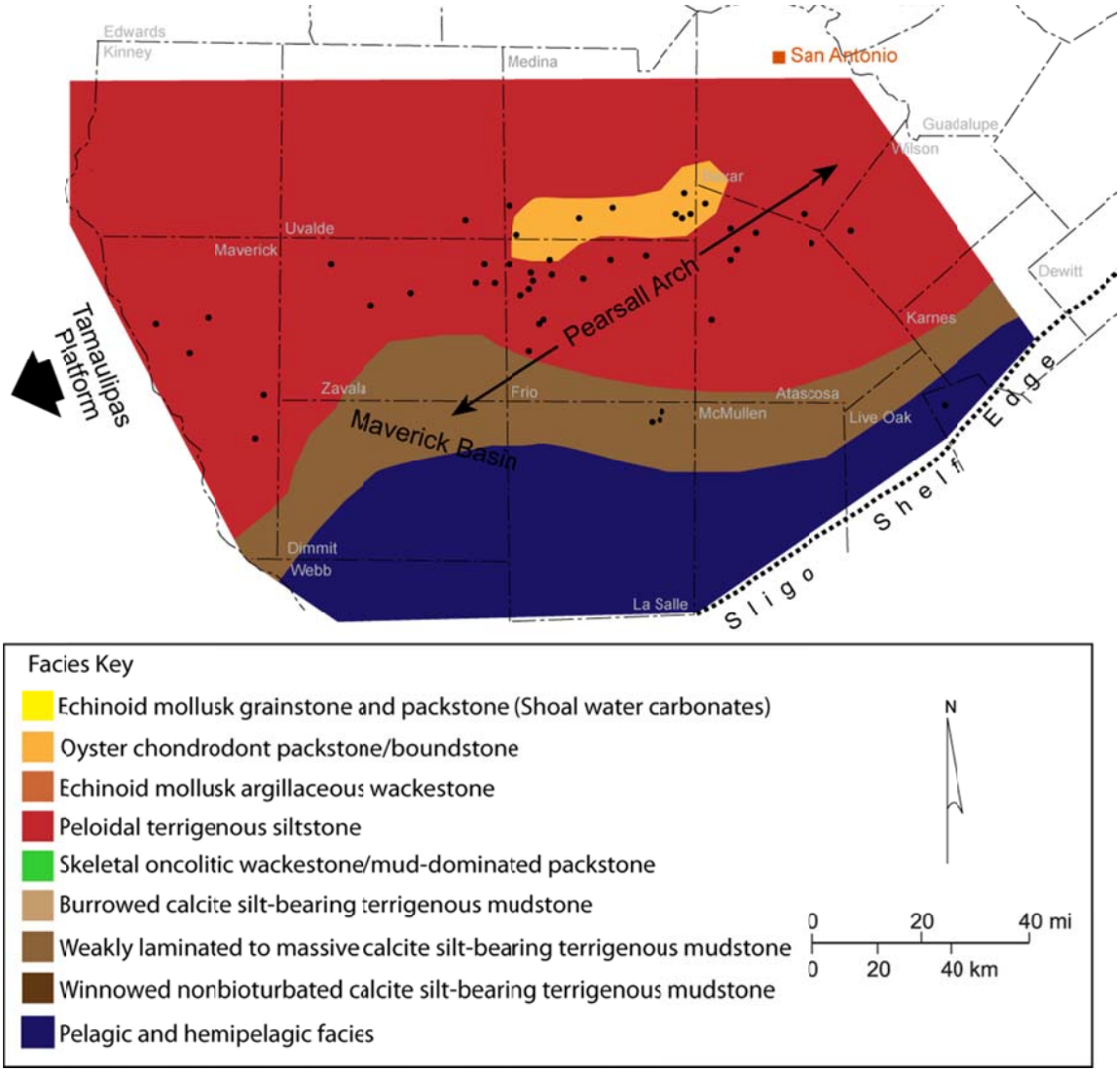

Figure 3.21: Upper Bexar Shale Member lithofacies map (Modified from Loucks, 1976).

LITHOFACIES VARIABILITY AND LITHOFACIES STACKING

In the Pearsall Formation, lithofacies vary both temporally and spatially with eustatic sea-level changes and with the onset and recovery from OAEs. Horizontal variations tend to be more process oriented and reflect changes in energy conditions, whereas vertical changes tend to correlate to changes in the oxygenation levels and associated environments.

Moving from updip to downdip there is a gradual change in lithofacies across the ramp based on changes in processes and depositional styles similar to what is observed in other mudstone systems such as the Fayetteville Shale (Handford, 1986) and the Eagleford Shale (Harbor, 2011). A schematic diagram of this gradual change as observed in the Pearsall Formation is shown in Figure 3.22. In the updip area the rocks tend to be high-energy deposits, such as grainstones, packstones, or siltstones. These deposits typically exhibit cross-bedding and other sedimentological features indicative of higher energy conditions and the siltstones commonly show signs of being deposited by storms such as hummocky cross stratification. Moving downdip the lithofacies grade into more terrigenous and weakly laminated to massive strata. This more distal strata was deposited by dilute turbidity currents, and contour currents transporting sediment along strike similar to much of the sedimentation in the Barnett Shale (Loucks and Ruppel, 2007). This strata contains thin-walled bivalves and other deep-water fauna. Bioturbation is responsible for the massive character and the lack of turbidites and tempestites. Still further downdip the facies grade into nonbioturbated winnowed lithofacies. This last lithofacies lacked coarser grained skeletal content even relative to other outer ramp facies. It is also one of the least bioturbated facies and preserved event beds. This facies grades into strata originally composed of pelagic and hemipelagic sediments. Pelagic foraminifera are abundant. In general, the carbonate content decreases from updip to downdip but in the seaward most lithofacies it increases in carbonate content as a result of deposition from of pelagic carbonate organisms.

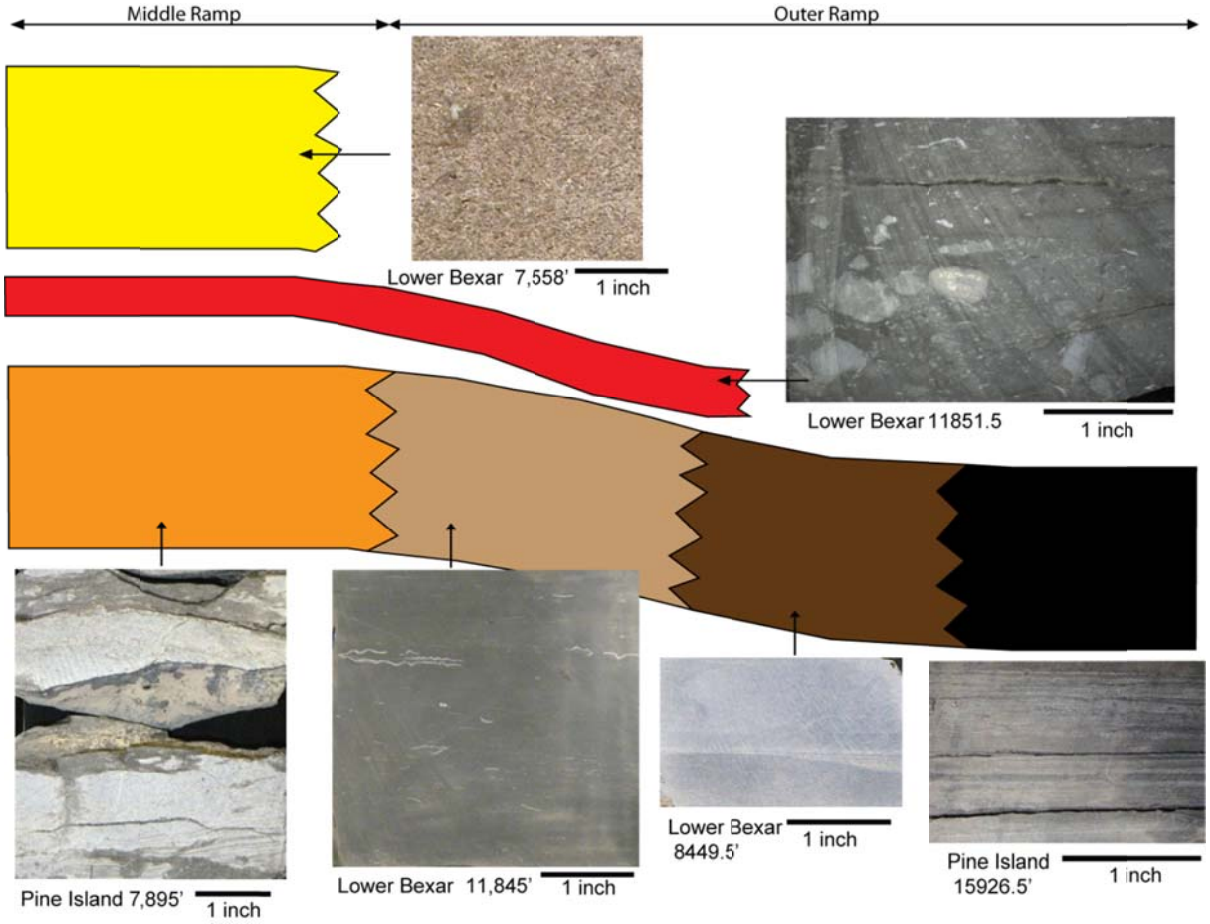

Figure 3.22 Horizontal facies variability. Facies grade from higher energy packstones, grainstones, and siltstones through lower energy massive to weakly laminated terrigenous mudstones, and finally into pelagic and hemipelagic facies. These lithofacies belts grade into each other. Debris flows (red) can transport material between facies zones.

Vertically, the sediments vary because of environmental change and eustatic events. These changes are described in Figure 3.23 and Figure 3.24 for the Pine Island Shale and lower and middle Bexar Shale Members.

Lithofacies stacking in the middle-ramp Pine Island Shale Member is discussed in Loucks (1976) and expanded here and in Figure 3.23. At the base of the Pine Island Shale Member, contact with the Sligo Formation there is an erosional surface as evidenced by a skeletal lag and scour surface. This is a third-order sequence boundary. The 2nd order MFS occurs above this as evidenced by laminated peloidal terrigenous siltstones and a decrease in sedimentary structures related to fair weather wavebase and storm activity. The oyster chondrodont biostrome occurs above the MFS, and in association with the OAE 1-A discussed in the next chapter. Moving further up in the section the facies become more calcareous and there is more evidence of shallow water processes occurring in the form of wave created features. The argillaceous wackestones also become more prevalent as the Pine Island Shale Member transitions into the lower Cow Creek Member, and the dominant organisms are echinoids and thin walled mollusks.

Lithofacies patterns in the outer ramp are difficult to discern as only one core is available from the outer ramp Pine Island Shale Member for analysis (Shell #1-R Roessler). Based on nannofossil data, the Roessler cored interval is at the top of the Pine Island Shale Member. The abundance of ammonites in the lower section of the core as well as the presence of *C. Margerelli*, a key nannofossil indicative of dysoxic conditions (Lees et al., 2005), suggests the core captures the top of the OAE 1-A.

The core displays alternating layers of pelagic and hemipelagic mudstone with intervening thin layers of Fe-rich dolomitic mudstone. The stacking is thought to consist of interbedded layers of pelagic and hemipelagic facies. The pelagic facies, based on log signature, appears to be more dominant in the middle of the Pine Island section, which

may be equivalent to the oyster chondrodont biostrome in the middle ramp. At the base of the Pine Island according to Bebout et al. (1981) the contact with the Sligo Formation in the outer ramp area is gradational, where it is erosive in the middle ramp. At the top of the outer ramp Pine Island Shale Member, the hemipelagic facies appears to be more common and this eventually grades into argillaceous wackestones of the Lower Cow Creek.

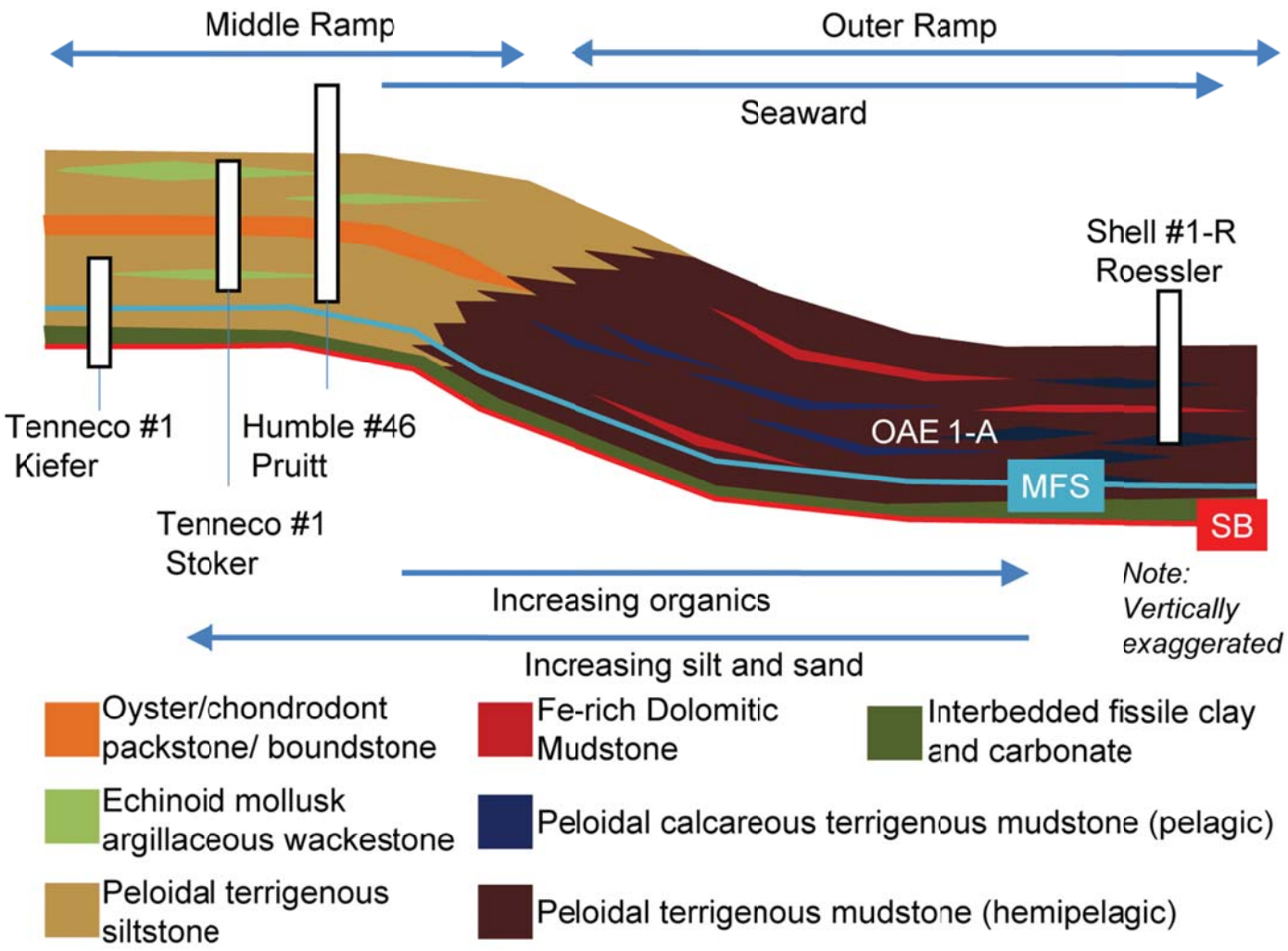

Figure 3.23 Pine Island Shale lithofacies stacking.

In the lower Bexar Shale Member the lithofacies stacking is illustrated in figure 3.24. The stacking is distinctly different in the middle ramp due to the development of shoal water complexes which overly a very thin peloidal terrigenous siltstone. In the outer ramp the terrigenous facies become far more prevalent. At the base of the section near the top of the Cow Creek Member, lime mudstones are well developed on top of the Skeletal oncolitic wackestones and mud dominated packstones of the upper Cow Creek Member. This grades into a terrigenous matrix of the burrowed calcite silt bearing terrigenous mudstone, which features *Planolites* burrows similar to the lime mudstone, but is also weakly laminated. The MFS of the third order sequence is at the top of this package on the basis of wireline logs and lamination. Above the MFS the winnowed nonbioturbated calcite silt bearing terrigenous mudstone is dominant and the expression of the regional OAE in the lower Bexar Shale. This facies also features some elements of a pelagic and hemipelagic facies. Moving upward in the section the facies become richer in skeletal material as the OAE subsides and shallowing associated with the top of the lower Bexar 3rd order sequence. Following the sequence boundary, massive to weakly laminated to massive calcite silt-bearing terrigenous mudstones become dominant in the regressive portion of the middle Bexar Shale Member. This sequence is unaccompanied by an OAE.

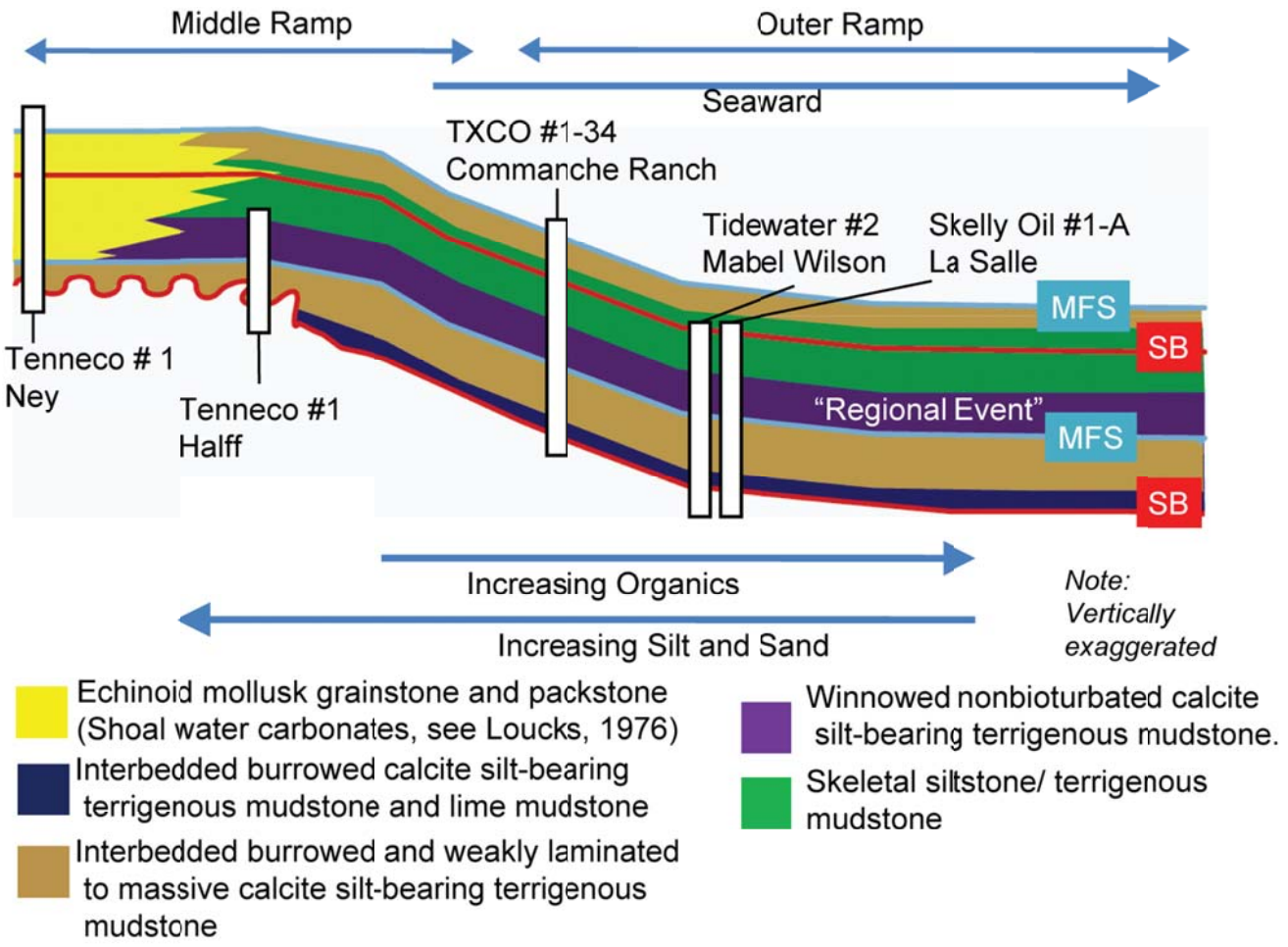

Figure 3.24: Lower Bexar Shale lithofacies stacking.

Chapter 4: Depositional Setting and Oceanic Anoxic Events

GENERAL STATEMENT

Environments of deposition during some periods of Pearsall time were strongly influenced by OAEs, which occurred during marine transgression. OAEs are identified in the stratigraphic record by physical changes in sedimentology as well as by anomalies in global carbon cycling detected by analyzing $\delta^{13}C$ secular curves. In this chapter, the OAEs during Pearsall time and their effects on deposition and associated facies are reviewed. Biostratigraphy is discussed as it constrains the timeframe of the OAEs and the $\delta^{13}C$-based chemostratigraphy. In contrast to the chemostratigraphy the biostratigraphy does not necessarily provide a complete or detailed a temporal record. After establishing the timescales and stratigraphic locations of the OAE events using chemostratigraphy, two depositional settings are proposed: (1) an OAE-dominated setting and (2) an environmentally "normal" setting. These are followed by a model for transition between the two depositional settings. This overall depositional model is applied to the Pearsall Formation in an effort to integrate the stratigraphy, OAEs, and facies.

LOWER CRETACEOUS OCEANIC ANOXIC EVENTS

Oceanic anoxic events were first recognized by Schlanger and Jenkyns (1976) who noted the contemporaneous deposition of black shales around the world (Schlanger and Jenkyns, 1976; Jenkyns, 1980). In the Pine Island Shale, lower Bexar Shale, and upper Bexar Shale Members the OAEs coincide with regional third-order transgression. Not all transgressions in the Pearsall Formation, however, are accompanied by these OAEs as is the case of the upper Cow Creek and middle Bexar Shale Member third-order sequences. During OAEs, the oxygen minimum zone, normally located at depth in thousands of feet of water (Sliter, 1989), expands and episodes of extreme dysoxia occur

on the shelf and over other topographic highs (Wignall, 1994). The events are attributed to changes in global carbon cycling, as observed in $\delta^{13}C$ ratios (Kump and Arthur, 1991). The OAE events induce increases in primary biological productivity (Leckie et al., 2002). The increase in productivity leads to a high production of organic matter; the decomposition of which drives shallow-water hypoxia, and creates conditions for the preservation of organic matter.

OAEs are accompanied by changes in the global marine environment, which alter the global cycling of carbon (Jones and Jenkyns, 2001). The OAEs are generally marked by increases in ^{12}C over time followed by a decrease in the ^{12}C because of ^{12}C incorporation in sequestered organic matter (Weissert, 1989; Leckie et al., 2002; Erba et al., 2004; Weissert and Erba, 2004; Follmi et al., 2006; Jarvis et al., 2006). The changes in the carbon isotope ratios are reported as changes in the $\delta^{13}C$ ratio relative to the V-PDB standard discussed in the methods section. The increase in light weight ^{12}C in the system that trigger the OAEs was produced external to the study area (Phelps, 2011).

The most common explanation for the increase in the availability of light carbon to both carbonate and organic matter during Pearsall time was an increase in the rate of seafloor spreading and the emplacement of large igneous provinces (LIPs) (Larson 1991; Coffin and Eldholm, 1994; Bralower, 1999; Leckie, 2002). Other explanations include the input of land-derived organic matter, rich in ^{12}C (Schlanger and Jenkyns, 1976) and the release of ^{12}C-rich methane hydrates (Vehrenkamp, 2010).

These tectonic events are thought to have two consequences. First, increased spreading and emplacement of LIPs can cause sea level rises up to 300 m (Miller et al, 2005) and these rise in sea level are unrelated to the Milankovitch controlled changes in sea level. Second, the increase production of oceanic crusts caused volcanic degassing and increased hydrothermal activity at the sites of the LIPs and mid-ocean ridges (Jones

and Jenkyns, 2001). This had direct consequences for climate change, increasing the partial pressures of CO_2 in the atmosphere and ocean, altering ocean water acidity, as well as adding other nutrients such as Fe and Mg ions to the ocean (Jones and Jenkyns 2001).

Changes in environments of deposition accompanying the onset of an OAE will result in physical changes in the mineralogy of the sediment and types of biota because of the addition of both ions and CO_2 to the global environment. The addition of Fe and Mg ions are nutrients for the lower part of the food chain in the ocean, which promotes higher primary productivity (Jones and Jenkyns, 2001). Higher productivity drives the creation or expansion of an oxygen-minimum zone (OMZ) within the water column as decomposing organism remove oxygen from the water column (Demaison and Moore 1980; Arthur and Sageman 1994). The OMZ normally occurs at water depths of 500 to 2000 m, but under OAE conditions it can rise to within 50 m of the surface (Southam et al., 1982, Wignall, 1994). This enables the preservation of organic matter in relatively shallow environments, so long as the environments are not oxygenated by surface processes such as wind and wave action. The effect of CO_2 is multifold. The rise in the partial pressures of CO_2 in the oceans acidified them and contributes to a biocalcification crisis (Erba, 1994; Bralower et al., 1999; Erba et al., 2010). This had adverse effects on many phototrophic organisms and led to changes in the biota, notably a change from a choralgal fossil assemblage to a foramol assemblage during the OAEs (Phelps. 2011). Particularly susceptible to these changes were nannococcids, which experienced extinction and radiation events, and rudists, which largely disappeared during Pearsall time (Erba, 1994; Erbacher et al.1996). This OAE-related change in biota was critical in driving the transition from the flat-topped rimmed platform during the deposition of the

Sligo Formation to the development of distally steepened ramp morphology during the deposition of the Pearsall Formation.

The addition of the CO_2 to the atmosphere and ocean was also a key driver for global warming which had several consequences. The global warming accelerated the hydrological cycle, which produced an increase influx of siliciclastic material into the basin and resulted in deposition of terrigenous mudrocks (Weissert and Erba, 2004). Additional effects of the global warming were worldwide in extent (Jones and Jenkyns, 2001). These effects included sluggish seawater circulation related to the minimization of longitudinal temperature differences and thus minimized thermohaline circulation (Huber, 2002) which further promoted continued periods of anoxia in the world's oceans (Arthur and Sageman, 1994). Also zonal wind velocities increased (Jones and Jenkyns, 2001), driving bottom currents similar to the loop current present in the Gulf of Mexico today (Shanmugam, 2008). These currents may have caused upwelling when they encountered the shelf edge (Hay and Brock, 1992), which drove upwelling. A similar situation may have occurred along the Pearsall shelf edge (Stricklin et al.,1991). This upwelling brought the nutrients, injected by the volcanic activity into the ocean, to the surface to fuel the surface productivity which ultimately led to anoxia and enhanced TOC preservation.

BIOSTRATIGRAPHY

General Statement

Biostratigraphic data are used to link chemical $\delta^{13}C$ data and lithological trends to a temporal framework. Nannofossil data was provided by Jason Jeremiah from Shell Petroleum Company and the ammonite data was provided by Peter Rawson affiliated with the University of Hull at Scarborough. Because of the rarity of ammonites and poor

fossil recovery related to the biocalcification crisis, biostratigraphic data only serves to ground truth temporal trends discussed in the context of the $\delta^{13}C$ data.

Ammonite Biostratigraphy

The ammonite zonations are from Young (1986). From outcrops on the San Marcos Arch, he identified three ammonite zones within Aptian time. Other workers have identified additional zones in Aptian time below Young's lowest zone (Follmi, 2006), but these zones originated in Tethys Ocean and were not identified in this study. Young's three ammonite zones are the *Kasanskyella spathi* zone equivalent to the Bexar Shale Member, the *Dufrenoyia justinae* zone equivalent to the Cow Creek Member, and the *Dufrenoyia rebeccae* zone equivalent to the Pine Island Shale Member (Young, 1986; Mancini and Puckett, 2005).

Ammonites identified in the cores for this study match the zones delineated for Aptian time on the San Marcos Arch. *K. spathi* is found in the lower Bexar Shale Member, *D. justinae* is found in the distal Cow Creek Member, and *D. rebeccae* is found in the upper part of the Pine Island Shale Member. However, the ammonites found and identified do not constrain the upper and lower boundary of the section. In the Pine Island Shale Member all of the identifiable ammonites are located near the top of the member making it unclear if the Pine Island Shale Member is actually entirely within the *D. rebeccae* zone. The ammonites found near the base of the section are juvenile, and therefore not clearly identifiable. Therefore, the ammonite data does not narrowly constrain the timing of the flooding of the Sligo platform or the onset of shale deposition during Pine Island Shale time. Similarly, no ammonites could be found in the upper or middle Bexar Shale Members. Therefore, the age of top of the Pearsall interval cannot be constrained beyond recognizing that the lower Bexar Shale Member is in the *K. spathi*

zone using the ammonite data. Consequently, on the basis of ammonite data, it is unclear if the upper Bexar Shale Member extends into Albian time.

Nannofossil Biostratigraphy

The Pearsall Formation spans the whole of Aptian time and may stretch into Albian time and is believed to include part of the NC6 zone, the NC7 zone, and part of the NC8 zone (Bralower, 1999). The OAEs are times of major extinction and radiation of nannofossils aiding in the identification of the zones (Erba 1994; Erbacher et al., 1996). Nannofossil zones are taken from Roth (1978). The NC6 zone is defined by the nannococcid crisis, a mass extinction, described by Erba (1994) and is roughly equivalent to the Pine Island Shale Member and the OAE 1-A. The NC7 zone is defined by the first appearance of the fossil *Eprolithus floralis* and is equivalent to the Cow Creek Member and much of the Bexar Shale Member. The NC8 zone, considered Albian in age, is defined by the first appearance of *Prediscosphaera columnata* (Roth, 1978; Herrle et al, 2003)*;* it is interpreted to be equivalent to the upper Bexar Shale Member and the OAE 1-B.

The Pearsall nannofossil data lack clear markers delineating the nannofossil zones, with the exception of the base of the NC7 zone. Most of the samples analyzed in the Sligo Formation are barren or inconclusive. Deposition of the Pearsall Formation is known to start in the NC6 zone. This zone contains within it the nannoconid crisis (Erba, 1994). This zone coincides with the OAE 1-A. However, during this time the fossil *Cyclagelopshaera margerelii* experienced an acme. *C. margerelii* has been shown to be resistant to conditions of overly nutrified waters prospered in environments with anoxic bottom waters (Lees et al., 2005) similar to those produced by OAEs.

NC7 is marked by the first appearance of the *E. floralis* which coincides with the end of Pine Island Shale Member deposition in the study area and the end of the OAE 1-A. Prior to the start of the NC7 zone, diversity levels seen in the Pearsall cores are exceedingly low. They climb rapidly in NC7 and it appears that there is a change in the fossil assemblage during the OAE regional event. *C. margerelii* also reappears in the data during the regional OAE event in the Pearsall but its appearance is fleeting. The extinction of *C. margerelii* occurs sometime before the OAE 1-B and the onset of NC8 in the Bexar Shale Member, (Jason Jeremiah, Shell Oil Company, personal communication).

NC8 is the first Albian nannofossil zone. *P. columnata*, the marker for NC8, was not found in South Texas area core material, even in the distal Glen Rose Formation which is definitely Albian in age (Goldhammer and Johnson, 2001; Phelps, 2011). Therefore, the nannofossil record in the core data from the study area did not record the start of Albian time or the NC8 zone. The data from Bralower et al. (1999) in Mexico, in conjunction with chemostratigraphy, however, can be used to correlate the Aptian/Albian boundary into the South Texas area. Also, it appears that *E. floralis*, experienced a relative acme in the OAE 1-B event. This acme is believed to occur because the OAE created a biocalcification crisis and *E. floralis,* which has been shown to be resistant to dissolution (Bralower, 1988), was preferentially preserved, whereas other fossil dissolved. The OAE 1-B is typically dated as Albian in age. The acme of *E floralis* coincides with this event in the upper Bexar Shale Member and leads to the interpretation that the Pearsall Formation extended across the Aptian-Albian time boundary.

CHEMOSTRATIGRAPHY

Introduction to Secular Carbon Isotope Curve Stratigraphy

OAEs can be traced globally through the use of secular carbon isotope curves. The isotopic composition of sea water fluctuates through time. The available carbon isotopes, are incorporated into carbonate or organic matter so that the $\delta^{13}C$ ratio of the organic or carbonate material reflects the $\delta^{13}C$ ratio of the seawater in which it was formed. Negative excursions of the curve occur when light carbon ^{12}C is added to the system and incorporated into organic matter and carbonate. Negative excursions relate to volcanic degassing and other processes discussed in the previous paragraphs. Positive excursions occur when organic matter containing relatively light carbon is sequestered by burial and preservation of organic matter, removing the light carbon from the system and making the $\delta^{13}C$ ratio of the remaining carbon heavier. Commonly these isotopic curves for organic carbon and carbonate carbon move in unison around their respective averages, however, in some circumstances, variations in isotopic composition are closely related to the type and chemical reactivity of organic matter causing the organic curves to deviate from the local trend (Kump and Arthur, 1999). The OAEs can be detected by excursions in the carbon isotope curve.

Reference Secular Carbon Isotope Curves for Lower Cretaceous Strata

The secular carbon isotope curves prepared for the present study of the Pearsall interval are compared to secular carbon isotope curves from the literature (Figure 4.1) (Moullade et al., 1998; Bralower, 1999; Herrle et al., 2004; Follmi, 2006; Vehrenkamp, 2010; Phelps, 2011). The two key comparison curves are in equivalent rock units adjacent to the study area. One curve originates from Mexico (Bralower, 1999) and the other originates from the San Marcos Arch (Phelps, 2011). The San Marcos Arch curve is

derived from $\delta^{13}C_{carb}$ values of a shallow-water carbonate succession. The curve from the La Pena section in Mexico was produced using $\delta^{13}C_{org}$ from organic matter and shows three well-defined OAEs in the Pearsall. (Bralower, 1999). These reference curves are supplemented by other established $\delta^{13}C$ curves from other areas in the world, which were reviewed in Phelps (2011). One of these curves comes from the Viscontian Trough which was in the western part of Tethys. It was sampled in southeast France, but at the time of deposition was not far removed from the paleo-Gulf of Mexico (Follmi, 2006). The other additional curve comes from Oman, where rocks temporally equivalent to the Pearsall Formation are large oil and gas reservoirs (Vehrenkamp, 2010). Dating of these curves has been accomplished through calibration to nannofossil, planktonic foraminifera, and ammonite data (Bralower, 1999; Follmi et al., 2006). Specific intervals have been assigned stratigraphic names. Menegatti et al. (1998) and Bralower (1999) both use C2-C8 for the Pearsall interval, whereas Bralower (1999) extends the nomenclature to C2-C13. These intervals can be identified on both other secular $\delta^{13}C$ reference curves, and on secular $\delta^{13}C$ taken from the study area, and used to correlate along with stratigraphic and fossil data.

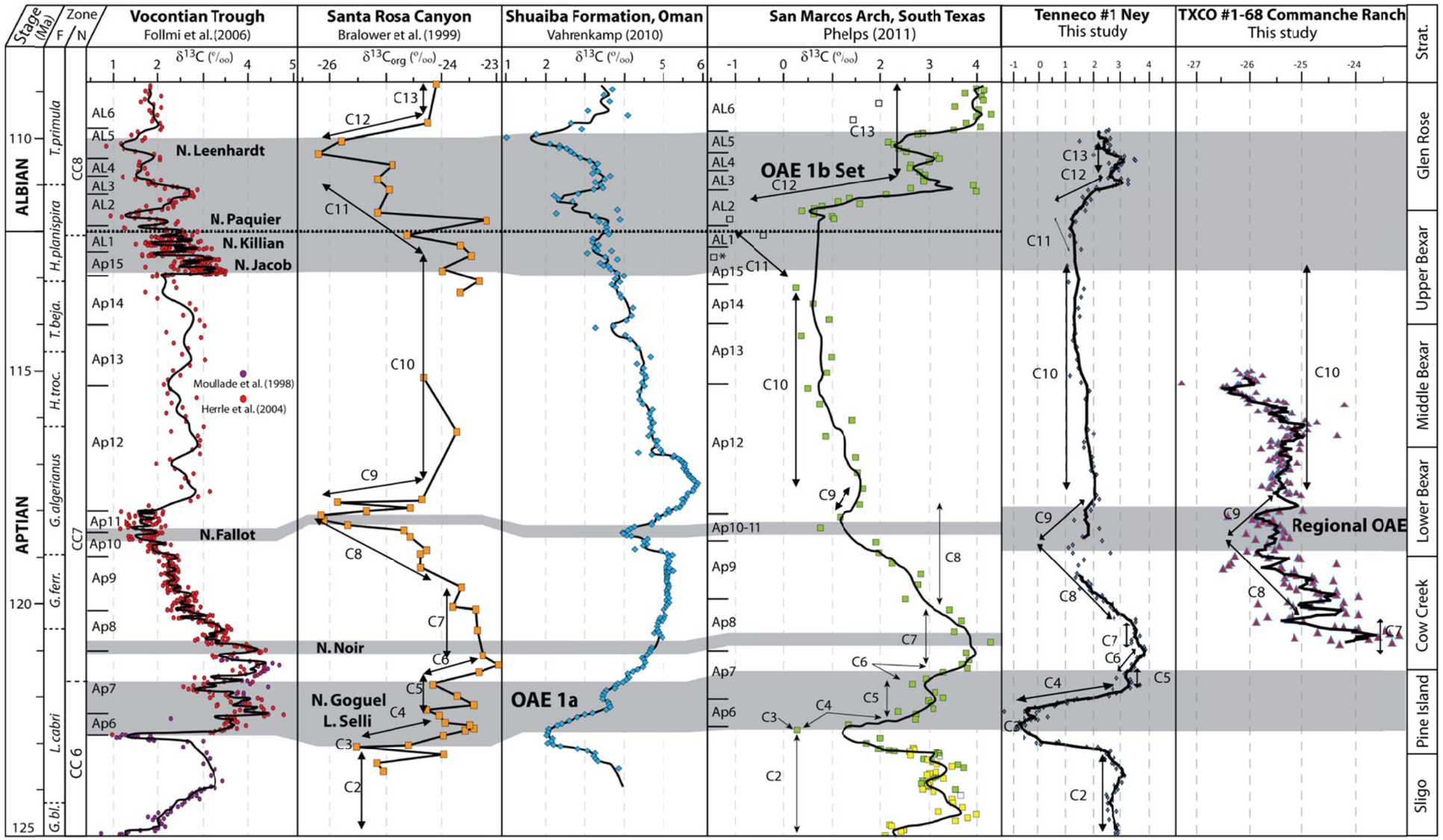

Figure 4.1: Secular carbon isotope reference curves and correlations to new curves with respect to time. Curves complied from Follmi, et al.2006; Bralower et al, 1999; Vahrenkamp, 2010; Phelps, 2011, and this study. Chemostratigraphic segments C2-C13 are from Menegatti et al. 1998 and Bralower, 1999. Figure reproduced and modified with permission by R. Phelps.

South Texas Pearsall Secular Carbon Isotope Curves

Ney Secular Carbon Isotope Curve

Isotope samples were taken every 2 to 3 feet through the Tenneco #1 Ney well (Figure 1.4). The values of $\delta^{13}C_{carb}$ range from 3.9‰ to -1.4‰. These values were compared to $\delta^{18}O$ values (Figure 4.2). Where $\delta^{18}O$ values indicate meteoric diagenesis, commonly in grainstones positioned at sequence boundaries, the $\delta^{13}C_{carb}$ values are removed as these samples are thought to reflect diagenetic $\delta^{13}C_{carb}$ values and not the $\delta^{13}C$ of the seawater at the time of deposition (Goa and Land, 1991). Burial diagenesis was also considered as it could theoretically be responsible for altering the $\delta^{13}C$ ratio. Various authors have suggested that if burial diagenesis was the controlling factor $\delta^{18}O$ and $\delta^{13}C$ values would correlate. In the case where burial diagenesis is not the controlling factor $\delta^{13}C$ values would reflect the original composition of the seawater, while the $\delta^{18}O$ values would reflect diagenesis and they would not correlate (McKenzie 1978, Weissert 1989, Menegetti et al., 1998). The isotope samples from the Ney well do not show any correlation between $\delta^{18}O$ and $\delta^{13}C$ values (Figure 4.2). Additionally $\delta^{13}C_{carb}$ values that were more than 2.0‰ off of the local trend were removed as these values are probably inconsistent with the isotopic values of seawater at the time of deposition.

In the Ney core a five point moving average of the $\delta^{13}C_{carb}$ was used in conjunction with the individual data points to better identify changes in the secular carbon curve. The $\delta^{13}C$ trends C2 to C13 are identified as shown in Figure 4.2 in conjunction with formation tops. These curve cover from an interval within the upper Sligo Formation to within the lower Glen Rose Formation and can be compared closely to the composite curve Phelps (2011) developed on the San Marcos Arch (Figure 4.4).

The OAE 1-A and 1-B positive excursions are readily identifiable, coinciding with the C4 and C12 events. The OAE 1-A event is clearly identified with the C3 and C4 intervals. The Late Aptian regional event coincides with the C8 and C9 in the lower Bexar Shale Member. Its signature is, however, relatively poor. Finally the OAE 1-B event is identified by the C11 and C12 intervals and while the C12 interval distinct, the C11 interval is not well developed.

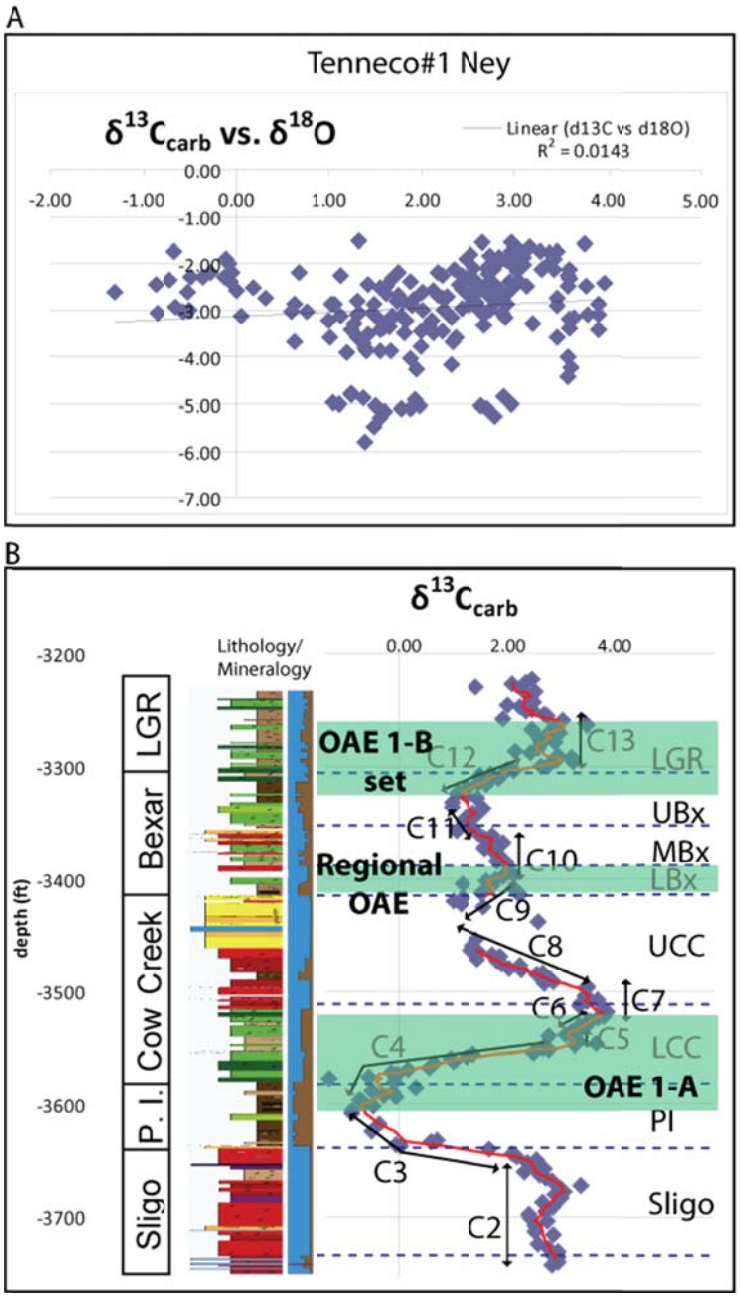

Figure 4.2: Ney secular $\delta^{13}C$ carbon isotope curve. (A) Graph shows the correlation between $\delta^{13}C$ and $\delta^{18}O$ as well as the low R^2 value which indicates little to no correlation. (B) Graph shows the secular isotope curve with respect to lithology and mineralogy. See Figure 2.10 for mineralogy and facies key. The OAEs are highlighted in green.

Commanche Ranch Secular Carbon Isotope Curve

The Commanche Ranch core was sampled for organic $\delta^{13}C_{org}$ isotopes only. Because of its paleogeographic position is such that it does not appear to exhibit a large change in organic matter type being deposited during the C9-C10 interval as did the La Salle County cores. This is because it was deposited the influence of siliciclastic sedimentation near the San Marcos Arch. The $\delta^{13}C_{org}$ values range between -26.34‰ to -23.06‰ and are shown in Figure 4.3. No $\delta^{18}O$ isotopes were analyzed to use in identifying diagenetic effects.

A five point running average was used and the C7-C10 intervals are identified with fair confidence for comparison to the Ney and Santa Rosa Canyon secular isotope curves. Because the Commanche Ranch curve is not a shallow water curve it compares well with the Viscontian Trough secular isotope curve shown on figure 4.1. Also the Regional OAE event was identified within the C8 and C9 intervals. In this well it coincided with the nonbioturbated winnowed facies.

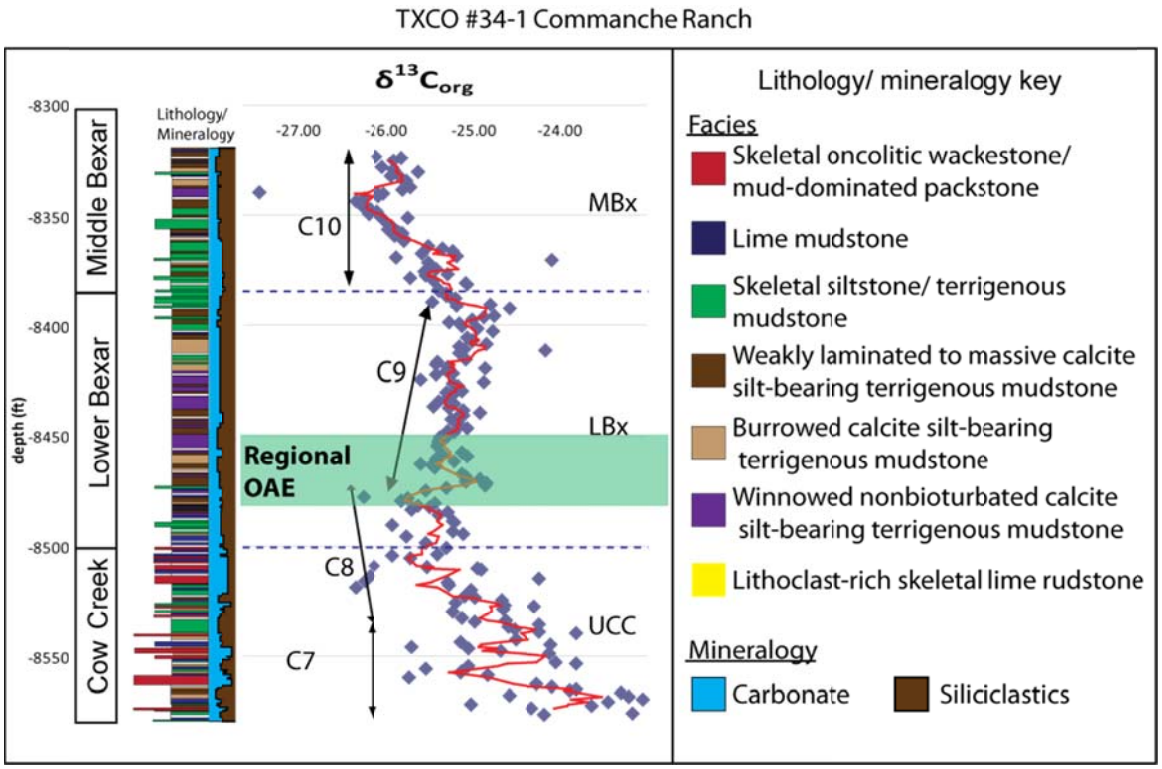

Figure 4.3: Commanche Ranch secular carbon isotope curve. The Graph shows the $\delta^{13}C_{org}$ isotope curve with respect to depth, facies, and mineralogy.

La Salle and Wilson Secular Carbon Isotope Curves

The Tidewater #2 Mabel Wilson and the Skelly #1-A La Salle were sampled for both carbonate and organic carbon isotopes (Figure 1.4). Both the organic and carbonate $\delta^{13}C$ values relative to depth and the comparison between $\delta^{18}O$ and $\delta^{13}C_{carb}$ are shown in Figure 4.4. $\delta^{13}C_{org}$ ranges between -24.17‰ and -27.07‰ in the La Salle core and between -24.67‰ to -27.40‰ in the Wilson core. In the La Salle core $\delta^{13}C_{carb}$ values range between 2.21‰ and -2.37‰ and in the Wilson well values of $\delta^{13}C_{carb}$ range between 2.85‰ and -1.93‰. From a comparison of $\delta^{18}O$ with the stratigraphy and depth there appears to be very little evidence of meteoric water influx during diagenesis in the outer ramp. Also the $\delta^{18}O$ and $\delta^{13}C_{carb}$ have a very low correlation coefficient indicating

diagenesis has not altered the $\delta^{13}C_{carb}$ values (Figure 4.2). Also the $\delta^{13}C_{carb}$ and $\delta^{13}C_{org}$ also had a low-correlation coefficient in both the La Salle and Wilson wells.

Similar to in the Ney core five-point running averages of the $\delta^{13}C_{carb}$ and $\delta^{13}C_{org}$ data were used. Attempts were made to identify the C7-C10 intervals in these cores but the trends relating to these proved elusive. Nonetheless the wells correlate closely with each other. The poor identification of the C7-C10 zones is shown in Figure 4.4. The organic isotopes are more problematic than the curves derived from carbonate material. In both cores there is a large change in organic isotope values in the middle of the lower Bexar Shale Member. This could be related to a change in the type of kerogen in the cores near the MFS of the lower Bexar Shale Member as different types of kerogen have different $\delta^{13}C_{org}$ average values (Wignall, 1994). There is a debate as to whether marine or terrestrial organic matter had a lighter $\delta^{13}C$ ratio or vice versa in the Cretaceous Period (Dean et al, 1986; Wignall, 1994). Also rock pyrolysis data do not conclusively separate marine from terrestrial kerogen in this area, as the R_o values are greater than 1 (Peters, 1987). Potential variations in the type of organic matter could be attributed to the paleogeographic position in the Atascosa Trough near both the carbonate factories on Pearsall Arch and the siliciclastic sedimentation in the area the San Marcos Arch (Figure 2.11). Organic diagenesis may have also altered the carbonate-derived curves as various mixtures of carbonate carbon isotopes were available. Given the difficulties identifying the C7 – C10 intervals, the curves were not used in correlation.

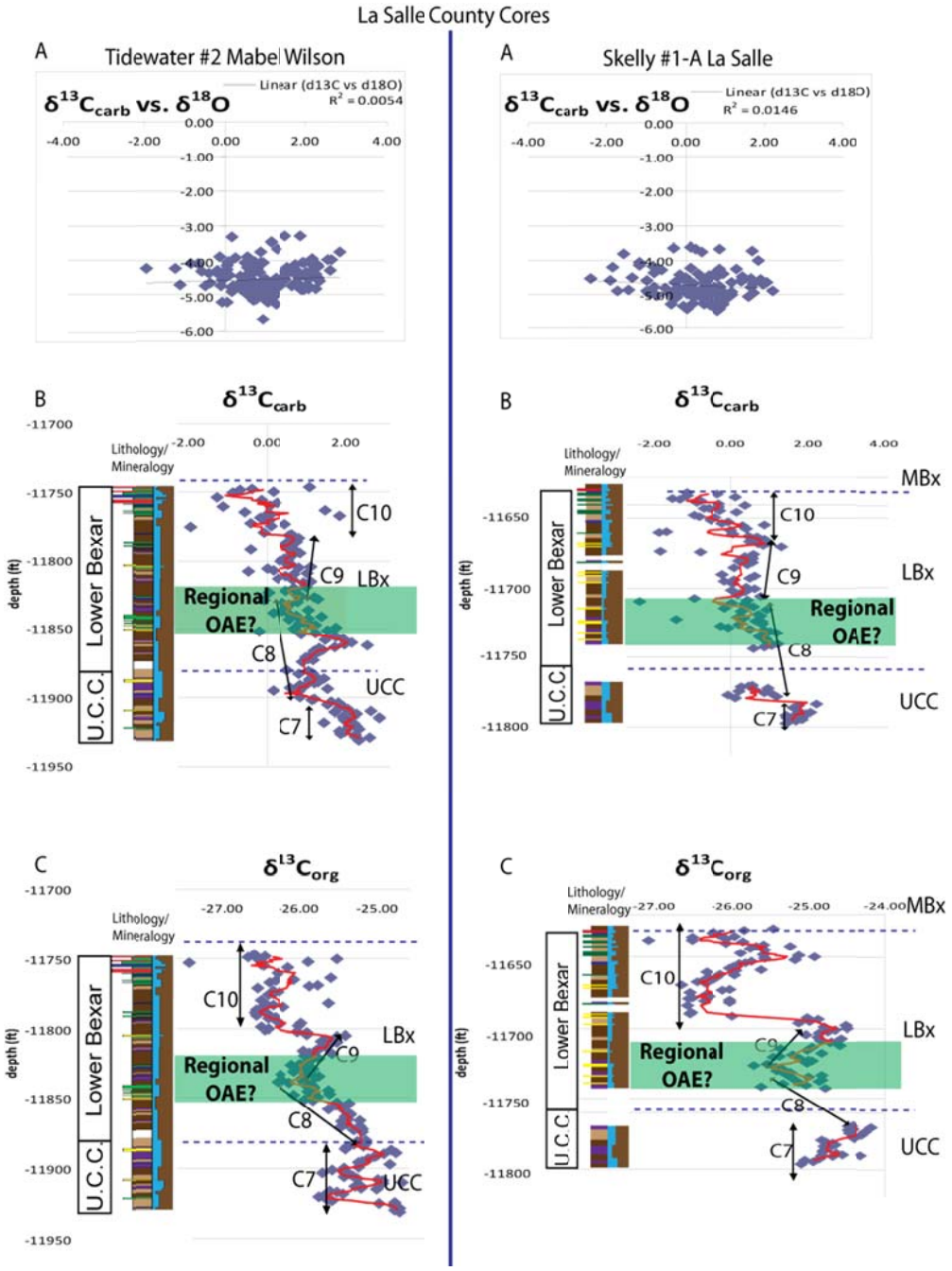

Figure 4.4: Mabel Wilson secular carbon isotope curve and La Salle secular isotope curve. (A) shows the comparison of $\delta^{13}C_{carb}$ and $\delta^{18}O_{carb}$ for both wells. (B) The graphs shows the $\delta^{13}C_{carb}$ isotope curve with respect to depth, facies, and mineralogy. (C) shows the $\delta^{13}C_{org}$ isotope curve with respect to depth facies and mineralogy. The facies and mineralogy key can be found in figure 4.3.

Secular Carbon Isotope Curve Correlations

The identification of the C2-C13 intervals allows correlations between distant stratigraphic sections that have different thicknesses. The stratigraphic sections also occur in different paleogeographic settings and facies-independent correlation can be accomplished. This is consistent with Swart et al. (2009) who found $\delta^{13}C_{carb}$ ratios to be independent of facies in the modern and previous studies in the ancient by Amodio et al. (2008). The correlations can also be used to trace OAE-dependent TOC and mineralogical changes between the wells as observed in the Santa Rosa Canyon section and the cores in the study area (Bralower, 1999; this study).

Correlations are good between the TXCO #68-1 Commanche Ranch secular isotope curve, the Tenneco #1 Ney secular isotope curve, and the reference curves (Figure 4.1). Key stratigraphic surfaces within the Pearsall Formation, biostratigraphic data, and the identification of the C2-C13 intervals were used in these correlations. The La Salle County secular isotope curves are not incorporated into the regional correlations as confidence in these correlations is low. Even though the carbon isotope curves match between these wells the curves did not match curves in other wells in light of stratigraphic framework. The correlations between the Commanche Ranch, the Ney secular isotope curves and reference curves are shown relative to time in Figure 4.1.

The purpose of correlations between the wells in the study area is to identify if the OAE signals are stratigraphically equivalent and if so, it allows the tracing of changes in rock characteristics in the study area. The strata containing the OAEs are either source rocks or temporally equivalent to source rocks. There are three OAE-type correlative zones in the Pearsall section and shaded gray in Figure 4.1. OAE isotopic excursions commonly are marked by decreases $\delta^{13}C$ ratios followed by an increase in the $\delta^{13}C$ ratios.

The positive excursion in the $\delta^{13}C$ ratios is the part of the event where TOC is preserved. These events cause a decline in carbonate content and an increase in TOC.

Ocean Anoxic Event 1-A

The OAE 1-A is amongst the best documented OAE events globally (Li et al., 2008). It coincides with the emplacement of the Ontong-Java LIP (Bralower, 1999). The event is easily found in all of the reference secular curves near the beginning of Aptian time. The OAE 1-A includes the C3-C6 intervals and was readily identified in the Pine Island Shale Member in the Ney well both in terms of sedimentology and by the secular isotope excursion. This event coincides with the deposition of terrigenous mudrocks over the older Sligo Shelf during a second-order maximum flooding event. Some calcareous skeletal-dominated material was deposited in the updip area but this accumulation was related to oxygenation from surface waters. Downdip the sediment is dominated by pelagic and hemipelagic facies with little to no benthic faunal content. High TOC is also observed in Shell #1-R Roessler well downdip and attributed to anoxic to dysoxic conditions, however, the water column was probably not euxinic as small pyrite framboids indicative of euxinic water (Raiswell and Berner, 1985) were not found in the Pine Island Shale Member.

Regional Event

The late Aptian regional event coincides with the lower Bexar Shale Member interval and the transition between the C8 and C9 intervals in the $\delta^{13}C$ curves (Figure 4.4). It is described as either a late Aptian regional event by Bralower (1999) or as the N. Fallot event by Follmi et al. (2006). It is the least recognizable of the OAEs in the $\delta^{13}C$ curves and the true regional extent of it is not known as it appears to be largely confined to the paleo-Gulf of Mexico and western Tethys (Follmi, 2006; Phelps, 2011). It is also

not linked with the emplacement of a LIP or other tectonic events (Bralower, 1999), although seafloor spreading was ongoing at a rapid pace (Larsen, 1991). The OAE appears to have started within the upper Cow Creek Member interval, as this is where the $\delta^{13}C$ begins to decline. High TOCs are found in the lower Bexar Shale Member. The strata in this interval is dominantly terrigenous with significant calcite silt derived from disaggregation of inoceramid shells., The inoceramid shells the lower Bexar Shale Member facies may suggest that parts of the water column during this event were dysoxic. There is no indication that the water column was euxinic during this time.

Ocean Anoxic Event 1B

The OAE 1-B is actually a series of events but it is expressed as only one event in the paleo-Gulf of Mexico (Follmi, 2006; Phelps 2011). This event coincides with the emplacement of the Kerguelen LIP in the South Pacific (Coffin and Eldholm, 1999), which is thought to drive the event. The event lasted through the C11-C12 intervals identified by Bralower (1999). The decline in the $\delta^{13}C$ ratio is not entirely evident in many areas for the C11 interval, however, the $\delta^{13}C$ ratio positive excursion is prominent in the Ney secular isotope curve (Figure 4.1). The sedimentology of the upper Bexar Shale Member during OAE 1-B interval is also similar to the sedimentology of the Pine Island Shale Member OAE 1-A interval on the middle ramp. Unfortunately, this interval was not sampled in the outer ramp area of this study.

SEDIMENTATION RATES

Sedimentation rates were calculated for all of the Pearsall members in the Ney core and in other wells where a complete member was cored. The rates were calculated based on the stratigraphic surfaces and carbon stratigraphic zones in terms of cm/ky. These sedimentation rates are averaged across the total time of deposition of each unit.

These rates do not account for erosion processes; therefore they are minimum sedimentation rates. They also do not account for geologically instantaneous processes such as periodic very rapid pulses of sedimentation separated by long periods of no sedimentation.

The calculated average rate of deposition during the complete Pearsall time in the Tenneco #1 Ney well is 1.01 cm/ky. Individual member rates are as follows: Pine Island Shale Member is 0.90 cm/ky; Cow Creek Member is 2.35 cm/ky; lower Bexar Shale Member is 0.38 cm/ky; middle Bexar Shale Member is 0.35 cm/ky; and upper Bexar Shale Member is 0.55 cm/ky. These rates closely match the sedimentation rates as reported by Phelps (2011) from the San Marcos Arch. On the basis of the isotope curve from his study presented in figure 4.4. He calculated rates in the Bexar Supersequence of 0.5 cm/ky and rates if 0.6 cm/ky in the James Supersequence.

Sedimentation rates were also calculated from the TXCO # 34-1 Commanche Ranch data set, the Tidewater Oil #2 Mabel Wilson data set, and the Skelly Oil #1-A La Salle data set for the lower Bexar Shale Member. Average sedimentation rates in the lower Bexar Shale Member are 1.2 cm/ky in the La Salle well, 1.4cm/ky in the Wilson well, and 2.2 cm/ky in the Commanche Ranch well. This is very similar to the rates calculated for the Santa Rosa canyon section for the OAE 1-A events in Li et al.(2008)' Using chemostratigraphic methods, biostratigraphic methods and other stratigraphic methods to estimate time, Li et al. (2008) calculated sedimentation rates between 1.9 and 2.2 cm/ky in the Santa Rosa canyon section in Mexico.

Sedimentation rates are dominantly a product of accommodation. The extremely slow rates of less than 1.0 cm/ky in the Tenneco #1 Ney well and on the San Marcos Arch (Phelps, 2011) are limited by the shelf setting. They also reflect the ability of carbonates to aggrade more aggressively and fill accommodation.

In the Ney well the rates are lower in the lower Bexar Shale Member because of the OAE event and the inability of clastics to aggrade aggressively during transgression (Pomar, 2001). In the upper Bexar Shale Member the rates appear to be higher than in the middle and lower Bexar Shale Members because there was more accommodation as the upper Bexar Shale Member contained within a second-order flood.

In the Maverick Basin, in the Commanche Ranch, Wilson, and La Salle wells rates are higher as there was more accommodation. Hence these rates are closer to the rates in the Santa Rosa Canyon section which is thought to have been deposited in deeper water (Bralower et al, 1999). These rates, even at 2cm/ky are however relatively slow (Bhattacharya and MacEachern, 2009; Phelps 2011). This narrows the range of potential depositional processes as discussed in the prior facies section.

DEPOSITION SETTING SUMMARY

General statement

The history of the Pearsall Formation reflects transitions back and forth from a stressed OAE environments (Figure 4.5) to a normal marine environments (Figure 4.6). Figure 4.5 and 4.6 describe the two end-member depositional environments active during Pearsall time.

The Pearsall Formation records three transitions among the end-members. An overall model to describe this transition was developed by Phelps (2011) (Figure 4.7). Phelps (2011) delineated four stages in his model: the equilibrium stage, the crisis stage, the anoxic/ dysoxic stage, and the recovery stage. Following the recovery stage is a return to the equilibrium stage. The model reflects how the environment responds to the perturbations which cause OAEs. The Pearsall Formation contains the perturbations of the OAE 1-A, the late Aptian regional event, and the OAE 1-B. Figure 4.5 displays the

OAE-dominated setting which reflects the anoxic to dysoxic stage, whereas Figure 4.6 displays the equilibrium/late recovery setting. Following a description of these two end-member depositional settings, the following sections will discuss the Pearsall members with respect to the overall depositional model presented in Figure 4.7.

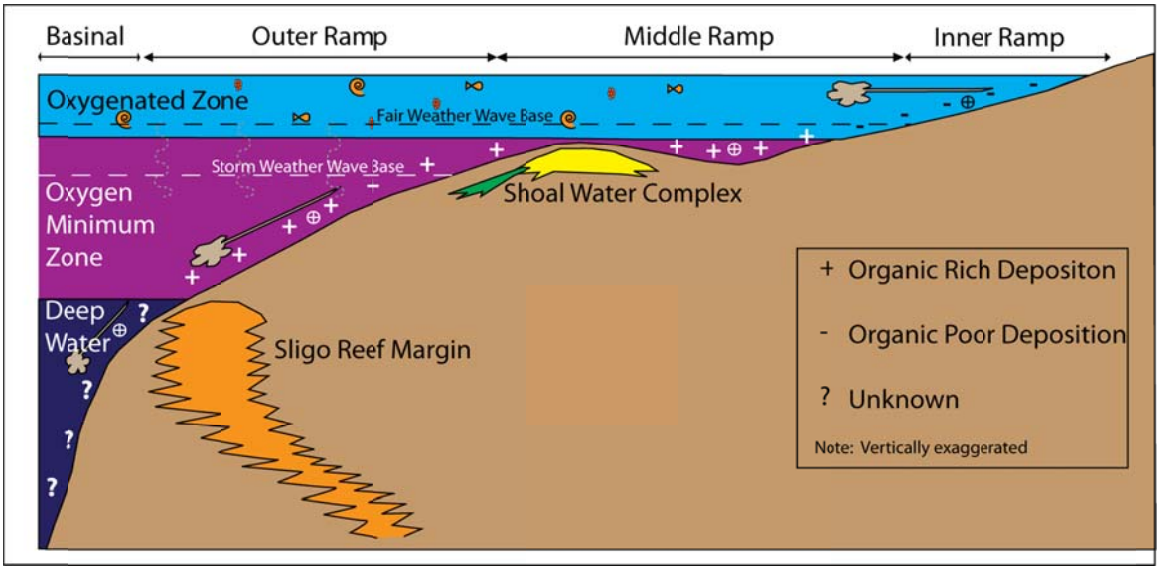

Figure 4.5: OAE depositional setting. The OAE depositional setting is distinguished by the development of a large oxygen minimum zone, the turning off of the carbonate factory, and by the high production of biota in surface waters.

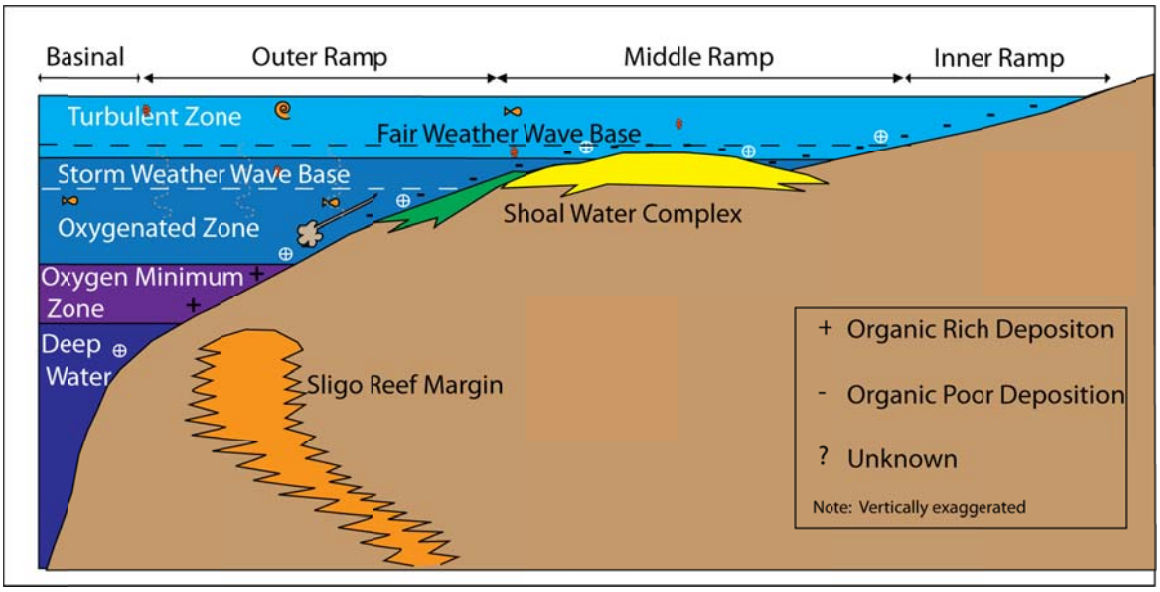

Figure 4.6: Normal marine shelf depositional setting. The flooded shelf or "normal" depositional setting is distinguished from the OAE depositional setting by the small or absence of an oxygen minimum zone and the active benthic carbonate factory.

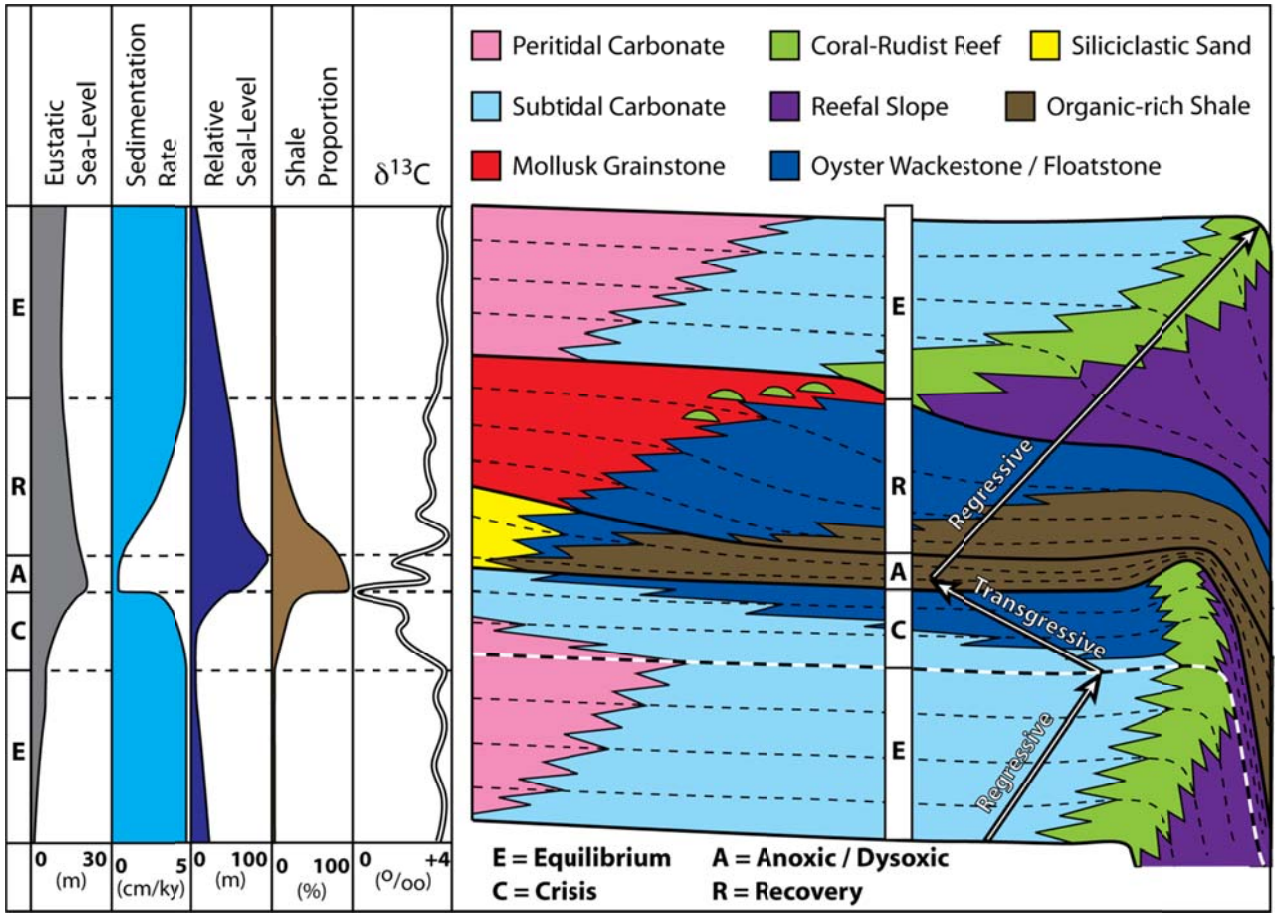

Figure 4.7: OAE depositional model. The schematic diagram from Phelps (2011) shows the effect of OAEs on cycles The Pearsall Formation features three of these cycles. Figure reproduced with permission by R. Phelps.

OAE Depositional Setting

The OAE depositional environment is one of end-member of the depositional environments and corresponds to the anoxic/dysoxic part of the model by Phelps (2011). Figure 4.5 depicts the key aspects of this depositional environment. During this time the water column was stratified with respect to oxygen. There were an oxygenated zone, a dysoxic to anoxic oxygen-minimum zone, and a deep-water distal basinal zone which probably had a higher oxygen content than the oxygen minimum zone. Wind-driven bottom currents (Shanmugam, 2008) created upwelling (Hay and Brock, 1992) bringing nutrients into the upper part of the oxygenated water column. A very active biologic community developed and thrived on these nutrients in the shallow-surface waters. Suspension sediment originated in these shallow waters producing the hemipelagic and pelagic facies. The benthic carbonate factory was largely shutdown and most of the terrigenous sediment was either transported downslope in dilute turbidity flows producing poorly laminated to massive deposits commonly seen in the outer ramp facies. The currents which drove the upwelling may have also reworked the deeper water sediments (Wignall, 1994). TOC was preserved in the dysoxic to anoxic outer ramp setting, whereas TOC was not preserved in the more oxygenated middle and inner ramp.

Normal Marine Depositional Setting

The normal flooded shelf depositional setting (Figure 4.6) differs from the OAE depositional setting in several ways. First, the water column was not overly nutrified and thus there was a less active pelagic fauna. Without the surplus of biological activity to remove oxygen from the water column, the Gulf of Mexico had a normal oxygenation regime with oxygen decreasing with depth, but rarely reaching dysoxic or anoxic conditions. The primary source of sediment was the carbonate shoal-water complexes

which developed in shallow-water. These shoals were predominantly grain-rich deposits with minor reef development and were surrounded by aprons of oncolids and muddy skeletal sediments. Given enough time the shoals and the patch reefs, similar to those developed in the shoal water complexes during the Pearsall, would prograde far enough to form a shelf margin reef, as they did in the Glen Rose, and as seen in the equilibrium stage of Figure 4.7. In deeper water a benthic fauna developed producing skeletal terrigenous mudstones and argillaceous wackestones.

Depositional Settings of the Upper Sligo and Pearsall Formations

Upper Sligo Formation

The upper Sligo Formation comprises the transition from equilibrium to crisis stage in the model presented in Figure 4.7. The upper Sligo was deposited during a transgression. This caused the landward-most carbonate facies to back step while the shelf-edge reef aggraded. The updip facies of the upper Sligo in the study area are predominantly ooids and rudist dominated grainstones and boundstone. (Bebout, 1977; Foster, 2003; Phelps, 2011) The secular carbon isotope curves from this section, however, indicate that overall the environment changed as it built up to OAE conditions. The fauna did not respond to these changes until later during Pine Island Shale deposition. Figure 4.6 best describes the depositional environment at this time, however, during Sligo time a shelf-margin reef was present and actively producing sediment.

Pine Island Shale Member

The Pine Island Shale Member was deposited during the anoxic to dysoxic stage in Figure 4.7, which corresponds to the OAE 1-A event. This occurred in conjunction with the second-order maximum flood of the James Supersequence (Figure 2.9). During this time sedimentation rates were low. On the middle ramp, in the topographically high

areas within the oxygenated zone, an oyster chondrodont biostrome developed, but elsewhere most of the sedimentation was dominated by pelagic and transported sediment. This can be observed in the facies map presented in Figure 3.16. Deposition of the Pine Island Shale Member continued until the recovery stage took effect, however, most of its deposition occurred in the anoxic/dysoxic period under conditions illustrated in Figure 4.5. The recovery was not time-synchronously, but occurred slowly as conditions near shore improved first allowing the carbonates of the lower Cow Creek Member to prograde.

Lower Cow Creek Member

The lower Cow Creek Member contains the lower portion of the recovery interval seen in Figure 4.7. As such, it became dominated by wackestones and terrigenous mudstones. As conditions improved on the ramp and organisms began to recolonize previously hostile areas that were dominated by terrigenous mudstone deposition deposited in the oxygen minimum zone. TOC was still preserved in the deep basin as the OAE conditions probably persisted there producing a continued change in the $\delta^{13}C$ secular isotope curve in the lower Cow Creek Member. Near the Burro Salado Arch (Figure 2.11),updip carbonate shoals and muddy carbonate sand began to form and prograde seaward as seen in the facies map in Figure 3.17.

Upper Cow Creek Member

The upper Cow Creek Member contains the late recovery period and equilibrium state, interrupted by the Late Aptian Regional event and associated transgression (Figure 4.7, Figure 4.6). Shoal-water complexes were active and developed during this period. Adjacent to the shoals were oncolid aprons. Patch reefs, similar to those drawn in the overall model, also developed in the area of the shoals. Beyond the oncolid apron muddy

skeletal sediments were deposited. Further out on the ramp terrigenous sediment was deposited by, contour currents, dilute turbidity currents, deeper water bottom currents and hemipelagic to pelagic suspension.

Lower Bexar Shale Member

During lower Bexar Shale time, Pearsall sedimentation experienced the stages of crisis, anoxic/dysoxic, and recovery. This late Aptian regional event was not as widespread as the OAE 1-A or 1-B (Bralower, 1999; Follmi, 2006; Phelps, 2011). The crisis phase began in the upper Cow Creek Member and continued through into the lower Bexar Shale Member. As such, the patch reefs that had developed in the Middle ramp ceased to exist as the oxygen minimum zone formed and a clastic shoreline developed. During this time a peloidal siliciclastic silts were deposited updip and facies with minor bioturbation formed on the outer ramp. TOC deposition and preservation coincided with the development of these outer ramp facies. This is summarized in Figure 4.5. Ultimately the system entered the recovery phase and a shoal-water complex developed where previous terrigenous sediments had persisted. The shoals prograded as the conditions moved from the OAE environment to the equilibrium environment shown in Figure 4.6. The dominant facies relationships are shown in Figure 3.19.

Middle Bexar Shale Member

The middle Bexar Shale Member is an example of a transgression unaccompanied by an OAE (Figure 1.1). During the transgression, low TOC muds and skeletal terrigenous mud were deposited. Following the transgression ooid shoals developed on the middle ramp. Middle Bexar Shale deposition may have represented the crisis period leading up to the OAE, but this was not clear on the basis of the sedimentology. As such most of the deposition can be summarized by Figure 4.6.

Upper Bexar Shale Member

The upper Bexar Shale Member is the expression of the OAE 1-B event. Its depositional environment is summarized by Figure 4.5 and the its strata were deposited during the anoxic/dysoxic phase of the model. It is also the maximum flood of the Bexar Supersequence. Deposition was very similar to that of the Pine Island Shale Member in the middle ramp area. It is thought that, like the Pine Island Shale and lower Cow Creek Members, the boundary between the upper Bexar Shale Member and overlying Lower Glen Rose Formation is not time synchronous.

Lower Glen Rose Formation

The Lower Glen Rose Formation is dominated by the depositional environment described in Figure 4.6. It also is the recovery and equilibrium phase following the OAE 1-B event. This is evidenced by the patch reefs described by Bay (1982) and Aconcha (2008) and shown in Figure 4.7 prior to the ultimate establishment of the Stuart City Reef Margin.

Chapter 5: Pearsall Shale-Gas System

INTRODUCTION

In the 1970's, South Texas was looked upon as one of the next great petroleum provinces in the United States and world (Cook, 1979). Drilling, however, rarely extended into the Pearsall Formation. While most of the penetrations of the Pearsall Formation tested wet, there were a several encouraging tests in the Pearsall Formation and other deep formations (Ewing, 2010).

Many of the Pearsall tests were unsuccessful because the porous, middle ramp shoal-water complexes lack an updip seal; consequently, petroleum was not trapped (Loucks, 1976). Nonetheless, the formation is known for its oil and gas shows in South Texas (TXCO, 2009). The only early, sizable, conventional production from the Pearsall Formation has been produced from the Los Quatros Field in Maverick County. Most of this production comes from only a few wells, such as the Apache #2 Maverick County well, which has produced approximately 4 BCF since 1979 (IHS scout ticket). The majority of these wells in the Los Quatros Field perforated both the lower Bexar Shale and Cow Creek Members, thus not allowing the assignment of reserves to individual reservoirs. Some of these wells were overpressured. Fractures noted in cored wells has raised the speculation that natural fractures may be necessary for production (Clarke, 2007). In La Salle County, the Auld-Shipman #1 Mabel Wilson well had an IP test of 2.35 MMCF per day with a 14/64 choke. Additionally the #1 Mabel Wilson well in La Salle, County tested some liquid hydrocarbon and had a GOR of 49,400 CFB (IHS scout tickets). Other wells such as the Skelly #1 Winkler well in Atascosa County have also tested oil but not in commercial quantities (IHS scout ticket).

Recent wells have specifically targeted the lower Bexar Shale Member as a shale-gas target. These wells target the Pearsall Formation where it is overpressured. This

overpressuring, based on pressure calculations using mud weights, appears to occur sporadically in the area of Maverick, Zavala, and Dimmit Counties (Figure 5.1). Wells drilled horizontally in the Pearsall have had relatively good results, with one well, the Anadarko #62-3H Tovar, in southern Maverick County, reporting an IP near 8 MMCF per day (Hackley, 2011). Other wells, including the Redemption Oil and Gas #1-1H Shook well, which was drilled October, 2009 and had an IP of 5.1 MMCF per day, in northwest Dimmit County, has now maintained production for several months, producing on average over 1 MMCF per day (IHS scout ticket).

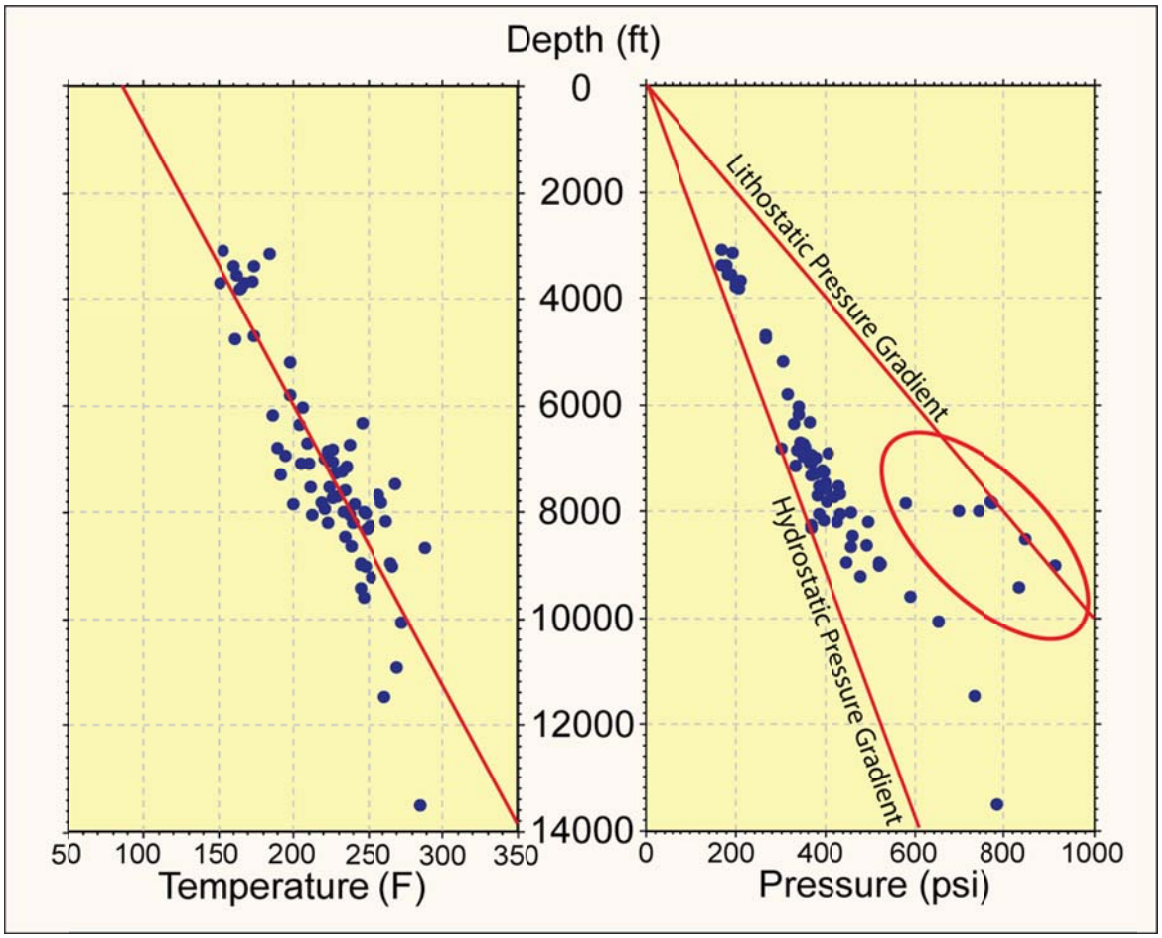

Figure 5.1: Cross plots of temperature and pressure against depth from Maverick, Dimmit, and Zavala Counties. Pressure was calculated from mud weights and bottom-hole temperatures were corrected for circulation time. The pressures within the red ellipse indicate over strong overpressuring in the Pearsall Formation. Most of the pressure data actually show some over pressuring as it falls to the right of the hydrostatic pressure line.

PETROLEUM SYSTEM

The outer ramp petroleum system is an unconventional shale-gas system in that it is simultaneously the reservoir, source, and seal. Key shale-gas reservoir parameters are TOC, maturity, kerogen type, and porosity. These parameters are discussed in this chapter.

In the Pearsall Formation three potential unconventional reservoir zones are identified based on their mineralogy, TOC, and maturity: Pine Island Shale Member, lower Bexar Shale Member, and upper Bexar Shale Member. Only the lower Bexar Shale Member is currently being exploited and produced. Figures 5.2 and 5.3 show the isopach maps of two of the potential unconventional reservoirs. These maps show the general thickness trends of the potential reservoir intervals, however, TOC and maturity must be incorporated to define the actual potential fairway.

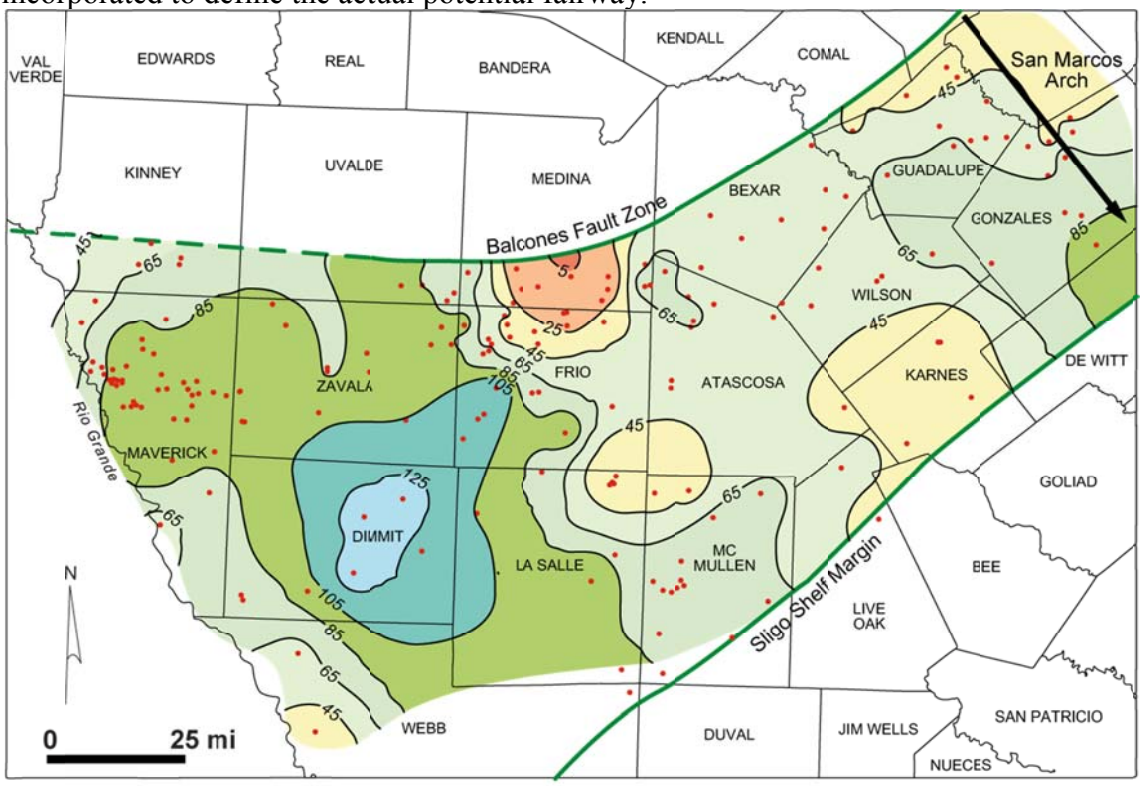

Figure 5.2: Lower Bexar Shale Member mudrock isopach map. The carbonate shoals are not included in this isopach map.

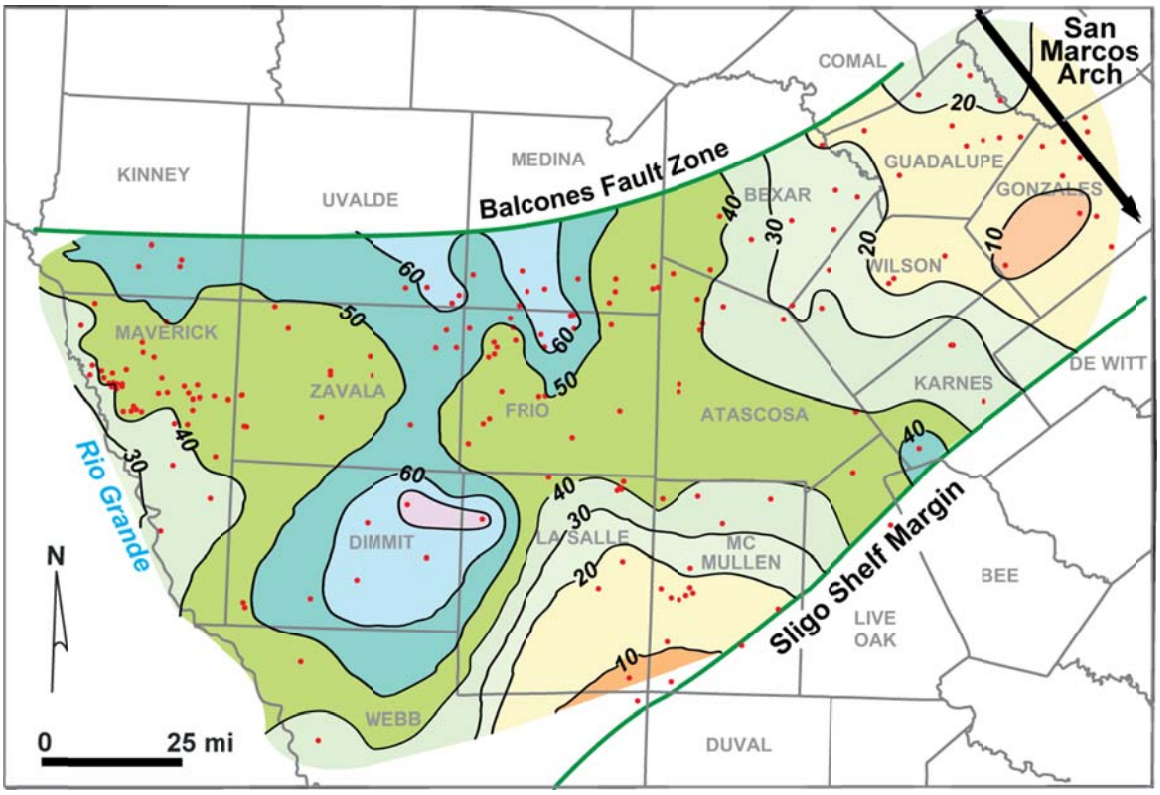

Figure 5.3: Pine Island Shale Member isopach map.

TOTAL ORGANIC CARBON AND THERMAL MATURITY

General Statement

Organic carbon can be analyzed through rock pyrolysis (Espitalie et al., 1977). and the majority of the work regarding TOC for this study was done by this method. Rock pyrolysis data gives the amount and quality of kerogen in the rock and provides an estimation of whether the kerogen will produce gas or oil.

The preserve amount of TOC depends on several factors, including production, destruction, and dilution of organic matter (Passey et al., 2010). The OAE-driven processes, which occurred during Pearsall time, promoted the production and preservation of organic matter (Schlanger and Jenkyns, 1976; Weissert, 1989). They also suppressed dilution in the Maverick Basin as the carbonate factory was largely shut

down. (Arthur and Schlanger, 1979; Follmi et al., 1994; Weissert et al., 1998) However, the Pearsall Formation has undergone enough maturation that late destruction of organic matter through catagenic processes and the production of oil and gas needs to be considered (Raiswell and Berner 1987).

Rock pyrolysis data can be used to determine kerogen type based hydrogen index (HI) and oxygen index (OI) which is derived from the TOC, S_2, and S_3 data. S_2 values can be low for several reasons: (1) because of maturation of the organic matter, (nor reason given for argillaceous rock; give it here) in argillaceous rocks, and in rocks with low TOC (Peters, 1986). In the Pearsall Formation the less mature samples also coincide with the area of low TOC deposition making it hard to obtain data on the kerogen type. Also many of the analyses performed on samples from the high TOC area did not yield usable information on kerogen type or R_o. Samples with higher R_o are also more likely to correspond to an apparent type III kerogen. This is because type II kerogen depletes more than type III kerogen during maturation, losing approximately 60% of the original organic carbon, whereas type III kerogen only loses about 30% (Raiswell and Berner 1987).

Pine Island Shale Member

Kerogen Type

Information derived from rock pyrolysis was supplemented by visually observed macerals in core and thin section using standard light microscopy and a hand lense. Throughout the outer ramp Pine Island Shale Member organic material with a coffee ground-like texture was noted. Where observed in thin section, theses macerals appear to be woody material. A very large piece of woody material with cellular texture was noted in the Shell #1-R Roessler core at the paleo-Sligo Shelf Margin. This piece of wood was

wider than the 5 cm-wide core and approximately 13 mm in height. In some of the cores, wavy organic-rich laminae are also preserved. These wavy laminae are thought to be bacterial mats (O'Brien, 1996). This suggests the presence of both type marine II kerogen and terrestrial type III kerogen.

The reliable rock pyrolysis data, according to Daniel Jarvie (Geomark Geochemistry, personal communication), are plotted on a pseudo Van-Krevelen diagram in Figure 5.4 (Peters, 2002). All of this data came from the middle ramp. This diagram suggests that the Pine Island Shale Member has both type II and III kerogen present in the updip area proximal to the terrestrial source. Given this evidence, plus the visual confirmation of type III kerogen in the outer ramp area, it is concluded that both type II and type III kerogen are present throughout the Pine Island Shale Member in the Maverick Basin. It is probable that additional type I and II kerogen was present in the downdip area and that it was not detected because of the high degree of maturation and limitations of the rock pyrolysis method in argillaceous rocks.

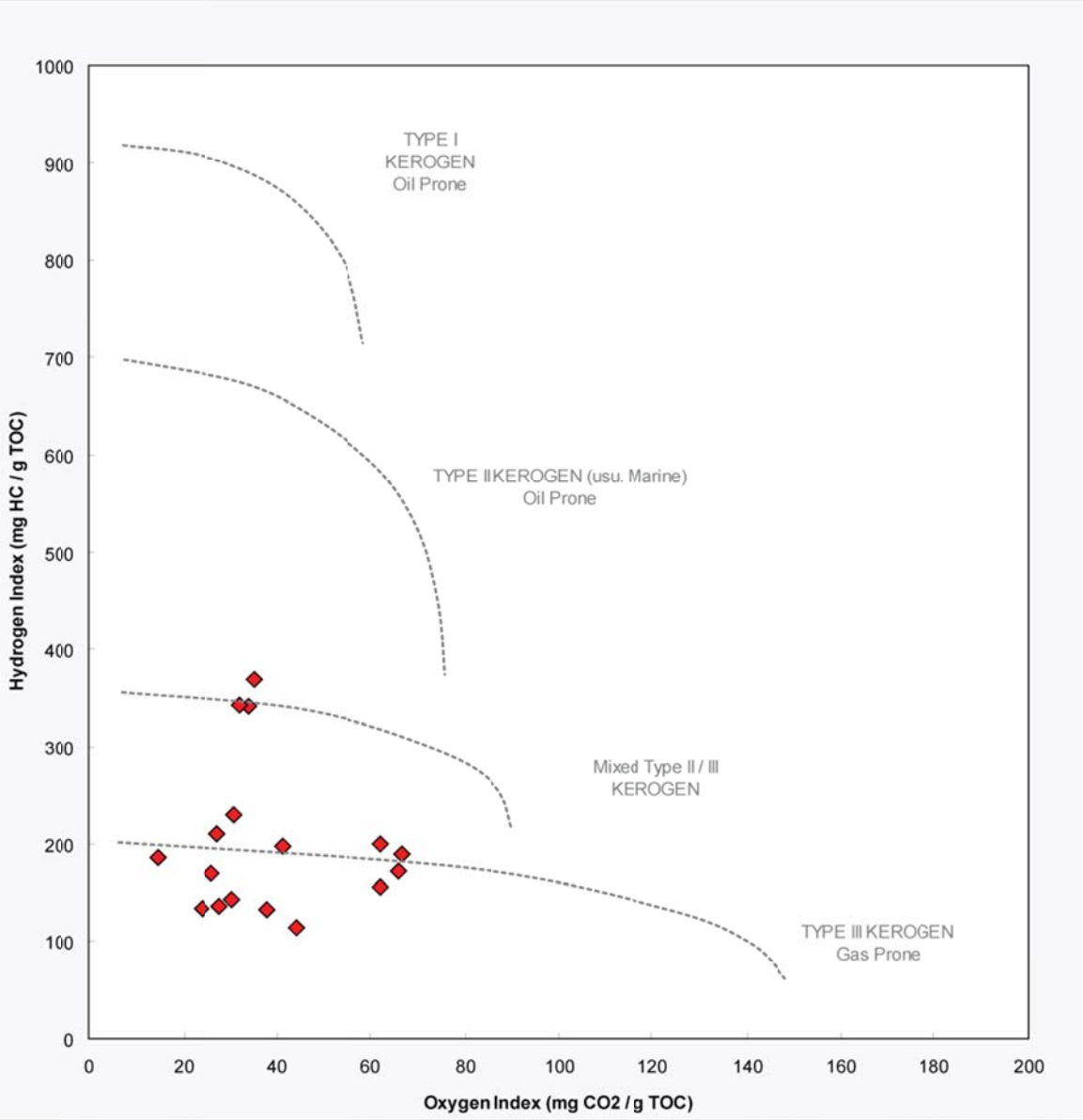

Figure 5.4: Pine Island Shale Member kerogen type. The samples are predominantly from the middle ramp area where maturities are low. In the outer ramp less type III kerogen is expected because of the distances to terrigenous sources.

TOC Abundance and Distribution

The Pine Island Shale Member TOC map (Figure 5.5) was compiled from data throughout the whole Pine Island Shale section. Only whole core mudrock samples were

used for rock-pyrolysis analysis. Some of these samples were collected by the USGS (Hackley, 2009) and others were collected specifically for this study. The TOC data presented Figure 5.5 represents an average TOC for the whole Pine Island section in the given well as opposed to the maximum TOC values present. The TOC values correlate to estimated water depths during Pine Island deposition. Low values (0.2% to 0.3%) are centered over the topographically high Pearsall Arch. Higher TOC values are located seaward of the Pearsall Arch across areas that were deep enough at the time of deposition to be anoxic to dysoxic. These TOC values are at or near 1%, but their higher R_o values need to be taken into account because some of the organic matter was destroyed during maturation. With the increased water depth there was increased anoxia and less biological activity, creating favorable conditions for the preservation of organic matter. Therefore, the amount of TOC deposited during the OAE-1A reflected water depth and level of oxygenation.

A TOC profile was developed for the Shell #1-R Roessler core (Figure 5.6) in northern Bee County. It was found that TOC has a strong positive correlation with the pelagic carbonate content. The pelagic carbonate content was a function of deeper water suspension sedimentation on the outer ramp where bottom conditions were dysoxic to anoxic. These conditions were ideal for the accumulation of organic as organic production rates were high, destruction of organics was low, and dilution of the organics with siliciclastic and carbonate material was low (Passey et al., 2010).

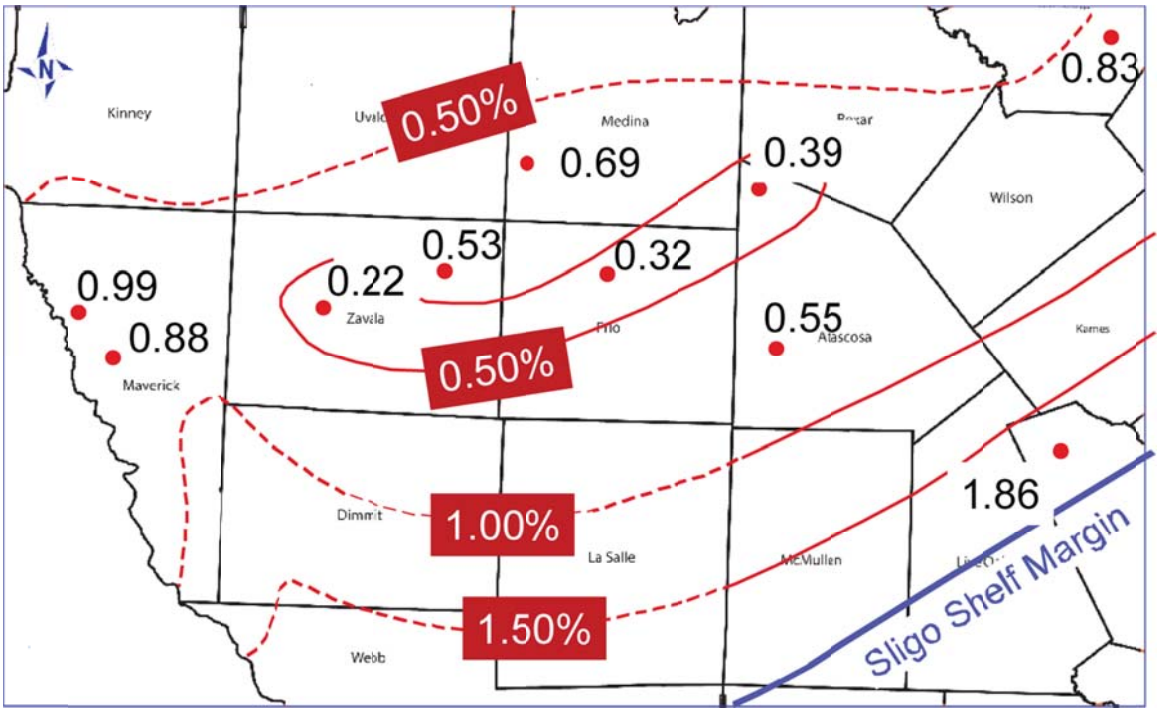

Figure 5.5: Pine Island Shale Member TOC trend map. The map presents a trend from generally lower values up dip to higher values downdip, except across the Pearsall Arch, which may have been the shallowest area on the middle ramp.

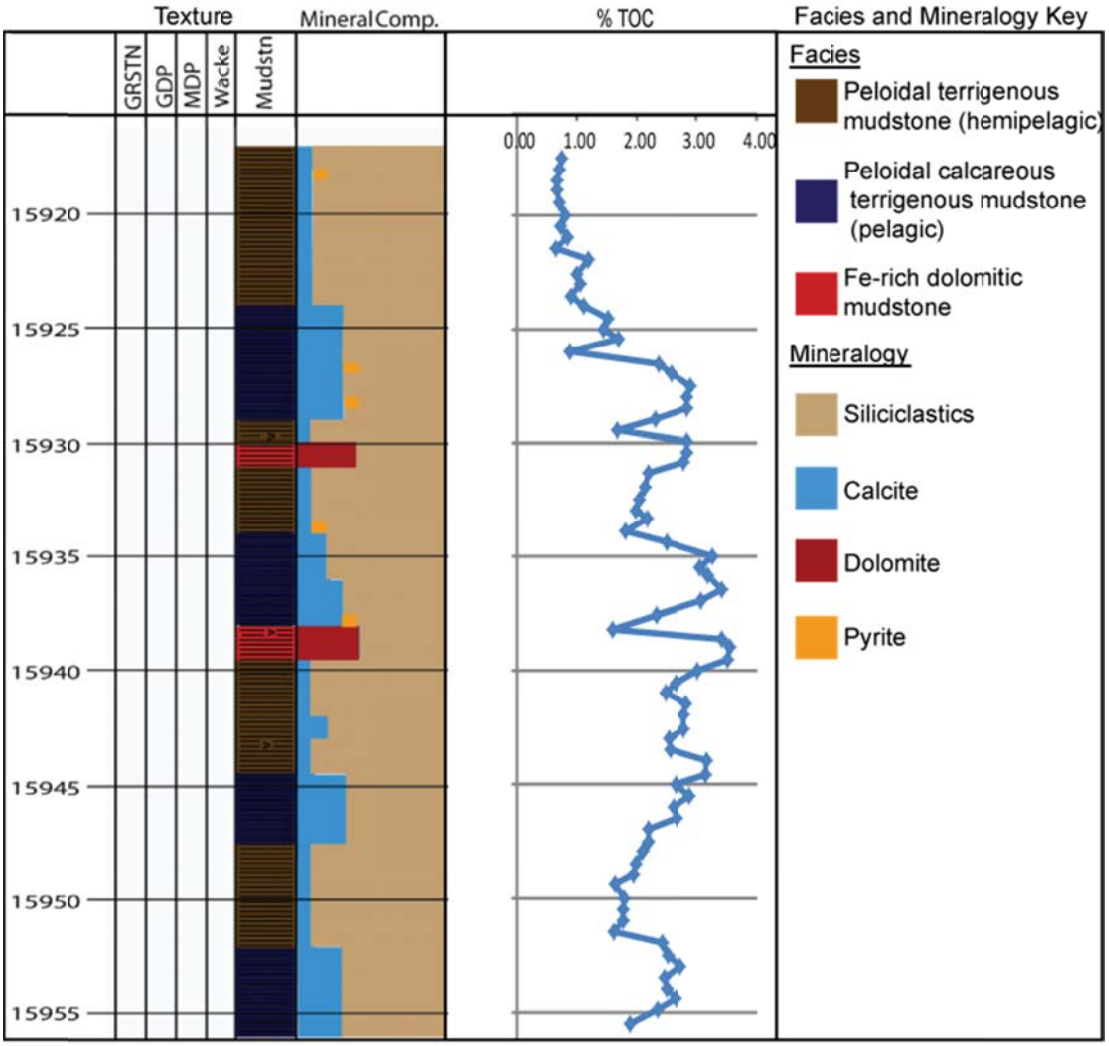

Figure 5.6: TOC profile of the Pine Island Shale Member in the Shell #1-R Roessler well. Higher TOC values correlate to the more calcareous pelagic-rich intervals

Maturation

The thermal maturity, along with the kerogen quantity and type, determines what kind of hydrocarbons a source rock will generate (Peters, 2002). It is also sheds light on the burial history of a rock as the character and properties of kerogen change with time and temperature. The Pine Island Shale and lower Bexar Shale Members are separated approximately by 200 feet of section, thus in anyone well the R_o values are nearly the

same. Therefore, in constructing R_o maps for either the Pine Island Shale or lower Bexar intervals, the R_o data from both units can help define the general contour patterns (Figure 5.7, Figure 5.8).

R_o values were derived from rock pyrolysis data or optically observed by the USGS (Hackley, 2009). The R_o values generally increase in the downdip direction reflecting progressively deeper burial depths. However, it is important to note that the Pearsall Formation in the Maverick Basin was not subjected to a uniform burial history. The Maverick Basin can be divided up into several areas of contrasting burial history. In the western part of the study area, around the Chittim Arch (Figure 2.4), R_o reflects the earlier and greater subsidence in the area of the Triassic rift rather than the later uplift. This area experienced approximately 1-2 km of uplift (Ewing, 2003) during the Laramide uplift. Prior, deep burial accounts for R_o values above 1.5% at depths of approximately 8000 ft. in Maverick County (Figure 5.7). These maturities are close to the maturities of samples taken from depths near 16,000 ft. in the outer ramp section near the San Marcos Arch. The central and eastern half of the Maverick Basin did not experience as much initial burial or later Laramide uplift as the outer ramp area or western portion of the Maverick Basin. These samples have R_o values between 0.5% and 1% (Figure 5.7) which conforms roughly to the burial history curve developed by Elisabeth Rowan (USGS, written communication, 2011) seen in Figure 5.9 from central Frio County. This burial history analysis should be representative though-out the central and eastern portion of the study area reflecting passive margin conditions with limited erosion updip towards the Llano uplift.

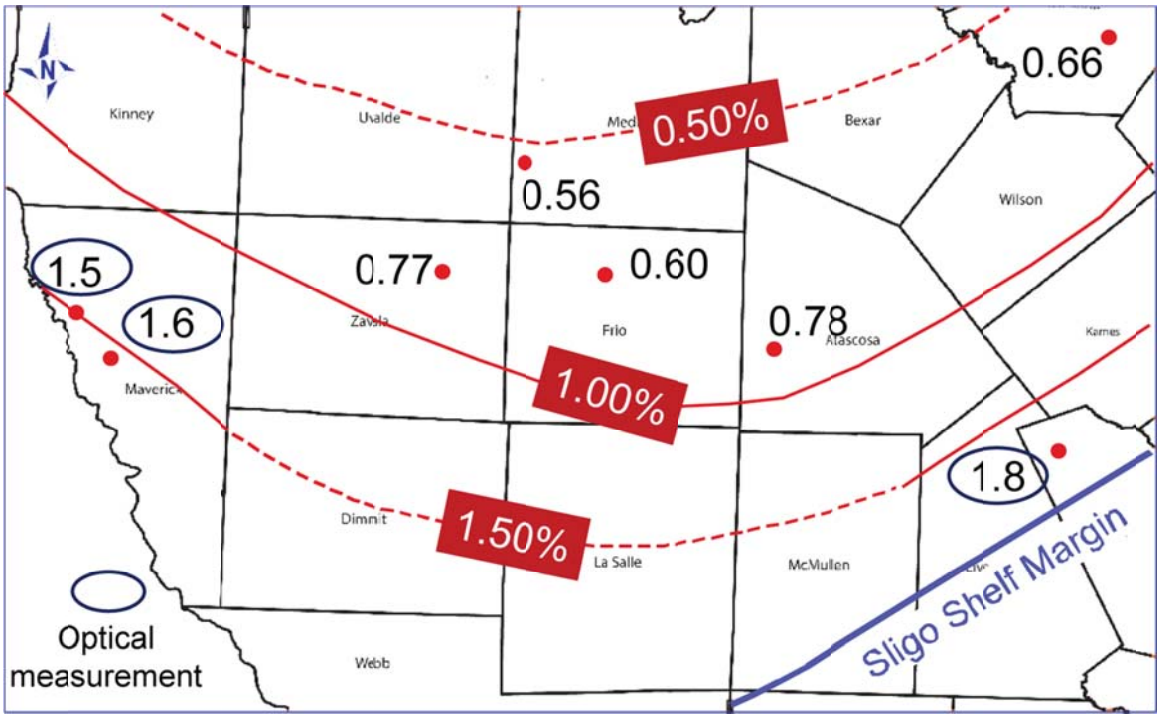

Figure 5.7 Pine Island Shale Member R_o trend map. Optical measurements from Hackley, 2009.

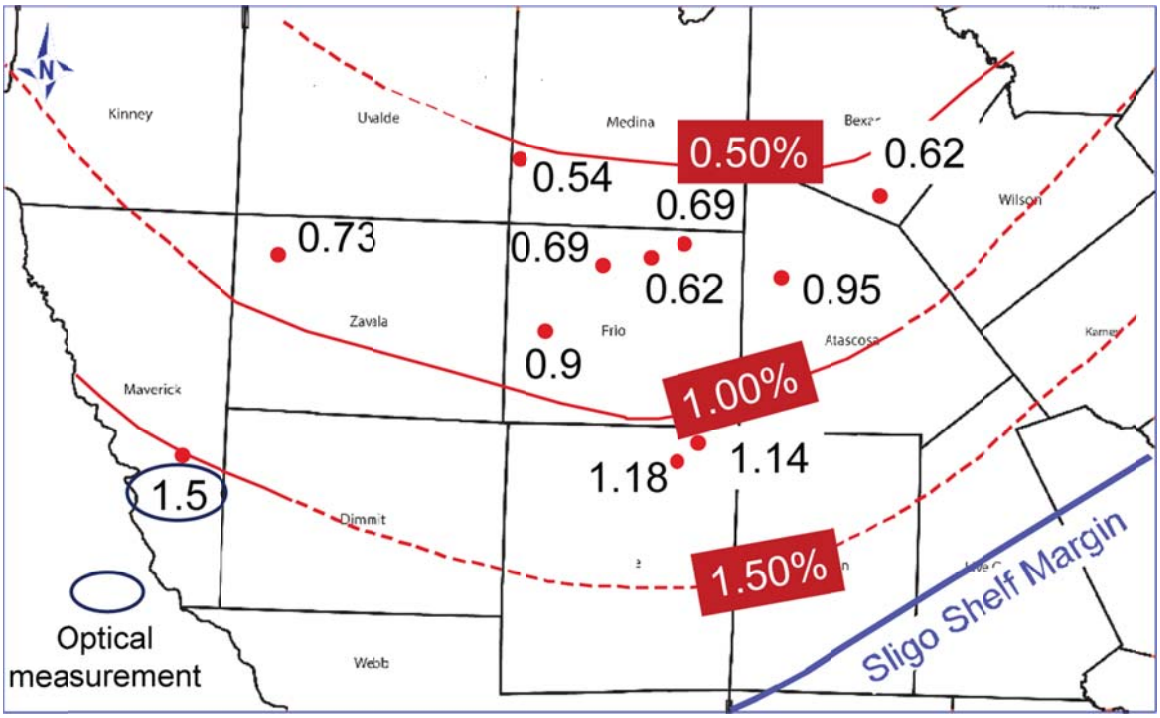

Figure 5.8: Lower Bexar Shale Member R_o trend map. Optical measurements from Hackley, 2009.

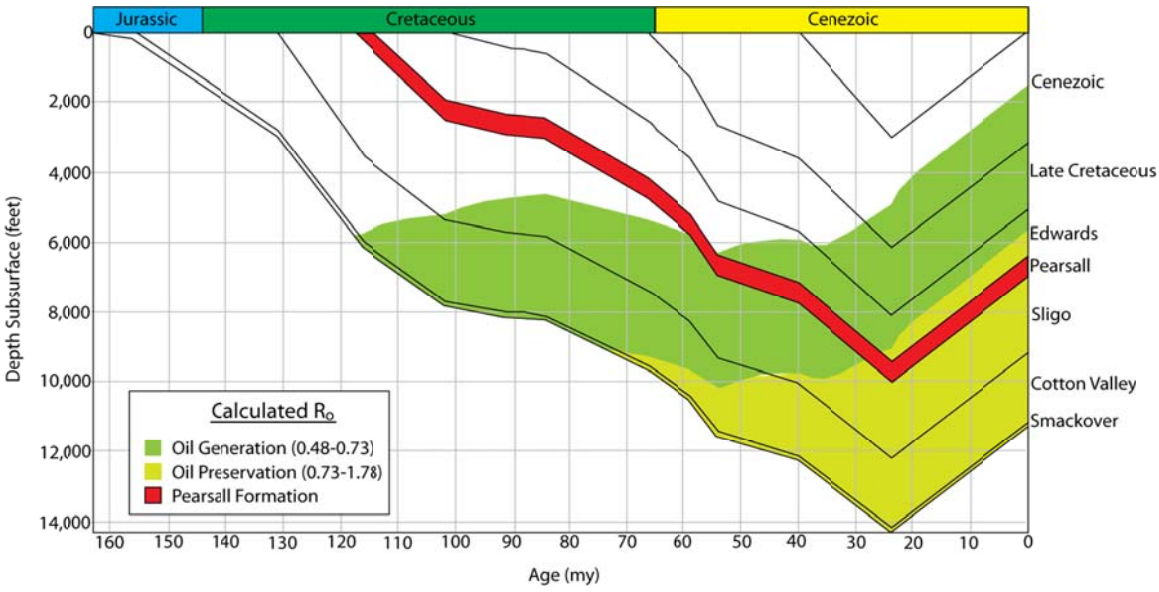

Figure 5.9: Burial history curve from central Frio County. Modified from E. Rowan, (USGS, written communication, 2011).

Lower Bexar Shale Member

Kerogen Type

Data on lower Bexar Shale kerogen characteristics were derived from visual observations, organic matter typing, and rock pyrolysis. Coffee-ground-textured organic material was identified in the lower Bexar Shale Member but less frequently than in the Pine Island Shale Member. Also no large pieces of wood were found in the lower Bexar Shale Member. Kerogen identified in Medina and Bexar Counties is dominantly type I and II through organic matter typing by Weatherford. The recognition of type I and II kerogen in the proximal area suggests that similar kerogen would be found further from the coastline where terrigenous material is less prevalent.

Similar to the Pine Island Shale Member, maturation of the lower Bexar Shale Member plays a key role in the rock pyrolysis values in the downdip section. Rock pyrolysis indicated that the lower Bexar Shale Member kerogen is predominately II/III updip and type III downdip based on the HI and OI values (Figure 5.10). The identification of type III kerogen in the outer ramp area is a function maturation and consequent degradation of the kerogen. In Figure 5.10, the samples with Ro higher than 0.9 are shown in blue. They all come from outer ramp wells and plot as type III kerogen; however, this may be a result of maturation (Peters, 2002). As with the Pine Island Shale Member, most of the wells with optically assessed R_o values higher than one (Hackley, 2009) did not yield viable calculated R_o data. In conclusion, the lower Bexar Shale Member contains a mixture of type II and III kerogen in the thermally less mature middle ramp area and likely contains a mixture of type II and III kerogen in the more mature outer ramp area; however the origin of the kerogen in the outer ramp is obscured by the effects of burial and maturation.

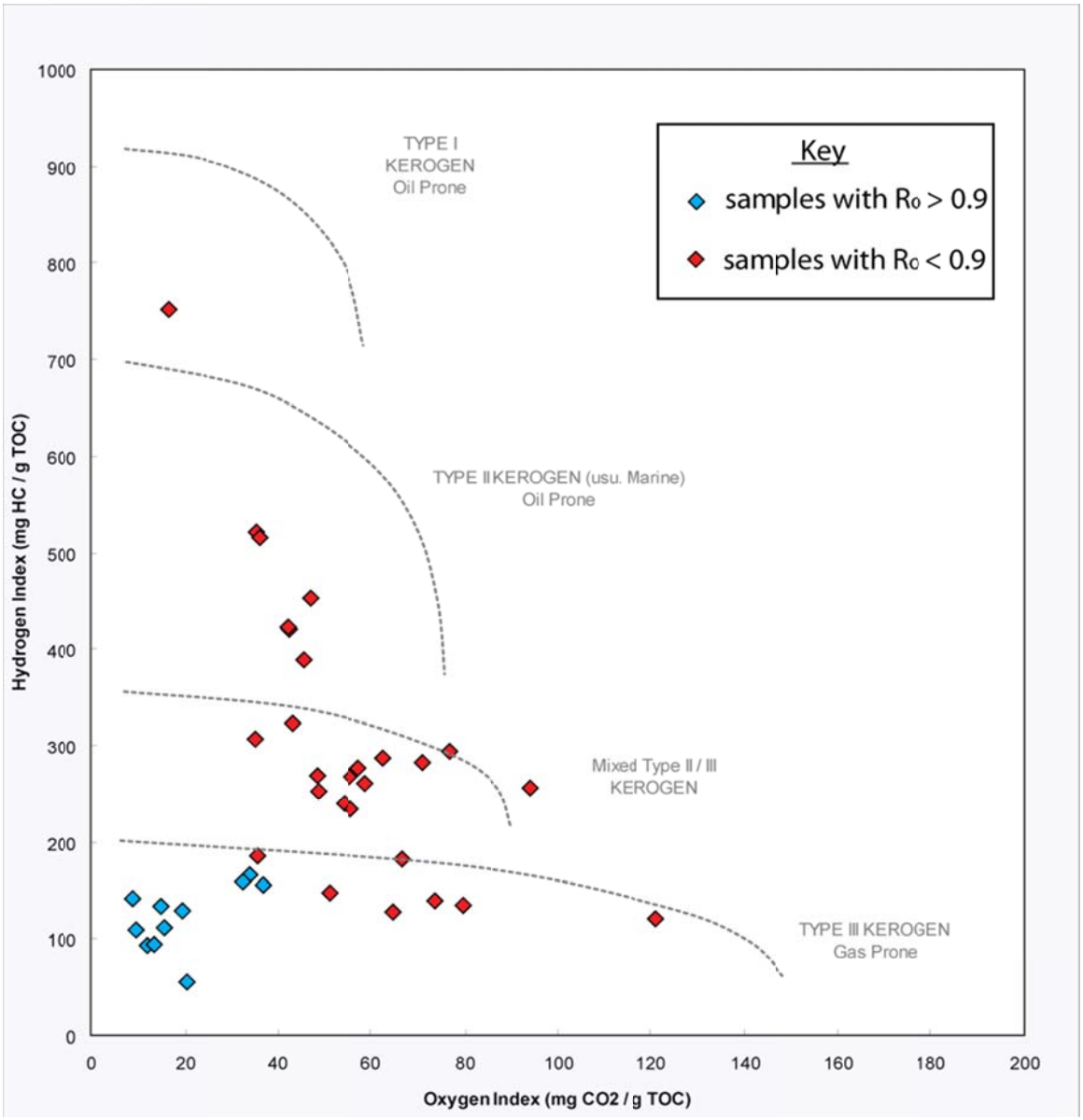

Figure 5.10: Lower Bexar Shale Member kerogen types.

TOC Abundance and Distribution

In the lower Bexar Shale Member, core material for TOC samples were only available in the interval immediately above the top of the Cow Creek Member (Figure 6.11). This horizon did not coincide with peak OAE TOC deposition. The lower Bexar

Shale Member has higher overall average TOC relative to the Pine Island Shale Member. The effect of the Pearsall Arch is also much less pronounced as TOC values in this area are between 0.6% and 1.5%. In the Maverick Basin area values were consistently higher and generally above 1%.

TOC profiles for the outer ramp area show that maximum TOC in the most kerogen-rich part of the lower Bexar Shale Member is between 2% and 5% (Figure 5.12). This is true even in areas with R_o above 1.0. These values coincided with the lithofacies interpreted as having been deposited under the most anoxic conditions. A weak correlation of higher TOC with pelagic carbonate content was observed and discussed earlier.

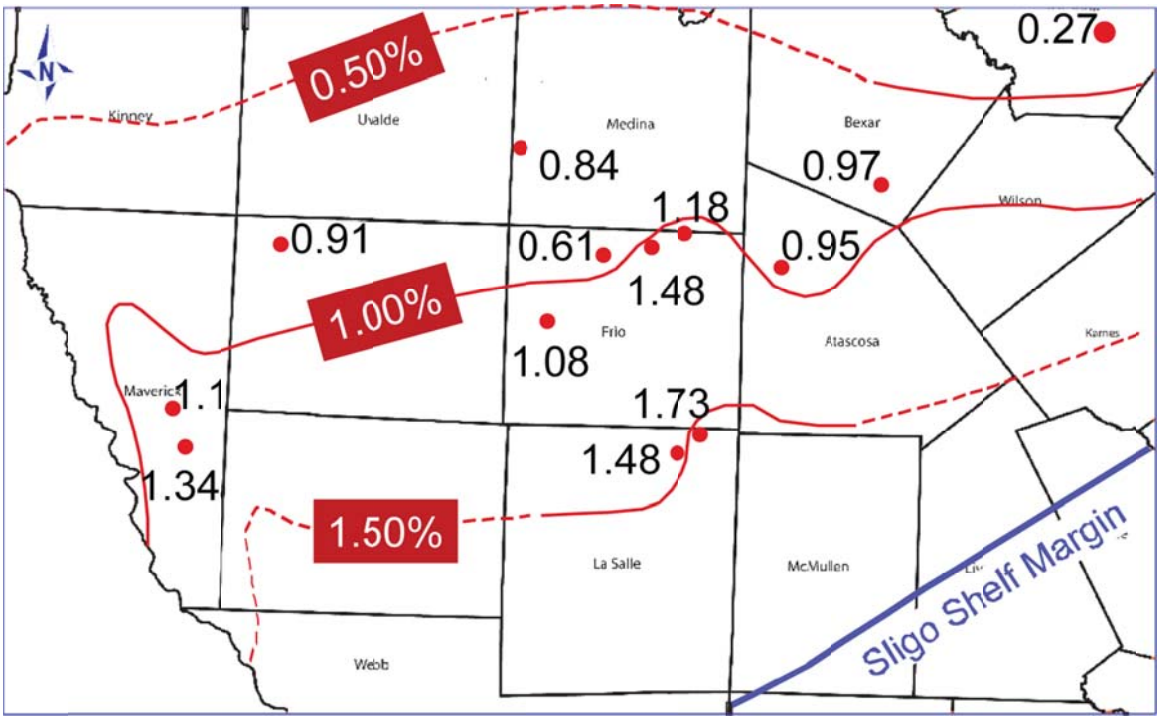

Figure 5.11: Lower Bexar Shale Member TOC trend map.

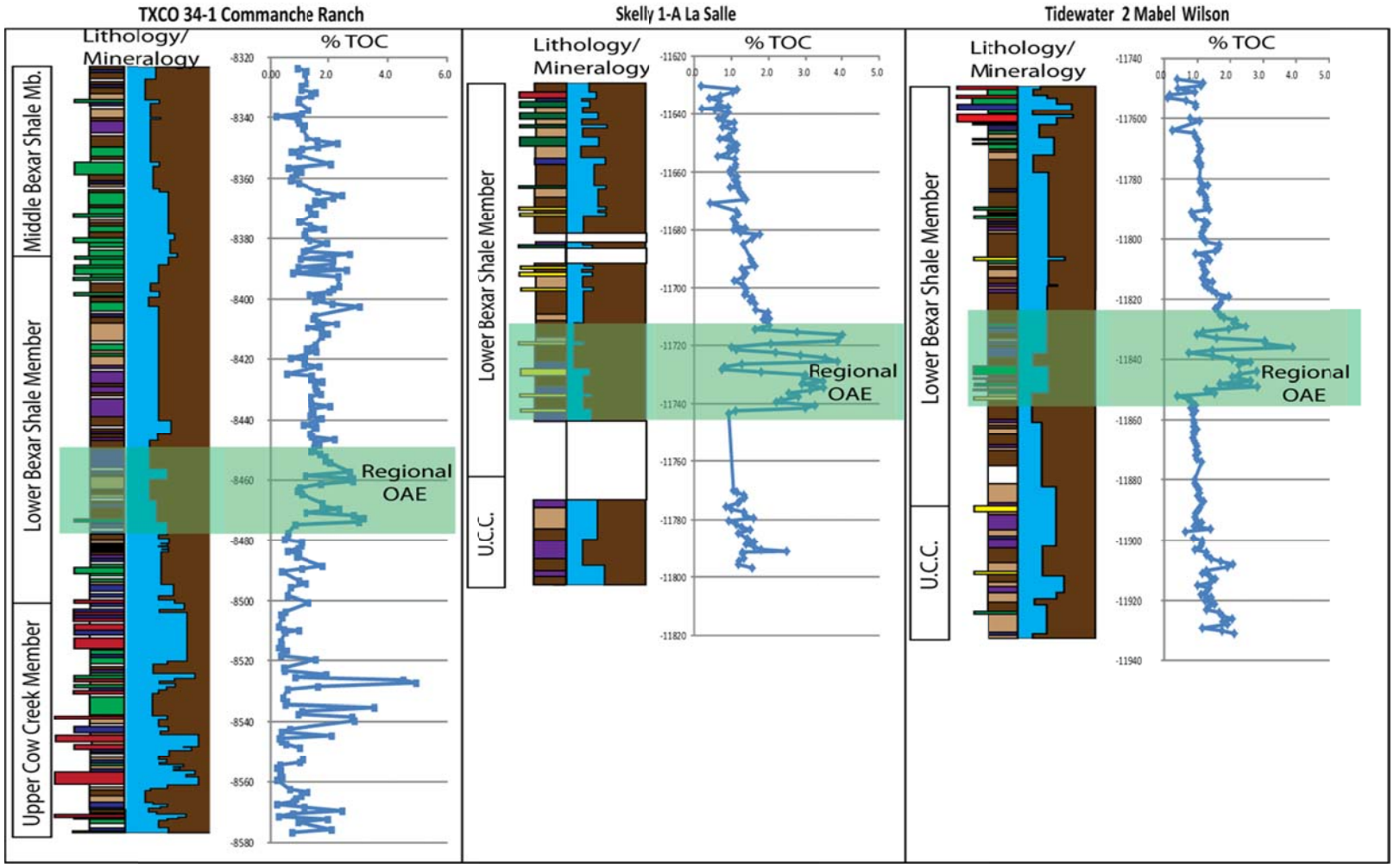

Figure 5.12: Lower Bexar Shale Member TOC profiles. The facies and mineralogy key can be found in figure 4.3.

Maturation

The maturation of the lower Bexar Shale Member responded to the same processes and burial history as the Pine Island Shale Member. Discussion of the maturation of the lower Bexar Shale Member was coupled with the maturation of the Pine Island Shale Member in the previous section.

PORE TYPES

General Statement

The Pearsall mudrock show no visible pores using petrographic methods. SEM analysis on ion-milled samples were necessary to define the pore networks in the Pearsall mudrocks (Hull and Loucks, 2010). The Pearsall mudrocks in Maverick County have approximately 8% bulk porosity where porosity was measured using crushed-rock analysis techniques (Luffel et al., 1992). Observed pores in the Pearsall mudrocks range from equant pores near 5 nanometers in diameter to elongate pores 0.5 microns wide and several microns long. The pores in mudstones can be classified as interparticle, intraparticle, and organic-matter pores (Figure 5.13) (Loucks et al., 2010; in press, 2012).

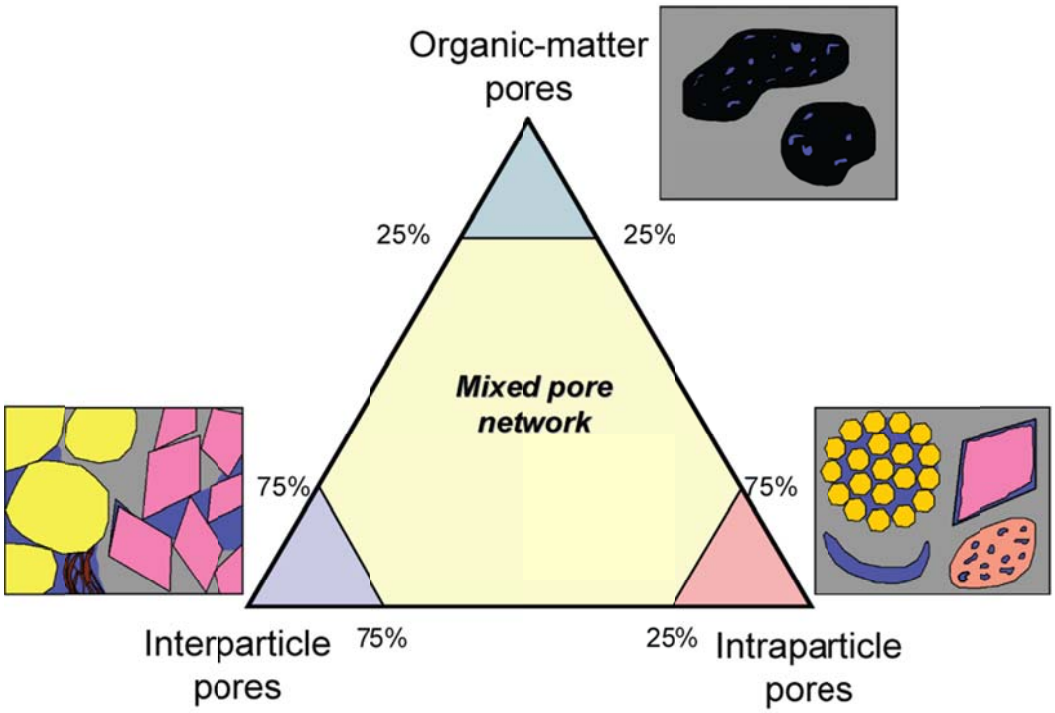

Figure 5.13: Mudrock pore nannopore classification (Loucks et al., 2010; in press, 2012).

Organic-Matter Pores

Organic-matter (OM) pores (Loucks et al., 2010) occur inside organic material and were first described in the Barnett Shale where they are the primary pore network (Loucks et al., 2009). These pores develop during maturation, starting at a R_o of 0.6%. (Loucks et al., 2009). These pores seem to form preferentially in type I and II kerogen as original type III kerogen rarely shows pores (Loucks et al., in press, 2012). Pores hosted within OM appear to form networks indicating that they are likely interconnected and form a permeability network within the grain (Loucks et al., 2009; Ambrose et al., 2010). As such the porosity contributed by organic matter is considered largely effective (Loucks et al.2009; Ambrose et al., 2010) because internal grain network likely connects to other interparticle pores.

OM pores occur in both the lower Bexar Shale and Pine Island Shale Members (Hull and Loucks, 2010) (Figure 5.14). Not all organic macerals develop pores even when mature. This is evidenced in SEM images from the TXCO #34-1H Commanche Ranch well (Figure 5.14) in which some organic macerals have no pores (Figure 5.14C). In some samples it appears that the whole organic grain may not develop pores, but that pores may develop in specific zones such as around the edge of the grain (Figure 5.14F). Also the organic macerals can take the form of pseudomatrix and be deformed and compacted around and between grains (Figure 5.14B), while other macerals can be in pressure shadows and the organic grains remain relatively undeformed (Figure 5.14 A, D).

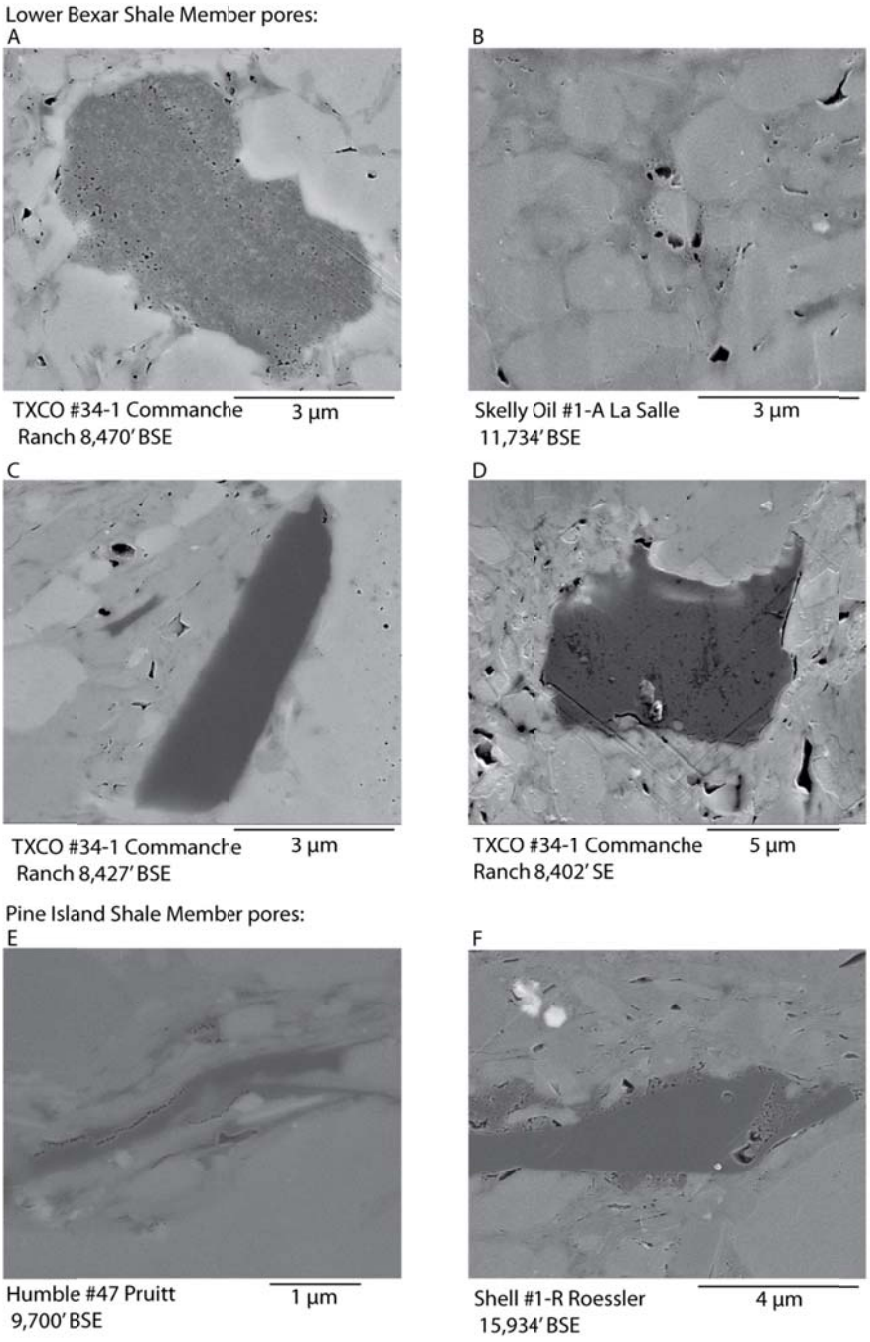

Figure 5.14: Organic-matter pores. (A) OM with a well-developed internal pore network. (B) OM behaving as pseudomatrix. (C) OM which has not developed porosity. (D) OM with partially developed internal pore network. (E) OM with long narrow pores. (F) OM which has developed porosity in some parts only.

Interparticle Pores

Interparticle pores in mudstones occur between grains (Loucks et al., 2010). Such pores are common in clay-rich matrix. They are also common around silt grains as the silt grains disrupt the compaction processes, thereby holding pores open (e. g. Krushin, 1997; Katsube and Williamson, 1998; Dewhurst et al., 1998; Milliken and Reed, 2009). These pores, however, can be reduced by cementation, compaction, and other porosity reducing processes similar to those which affect pores visible with the unaided eye (Milliken and Day-Stirrat, 2010).

Figure 5.15 shows examples of interparticle pores and pore networks from the Pearsall Formation. In both the Pine Island Shale and lower Bexar Shale Members, relatively low-magnification images show a multiplicity of pores in the mudstones that are likely interconnected (Figure 5.15 B, F). Interparticle pores are the most common pores seen in the Pearsall mudstones (Hull and Loucks, 2010). They tend to be triangular in shape and distributed throughout the rock (Figure 5.15 A, C). The pores also commonly occur between clay floccules. In some samples, interparticle pores appear enhanced by dissolution of the surrounding grains (Figure 5.15 D, E). The pores range in size from up to a quarter micron wide and several microns to tens of nanometers long. Some pores show evidence of being relic bubbles in hydrocarbons such as seen in the triangular pore in the upper right of the photograph from the Humble Pruitt (Figure 5.15 E).

The interparticle pore system should be mostly effective because pores are in conventional reservoirs. The pores seem to occur in small groups and areas. It is not known if these clusters of pores are connected or if hydraulic fracturing is required to connect them and make them effective.

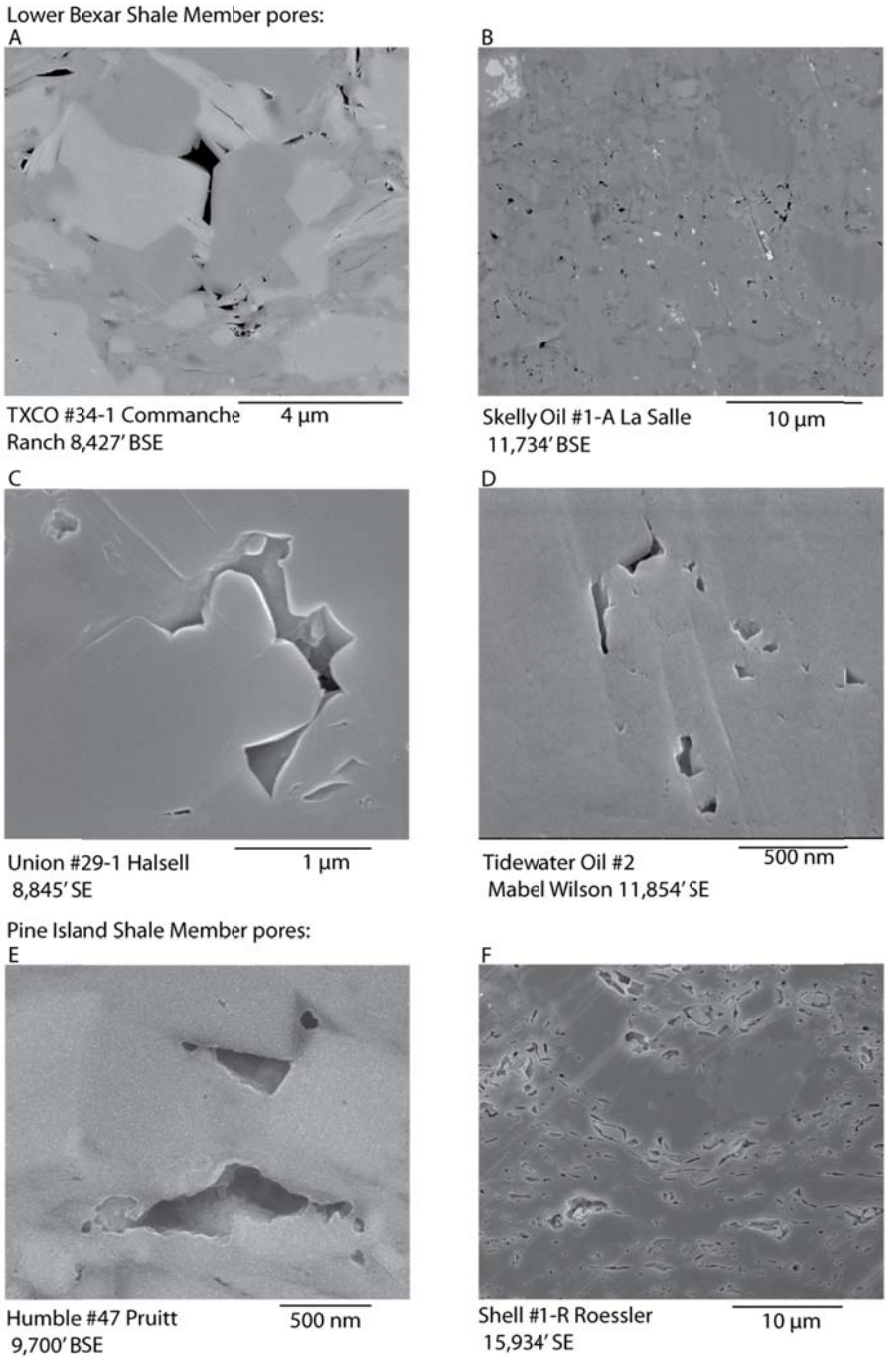

Figure 5.15: Interparticle pores. (A) Pores clustered around large silt grains. (B) Example of the lower Bexar Shale Member porosity network. (C) Large pores enhanced by dissolution. (D) Small pores around silt grain. (E) Triangular pores, and hydrocarbon filled pores in the Pine Island Shale Member. (F) An example of the Pine Island Shale Member pore network.

Intraparticle Porosity

Intraparticle pores occur within grain boundaries (Loucks et al., 2010) and are the most diverse form of pores in mudrocks. Some of the Pearsall pores are moldic, resulting from the dissolution of nannofossils or crystals (Hull and Loucks, 2010). The pores can also be formed by fluid inclusions and as intraplate space in mica or clay platelets. Some of intraparticle pores are less likely to be interconnected and therefore part of the effective porosity (Loucks et al., 2010). However, interparticle pores can also occur in other situations more unique to mudrocks. Framboidal pyrite can contain significant amounts of porosity within its rigid crystal structure (Loucks et al., 2009; Figure 5.16 F).

The pores Figure 5.16 A and E feature pores resulting from dissolution of carbonate crystals and skeletal grains. In both of the examples, rhombic dolomites have clearly been dissolved around the edges or in their entirety. In the lower left hand example there is also a crescent-shaped dissolution feature believed to be related to a skeletal grain. Figure 5.16 B shows a biotite intraparticle porosity along the cleavage planes. Figures 5.16 C shows a grain containing fluid inclusions. Figure 5.16 D shows a phosphate clast with submicron internal intraparticle pores.

The intraparticle pores are among the most likely to be preserved as they are generally protected from compaction by the structural support of the surrounding rigid grains. Also porosity created by dissolution at grain edges commonly occurs after compaction has already taken place. These pores are more likely to be connected to other pores because they are at the external edge of the grain.

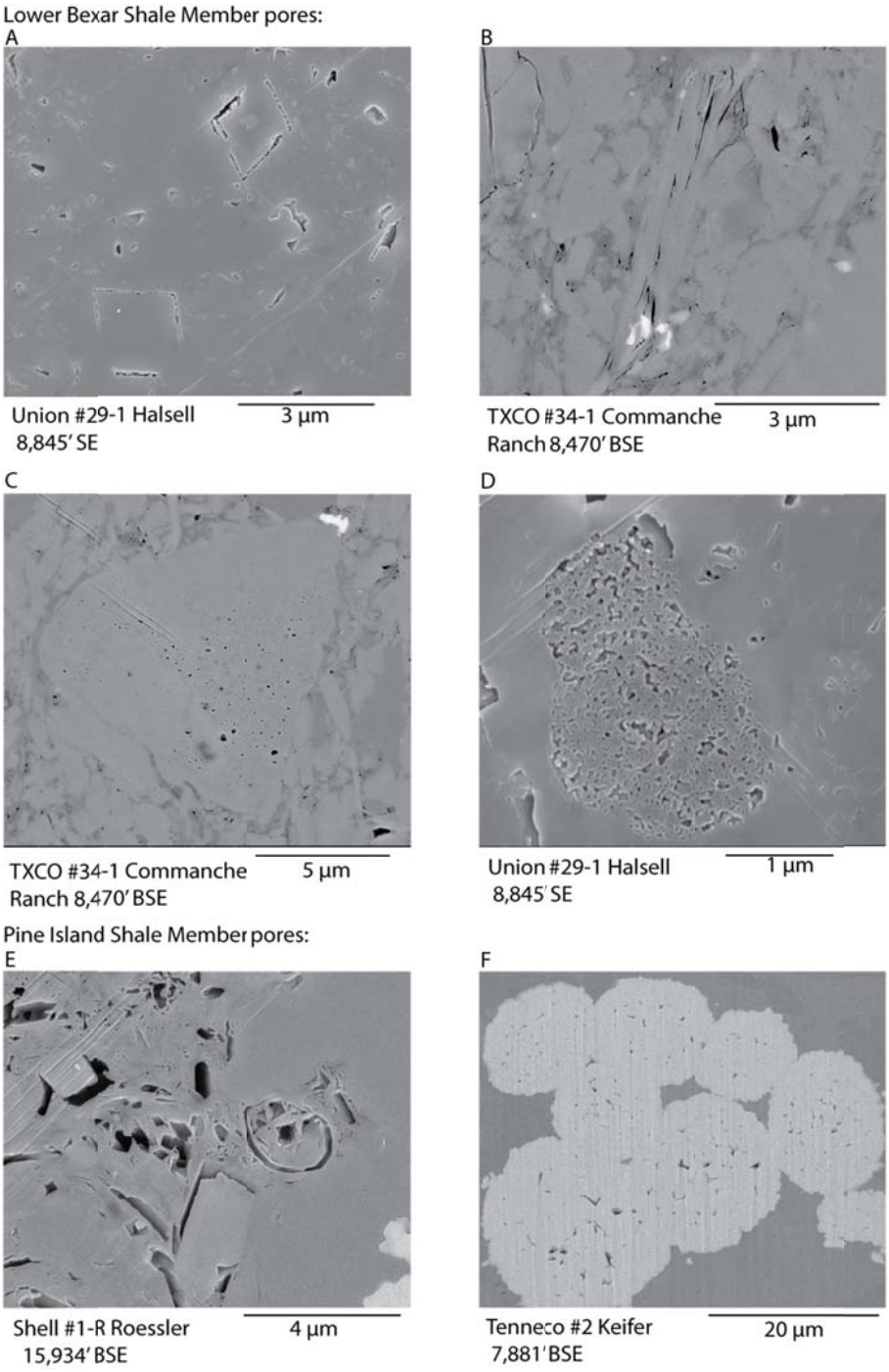

Figure 5.16: Intraparticle pores. (A) Pores after dolomite molds. (B) Pores in a biotite grain. (C) Fluid inclusions, ineffective porosity. (D) A phosphate clast with well-developed internal pore network. (E) Fossil and dolomite molds. (F) Pores within pyrite framboids.

Fracture Porosity

At least two generations of fractures are observed in the Cow Creek and lower Bexar Shale Members (Figure 5.17). Some of the fractures have associated pore space and are thought to be important for oil and gas production (Clarke, 2007). There are numerous fractures in the cores indicating that there are likely thousands of fractures in the subsurface. Nearly all of the outer ramp Bexar Shale Member cores feature subvertical calcite filled fractures. They are also planes of weakness in the rock that control breakage of the core. These fractures are open mode fractures and do not typically exhibit any offset across the fracture face. It is not possible to tell the exact length of the fractures as they cut across the face of the core but overall they are near vertical. No orientated core or image logs were available for this study, so the orientation of the fractures is not possible to discern. When a fracture terminates, a new fracture commonly appears a few millimeters away and continues (Figure 5.17 C). The offset of fractures does not appear to be related to changes in lithology as the fracture terminations, when observed, do not correspond to changes.

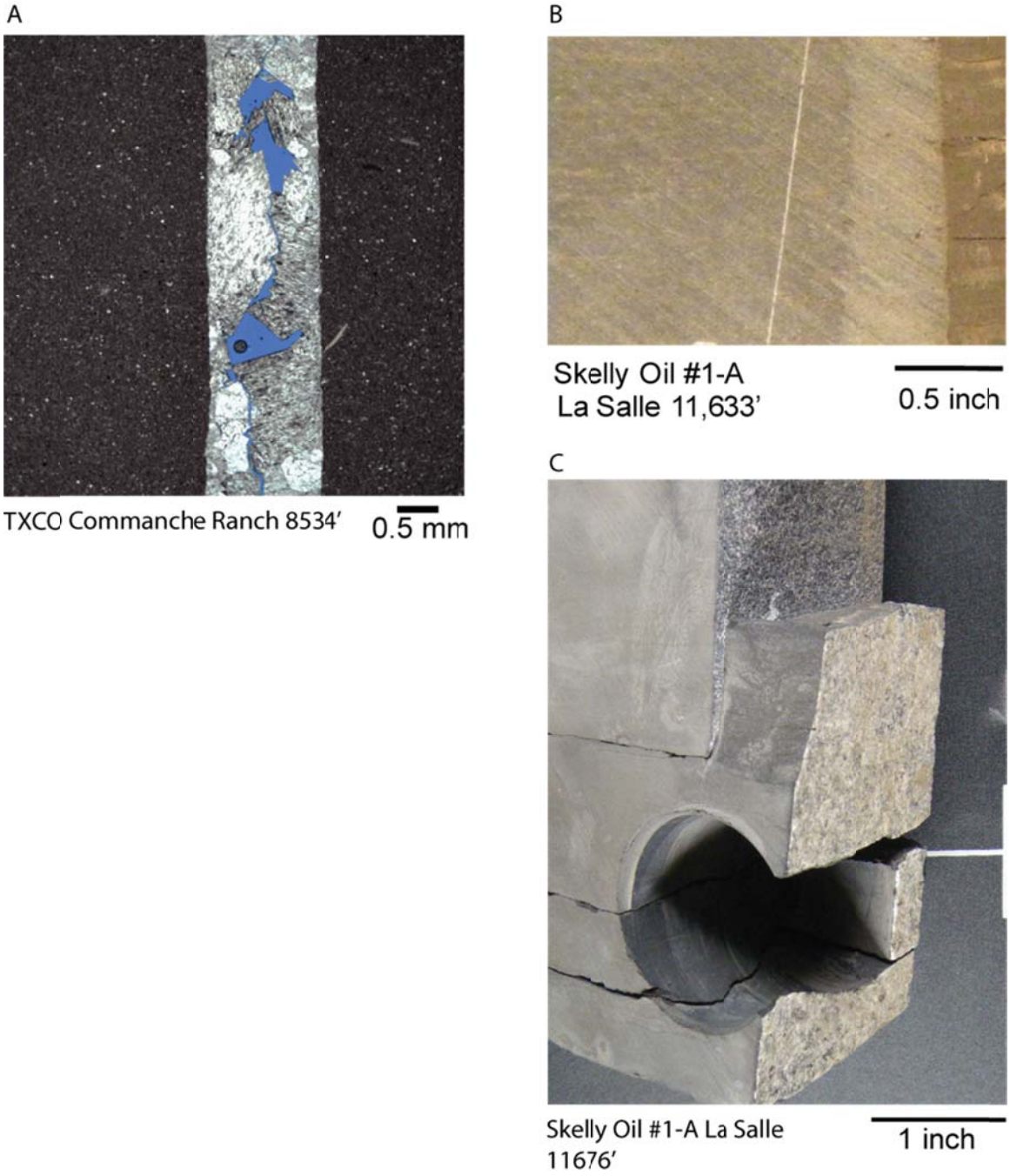

Figure 5.17: Subvertical fractures. (A) Open pores in the fracture. (B) Sealed cemented fracture. (C) Fracture surfaces covered in calcite cement and offset from each other.

Porosity and Permeability versus Mineralogy

In addition to SEM imaging of pores, crushed rock permeability and porosity analysis was available on one well (name of well is proprietary). Figure 5.18 shows the relationship between the porosity and permeability in the upper Cow Creek and lower Bexar Members. The data show a positive correlation between porosity and permeability if the carbonate and terrigenous mudstones are grouped together. The data points can be divided into three facies groups based on the kind of matrix present and the stratigraphic formation. The argillaceous carbonate matrix samples, wackestones, from the upper Cow Creek Member exhibit the lowest porosities and the largest range of permeability from 1 nd to 25 nd. The next group of samples is from the upper Cow Creek Member clay-rich terrigenous mudstones. These actually exhibited the best combination of porosity and permeability (as well as some of the highest TOC). It is thought that the high clay and organic content is associated with dominantly connected interparticle and organic pores. These terrigenous mudstones are interbedded with the argillaceous wackestones and are too thin to form good reservoirs. The final group is terrigenous mudstones from the lower Bexar Shale Member. These terrigenous mudstones have the highest permeability values and are producing as a shale-gas reservoir. Comparison of XRD mineralogy with porosity (Figure 5.19A) shows that the porosity has a positive correlation with clay content (Figure 5.19A) and that correlation with permeability is not very strong. Figure 5.19(C and B) shows a negative correlation with porosity and permeability.

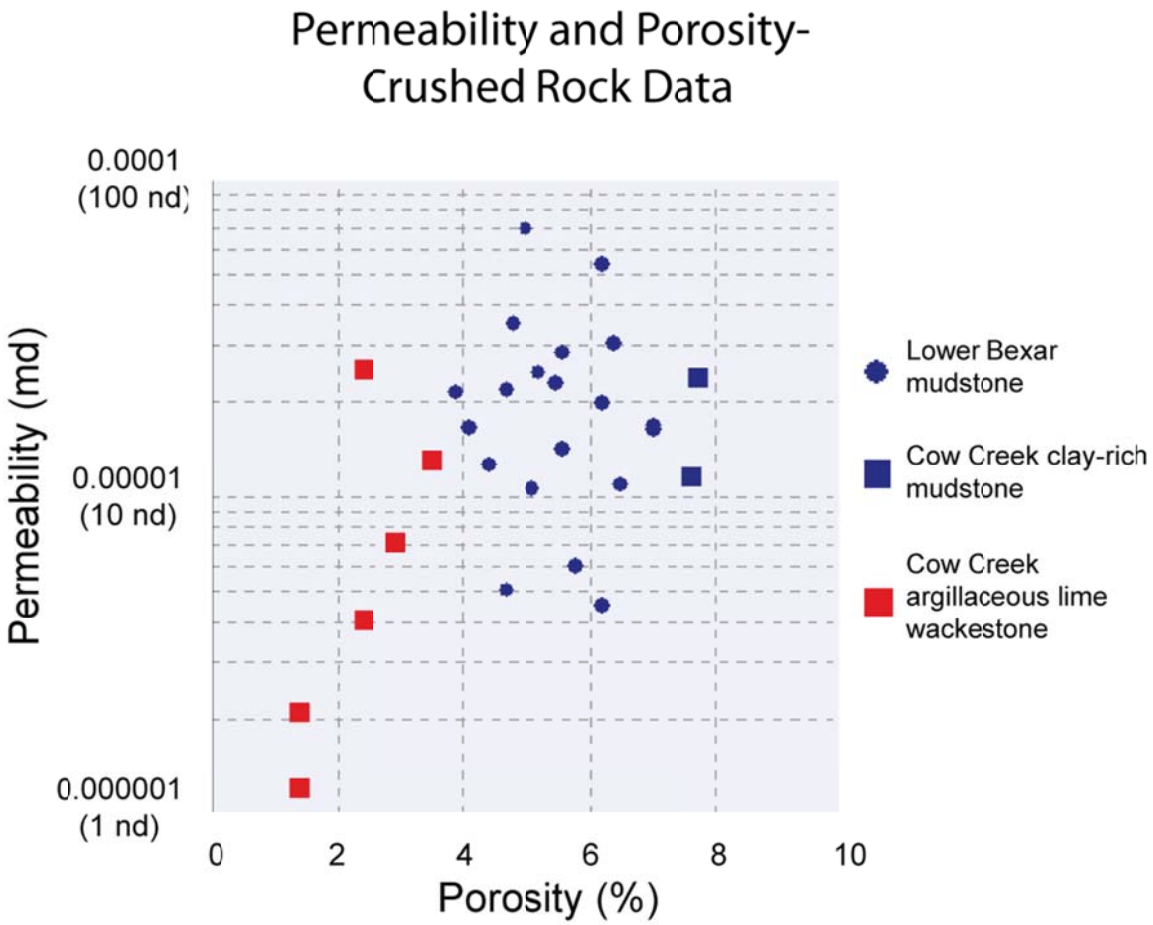

Figure 5.18: Porosity and permeability.

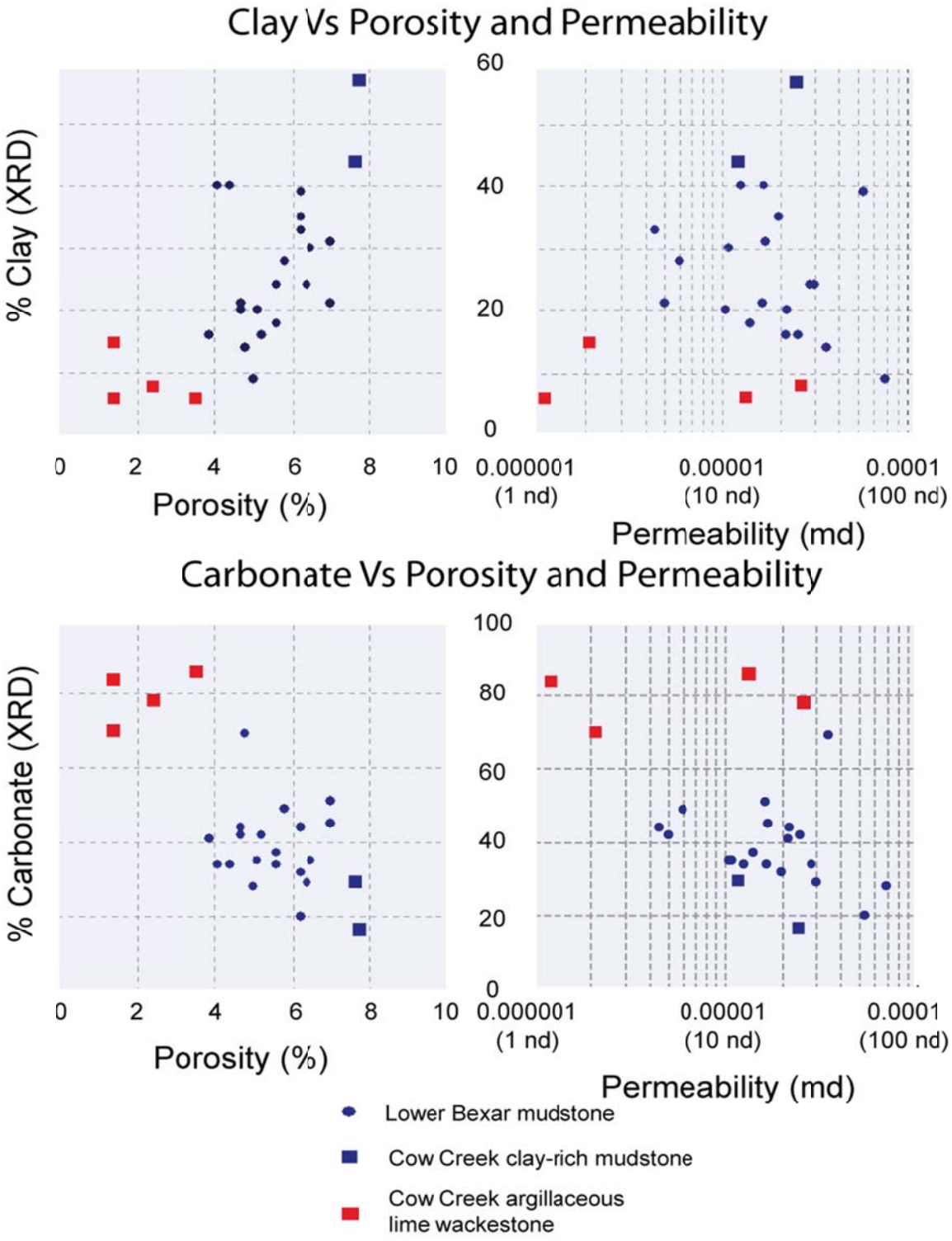

Figure 5.19: Porosity and permeability versus mineralogy.

Chapter 6: Conclusions

General Statement

The Pearsall Formation is a series of interbedded carbonate and siliciclastic units deposited primarily during Aptian time. They form a viable shale-gas system in South Texas that has yet to be fully exploited. The shale-gas system arises from the interaction of second-order transgressions, several OAEs, and deposition on a broad ramp on a drowned shelf.

Structure, Stratigraphy, and OAEs

The study area in South Texas is complicated both structurally and stratigraphically as a result of the paleostructures that existed during Pearsall deposition. The Pearsall Formation was deposited over 11.75 my (Phelps, 2011). It was deposited primarily between the maximum flooding events of two second-order sequences, and it has a second-order sequence boundary at the top of the Cow Creek Member in the middle of the formation. The formation as a whole can be divided into five third-order sequences that can be traced throughout the ramp.

In addition to these sequences and the eustatic events that created them, there are three OAEs recorded in the Pearsall Formation. These three events, the OAE 1-A, the late Aptian regional event, and the OAE 1-B, occurred at 122 my, 119 my, and 110 my, respectively. The OAEs coincided with flooding of the ramp and altered the degree of oxygenation of the water column, producing dysoxic to anoxic bottom conditions. A shift from carbonate-dominated sedimentation occurred during the OAE to siliciclastic-dominated sedimentation.

DEPOSITIONAL SYSTEMS AND FACIES

Deposition was dominated by environmental perturbations produced by the OAEs that induced changes in the depositional environments. During the deposition of the Sligo Formation, Cow Creek Member, and later carbonate formations, conditions favored a strong carbonate factory. During OAE deposition, deeper waters existed over much of the ramp, and the dominant depositional processes were dilute turbidity currents, hemipelagic plumb suspension deposition, and pelagic suspension deposition.

PETROLEUM SYSTEM

In the outer ramp the prospective producing units are the Pine Island Shale, lower Bexar Shale, and upper Bexar Shale Members. Each of these reservoirs is related to occurrences of OAEs. Several potential shale-gas facies were deposited in the outer ramp area during the OAEs. The weakly laminated to massive calcite-silt bearing terrigenous mudstone and the winnowed nonbioturbated calcite silt-bearing terrigenous mudstone are potential reservoir facies. These are the facies that produce shale-gas in the lower Bexar Formation in southern Maverick County.

High TOC is found in the pelagic facies and the nonbioturbated facies. These facies are more distal and accumulated in areas of increased subsidence particularly the areas underlain by the Triassic rift and by large quantities of Jurassic Salt.

The areas with thermal maturity in the oil window coincide with areas of low TOC on the San Marcos Arch, Pearsall Arch, and near the Burro Salado Arch. The areas with higher thermal maturity coincide with accumulations of higher TOC. These areas have maturity levels in the condensate to dry gas zone but have generally produced dry gas. These higher maturities are associated with uplift in the western part of the study area. To the east near the San Marcos Arch, there is a greater possibility for wet gas, but

the play area also constricts approaching the arch in that the area affected by dysoxia on the shelf may be smaller due to the paleostructure.

Pore networks were imaged in the key facies of the Pearsall Formation using the Ar-ion milled samples on the SEM. Nano- to micropore network includes interparticle, intraparticle, and organic-matter pores, with interparticle pores dominating. The interparticle pores are expected to have the best connectivity. Clay-rich facies also have greater permeability than do carbonate-rich facies.

The lithofacies maps combined with the TOC and maturation maps presented in this study suggest that a large area of the Pearsall outer ramp lithofacies should be prospective for shale-gas exploration. At the shelf edge is approached, depth may become an important economic factor. To trace the Pearsall shale-gas system into Mexico and/or into the East Texas Basin, investigations similar to the present study are necessary.

Appendices

Appendices can be accessed using the DVD at the back of this volume.

APPENDIX A: CORE DESCRIPTIONS

APPENDIX B: TOC AND ROCK-EVAL DATA

APPENDIX C: OTHER GEOCHEMICAL DATA

APPENDIX D: BIOSTRATIGRAPHIC DATA

APPENDIX E: THIN SECTION SCANS

References

Achauer, C.W. 1974. Deposition and diagenesis of the James Limestone (Lower Cretaceous) in the East Texas Basin (Abs.). Gulf Coast Association of Geological Societies, 24: 210.

Aconcha, E.S., Kerans, C. and Zeng, H. 2008. Seismic Geomorphology Applied to Lower Glen Rose Patch Reefs in the Maverick Basin, Southwest Texas. Transactions - Gulf Coast Association of Geological Societies, 58: 3-23.

Ambrose, R.J., Hartman, R.C., Diaz-Campos, M., Akkutlu, I.Y., and Sondergeld, C.H. 2010. New pore-scale considerations for shale gas in place calculations. SPE Unconventional Gas Conference, 23-25 February, 2010: 17pp.

Amodio, S., Ferreri, V., D'Argenio, B., Weissert, H. and Sprovieri, M. 2008. Carbon-isotope stratigraphy and cyclostratigraphy of shallow-marine carbonates; the case of San Lorenzello, Lower Cretaceous of southern Italy. Cretaceous Research, 29: 803-813.

Amsbury, D.L. 1974. Stratigraphic petrology of lower and middle Trinity rocks on the San Marcos platform, south-central Texas. Geoscience and Man, 8: 1-35.

Amsbury, D.L. 1996. Pearsall (Aptian Cretaceous) subsurface to outcrop sequence stratigraphy, central Texas. Transactions - Gulf Coast Association of Geological Societies, 46: 1-7.

Arntz, W.E., Tarazona, J., Gallardo, V.A., Flores, L.A., and Salzwedel, H. 1991. Benthos communities in oxygen deficient shelf and upper slope areas of the Peruvian and Chilean Pacific coast, and changes caused by El Nino. In Modern and ancient shelf anoxia (Eds. R.V. Tyson and T.H. Pearson), pp. 131-154. Geological Society Special Publication, 58.

Arthur, M.A. and Sageman, B.B. 1994. Marine black shales; depositional mechanisms and environments of ancient deposits. Annual Review of Earth and Planetary Sciences, 22: 499-551.

Arthur, M.A., Dean, W.E, and Stow, D.A.V. 1984. Models for the deposition of Mesozoic-Cenozoic fine-grained organic-carbon-rich sediment in the deep sea. In Deep-water processes and facies. eds. D.A.V. Stow and D.J.W. Piper. Geological Society Special Publication, 15: 527-562.

Arthur, M.A. and Schlanger, S.O. 1979. Cretaceous 'oceanic anoxic events' as causal factors in development of reef-reservoired giant oil fields. AAPG Bulletin, 63: 870-885.

Bay, A.R. 1982. Evolution and porosity of carbonate shoaling cycles, Lower Cretaceous-lower Glen Rose, South Texas. Transactions - Gulf Coast Association of Geological Societies, 32: 101-119.

Bay, T.A., Jr. 1977. Lower Cretaceous Stratigraphic Models from Texas and Mexico. In: Cretaceous Carbonates of Texas and Mexico: Applications to Subsurface Exploration (Eds D.G. Bebout and R.G. Loucks), Report of Investigations No 89, pp. 12-30. University of Texas at Austin, Bureau of Economic Geology, Austin, TX.

Bebout, D.G. 1977. Sligo and Hosston depositional patterns, subsurface of South Texas. Report of Investigations - Texas, University, Bureau of Economic Geology79-96.

Bebout, D.G., Budd, D.A. and Schatzinger, R.A. 1981. Depositional and diagenetic history of the Sligo and Hosston formations (Lower Cretaceous) in South Texas. Report of Investigations - Texas, University, Bureau of Economic Geology. University of Texas at Austin, Bureau of Economic Geology: Austin, TX, United States, United States, 70 pp.

Bebout, D.G. and Loucks, R.G. (Eds) 1977. Cretaceous Carbonates of Texas & Mexico - Applications to Subsurface Exploration. (Ed W.L. Fisher), Report of Investigations, 89. Bureau of Economic Geology, The University of Texas at Austin, Austin, TX, 332 pp.

Bebout, D.G. and Schatzinger, R.A. 1978. Distribution and geometry of an oolite-shoal complex; Lower Cretaceous Sligo Formation, South Texas. Transactions - Gulf Coast Association of Geological Societies, 28, Part 1: 33-45.

Berner, R.A. 1970. Sedimentary Pyrite Formation. American Journal of Science, 268: 1-23.

Bhattacharya, J.P., MacEachern, J.A. 2009. Hyperpycnal Rivers and Prodeltaic Shelves in the Cretaceous Seaway of North America. Journal of Sedimentary Research, 79, 184-209

Blakey, R. 2005. Paleogeography and geologic evolution of North American; images that track the ancient landscapes of North America: http://www2.nau.edu/rcb7/nam.html (accessed July 16, 2011).

Boggs, S. Jr. 2006. Principles of sedimentology and stratigraphy: Upper Saddle River, NJ, Pearson Prentice Hall, 662pp.

Bralower, T.J. 1988. Calcareous nannofossil biostratigraphy and assemblages of the Cenomanian-Turonian boundary interval: implications for the origin and timing of oceanic anoxia. Paleoceanography, 3: 275-316.

Bralower, T.J., CoBabe, E., Clement, B., Sliter, W.V., Osburn, C.L. and Longoria, J. 1999. The record of global change in Mid-Cretaceous (Barremian-Albian) sections from the Sierra Madre, northeastern Mexico. Journal of Foraminiferal Research, 29: 418-437.

Bushaw, D. 1968. Environmental synthesis of east Texas Lower Cretaceous: Transactions - Gulf Coast Association of Geological Societies, 18: 416-438.

Cartwright, J.A. and Dewhurst, D.N. 1998. Layer-bound compaction faults in fine-grained sediments. Geological Society of America Bulletin, 110: 1242-1257.

Clarke, R. 2007. Basin Focus: Maverick Basin. Oil and Gas Investor: 4pp.

Coffin, M.F., Eldholm, O. 1994. Large Igneous Provinces Crustal Structure, Dimensions, and External Consequences: Reviews of Geophysics, 32: 1-36.

Cook, T.D. 1979. Exploration history of South Texas Lower Cretaceous carbonate platform. AAPG Bulletin, 63: 32-49.

Day-Stirrat, R.J., Milliken, K.L., Dutton, S.P., Loucks, R.G., Hillier, S., Aplin, A.C., and Schleicher, A.M.. 2010. Open-system chemical behavior in deep Wilcox Group mudstones, Texas Gulf Coast, USA. Marine and Petroleum Geology, 27: 1804-1818.

Demaison, G.J. and Moore, G.T.. 1980. Anoxic environments and oil source bed genesis. Organic Geochemistry, 2: 9-31.

Drosser, M.L., and Bottjer, D.J. 1986. A semiquantitative field classification of ichnofabric: Journal of Sedimentary Research, 56, 4: 558-559.

Dunham, R.J. 1962. Classification of carbonate rocks according to depositional texture: in (Ham, W.E., eds.), Classification of carbonate rocks: AAPG Memoir 1: 62-84.

Erba, E. 1994. Nannofossils and superplumes: The Early Aptian "nannoconid crisis". Paleoceanography, 9: 483-501.

Erba, E., Bottini, C., Weissert, H.J. and Keller, C.E. 2010. Calcareous nannoplankton response to surface-water acidification around Oceanic Anoxic Event 1a. Science, 329: 428-432.

Erbacher, J. and Thurow, J. 1997. Influence of oceanic anoxic events on the evolution of Mid-Cretaceous Radiolaria in the North Atlantic and western Tethys. Marine Micropaleontology, 30: 139-158.

Erbacher, J., Thurow, J. and Littke, R. 1996. Evolution patterns of radiolaria and organic matter variations: A new approach to identify sea-level changes in mid-Cretaceous pelagic environments. Geology, 24: 499-502.

Espitalie, J., Madec, M., Tissot, B., Menning, J.J. and Leplat, P. 1977, Source rock characterization method for petroleum exploration, *in* Preprints- Offshore Technology Conference, Houston, Tx: Dallas, Tx, Offshore Technology Conference, 3, 9: 439-444.

Ewing, T.E. 2003. Review of the Tectonic History of the Lower Rio Grande Border Region, South Texas and Mexico, and Implications for Hydrocarbon Exploration. Sipes Newsletter, 40: 16-21.

Ewing, T.E. 2010. Pre-Pearsall Geology and Exploration Plays in South Texas. Transactions - Gulf Coast Association of Geological Societies, 60: 241-260.

Folk, R.L. 1980. Petrology of sedimentary rocks: Austin, Texas, Hemphill Publishing Co., 182pp.

Follmi K.B. and Grimm K.A., 1990. Doomed pioneers: Gravity-flow deposition and bioturbation in marine oxygen-deficient environments. Geology, 18: 1069-1072.

Follmi, K.B., Godet, A., Bodin, S. and Linder, P. 2006. Interactions between environmental change and shallow water carbonate buildup along the northern Tethyan margin and their impact on the Early Cretaceous carbon isotope record. Paleoceanography, 21: 1-16.

Forgotson, J.M., Jr. 1957. Stratigraphy of Comanchean Cretaceous Trinity group [Gulf Coastal Plain]. Bulletin of the American Association of Petroleum Geologists, 41: 2328-2363.

Foster, T.R. 2003.The evolution of a Lower Cretaceous carbonate platform within a divergent margin setting: The Cupido Formation, northeastern Mexico. The University of Texas at Austin, Austin, 226 pp.

Fritz, D.A., Belsher, T.W., Medlin, J.M., Stubbs, J.L., Wright, R.P. and Harris, P.M. 2000. New exploration concepts for the Edwards and Sligo margins, Cretaceous of onshore Texas. AAPG Bulletin, 84: 905-922.

Gao, G. and Land, L.S. 1991. Early Ordovician Cool Creek Dolomite, middle Arbuckle Group, Slick Hills, SW Oklahoma, USA; origin and modification. Journal of Sedimentary Research, 61: 161-173.

Goldhammer, R.K. and Johnson, C.A. 2001. Middle Jurassic-Upper Cretaceous paleogeographic evolution and sequence-stratigraphic framework of the Northwest Gulf of Mexico rim. In: The western Gulf of Mexico basin; tectonics, sedimentary basins, and petroleum systems (Eds C. Bartolini, R.T. Buffler and A. Cantu-Chapa), AAPG Memoir 75, pp. 45-81. American Association of Petroleum Geologists : Tulsa, OK, United States, Tulsa, OK.

Hackley, P.C., Dennen, K., Gesserman, R., and Ridgley, J.L. 2009. Preliminary investigation of the thermal maturity of Pearsall Formation shales in the Maverick Basin, South Texas. AAPG Annual Convention, Denver, Co.

Hackley, P. 2011. USGS Assessment of Undiscovered Shale Gas Resources in the Lower Cretaceous Pearsall Formation, Maverick Basin, South Texas (Abs). AAPG Annual Conference and Exhibition, Houston, Tx.

Hallock, P. and Schlager, W. 1986. Nutrient excess and the demise of coral reefs and carbonate platforms. Palaios, 1: 389-398.

Handford, C.R. 1986. Facies and bedding sequences in shelf-storm-deposited carbonates; Fayetteville Shale and Pitkin Limestone (Mississippian), Arkansas. Journal of Sedimentary Research, 56: 123-137.

Harbor, R. 2011. Facies Characterization and Stratigraphic Architecture of Organic-Rich Mudrocks, Upper Cretaceous Eagle Ford Formation, South Texas. University of Texas at Austin, Austin, Tx. 186pp.

Hay, W.W., and Brock, J.C., 1992. Temporal variation in intensity of upwelling off southwest Africa. Geological Society Special Publications, 64: 463-497.

Herrle, J.O., Koessler, P., Friedrich, O., Erlenkeuser, H. and Hemleben, C. 2004. High-resolution carbon isotope records of the Aptian to lower Albian from SE France and the Mazagan Plateau (DSDP Site 545); a stratigraphic tool for paleoceanographic and paleobiologic reconstruction. Earth and Planetary Science Letters, 218: 149-161.

Huber, B.T., Norris, R.D. and MacLeod, K.G. 2002. Deep-sea paleotemperature record of extreme warmth during the Cretaceous. Geology, 30: 123-126.

Hughes, D.J. 1968. Salt tec5tonics as related to several Smackover fields along the northeast rim of the Gulf of Mexico Basin. Transactions - Gulf Coast Association of Geological Societies, 18: 320-330.

Hughes, E.N. 2011. Chemostratigraphy and paleoenvironment of the Smithwick Formation, Fort Worth Basin, San Saba County, Texas. University of Texas at Arlington, Arlington, Tx. 94pp.

Hull, D.C., and Loucks R.G. 2010. Depositional systems and stratal architecture of the Lower Cretaceous (Aptian) Pearsall Formation in south Texas. Transactions - Gulf Coast Association of Geological Societies, 60: 901-906.

Imlay, R.W. 1945. Subsurface Lower Cretaceous formations of south Texas. Bulletin of the American Association of Petroleum Geologists, 29: 1416-1469.

Inden, R.F. and Moore, C.H. 1983. Beach environment. AAPG Memoir, 33: 211-265.

Jarvie, D. M. and Tobey, M.H. 1999. TOC, rock-eval, or SR. analyzer interpretive guidelines. Humble Geochemical Services Division. 16pp.

Jenkyns, H.C. 1980. Cretaceous anoxic events; from continents to oceans. Journal of the Geological Society of London, 137, Part 2: 171-188.

Jenkyns, H.C. 1995. Carbon-isotope stratigraphy and paleoceanographic significance of the Lower Cretaceous shallow-water carbonates of Resolution Guyot, Mid-Pacific Mountains. Proceedings of the Ocean Drilling Program, Scientific Results, 143: 99-104.

Jenkyns, H.C. 2003. Evidence for rapid climate change in the Mesozoic-Palaeogene greenhouse world. Philosophical Transactions - Royal Society London, 361: 1885-1916.

Jones, C.E. and Jenkyns, H.C. 2001. Seawater strontium isotopes, oceanic anoxic events, and seafloor hydrothermal activity in the Jurassic and Cretaceous. American Journal of Science, 301: 112-149.

Kaminski, M.A., Boersma, A., Tyszka, J., and Holbourn, A.E.L. 1993. Response of deep-water agglutinated foraminifera to dysoxic conditions in the California Borderland basins. In: (Kaminski, M.A., Geroch, S., and Gasifski, M.A. eds. Proceedings of the fourth international workshop on agglutinated foraminifera, Krakow Poland, September 12-19, 1993. Grzybowski Foundation special publication, 3: 131-140.

Katsube J. and Williamson, M. 1998. Shale petrophysical characteristics: permeability history of subsiding shales; in Shales and Mudstones II, (eds) J. Schieber, W. Zimmerle, and P.S. Sethi; Stuttgard, Germany. 69-91.

Kelling, G. and Mullins, P.R., 1974. Graded limestones-quarzite couplets: Possible storm deposits from the Moroccan Carboniferous, Sedimentary Geology, 13: 161-190.

Kerans, C. and Loucks, R.G. 2002. Stratigraphic setting and controls on occurrence of high-energy carbonate beach deposits; Lower Cretaceous of the Gulf of Mexico. Transactions - Gulf Coast Association of Geological Societies, 52: 517-526.

Krushin, J.T. 1997. Seal capacity of non-smectite shale, in R.C. Surdam ed. Seals traps and the petroleum system. AAPG Memoir 67, 31-47.

Kump, L.R. and Arthur, M.A. 1999. Interpreting carbon-isotope excursions: carbonates and organic matter. Chemical Geology, 161: 181-198.

Lamb, M.P., Myrow, P.M., Lukens, C., Houck, K. and Strauss, J. 2008. Deposits from wave-influenced turbidity currents: Pennsylvanian Minturn Formation, Colorado, USA. Journal of Sedimentary Research, 78: 480-498.

Larson, R.L. 1991. Latest pulse of Earth: Evidence for a mid-Cretaceous superplume. Geology, 19: 547-550.

Larson, R.L. and Erba, E. 1999. Onset of the mid-Cretaceous greenhouse in the Barremian-Aptian: Igneous events and the biological, sedimentary, and geochemical responses. Paleoceanography, 14: 663-678.

Law, C.A. 1999. Evaluating source rocks, in Beaumont E.A, and Foster, N.H. eds., Exploring for oil and gas traps. AAPG treatise of petroleum geology, 6-4 – 6-41.

Leckie, R.M., Bralower, T.J. and Cashman, R. 2002. Oceanic anoxic events and plankton evolution; biotic response to tectonic forcing during the Mid-Cretaceous. Paleoceanography, 17.

Lees, J.A., Bown, P.R., and Young, J.R.. 2005 Photic zone palaeoenvironments of the Kimmeridge Clay Formation (Upper Jurassic, UK) suggested by calcareous nannoplankton palaeoecology. Palaeogeography, Palaeoclimatology, Palaeoecology, 235: 110-134.

Lehmann, C., Osleger, D.A. and Montanez, I. 2000. Sequence stratigraphy of Lower Cretaceous (Barremian-Albian) carbonate platforms of northeastern Mexico; regional and global correlations. Journal of Sedimentary Research, 70: 373-391.

Lehmann, C., Osleger, D.A., Montanez, I.P., Sliter, W.V., Arnaud-Vanneau, A. and Banner, J.L. 1999. Evolution of Cupido and Coahuila carbonate platforms, Early Cretaceous, northeastern Mexico. Geological Society of America Bulletin, 111: 1010-1029.

Lehrmann, D.J. and Goldhammer, R.K. 1999. Secular variation in parasequence and facies stacking patterns of platform carbonates; a guide to application of stacking-patterns analysis in strata of diverse ages and settings. Special Publication - Society for Sedimentary Geology, 63: 187-225.

Levin, L.A. 1994. Paleoecology and ecology of xenophyophores. Palaios, 9:32-41.

Li, Y.-X., Bralower, T.J., Montanez, I.P., Osleger, D.A., Arthur, M.A., Bice, D.M., Herbert, T.D., Erba, E. and Premoli Silva, I. 2008. Toward an orbital chronology for the early Aptian oceanic anoxic event (OAE1a, approximately 120 Ma). Earth and Planetary Science Letters, 271: 88-100.

Lopez, J.A. 1995. Salt tectonism of the U.S. Gulf Coast Basin. New Orleans Geological Society.

Loucks, R.G. 1976. Pearsall formation, Lower Cretaceous, south Texas : depositional facies and carbonate diagenesis and their relationship to porosity, The University of Texas at Austin, Austin, 362 pp.

Loucks, R.G. 1977. Porosity development and distribution in shoal-water carbonate complexes; subsurface Pearsall Formation (Lower Cretaceous), South Texas. In: Cretaceous Carbonates of Texas and Mexico: Applications to Subsurface Exploration (Eds D.G. Bebout and R.G. Loucks), Report of Investigations No 89, pp. 97-126. University of Texas at Austin, Bureau of Economic Geology : Austin, TX, United States, Austin, TX.

Loucks, R.G., Abel, C., and ver Hoeve, M. 1996. Paleostructure association, lithofacies architecture, and reservoir quality of the Upper James Lime (Pearsall Fm, Lower Cretaceous) in the Poplarville Field, Pearl River Co., Mississippi. Transactions - Gulf Coast Association of Geological Societies, 46: 235-248.

Loucks, R.G. 2002. Controls on reservoir quality in platform-interior limestones around the Gulf of Mexico; example from the Lower Cretaceous Pearsall Formation in South Texas. Transactions - Gulf Coast Association of Geological Societies, 52: 659-672.

Loucks, R.G. and Ruppel, S.C. 2007. Mississippian Barnett Shale: Lithofacies and depositional setting of a deep-water shale-gas succession in the Fort Worth Basin, Texas. AAPG Bulletin, 91: 579-601.

Loucks, R.G., Reed, R.M., Ruppel, S.C., and Jarvie, D.M. 2009. Morphology, genesis, and distribution of nanometer-scale pores in siliceous mudstones of the Mississippian Barnett Shale. Journal of Sedimentary Research, 79: 848-861.

Loucks, R. G., Reed, R. M., Ruppel, S. C., and Hammes, U., 2010, Preliminary classification of matrix pores in mudstones: Gulf Coast Associations of Geological Societies Transactions, 60.

Loucks, R.G., Reed, R.M., Ruppel, S.C., and Hammes, U. Spectrum of pore types and networks in mudrocks and a descriptive classification for matrix-related mudrock pores. AAPG Bulletin, in press.

Lozo, F.E. and Smith, C.I. 1964. Revision of Comanche Cretaceous stratigraphic nomenclature, southern Edwards Plateau, southwest Texas. Transactions - Gulf Coast Association of Geological Societies, 14: 285-306.

Lozo, F.E. and Stricklin, F.L., Jr. 1956. Stratigraphic notes on the outcrop basal Cretaceous, central Texas. Transactions - Gulf Coast Association of Geological Societies Transactions, 6: 67-78.

Luffel, D.L. and Guidry, F.K. New core analysis method for measuring rock properties in Devonian shale. Journal of Petroleum Technology: 1184-1190.

MacQuaker, J.H.S., Keller, M.A., Davies, S.J. 2010. Algal blooms and "marine snow": Mechanisms that enhance preservation of organic carbon in ancient fine-grained sediments. Journal of Sedimentary Research, 80: 934-942.

Mancini, E.A. and Puckett, T.M. 2002. Transgressive-regressive cycles in Lower Cretaceous strata, Mississippi Interior Salt Basin area of the northeastern Gulf of Mexico. Cretaceous Research, 23: 409-438.

Mancini, E.A. and Scott, R.W. 2006. Sequence stratigraphy of Comanchean Cretaceous outcrop strata of Northeast and South-Central Texas; implications for enhanced petroleum exploration. Transactions - Gulf Coast Association of Geological Societies, 56: 539-550.

Mazzullo, S.J. 2000. Organogenic dolomitization in peritidal to deep-sea sediment. Journal of Sedimentary Research, 70: 10-23.

McKenzie, J.A., Bernoulli D., and Garrison, R.E. 1978. Lithification of pelagic-hemipelagic sediments at DSDP site 373: Oxygen isotope alternation with diagenesis, Initial Report Deep Sea Drill Project, 42A: 473-748.

Menegatti, A.P., Weissert, H., Brown, R.S., Tyson, R.V., Farrimond, P., Strasser, A. and Caron, M. 1998. High-resolution delta ^{13}C stratigraphy through the early Aptian 'Livello Selli' of the Alpine Tethys. Paleoceanography, 13: 530-545.

Miller K.G., Kominz, M.A., Browning, J.V., Wright, J.D., Mountain, G.S., Katz, M.E., Sugarman, P.J., Cramer, B.S., Christie-Blick, N., and Pekar, S.F.. 2005. The Phanerozoic record of global sea-level change. Science 310: 1293–1298.

Moullade, M., Kuhnt, W., Bergen, J.A., Massed, J.P. and Tronchetti, G. 1998. Correlation of biostratigraphic and stable isotope events in the Aptian historical stratotype of La Bedoule (Southeast France). Comptes Rendus de l'Academie des Sciences, Serie II. Sciences de la Terre et des Planetes, 327: 693-698.

Mount, J.F. 1984. Mixing of siliciclastic and carbonate sediment in shallow shelf environments. Geology, 12: 432-435.

Mulder, T., Alexander, J. 2001. The physical character of sub-aqueous sedimentary density flows and their deposits: Sedimentology, 48: 269-299.

O'Brien, N.R. 1996. Shale lamination and sedimentary processes, *in* Kemp., A.E.S. ed., Palaeoclimatology and palaeoceanography from laminated sediments: Geological Society Special Publication, 116: 23-36.

O'Brien, N.R., Nakazawa, K. and Tokuhashi, S. 1980. Use of clay fabric to distinguish turbiditic and hemipelagic siltstones and silts. Sedimentology, 27: 47-61.

Passey, Q.R., Bohacs, K.M., Esch, W.L., Klimentidis, R., Sinha, S. 2010. From oil-prone source rock to gas-producing shale reservoir—geologic and petrophysical characterization of unconventional shale-gas reservoirs. SPE paper 131350 presented at the CPS/SPE international oil & gas conference and exhibition China, Beijing, China.

Pemberton, S.G., MacEachern, J.A., Gingras, M.K., and Saunders, T.D.A. 2008. Biogenic chaos. Cryptobioturbation and the work of sedimentologically friendly organisms. Palaeogeography,Palaeoclimatology, Palaeoecology, 270: 273-279.

Peters, K.E. 1986. Guidelines for evaluating petroleum source rock using programmed pyrolysis. AAPG Bulletin, 70: 318-329.

Peters, K.E., Walters, C.C., and Moldowan, J.M. 2005. The biomarker guide, 2nd ed: Cambridge, U.K., Cambridge University Press: 1,155pp.

Phelps, R.M. 2011. Middle-Hauterivian to Lower-Campanian Sequence Stratigraphy and Stable Isotope Geochemistry of the Comanche Platform, South Texas. University of Texas at Austin, Austin, Tx. 242pp.

Pike, J., Bernhard, J.M., Moreton, S.G., and Butler, I.B. 2001. Microirrigation of marine sediments in dysoxic environments: Implications for early sediment fabric formation and diagenetic processes, Geology, 29: 923–926.

Pindell, J. and Kennan, L.: Kinematic Evolution of the Gulf of Mexico and the Caribbean. In: D. Fillon (ed.): Gulf Coast Section Society of Economic Paleontologists And Mineralogists Foundation, 2001, pp.32.

Pomar, L. 2001. Ecological control of sedimentary accommodation: evolution from a carbonate ramp to rimmed shelf, Upper Miocene, Balearic Islands. Palaeogeography, Palaeoclimatology, Palaeoecology, 175: 249-272.

Potter, P.E., Meynard, J.B., and Depetris, P.J. 2005. Mud and mudstones- Introduction and overview: Berlin, Heidelberg, Springer-Verlag, 297p.

Pratt, L.M., Arthur, M.A., Dean, W.E. and Scholle, P.A. 1984. Paleoceanographic cycles and events during the Late Cretaceous in the Western Interior Seaway. In: Cretaceous Evolution of the Western Interior Basin of North America (Eds W.G.E. Caldwell and E.G. Kaufman), Special Paper 39. Geological Association of Canada, Special Paper 39.

Raiswell, R., and Berner, R.A. 1985. Pyrite formation in euxinic and semi-euxinic sediments. American Journal of Science, 285:710-724.

Raiswell, R., and Berner, R.A. 1987. Organic carbon losses during burial and thermal maturation of normal marine shales. Geology15: 853-856.

Rhodes, D.C., and Morse I.W. 1971. Evolutionary and ecological significance of oxygen-deficient marine basins. Letaia, 4: 413-428.

Rine, J.M. and Ginsburg, R.N. 1985. Depositional facies of a mud shoreface in Suriname, South America; a mud analogue to sandy, shallow-marine deposits. Journal of Sedimentary Research, 55: 633-652.

Ross, D.J. 1992. Sedimentology and depositional profile of a mid-Cretaceous shelf edge rudist reef complex, Nahal Ha'mearot, northwestern Israel. Sedimentary Geology, 79: 161-172.

Roth, P. H., 1978, Cretaceous nannoplankton biostratigraphy and oceanography of the northwestern Atlantic Ocean. Initial Reports of the Deep Sea Drilling Project, 44: 731–759.

Salvador, A. 1991. Triassic-Jurassic. In: The geology of North America (Ed A. Salvador), pp. 131-180. Geol. Soc. Am. : Boulder, CO, United States, Boulder, CO.

Scotese, C.R. 1997. Paleogeographic Atlas, PALEOMAP Progress Report 90-0497, Arlington, Texas, Department of Geology, University of Texas at Arlington, 45pp.

Schieber, J. 1998. Sedimentary features indicating erosion, condensation, and hiatus in the Chattanooga Shale of Central Tennessee: Relevance for sedimentary and stratigraphic evolution. in Shales and Mudstones II, (eds.) J. Schieber, W. Zimmerle, and P.S. Sethi; Stattgard, Germany. 69-91.

Schieber, J. 1998. Possible indicators of microbial mat deposits in shales and sandstones: examples from the Mid-Proterozoic Belt Supergroup, Montana, USA. Sedimentary Geology, 120: 105-124.

Schieber, J., Southard, J., and Kevin, T. Accretion of mudstone beds from migrating floccule ripples. Science, 14: 1760-1763.

Schieber, J., Southard, J.B., and Schimmelmann, A. 2010, Lenticular shale fabric resulting from intermittent erosion of water-rich muds- Interpreting the rock record in the light of recent flume experiments: Journal of Sedimentary Research, 80: 119-128.

Schlager, W. 1991. Depositional bias and environmental change - important factors in sequence stratigraphy. Sedimentary Geology, 70: 109-130.

Schlager, W., Reijmer, J.J.G., and Droxler, A. 1994. Highstand shedding of carbonate platforms. Journal of Sedimentary Research, 64: 270-281.

Schlager, W. 2005. Carbonate Sedimentology and Sequence Stratigraphy. Concepts in Sedimentology and Paleontology, 8. Society of Economic Paleontologists and Mineralogists, Tulsa, OK, 200 pp.

Schlager W. 1999. Scaling of sedimentation rates and drowning of reefs and carbonate platforms. Geology, 27: 183-186.

Schlanger, S.O. and Jenkyns, H.C. 1976. Cretaceous oceanic anoxic events; causes and consequences. Netherlands Journal of Geosciences, 55: 179-184.

Scholle, P.A. and Arthur, M.A. 1980. Carbon isotope fluctuations in Cretaceous pelagic limestones; potential stratigraphic and petroleum exploration tool. AAPG Bulletin, 64: 67-87.

Scotese, C.R., Gahagan, L.M. and Larson, R.L. 1988. Plate tectonic reconstructions of the Cretaceous and Cenozoic ocean basins. Tectonophysics, 155: 27-48.

Scott, R.J. 2003. The Maverick Basin: New technology -- New Success. In: Structure and Stratigraphy of south Texas and Northeast Mexico: Applications to Exploration, CD ROM, pp. 18. GCSSEPM Foundation South Texas Geological Society.

Shanmugam, G. 2008. Deep-water bottom currents and their deposits. Developments in Sedimentology, 60: 59-81.

Sliter, W.V. 1989. Aptian anoxia in the Pacific Basin. Geology, 17: 909-913.

Sloss, L.L. 1963. Sequences in the Cratonic Interior of North America. Geological Society of America Bulletin, 74: 93-114.

Soutar, A., Johnson, S.R., Baumgartner, T.R. 1981. In search of modern depositional analogs to the Monterey Formation. *In* The Monterrey Formation and related siliceous rocks of California. (eds. R.E. Garrison and R.G. Douglas): 123-147

Southam, J.R., Peterson,W.H., and Brass, G.W. 1982. Dynamics of anoxia. Palaeogeography, Palaeoclimatology, Palaeoecology, 4, 183-198.

Stanley, S.M. and Hardie, L.A. 1998. Secular oscillations in the carbonate mineralogy of reef-building and sediment-producing organisms driven by tectonically forced shifts in seawater chemistry. Palaeogeography, Palaeoclimatology, Palaeoecology, 144: 3-19.

Stow, D.A.V. and Bowen, A.J. 1980. A physical model for the transport and sorting of fine-grained sediment by turbidity currents. Sedimentology, 27: 31-46.

Stow, D.A.V. and Piper D.J.W. 1984. Deep-water fine-grained sediments- Facies models: Geological Society of London Special Publications, 15: 611-646.

Stricklin, F.L., Jr., Smith, C.I. and Lozo, F.E. 1971. Stratigraphy of lower Cretaceous Trinity deposits of central Texas. - The University of Texas at Austin, Bureau of Economic , Report of Investigations No. 71, 63 pp.

Swart, P.K. and Eberli, G.P. 2005. The nature of the delta $\delta^{13}C$ of periplatform sediments; implications for stratigraphy and the global carbon cycle. Sedimentary Geology, 175: 115-129.

Swart, P.K., Reijmer, J.J.G. and Otto, R. 2009. A re-evaluation of facies on Great Bahama Bank; II, Variations in the delta $\delta^{13}C$, $\delta^{18}O$and mineralogy of surface sediments. Special Publication of the International Association of Sedimentologists, 41: 47-59.

Thompson, J.B., Mullins ,T.H., Newton, C.R., and Vercoutere, T.L. 1985. Alternative biofacies model for dysaerobic communities. Lethaia, 18: 167-179.

Tinker, S.W. 1985. Lithostratigraphy and biostratigraphy of the Aptian La Pena Formation, Northeastern Mexico and South Texas, and depositional setting of the Aptian Pearsall-La Pena Formations, Texas subsurface and Northeastern Mexico: Why is there not another Fairway Field?: M.S. Thesis, University of Michigan, Ann Arbor, 80 pp.

Thiede, J. and van Andel, T.H. 1977. The palaeo-environment of anaerobic sediments in the late Mesozoic South Atlantic Ocean. Earth and Planetary Science Letters, 22: 301-309.

Tucker, M.E. and Wright, V.P. 1990. Carbonate Sedimentology. Blackwell Scientific Publications, Oxford, 482 pp.

TXCO Resources 2009. The emerging resource company. Howard Weil 37th annual energy conference. New Orleans.

Vahrenkamp, V.C. 2010. Chemostratigraphy of the Lower Cretaceous Shu'aiba Formation: A d13C reference profile for the Aptian Stage from the southern Neo-Tethys Ocean. In: Barremian – Aptian stratigraphy and hydrocarbon habitat of the eastern Arabian Plate (Eds F.S.P. van Buchem, M.I. Al-Husseini, F. Maurer and H.J. Droste), GeoArabia Special Publication 4, pp. 107-138.

Waite, L.E. 2009. Stuart City trend of the Edwards Formation, south Texas, revisited: new data, new concepts. Bulletin of the South Texas Geologic Society, 50: 15-36.

Weissert, H. 1989. C-isotope stratigraphy, a monitor of paleoenvironmental change; a case study from the Early Cretaceous. Surveys in Geophysics, 10: 1-61.

Weissert, H. and Erba, E. 2004. Volcanism, CO2 and palaeoclimate: a Late Jurassic-Early Cretaceous carbon and oxygen isotope record. Journal of the Geological Society, 161: 695-702.

Weissert, H., Lini, A., Follmi, K.B. and Kuhn, O. 1998. Correlation of Early Cretaceous carbon isotope stratigraphy and platform drowning events; a possible link? Palaeogeography, Palaeoclimatology, Palaeoecology, 137: 189-203.

Wetzel, A. 1984. Bioturbation in deep-sea fine grained sediments: influence of sediment texture, turbidite frequency, and rates of environmental change. In Fine-grained sediments: deep water processes and facies (eds. D.A.V. Stow and D.J.W. Piper), 595-610. Geologic Society Special Publication, 15.

Wignall, P.B. 1991. Black Shales. Oxford, UK. Oxford University Press. 127pp.

Wignall, P.B., and Hallam, A. 1991. Biofacies, stratigraphic distribution and depositional models of British onshore Jurassic black shales. In Modern and ancient continental shelf anoxia (eds. R.V. Tyspn and T.H. Pearson.), pp. 291-309. Geological Society Special Publication, 58.

Wignall, P.B. and Newton R. 1998. Pyrite framboids diameter as a measure of oxygen deficiency in ancient mudrocks. American Journal of Science, 298: 537-552.

Wilson, P.A. and Norris, R.D. 2001. Warm tropical ocean surface and global anoxia during the Mid-Cretaceous period. Nature, 412: 425-428.

Winker, C.D. and Buffler, R.T. 1988. Paleogeographic evolution of early deep-water Gulf of Mexico and margins, Jurassic to Middle Cretaceous (Comanchean). AAPG Bulletin, 72: 318-346.

Young, K. 1986. Cretaceous, marine inundations of the San Marcos Platform, Texas. Cretaceous Research, 7: 117-140.

Vita

David C. Hull was born in Mobile, Alabama, and grew up in Fairfield, Connecticut. He attended the University of St. Andrews in St. Andrews, Scotland, for his undergraduate education and graduated in 2007 with a Master of Arts with Honours in economics and international relations. Subsequently, he worked as a petroleum landman in the Southern U.S. before enrolling for undergraduate geology courses at Texas A&M University. He did not receive a degree there but started his Masters of Science work at The University of Texas at Austin in 2009.

Permanent e-mail: david.christopher.hull@gmail.com

This thesis (report) was typed by David C. Hull.